HOST-PATHOGEN INTERACTIONS IN *PNEUMOCYSTIS* INFECTION

by

Taylor John Eddens

B.A., Washington and Jefferson, 2011

Submitted to the Graduate Faculty of

University of Pittsburgh School of Medicine in partial fulfillment

of the requirements for the degree of

Doctor of Philosophy

University of Pittsburgh

2016

UNIVERSITY OF PITTSBURGH

SCHOOL OF MEDICINE

This dissertation was presented

by

Taylor John Eddens

It was defended on

June 3rd, 2016

and approved by

Jeffrey Brodsky, Ph.D., Professor, Department of Biological Sciences

Mandy McGeachy, Ph.D., Assistant Professor, Department of Medicine

Doug Reed, Ph.D., Associate Professor, Department of Immunology

Dario Vignali, Ph.D., Vice Chair and Professor, Department of Immunology

Dissertation Advisor: Jay Kolls, M.D., Professor, Department of Pediatrics

HOST-PATHOGEN INTERACTIONS IN *PNEUMOCYSTIS* INFECTION

Taylor John Eddens, Ph.D.

University of Pittsburgh, 2016

Pneumocystis remains the most common opportunistic infection in patients with HIV/AIDS and can cause a life-threatening fulminant pneumonia. *Pneumocystis* pneumonia is re-emerging in the HIV-negative population, as immunosuppressive medications have greater use clinically. As the at-risk population increases, understanding the underlying host responses that can lead to protection against *Pneumocystis* becomes imperative. To that end, we characterized the early $CD4^+$ T-cell dependent eosinophilic response to *Pneumocystis murina*. Importantly, we demonstrated that eosinophils have potent anti-*Pneumocystis* activity both *in vitro* and *in vivo*.

However, eosinophils in the lung can also lead to pathology as seen in allergic airway inflammation in asthma. We therefore compared *Pneumocystis* to the common airway allergen, house dust mite, and demonstrated that the immune response to both pathogens was highly similar. *Pneumocystis* antigen exposure resulted in increased airway hyperresponsiveness and mucus production in a Th2-dependent and eosinophil-independent manner. From a translational standpoint, a subset of patients with severe asthma had increased anti-*Pneumocystis* IgG and IgE antibodies. Patients with high anti-*Pneumocystis* IgG levels had worsened cough and lung function as measured by spirometry, suggesting that *Pneumocystis* exposure may be correlated with worsened disease.

As *Pneumocystis* infection induces such a potent adaptive immune response, we next examined local immunity to *Pneumocystis*. Inducible bronchus associated lymphoid tissue (iBALT) has been characterized in several models of lung infection and contributes to protection.

Pneumocystis infection and exposure in a co-housing model resulted in the formation of iBALT structures in a CXCL13-dependent manner. Importantly, CXCL13 regulation appeared to be dependent on both Th2 and Th17 $CD4^+$ T-cells *in vivo* and in pulmonary fibroblasts *in vitro*.

The host response to *Pneumocystis* is limited in patients with global immunosuppression and the identification of novel drug and vaccine targets is lacking. Towards that end, we annotated the *Pneumocystis* genome and as proof-of-principle, demonstrated that the kinome (specifically VPS34) was druggable *in vitro*. Additionally, we utilized various –omics techniques to identify Meu10 and GSC-1 as novel vaccine targets capable of providing partial protection against *Pneumocystis*. Together, these studies identified novel protective and pathologic immune responses to *Pneumocystis* and enabled a top-down approach of anti-*Pneumocystis* therapeutic development.

TABLE OF CONTENTS

LIST OF TABLES

LIST OF FIGURES

PREFACE

"If we knew what we were doing, it wouldn't be called research."

-Albert Einstein

While this quote may seem like an inauspicious one to begin a dissertation defense with, I have two primary reasons for its selection. The first is that this quote reminds me of one of the many important lessons my mentor, Dr. Jay Kolls, imprinted on me during my time in his laboratory. Dr. Kolls continually reminded me to follow the data, as opposed to searching for results that would support a predetermined outcome. That philosophy led to at least two hours per week spent with Dr. Kolls, critically pouring over data and designing the next steps. This process led to the multiple successful projects contained within this defense and dozens of others that never got off the ground. But, it never mattered if my hypothesis was spot on or dead wrong. Instead, he taught me to evaluate every possible avenue that could explain the data and begin the next experiments. Find the phenotype, and chase it. That's what I have spent the last three and half years doing, and while the chase invariably led to many exhilarating and frustrating twists and turns, I am incredibly thankful for the journey and all he has taught me. It was truly an honor to work with such a brilliant scientific mind over the past three years.

Of course, Dr. Kolls was not the only mentor I have encountered over my training. I would like to thank Dr. Brian Campfield, a faculty member in the Kolls' lab, for seldom acting

like a faculty member. Dr. Campfield was an excellent role model on how to live a balanced life as a physician scientist and his advice, humor, and guidance throughout my PhD years were unbelievably important to my training. I also need to acknowledge Dr. Waleed Elsegeiny, a former graduate Student in the Kolls' lab. Waleed was always a willing teammate on our projects and his collaborations and training were instrumental in my development as a scientist. I would also like to acknowledge Dr. Kong Chen, William Horne, Dr. Pawan Kumar, Dr. Derek Pociask, and Dr. Mingquan Zheng. As past and present faculty members in the Kolls' lab, I always felt like I had a place I could to turn for guidance. To all the members of the Kolls' lab and my dissertation committee, thank you for pushing me to grow as a scientist.

Additionally, my training over the past three years was not limited to the bench top. I will forever be grateful to Dr. Allyson Larkin and Dr. Geoff Kurland for their clinical mentorship. Their efforts in guiding and relentlessly encouraging my growth as a physician scientist gave me confidence to pursue a lot of the work presented here. I would also like to thank Dr. Richard Steinman and the MSTP administration, past and present, for their continuing support.

The second reason for selecting the quote at the top of this preface dates back to when I first entered the University of Pittsburgh-Carnegie Mellon MSTP. My parents gave me a gift to celebrate my accomplishments, and it was a small, framed cartoon of Albert Einstein with that quote transcribed on the bottom. This cartoon sat on my desk and served as a reminder to stay patient and driven even as the science slowed down or got frustrating. More importantly however, it was a daily reminder of the loving support of my mom, dad, and brother, who never hesitated in their excitement for my training, even as I entered an eight-year program. To my friends and family, thank you for the fun trips, parties, and events over the past five years as when I look back in thirty years, I'm sure those will be the moments that I remember first. And

last but not least, I would like to thank my beautiful fiancé Dr. Katie Ryan. I realize that *Pneumocystis* is not a common topic at the dinner table in most households, but it certainly was in ours over the past three years. She has proofread more pages devoted to my research than she probably would ever care to. But her encouragement and support were unwavering. I thank you for all you do from the bottom of my heart.

It is only because of the people listed above, and many more, that these past three years have been as exciting, challenging, and fun as they were. In all sincerity, I thank you all.

1.0 INTRODUCTION

The title of this dissertation is probably shorter and more vague than most. However, it accurately reflects my dissertation studies in the Kolls' lab. I studied how *Pneumocystis* interacts with the host, and how the host appropriately—and sometimes inappropriately—responds to the fungus. This dissertation will discuss novel findings in the area of protective and pathologic immunity to *Pneumocystis*, the development of antifungals, and antigen discovery to prevent *Pneumocystis* infection (**Figure 1-1**). Each chapter will begin with a more host-centric or in-depth analysis of the prior work that led to that particular project. However, as the chapters contained within this dissertation cover a wide range of topics, this introduction will focus on the unifying theme of this project: *Pneumocystis*.

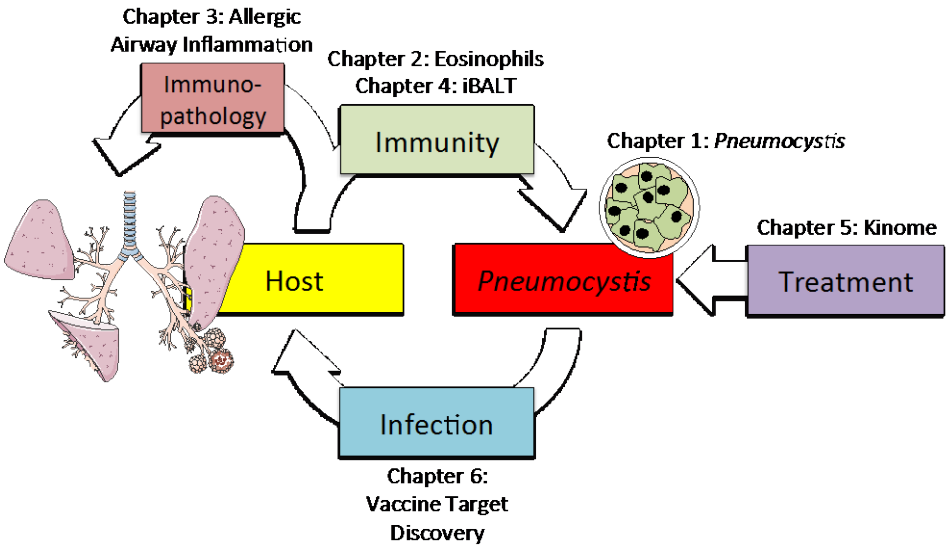

Figure 1-1. Visual outline of the host-pathogen interactions studied within this dissertation.

The majority of this introduction has been published in the following places:

Eddens T., Kolls J.K. 2015. Pathological and protective immunity to Pneumocystis infection. *Semin Immunopathol* 37:153-162.

Eddens, T., Kaloti, A. and Kolls, J.K. 2015. Pathogenesis of Pneumocystis jirovecii Pneumonia. In: Singh, S. K. ed. Human Emerging and Re-emerging Infections. Hoboken, NJ, USA: John Wiley & Sons, Inc., pp. 953–966.

1.1 *PNEUMOCYSTIS*: THE PATHOGEN

1.1.1 Epidemiology

The epidemiology of *Pneumocystis* can be categorized into the HIV and non-HIV populations. As described above, *Pneumocystis* first emerged as a common opportunistic infection in the HIV/AIDS population. As a result, anti-*Pneumocystis* prophylaxis was recommended for any individual with low $CD4^+$ T cell counts (<200 cells/μL), which led to a reduction in the incidence of infection (1). This reduction was furthered by the implementation of combined anti-retroviral therapy (cART) regimens (1). Within three years of the use of cART, *Pneumocystis* incidence (as measured by infection rates per 1,000 person-years) decreased by approximately half (1). Although the incidence of *Pneumocystis* has been reduced, a study by Walzer *et al*. demonstrated that the mortality of *Pneumocystis* pneumonia has largely been unchanged by the implementation of antiretroviral therapy (2). Prior to cART, mortality rates of *Pneumocystis* pneumonia in HIV patients were 10.1%; following cART, mortality rates were modestly reduced to 9.7% (2).

Despite the use of cART and anti-*Pneumocystis* prophylaxis, *Pneumocystis* pneumonia remains the most common serious opportunistic infection in HIV patients in the United States (1, 3, 4). One study reported 322 cases of *Pneumocystis* pneumonia in 2,622 patients with AIDS-defining events (3). Unsurprisingly, most cases of *Pneumocystis* in the developed world are in patients unaware of their HIV-positive status and/or patients not receiving prophylaxis or antiretroviral therapy (4).

In the developing world, *Pneumocystis* pneumonia is a common complicating factor in the HIV-positive population. *Pneumocystis* was detected in the bronchoalveolar lavage (BAL) fluid of 33% of HIV-infected patients presenting with a diffuse pneumonia in southern Africa

(5). Furthering those findings, additional studies in Africa have shown that HIV-positive patients with symptoms (e.g. cough/dyspnea) of pneumonia are likely to have *Pneumocystis* infection; the incidence of *Pneumocystis* in such populations were found to be between 37.2% and 48.6% in South Africa and Kenya, respectively (6, 7). Asian countries, such as Thailand, India, and Malaysia, also have high incidences of *Pneumocystis* infection in the HIV-positive population with diagnosis rates between 12.2-25% (8–10). Developing countries in South America, such as Chile and Venezuela, also report high incidences of *Pneumocystis* in HIV-positive patients with respiratory symptoms (~37%) (11, 12). More alarming than any individual percentage, the above studies all further the point that *Pneumocystis* remains a global clinical concern for patients with HIV/AIDS where prophylaxis and/or cART use is limited for a variety of reasons.

Pneumocystis is also re-emerging in developed countries in the HIV-negative population. A study conducted in Sweden demonstrated that 75% of patients presenting to the hospital with *Pneumocystis* pneumonia were HIV-negative (13). Another study conducted in the United Kingdom between 2000-2010 found that the number of hospital episodes of *Pneumocystis* pneumonia more than doubled during the study period, with transplant and hematologic malignancy patients representing the highest risk groups (14). In addition to malignancy and transplantation, several other conditions including autoimmune conditions and inherited immunodeficiencies have been implicated as emerging risk factors for *Pneumocystis* infection **(Table 1)** (3, 15–27).

Table 1-1. Conditions, procedures, and therapeutic agents that have been implicated in increasing the patient's risk for developing *Pneumocystis* pneumonia.

Conditions/procedures associated with *Pneumocystis* infection	Therapeutic agents associated with *Pneumocystis* infection
HIV	Corticosteroids
Hematologic malignancy	Alkylating agents (e.g. cyclophosphamide)
Solid tumors	Antimetabolite chemotherapeutics (e.g. methotrexate)
Hematopoietic stem cell transplantation	TNF inhibitors (e.g. Etanercept)
Solid organ transplantation	Azathioprine
Rheumatoid arthritis	Alemtuzumab
Severe combined immunodeficiency	Rituximab
Hyper-IgM syndrome	Sirolimus/Tacrolimus
Wegener's granulomatosis	Cyclosporine
Inflammatory Bowel Disease	
Collagen vascular disorders	

Although there are several immunologic changes associated with each of the above conditions, the immunosuppressive therapy for each disease undoubtedly contributes to the risk of developing *Pneumocystis* pneumonia **(Table 1)**. One such example is the use of Rituximab, a monoclonal antibody against the B-cell marker CD20, for the treatment of hematological malignancies such as diffuse large B-cell lymphoma. Martin-Garrido *et al*. found that approximately 30% of patients receiving Rituximab went on to develop *Pneumocystis* pneumonia over the course of the study period (28). Perhaps more troubling, acute respiratory failure was seen in 40% of patients with Rituximab-associated *Pneumocystis*, while mortality in these patients was as high as 30% (28). Although several other agents can increase a patient's risk for *Pneumocystis* **(Table 1-1)**, this example of Rituximab highlights two important points. First, the use of these targeted immunosuppressive agents has lead to a greater understanding of the immune response required to protect against *Pneumocystis* (see Immunity against *Pneumocystis* section). Rituximab selectively targets B-cells and leaves the often-implicated $CD4^+$ T cells intact; however, these patients are exquisitely susceptible to *Pneumocystis* to the

point where universal prophylaxis is being discussed. Second, similar to the findings described above with Rituximab, non-HIV cases of *Pneumocystis* tend to have increased morbidity (e.g. higher mechanical ventilation rates) and mortality than HIV-positive cases (29, 30). At this time, it remains unclear if the direct cause of the increased mortality is due to changes in the disease or differences in clinical management.

Since the first noticed cases of human *Pneumocystis* pneumonia (PCP) among malnourished children and preterm infants in Germany, there has been remarkable progression in our understanding of the pathogenesis of pediatric PCP. Maternal to fetal transmission of HIV led to an upshot in PCP diagnoses among infants and pediatric population in the pre-HAART and PCP prophylaxis era in the US. Currently, organ transplant and childhood hematological malignancies constitute the major risk factors for the development of PCP. Saltzman et al. (2012) conducted a retrospective review of 80 pediatric patients with PCP at Children's Hospital of Philadelphia admitted from 1996-2006 (31). In this cohort, HIV was the single most common associated underlying condition, accounting for 39% of the cases overall, but only in 15% of the cases since 1998. Transplant recipients and oncology patients together comprised another 39% of the cases, while another 9% of cases were attributed to primary immune deficiency. The remaining 9% of cases were associated with less well-recognized causes of susceptibility. High mortality was noted in the HIV and organ transplant groups. The probability of ICU admission and tracheal intubation was greater than 50% in all cases, although there was no increase in mortality associated with ICU admission or tracheal intubation in patients with underlying cancer or primary immune deficiency when compared to HIV-positive PCP. The cause of this discrepancy is unclear, although HIV patients could have had more complicating factors (31). Saltzman et al., (2012) also noted that prophylaxis provided incomplete protection in the

pediatric population, irrespective of the underlying condition, although they particularly noted the failure of prophylaxis among HIV patients (31). Pediatric HIV associated PCP is also a common problem in Argentina, which had the 6th largest pediatric AIDS population and a very high PCP attack rate (32, 33).

1.1.2 Clinical Features

Pneumocystis pneumonia in the HIV-positive population is generally characterized by a sub-acute onset of low-grade fever, nonproductive cough, and progressive dyspnea (34). Further nonspecific findings, such as tachypnea and tachycardia, can be found on physical exam, while the lung exam may range from normal to diffuse crackles upon auscultation (34). While the above characteristic presentation of *Pneumocystis* pneumonia is common in HIV-positive patients, HIV-negative patients can present much differently. Typically, the HIV-negative patients will have a more acute or fulminant presentation with substantial dyspnea, fever, and chills (15, 16). Furthermore, HIV-negative patients have a wider alveolar-arterial oxygen gradient and are more likely to require mechanical ventilation (15, 16).

1.1.3 Diagnosis

Radiologic methods are a useful first step in making a diagnosis of *Pneumocystis*, as most patients presenting with fever and dyspnea will receive a chest x-ray (CXR). The classic CXR of patients with *Pneumocystis* shows diffuse, bilateral interstitial and alveolar infiltrates **(Figure 1-2A)**. Less common findings, such as pneumatoceles, lobar infiltrates, and pneumothoraxes have

been reported (15, 16). Some patients presenting with *Pneumocystis* will have near normal or unimpressive radiographic findings, in which case higher resolution radiologic approaches are recommended, such as high-resolution chest CT (4, 16). Chest CT most commonly demonstrates ground glass opacity with relative peripheral sparing, although mosaic and diffuse patterns can be observed (35). Notably, the findings described above are not specific for *Pneumocystis* and a broad differential for opportunistic pneumonias (e.g. *Aspergillus*, *Mycobacterium avium*-complex) should be maintained (4).

It is also important to interpret radiologic findings in the context of the underlying immunosuppression. HIV-negative patients with *Pneumocystis* tend to have a greater extent of ground-glass opacity on chest CT (35). Moreover, HIV-negative *Pneumocystis* patients are more likely to have lung consolidations, perhaps reflecting a more robust host immune response (35).

Although radiologic methods, coupled with the appropriate clinical context, can highly suggest a diagnosis of *Pneumocystis*, the gold standard of diagnosis remains harvesting organism from bronchoalveolar lavage (BAL) fluid. Several stains can be utilized to identify *Pneumocystis* microscopically: Gomori-methenamine silver stain (GMS) **(Figure 1-2B)**, Wright-Giemsa, toluidine blue O, or Calcofluor white (34). Monoclonal antibodies conjugated to a fluorescent marker are also available to stain *Pneumocystis*. In fact, these conjugated monoclonal antibodies have greater sensitivity and specificity for detecting *Pneumocystis* than most non-immunofluorescent stains (34). In addition to BAL sampling, induced sputum samples can also be analyzed for *Pneumocystis* by the above stains, with monoclonal antibodies again having the highest sensitivity and specificity (15, 16). Importantly, HIV-negative patients with suspected *Pneumocystis* infection may have a negative induced sputum sample, as HIV-negative patients

tend to have a lower organism burden than their HIV-positive counterparts (15, 16). In HIV-negative patients, BAL is recommended (15, 16).

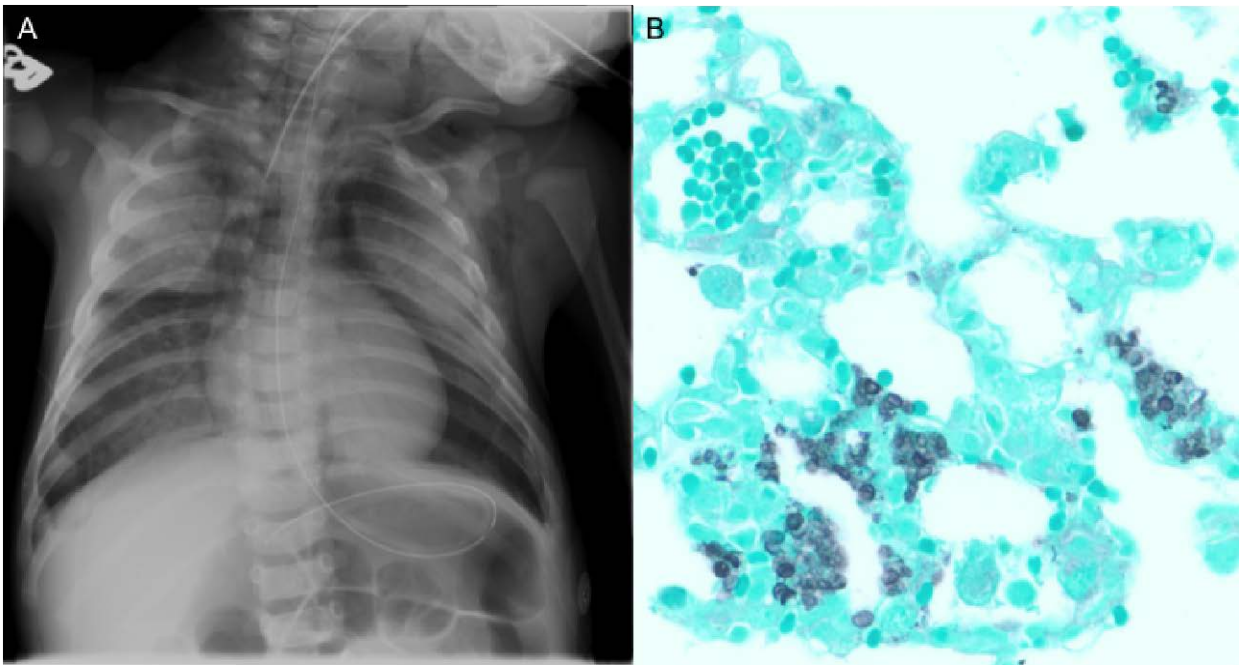

Figure 1-2. Radiographic and microbiologic diagnosis of *Pneumocystis*.

A. Chest radiograph of child with X-linked severe combined immunodeficiency showing bilateral ground glass infiltrates and air bronchograms consistent with *Pneumocystis* pneumonia. B. Gomori-methenamine silver stain (GMS) on *Pneumocystis* infected mouse lung, showing lung architecture (green) with *Pneumocystis* organisms (black) filling the alveolar spaces.

Several molecular techniques have been tested as a means to diagnose *Pneumocystis* from BAL or sputum samples. One such method developed in the 1990's was the use of a single-round polymerase chain reaction (PCR) to amplify the mitochondrial small subunit rRNA of *Pneumocystis* (36, 37). Since that time, the use of nested-PCR (two round PCR) has been used on several gene targets, such as dihydropteroate synthase (*DHPS*), dihydrofolate reductase (*DHFR*), major surface glycoprotein (*MSG*), and loci within the region coding for rRNAs (37).

While using the nested approach increases sensitivity to nearly 100%, this often comes at the cost of decreasing specificity due to the ability to detect colonized individuals who may not have active *Pneumocystis* pneumonia (37).

Newer techniques include the use of quantitative real-time PCR (qPCR) on many of the same targets described above. In addition to reduced turnaround times, qPCRs provide semi-quantitative data to discriminate the cases of colonized individuals from the truly infected individuals. As such, qPCRs for *Pneumocystis* tend to have high sensitivities, along with increased specificities when compared to nested techniques (37). One study that illustrates this point was conducted by Flori *et al*. and examined the diagnostic value of a qPCR test on *MSG* (38). In this study, which examined both HIV-positive and HIV-negative patients, the *MSG* qPCR test had a sensitivity of 100% and specificity of 98.6% (38). While this indicates such diagnostic tests can be optimized to have value in the clinical setting, implementing a qPCR test requires validating the gradations of *Pneumocystis* PCR product to distinguish colonization from infection in the heterogeneous population of the immunocompromised (37). At this time, this challenge still persists in the field and limits the clinical use of such tests.

Two serum markers, β-1,3-glucan and KL-6, have been evaluated as diagnostics for *Pneumocystis*. β-1,3-glucan is a component of the fungal wall, particularly of the ascus (see Microbiology of *Pneumocystis* below) and can enter the serum upon active infection. One study demonstrated that serum β-1,3-glucan above 100 pg/mL had a sensitivity of 100% and a specificity of 96.4% for diagnosing *Pneumocystis* pneumonia using a retrospective analysis (39). However, specificity for serum β-1,3-glucan testing is difficult to establish, as this test does not discriminate between fungal species. As such, serum β-1,3-glucan is often used as an adjunct to clinical suspicion and other diagnostic tests to confirm a *Pneumocystis* infection rather than a

stand alone diagnostic. Similarly, KL-6, a glycoprotein expressed on pneumocytes, can enter the serum in the setting of infectious lung disease. One study has shown that KL-6 levels are elevated in HIV-positive cases of *Pneumocystis*, but the generalizability of serum KL-6 to the HIV-negative population has yet to be demonstrated (40).

1.1.4 Microbiology of *Pneumocystis*

In the 1980's, molecular evidence began to arise that supported the notion that *Pneumocystis* belonged in the group Fungi as opposed to being classified as a protozoan. Edman *et al*. were the first to molecularly confirm the homology of *Pneumocystis* to fungi, such as *Saccharomyces cerevesiae,* by using alignments of the 16S rRNA (41). Several other groups corroborated the homology of the 16S rRNA to fungi and established homology between *Pneumocystis* and fungal mitochondrial gene sequences as well (42–44). Furthermore, one group demonstrated the presence of elongation factor-3 (EF-3), a protein specific to fungi, in *Pneumocystis* (45). Although more molecular evidence was uncovered, perhaps the most substantial evidence came in the context of the *Pneumocystis* genome project, when Cushion *et al*. made cDNA libraries of *Pneumocystis carinii* and subsequently sequenced the contigs; the vast majority of these sequences aligned to fungal species such as *S. cerevesiae* and *Schizosaccharomyces pombe* as opposed to protozoa (46).

Along with reclassifying the genus *Pneumocystis* into the group Fungi, researchers also discovered that genetic diversity existed between species of *Pneumocystis* isolated from different hosts. Originally, *Pneumocystis* was believed to be transmitted in a zoonotic fashion, until 1976 when Frenkel proposed that each *Pneumocystis* species was host-specific (47). After several other studies validated this theory, the genus *Pneumocystis* grew to contain several species. The

genus *Pneumocystis* encompasses five named species: *P. carinii, P. wakefieldiae, P. murina, P. oyrctolagi,* and *P. jirovecii* (48). *P. carinii,* which is isolated from rats, was the first to be discovered and is the most extensively studied organism within the genus. *P. wakefieldiae* is also isolated from rats and is the most genetically similar to *P. carinii*. *P. murina, P. oyctolagi,* and *P. jirovecii* appear to be the sole species found in mice, rabbits, and humans, respectively (as reviewed in (48). Interestingly, the amount of genetic variation between *P. carinii* and *P. jirovecii* suggests that these organisms diverged over 90-100 million years ago around the time of rodent-primate molecular divergence, which may explain why host-specificity appears to be so paramount to these organisms (49). In addition, several other unnamed species appear to have been isolated from other hosts such as non-human primates, ferrets, and horses (50–52).

One of the unique features shared by all the *Pneumocystis* species is the multiphasic life cycle that occurs within the alveolar space of the host (**Figure 1-3**). The ascus (cyst) form of *Pneumocystis* is circular or ovoid in shape and is approximately 4-7 μm in diameter (53, 54). The ascus form has a distinctive thick outer wall made of β-1,3-D-glucan, while within the ascus, eight ascospores mature (53–55). Following maturation, the ascospores will leave the ascus through a small pore and become the troph life form (53, 56). The troph life form appears to be the more metabolically active and replicative form of *Pneumocystis*. Trophs range in size from 2-8 μm and are more irregular in shape. Trophs are thought to replicate in both an asexual and sexual manner. Although most fungal species replicate asexually through a process known as "budding," trophs are thought to propagate via binary fission (57). Two trophs can also conjugate via the use of pheromone receptors and replicate sexually by fusing. Following fusion, the two previous trophs are now a single diploid early sporocyte, which divides using meiosis. This meiotic process is then followed mitosis, generating the eight ascospores (58). During the

division processes, the wall of the sporocyte thickens and hardens and returns the life cycle to the ascus stage.

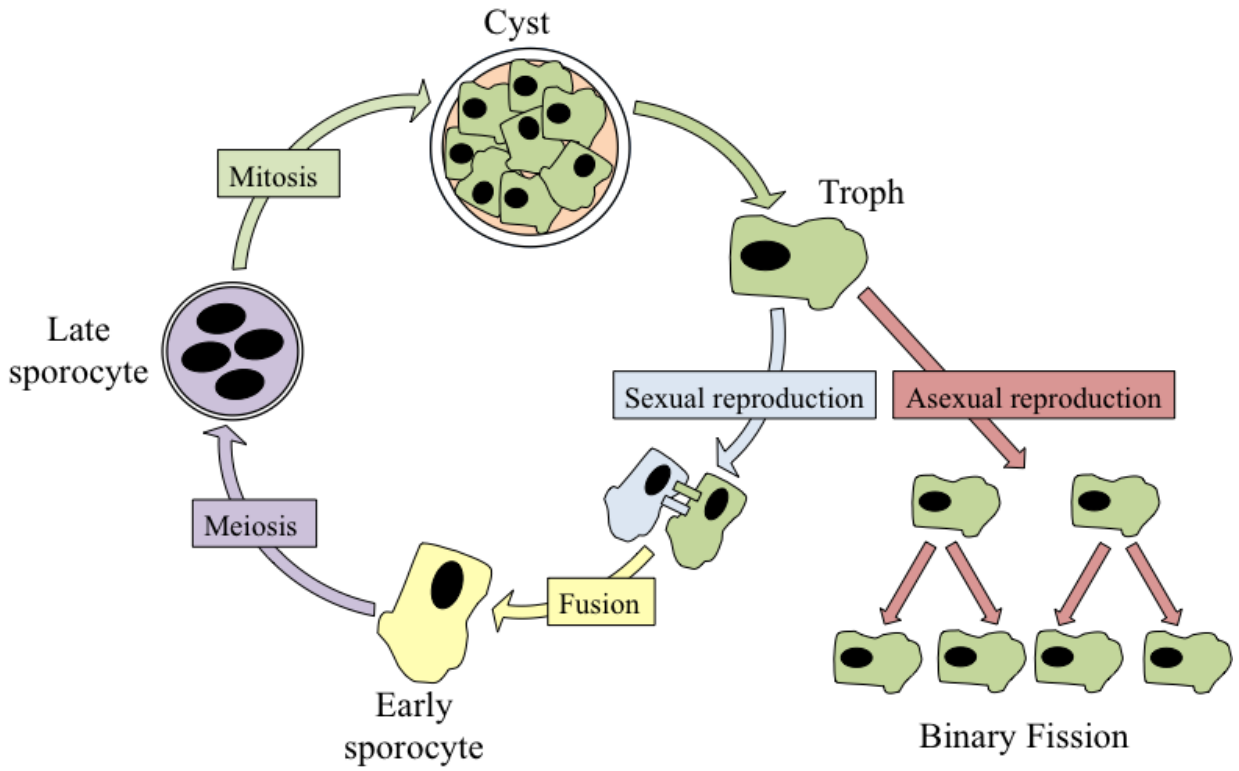

Figure 1-3. The *Pneumocystis* life cycle.

Pneumocystis cysts contain eight ascospores, which leave the cyst to become trophs. Trophs can reproduce asexually through binary fission, a process that results in two identical troph clones. Sexual reproduction can also occur, as two different trophs can fuse to become an early sporocyte. The early sporocyte will then undergo meiosis, forming four nuclei within the late sporocyte. The late sporocyte then thickens its wall and undergoes mitosis, resulting in a cyst.

One study by Cushion *et al*. examined the life cycle *in vivo*; in particular, they examined the effects of β-1,3-D-glucan synthase inhibitors on the ascus and troph population within the lung (55). Mice treated with anidulafungin had a decrease burden of asci in the lung, while the

level of trophs remained the same. More importantly, mice depleted of asci were no longer able to aerially transmit infection to immunodeficient mice, implicating the ascus as the infectious form. Using *in vivo* infection, a second study and unpublished data from our laboratory demonstrated the adherence of the troph life form to the type I pneumocyte in the lung (53). An additional study examined the *Pneumocystis* life cycle *in vitro*, despite the fact that a continuous axenic culture method for *Pneumocystis* has yet to be discovered (59). In this study, Martinez *et al*. showed that asci were capable of producing new trophs while the reverse (trophs becoming asci) did not occur. These results demonstrated that information regarding the *Pneumocystis* life cycle could be gleamed from *in vitro* studies, although the viability in culture is undoubtedly a confounding variable. Recently, a novel mechanism to grow *Pneumocystis jirovecii* has been reported using differentiated pseudostratified CuFi-8 cells, although the utility of such a culture system for propagating infection and/or directed therapy selection has yet to be determined (60). Further studies on the *Pneumocystis* life cycle would be greatly enhanced by any sustainable *Pneumocystis* culture method.

1.1.5 Transmission and Colonization

The most widely accepted theory of *Pneumocystis* transmission is that of aerosolized particles from host to host (16). However, various models of infection are still debated. The reactivation of latent infection theory postulates that initial infection occurs in infancy or early childhood, with reactivation later in life in the context of immune suppression. *Pneumocystis* DNA has been identified in the air surrounding apple orchards and the surface of pond water, indicating that it may be a ubiquitous organism in nature (15). Furthermore, seroprevalance of antibodies to

Pneumocystis is very common among children and has been observed in many parts of the world, thus supporting the theory that children are exposed to *Pneumocystis* early (16, 61). It is thought that in health, the infection is self-contained, but in the case of immunosuppression, the infection may reactivate.

The re-acquisition or *de novo* infection theory suggests *Pneumocystis* infection is actually re-acquired later in life after early childhood infection clearance, in the context of immune suppression. There is considerable evidence in support of this theory. PCP cases are known to have geographic clustering in the urban setting and genotypes found in patients with PCP are similar to those found in the current patient's environment but not those from his or her place of birth (15). Many studies have shown asymptomatic carrier state, particularly resulting by transmission of *Pneumocystis* from PCP patients to healthy hospital workers (62, 63). Additional evidence comes from animal studies that have demonstrated the transmission of *Pneumocystis* between immunocompetent and immunocompromised animals (64). Furthermore, asymptomatic carriage state has recently been observed in patients with non-HIV immunosuppression and pulmonary disease (65). Although asymptomatic carriage is common to both theories, the biggest difference between the *de novo* infection and the latent infection models is the length of time of colonization; in the latent infection model, colonization occurs early and may be stable at a low level until immunosuppression, while the *de novo* infection model suggests that infection is acquired after immunosuppression.

Given the presence of *Pneumocystis* colonization over time, several groups have begun to investigate the relationship between *Pneumocystis* and chronic lung diseases. Gingo et al. first documented respiratory abnormalities such as diffusion impairment and irreversible airway obstruction in patients with HIV in the era of combination antiretroviral therapy (66). The

development of chronic obstructive pulmonary disease (COPD) in non-human primates with persistent *Pneumocystis* colonization has also been demonstrated (67). Further, infection with *Pneumocystis* has been shown to be associated with the development of COPD in human subjects with and without HIV infection (68). These studies demonstrate that *Pneumocystis* can persist asymptomatically in the lung at low-levels (colonization) and that person-to-person transmission may result in frequent exposure in the population (64).

1.1.6 Protective Immunity to *Pneumocystis*

Much of what we have learned of the immune response to *Pneumocystis* has been gleaned from acquired and congenital immunodeficiencies leading to susceptibility, and many of these human conditions have also been successfully replicated in animal models. High dose corticosteroid treatment remains a risk factor and steroid-induced immunosuppression has been a widely used tool to induce infection in rodents (69, 70). Prior to the epidemic of the acquired immunodeficiency syndrome (AIDS), *Pneumocystis* infection in humans was associated with significant malnutrition or myelosuppressive chemotherapy for acute leukemia (71). When the epidemic of *Pneumocystis* infection was observed in AIDS, it was realized that the prevalence of *Pneumocystis* inversely correlated with the peripheral blood CD4+ T-cell lymphocyte count (72). This was recapitulated in a murine model where CD4+ T-cell depletion resulted in Pneumocystis pneumonia whereas CD4+ T-cell replete mice cleared the infection (73). Although CD4+ T-cells are essential, the specific T-cell subsets required remain unclear. Experimental *Pneumocystis* infection induces Th1, Th2, and Th17 responses in mice. Mice deficient in Th17 immunity have delayed clearance of the pathogen but ultimately clear the infection (74). Analogous to these findings, patients with STAT3 mutations that have a reduction in the number of antigen-specific

Th17 cells to *Candida albicans* (75) rarely develop clinical *Pneumocystis* infection (76). Interleukin (IL) 21 is a cytokine produced by T-follicular helper cells in the germinal center of secondary lymphoid tissues (77) as well as Th17 cells. IL-21 appears to play a key role in susceptibility to *Pneumocystis* as evidenced by a recent patient with an IL-21 receptor mutation who subsequently developed clinical *Pneumocystis* pneumonia (78).

B-cells also play a key role in susceptibility to infection. B-cell deficient mice are susceptible to infection (79), as well as patients with hyper IgM syndrome due to either mutations in CD40 or CD40 ligand (80, 81). Consistent with these findings, both *Cd40*$^{-/-}$ or *Cd40l*$^{-/-}$ mice are also susceptible to *Pneumocystis*. In addition to obvious effects on antibody production, the increased susceptibility of these patients may also be due to the fact that B-cells can function as critical antigen presenting cells during the infection (79). Antigen presentation by B-cells may also explain the fact that patients with mutations that affect antibody production such as common-variable or X-linked agammaglobulinemia can, but rarely, develop clinical *Pneumocystis* pneumonia (82). One caveat to the low incidence of *Pneumocystis* pneumonia in these patients, however, is that intravenous immunoglobulin is typically given prophylactically, which may mask some of the susceptibility to *Pneumocystis.* Despite the ambiguity associated with genetic immunodeficiencies, the use of anti-CD20 monoclonal antibodies in humans has emerged as a strong risk factor for *Pneumocystis* pneumonia, which further implicates the B-cell as an important cell type for the normal host defense against *Pneumocystis* (28). Thus the B-cell appears to be critical and the dual functions of antigen presentation and antibody production are likely important.

Further evidence suggests antibodies can provide protection against *Pneumocystis*. It has been demonstrated that antibodies can provide protective immunity by passive transfer of serum

elicited by immunization (83) or of monoclonal antibodies that recognize surface epitopes on the organism to immunodeficient mice (84). Thus, although the role of humoral immunity in conferring susceptibility in humans remains unclear, antibodies could still be exploited for prevention or therapy.

It is thought that ultimately macrophages are the key effector cells that actually clear the infection. Indeed, macrophage depletion increases organism burden in the lung (85). *Pneumocystis* has also been shown to induce apoptosis of lung macrophages and this could be a major host evasion strategy of the organisms (86). Non-opsonic phagocytosis and killing of the organism requires the c-type lectin receptor Clec7a (87). This pathway can be bypassed if the organism is opsonized with IgG (71). Complement also plays in a role in the antibody-mediated control of *Pneumocystis*, as mice deficient in complement treated with an anti-*Pneumocystis* monoclonal antibody had less protection against *Pneumocystis* than complement-replete, antibody treated mice (88). GM-CSF treatment of macrophages *in vitro* increases *Pneumocystis* killing (89), while GM-CSF administration *in vivo* can reduce *Pneumocystis* burden in susceptible mice (90). Moreover, GM-CSF deficient mouse strains develop *Pneumocystis* infection (91) and patients with anti-GM-CSF autoantibodies have increased susceptibility to *Pneumocystis* (92). Recently, it has been demonstrated that macrophages that have an alternative activation program have greater fungicidal activity (93).

In summary, much has been gleaned about the necessary components of the immune system required to clear *Pneumocystis* infection from both clinical studies on patients with genetic mutations and murine models using genetically modified mice. Importantly, however, the murine knockout models faithfully recapitulate clinical susceptibility conferred by analogous genetic mutations (**Table 1-2**). While no murine model will perfectly translate to human patients,

the table below suggests that using mice to study the essential components of immunity against *Pneumocystis* may accurately reflect those requirements in humans.

Table 1-2. Genes associated with *Pneumocystis* susceptibility in mice and men.

Loss of function Gene Mutation	Susceptibility to *Pneumocystis*	
	Human	**Murine**
RAG1	+	+
RAG2	+	+
CD40-CD40L	+	+
PRKDC	+	+
IL2RG	+	+
CD4	+	+
HLA/MHC Class II	+	+
IKBKG	+	N/I
ICOS	+	N/I
BTK	+	N/I
STAT3 (polymorphism)*	+	+
IL-21R*	+	+
Human (+): Clinical diagnosis in patients with mutation. Murine (+): Validated using experimental models. N/I: Not yet investigated. *: Unpublished observations		

1.1.7 Treatment

The first line therapy for active *Pneumocystis* infection and for *Pneumocystis* prophylaxis is trimethoprim-sulfamethoxazole (TMP-SMX) (**Table 1-3**). However, TMP-SMX can be associated with several side effects (e.g. rash, cytopenia) and is not recommended for patients with sulfa allergy (94–96). Interestingly, HIV-infected patients appear to be more likely to develop adverse side effects to sulfa drugs, further limiting the efficacy of TMP-SMX in the population at-risk for *Pneumocystis* infection (97). Several other treatments are indicated as second line therapies (e.g. pentamidine and dapsone) but such regimens tend to have much higher treatment failure rates (94, 95).

Table 1-3. Current treatment regimens for *Pneumocystis.*

Regimen	Dosage	Treatment Failure Rate	Common Adverse Effects	Mortality
Trimethoprim-Sulfamethoxazole (First Choice)	15-20 mg/kg, IV or orally	21%	Cytopenia, skin reactions, hepatitis, pancreatitis, renal insufficiency, anaphylaxis, GI disturbance	Up to 15%
Dapsone + Trimethoprim	5mg/kg 3 times daily orally	39%	Skin rash, fever, methemoglobinemia, GI disturbance	~20%
Atovaquone	750 mg 2-3 times orally	36%	Skin rash, fever, GI disturbance, hepatitis	~20%
Clindamycin and primaquine	600mg 4 times daily IV or 350-400mg 4 times a day orally	35%	Skin rash, fever, neutropenia, GI disturbance, hepatitis	19%
Pentamidine (Alternate choice moderate to severe PCP)	4mg/kg daily IV	40% or higher	Hypotension, cardiac arrhythmias, calcium, magnesium and potassium level disturbance, renal insufficiency, pancreatitis, hypoglycemia, neutropenia, hepatitis	>= 24%

2.0 EOSINOPHILS CONTRIBUTE TO EARLY CLEARANCE OF *PNEUMOCYSTIS MURINA* INFECTION

Adapted from:

Eosinophils contribute to early clearance of *Pneumocystis murina* infection

Taylor Eddens[1,2], Waleed Elsegeiny[1,2], Michael P. Nelson[4], William Horne[1], Brian T. Campfield[1,3], Chad Steele[4] and Jay K. Kolls[1]

[1]Richard King Mellon Foundation Institute for Pediatric Research, Children's Hospital of Pittsburgh of UPMC, Pittsburgh, Pennsylvania, USA.

[2]University of Pittsburgh School of Medicine, Department of Immunology, Pittsburgh, Pennsylvania, USA

[3]Division of Pediatric Infectious Diseases, Department of Pediatrics, University of Pittsburgh School of Medicine, Pittsburgh, Pennsylvania, USA

[4]Department of Medicine, University of Alabama at Birmingham, Birmingham, AL

These data are reported in the *Journal of Immunology*, 2015. 195:185-193.

2.1 INTRODUCTION: BIOLOGY OF EOSINOPHILS

Eosinophils were first described in 1879, when Dr. Paul Ehrlich noted the presence of a highly granular cell in the blood that stained strongly with acidophilic dyes (98). Eosinophils are derived from the myeloid lineage and circulate in low abundance in the serum with a very short half-life of approximately 18 hours (98, 99). Eosinophils can also enter tissues under homeostatic conditions, with the gastrointestinal tract representing the largest repository (100). In states of disease or inflammation, eosinophils can be detected in virtually any organ by histologic analysis. In addition to the unique morphology of eosinophils, these cells can also be recognized by expression of several surface receptors. For one, murine eosinophils express sialic acid-binding Ig-like lectin-F (SiglecF) while human eosinophils express Siglec-8 (99). In addition to being a useful marker for detection of eosinophils by flow cytometry, Siglec-F appears to bind mucins in the airway and may play a role in mediating eosinophil homeostasis (101, 102).

Another key surface receptor expressed by eosinophils is the IL-5 receptor alpha chain (IL-5Rα). IL-5, a cytokine released by Th2 and ILC2 cells, can travel through the circulation to the bone marrow where it acts on granulocyte/monocyte progenitors and eosinophil progenitors to give rise to eosinophils (103). In addition to being required for eosinophilopoiesis, IL-5 is a pro-survival factor in mature eosinophils and appears to prevent apoptosis (104). IL-5 signals through a heterodimeric receptor complex comprised of IL-5Rα and CSF2RB, a shared beta subunit with cytokines GM-CSF and IL-3 (105, 106). Binding of IL-5 to its receptor activates JAK2 and STAT5, in addition to several other proliferative signals such as PI3K and the MAPK pathways (105).

Several other mediators in the development of eosinophils have been discovered and exploited for the study of eosinophils *in vivo*. Eosinophil lineage commitment is dependent on

several transcription factors, including GATA1, PU.1, IFN consensus sequence binding protein, and C/EBP family members (99). GATA1 appears to be the most important transcription factor for eosinophilopoiesis, as deletion of the high-affinity double palindromic GATA1 site in the *Gata1* promoter leads to the complete ablation of eosinophil development (107). Impressively, despite erythroid and megakaryocytic cells requiring GATA1 expression, this deletion appears to abrogate eosinophilopoiesis and modify the differentiation of basophils (107, 108). We, along with several other groups, have used these mice to explore the role of eosinophils *in vivo*.

One key functional component of the eosinophil is the component that allowed for its differentiation via staining: the granule. Eosinophil granules contain a number of proteins, including major basic protein (MBP), eosinophil peroxidase, eosinophil cationic protein, and eosinophil-derived neurotoxin. These four proteins are highly cationic, and once released, are thought to cause damage to surrounding cells by damaging both self and non-self membranes (109). This lack of specificity has led to the study of the mechanisms of degranulation, as the eosinophil was presumed to release its contents completely and without discrimination (98). However, more recent studies have demonstrated that eosinophils secrete cytotoxic mediators in a more controlled fashion called ‘piecemeal degranulation’ (110, 111). Piecemeal degranulation also explains how an eosinophil can release a certain mediator and remain viable and responsive to subsequent stimuli (98). This controlled degranulation also explains how eosinophils can help modulate the immune system; eosinophils have been shown to secrete CCL17, CCL22 (Th2 recruitment factors), APRIL (plasmablast survival factor), and IL-4 and IL-13 (cytokines promoting alternatively activated macrophage development) (98). Additionally, eosinophils are capable of stimulating antigen-specific T-cell responses through MHC class II and CD80/86 expression (112).

Despite clear interactions with the immune system, the role of eosinophils in mediating clearance of pathogens remains somewhat controversial. Historically, eosinophils were thought to mediate host defense against helminthic infections, as histologic analysis of infected tissue revealed eosinophils and parasites in close proximity (98). Studies using recombinant eosinophilic cationic protein and major basic protein *in vitro* also demonstrated anti-helminthic properties against *Schistosoma mansoni* infection (113, 114). However, as newer genetic tools have become available for *in vivo* manipulation, the role of eosinophils in anti-parasitic defense became less clear. For example, eosinophil-deficient GATA1-/- knockout mice fail to develop *Trichinella spiralis* infection and have increased activity of nitric oxide synthase in the local macrophage milieu (115, 116). These findings were also recapitulated in a second eosinophil-deficient mouse model, TgPHIL, which express diphtheria toxin under the control of the eosinophil peroxidase promoter (115, 116). While undoubtedly more studies need to be performed with different parasitic infections, these more recent studies do raise the possibility that the parasite is skewing the immune response towards a Th2-eosinophil axis to allow persistence, as opposed to providing protection to the host.

However, eosinophils do appear to have beneficial properties in the context of host defense against other pathogens. Much like the early studies with parasites, eosinophilic granules have antibacterial and antiviral properties *in vitro* (117, 118). Unlike the parasitic studies, however, the protective effects of eosinophils in the setting of bacterial and viral infections were replicated *in vivo*. Transgenic eosinophilic mice overexpressing IL-5 had increased survival against a lethal *Pseudomonas* infection (119). Likewise, IL-5 transgenic mice have increased clearance of respiratory syncytial virus (RSV) and increased survival following lethal challenge with pneumovirus (98, 120).

Similarly, eosinophils appear to have antifungal properties. One study by Lilly *et al*. demonstrated that eosinophilic granules are fungicidal using a transwell assay with *Apsergillus fumigatus* (121). An additional study found that human eosinophils are capable of recognizing and damaging the cell wall of *Alternaria*, a fungal species associated with asthma and allergic airway disease (122). While a large portion of the literature on eosinophils is focused on allergic airway disease, here we will discuss protective effects of eosinophils in response to another fungal pathogen, *Pneumocystis*. The role of eosinophils in asthma will be discussed in Chapter 3.

2.2 RATIONALE AND HYPOTHESIS

The conventional mediators of immunity against *Pneumocystis* include antibodies and macrophages. However, anti-*Pneumocystis* antibodies form and perform opsonic phagocytosis with macrophages after *Pneumocystis* clearance has already begun, suggestive of a different antifungal immunologic mechanism early in infection. To investigate immunologic responses that may mediate clearance of *Pneumocystis*, we used RNA sequencing of whole lung at day 14 of *Pneumocystis murina* infection in CD4-depleted (which develop chronic progressive infection) and wild type C57BL/6 mice (which clear by 4 weeks). This unbiased approached revealed a strong eosinophil signature.

2.3 MATERIALS AND METHODS

Mice

C57BL/6 mice, *Rag1-/-* knockout mice on a C57BL/6 background, BALB/c mice, and *Gata1^{tm6Sho}/J* mice were all ordered from The Jackson Laboratory (107). Mice were all 6-8 week old females and were bred in the Rangos Research Building Animal Facility. All use of laboratory animals was approved and performed in accordance with the University of Pittsburgh Institutional Care and Use Committee.

Pneumocystis infection time course and primary infections

Twenty-five C57BL/6 female mice were CD4-depleted using weekly intraperitoneal administration of 0.3 mg of GK1.5 monoclonal antibody per mouse and were subsequently challenged with 2.0 x 10^6/mL *Pneumocystis murina* cysts using oropharyngeal inoculation as previously described (83, 123, 124). Twenty-five age-matched C57BL/6 female mice were inoculated at the same time, but were not CD4-depleted. Five mice from each group were then sacrificed at day 0, 3, 7, 10, and 14. Four BALB/c and *Gata1^{tm6Sho}/J* mice were also inoculated with *Pneumocystis* oropharyngeally and sacrificed at day 14. Six uninfected BALB/c mice were used as naïve controls.

RNA isolation and qRT-PCR

Lung RNA was purified using Trizol® Reagent (Life Technologies). Briefly, lungs were homogenized and following the addition of chloroform, RNA in the aqueous phase was collected and precipitated in isopropanol. Following centrifugation, the RNA was washed with 75% ethanol, centrifuged again, and then resuspended in nuclease-free water. Following incubation at

55°C, RNA was quantified using a Nanodrop and 1 μg of RNA was converted to cDNA using iScript™ cDNA synthesis kit per manufacturer's instructions (Bio-Rad). *PC* burden was then quantified using SsoAdvanced qRT-PCR universal probes supermix (Bio-Rad) using primers and a probe specific for *Pneumocystis murina* small subunit (SSU) rRNA with a standard curve of known *Pneumocystis* SSU rRNA concentrations. SSU primer and probe sequences are as follows:

F: 5'-CATTCCGAGAACGAACGCAATCCT; R: 5'- TCGGACTTGGATCTTTGCTTCCCA; Probe: 5'- TCATGACCCTTATGGAGTGGGCTACA. Other primers used include: *Prg2*, *Epx*, *Il5, Clca3, Muc5ac, Muc5b,* and *Il13* (Applied Biosystems). Prior to sequencing, the RNA was further purified using a Qiagen RNA cleanup kit with DNAse treatment.

RNA sequencing

Total RNA from mouse whole lung was used to perform RNA sequencing. Each sample was assessed using Qubit 2.0 fluorometer and Agilent Bioanalyzer TapeStation 2200 for RNA quantity and quality. Library preparation was done using Illumina TruSeq Stranded mRNA sample prep kit. The first step in the workflow involves purifying the poly-A containing mRNA molecules using poly-T oligo attached magnetic beads. Following purification, the mRNA was fragmented into small pieces using divalent cations. The cleaved RNA fragments were copied into first strand cDNA using reverse transcriptase and random primers. Strand specificity was achieved by using dUTP in the Second Strand Marking Mix, followed by second strand cDNA synthesis using DNA Polymerase I and RNase H. These cDNA fragments then have the addition of a single 'A' base and subsequent ligation of the adapter. The products are then purified and enriched with PCR to create the final cDNA library. The cDNA libraries are

validated using KAPA Biosystems primer premix kit with Illumina-compatible DNA primers and Qubit 2.0 fluorometer. Quality is examined using Agilent Bioanalyzer Tapestation 2200.The cDNA libraries will be pooled at a final concentration 1.8pM. Cluster generation and 75 bp paired read single-indexed sequencing was performed on Illumina NextSeq 500's.

Raw reads from an Illumina NextSeq 500 in fastq format were trimmed to remove adaptor/primer sequences. Trimmed reads were then aligned using BWA (version 0.5.9, settings aln -o 1 -e 10 -i 5 -k 2 -t 8) against the mouse genomic reference sequence. Additional alignment and post-processing were done with Picard tools (version 1.58) including local realignment and score recalibration (not duplicate marking) to generate a finale genomic aligned set of reads. Reads mapping to the genome were characterized as exon, intron, or intergenic (outside any annotated gene) using the matched annotation for the genomic reference sequence. The remaining unmapped reads from the genomic alignment were then aligned to a splice reference created using all possible combinations of known exons (based on annotation described above) and then categorizing these as known or novel splice events. This aligned data was then used to calculate gene expression by taking the total of exon and known splice reads for each annotated gene to generate a count value per gene. For each gene there was also a normalized expression value generated in two ways: 1) Reads per Mapped Million (RPM), which was calculated by taking the count value and dividing it by the number of million mapped reads, 2) Reads per Mapped Million per Kilobase (RPKM), which was calculated by taking the RPM value and dividing it by the kilobase length of the longest transcript for each gene. The RPM values are subsequently used for comparing gene expression across samples to remove the bias of different numbers of reads mapped per sample. RPKM values were subsequently used for comparing relative expression of genes to one another to remove the bias of different numbers of mapped

reads and different transcript lengths. In addition to gene expression measurements, nucleotide variation was also detected using the GATK (version 1.3-25, -dcov 2000 -stand_call_conf 30.0 -stand_emit_conf 10.0 -A DepthOfCoverage -A BaseCounts -A AlleleBalance), which identified single nucleotide and small insertion/deletion (indel) events using default settings. Mapped exonic reads per WT sample: 44,291,011; 23,432,350; 41,004,408; and 41,308,864. Mapped exonic reads per GK1.5 sample: 23,305,058; 43,821,698; 122,834,770; and 29,805,804. Data were then filtered on a quality score of 20 and probed for eosinophil associated genes: *Ear11, Ear5, Ccl8, Ccl24, Ccr3, Prg2, Ccl11, Ccl7, Il13, Ear10, Il5ra, Ear2, Csf2rb, Ccl5, Il5, Ear1, Il4* (did not pass quality filter), and *Epx* (did not pass quality filter).

Data Availability

The RNA sequencing data contained in this paper is publicly available through the Sequence Read Archive BioProject number: PRJNA276259. Further information can be found at: http://www.ncbi.nlm.nih.gov/bioproject/.

Bronchoalveolar lavage

Wild type C57BL/6, and GK1.5 treated mice infected with *Pneumocystis* were anesthetized at day 14 post-infection and a 20g Exel Safelet Catheter (Exel International Co.) was inserted in the cricoid cartilage. The needle was then removed and 1 mL aliquots were inserted and removed from the lung using a 1 mL syringe (10 mL total). Bronchoalveolar lavage (BAL) cells were then spun at 300xg for 10 minutes, resuspended in PBS, and counted using Trypan Blue stain. $1x10^6$ cells were then transferred to a round bottom 96-well plate for staining and the remainder of cells

was transferred to Trizol® Reagent for RNA isolation (as described above). Naïve (uninfected) mice were also examined as a control.

IL-5 and Eotaxin-1 Luminex on lung homogenate

Lung was collected in PBS containing protease inhibitors (Roche) and homogenized. We used a Bio-Plex Pro™ Assay (23-plex, Bio-Rad) according to the manufacturers recommendations. Briefly, the plate was treated with Bio-Plex assay buffer, followed by vortexing and two washes. Lung homogenates (undilulted), standards, and blanks were then added to the plate and incubated at room temperature for one hour shaking at 850 rpm, covered. Following three washes, detection antibodies were then diluted and added to each well. The plate was incubated as above. Following three washes, diluted SA-PE was added to each well and incubated at room temperature for 20 minutes on shaker. The plate was then washed three times and resuspended in assay buffer and beads were quantified using a Bio-Plex® MAGPIX™ (Bio-Rad).

Flow cytometry

BAL cells or cells from digested lung ($1x10^6$ total) were spun at 300xg for 3 minutes, resuspended in PBS, and pelleted once more. Cells were then resuspended in PBS containing 2% heat-inactivated fetal bovine serum and 0.4 μg of anti-CD16/CD32 (eBioscience, clone: 93). Following a 15 minute incubation at 4°C, cells were stained with the following antibodies: SiglecF-PE (BD Pharmigen™, clone: E50-2440), CD11b-APC (BioLegend, clone: M1/70), GR1-PE-Cy7 (BD Pharmigen™, clone:RB6-8C5), CD11c-FITC (eBioscience, clone: N418), and F4/80-APC-e780 (eBioscience, clone: BM8). Following an hour incubation at 4°C, cells were

washed with PBS, pelleted, and fixed (BD CytoFix™). Cells were then analyzed using a BD LSRII Flow Cytometer with compensation via OneComp eBeads (eBioscience).

Eosinophil culture and Pneumocystis killing assay

Bone marrow-derived eosinophils were generated using a previously described protocol (121, 125). Briefly, bone marrow was isolated from naïve BALB/c mice and cells plated at 1 x 10^6 cells/ml in RPMI 1640 containing 20% FBS (Irvine Scientific, Santa Ana, CA), 2 mM Glutamine, 25 mM HEPES, 1X MEM nonessential amino acids, 1 mM sodium pyruvate (all from Life Technologies BRL, Rockville, MD), 50 μM β-mercaptoethanol (Sigma-Aldrich, St. Louis, MO), 100 ng/ml stem cell factor and 100 ng/ml FLT3-L (both from Peprotech). After 4 days, cells were replated in the above media supplemented with 10 ng/ml IL-5. After 10 days, bone marrow cells were fully differentiated into eosinophils. As previously reported (125), samples of 1x10^5 cells were taken for RNA analysis each time media was changed for real time PCR analysis of *Epx* for eosinophil development and *Mpo* (Applied Biosystems) for neutrophil development. In addition, cells were cytospun onto glass slides, Giemsa stained and analyzed for morphology and purity by a murine pathologist in the Comparative Pathology Laboratory at the University of Alabama at Birmingham. On the tenth day, bone marrow-derived eosinophils were enumerated and utilized in experiments. Bone marrow-derived eosinophils (1 x 10^5) were then co-cultured with 1 x 10^3 *Pneumocystis* cysts in 100 μL for 18 h at 37°C and 5% CO_2 alone or in the presence of 10 ng/mL of IL-4 and IL-13. Controls included *P. murina* cultured in the absence of eosinophils as well as in the presence or absence of IL-4 and IL-13. Total RNA was isolated from the contents of each well using TRIZOL LS reagent (Invitrogen, Carlsbad, CA) and *Pneumocystis* SSU burden was calculated as above. Percent killing was defined as previously

described (87).

pIL5 and pCMV hydrodynamic injection

An untagged, murine IL-5 expression vector (pIL5, Origene, MC208784) and an empty vector pCMV6 control (Origene, PS100001) were grown in Mix and go *E. coli* (Zymo Research) in 200 mL of LB containing kanamycin and were prepared using an EndoFree Plasmid Maxi Kit (Qiagen) per manufacturer's instructions. Following quantification of vector, 10 μg of vector was added to 2 mL of Ringer's solution (0.9% NaCl, 0.03% KCL, and 0.016% $CaCl_2$) and injected intravenously via the tail vein within 5 seconds, as previously described (126, 127).

IL-5 ELISA

Serum IL-5 was quantified using BioLegend ELISA MAX™ Mouse IL-5 ELISA kit per manufacturer's instructions. Briefly, a 96-well plate was coated with capture antibody and stored overnight at 4°C. Following washes with PBS + 0.05% Tween-20, the plate was blocked with assay diluent for 1 hour at room temperature. Serum samples (diluted 1:20) and IL-5 standard were diluted in assay diluent, added to the plate, and incubate overnight at 4°C. Detection antibody and diluted Avidin-HRP were then added to the plate, with washes in between additions, and the plate was developed with TMB substrate in the dark. Absorbance was then measured at 450 nm.

Lung digestion

The right superior lobe of lung was physically digested using scissors, followed by an hour and a half incubation in collagenase/DNase in a 37°C shaker at 250 rpm. Single cell suspensions were

then strained using a 70 μm filter, pelleted, and then resuspended in 10 mL PBS. Following enumeration using Trypan Blue, cells were stained for flow cytometry as described above.

Histology

The left main bronchus was clamped using forceps and 250 μL of 10% formalin was injected into the bronchus. The lung tissue was then submerged in 10% formalin, paraffin-embedded, and processed by the Children's Hospital of Pittsburgh Histology Core. Sections were then stained from H&E and PAS.

Statistics

All statistics were performed using GraphPad Prism 6. Briefly, an unpaired, two-tailed Student's T test with a $p<0.05$ considered significant was used for all studies except for the BALB/c pIL-5 treatment. Given the non-Gaussian distribution for the BALB/c pIL-5 treatment, a Mann-Whitney nonparametric rank test was performed with a $p<0.05$ considered significant. For studies with three groups, a one-way ANOVA with Tukey's multiple comparisons was used with a $p<0.05$ considered significant. A Kruskal-Wallis nonparametric test with Dunn's multiple comparison's test was used for gene expression analysis in the BALB/c primary challenge experiment with a $p<0.05$ considered significant. Linear regression was also performed using Prism and Pearson's correlation coefficient calculations were performed.

2.4 RESULTS

2.4.1 RNA sequencing of whole lung identifies an eosinophil signature early in *Pneumocystis* infection

To further understand the role of $CD4^+$ T-cells in *Pneumocystis* infection, we examined *Pneumocystis* burden in wild type and GK1.5 treated, CD4-depleted C57/Bl6 mice. In this study, at day 14 using quantitative real time PCR, wild type mice begin to clear infection as CD4-depleted mice had a higher fungal burden at this time point (**Figure 2-1A**). As an unbiased approach to investigate potential mechanisms of fungal clearance, we used RNA sequencing of whole lung at this time point to examine the signatures of potential effector cells. Strikingly, several genes associated with eosinophil function and recruitment, such as *Prg2* (major basic protein), *Il5ra* (IL-5 receptor alpha), *Ccr3*, *Ccl11* (eotaxin-1), *Ccl24* (eotaxin-2), were all significantly upregulated at day 14 of infection in wild type animals (**Figures 2-1B and 2-1C**). Another specific eosinophil marker, eosinophil-associated ribonculease 2 (*Ear2*), was also significantly upregulated in wild type animals, while less specific eosinophil-associated ribonucleases (*Ear5, Ear10, Ear11*) also had higher expression in wild type animals. Importantly, in addition to a robust eosinophil signature at day 14 in wild type animals, IL-5 had significantly higher expression in wild type animals at the transcriptional level at day 7 and day 10 post-infection with *Pneumocystis* (**Figure 2-1D**). Importantly, *prg2*, an eosinophil associated gene, had a 10-fold increase in expression at day 14 by qRT-PCR, similar to that detected by RNA sequencing (**Figure 2-1D**). Furthermore, protein levels of IL-5 and eotaxin-1 (CCL11) were significantly higher in wild type animals at day 14 when compared to CD4-depleted mice (**Figure 2-1E**).

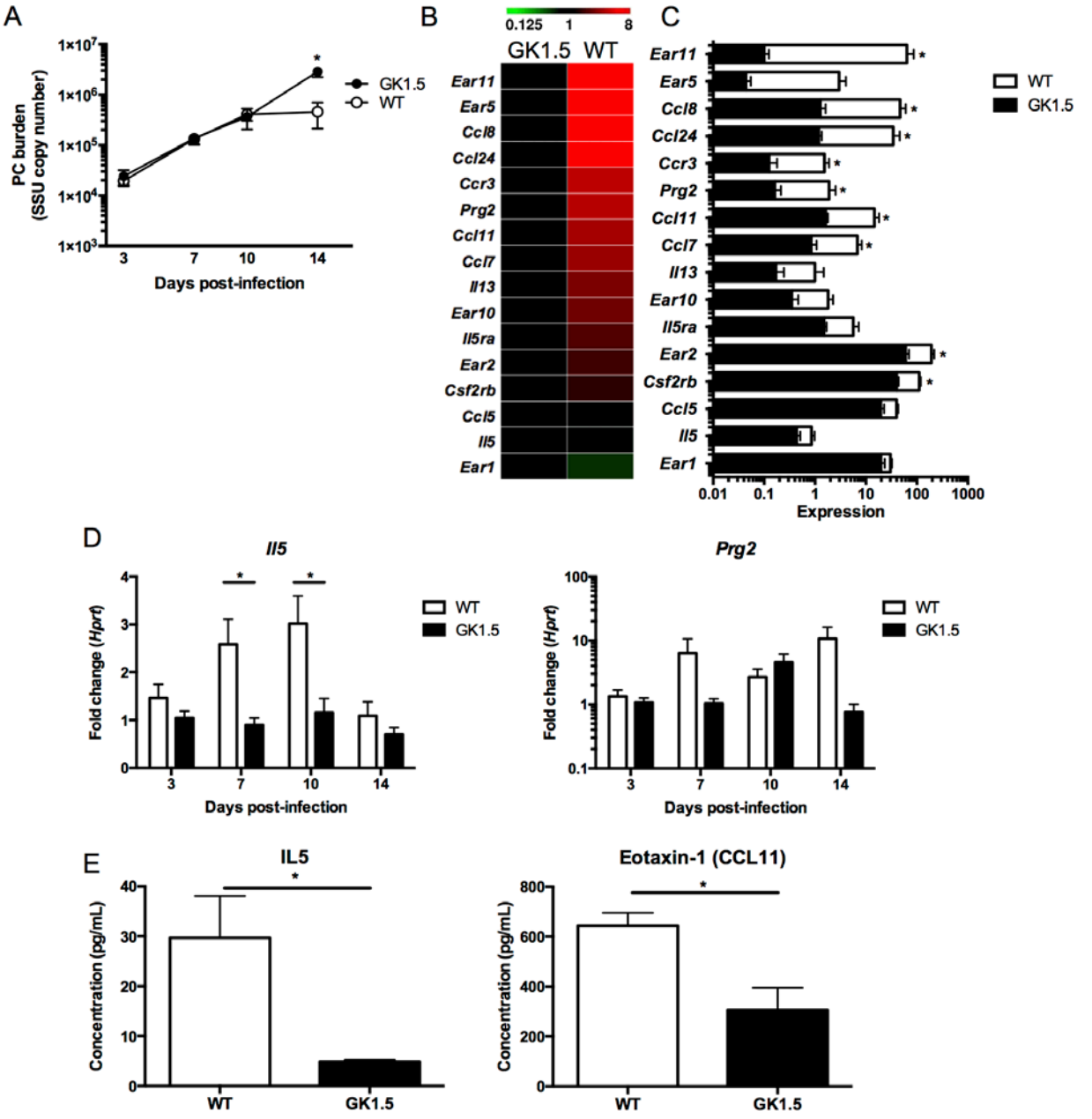

Figure 2-1. RNA sequencing of whole lung shows a prominent CD4-dependent eosinophil signature at day 14 of *Pneumocystis* infection.

A. Wild type or GK1.5 treated CD4-depleted C57BL/6 mice were infected with 2.0 x 10^6 cysts/ml of *Pneumocystis* and were sacrificed at day 3, 7, 10, or 14 following infection (*n*=5 at each time point). *Pneumocystis* burden was calculated by qRT-PCR of the small subunit ribosomal RNA and a significant decrease was seen at day 14 ($p<0.01$ by Student's t-test). B. RNA sequencing of whole lung RNA at day 14 in GK1.5 treated and wild type mice shows increase in expression in genes associated with eosinophils (*n*=4 in each group). C. Histogram of expression values

from heat map in B with * indicating $p<0.05$ by Student's t-test. D. *Il5* expression over the course of *Pneumocystis* infection normalized to *Hprt* and GK1.5 day 3 (fold change) shows increase of *il5* at day 7 and 10 in wild type mice (* $p<0.05$, Student's t-test). Similar to the expression pattern seen by RNA sequencing, a ten-fold increase in *Prg2* is seen at day 14 by qRT-PCR ($p>0.05$). E. IL-5 and Eotaxin-1 (CCL11) protein levels in lung homogenate at day 14 as determined by luminex (* $p<0.05$).

2.4.2 Eosinophils are present in bronchoalveolar lavage fluid early in *Pneumocystis* infection

To further clarify the $CD4^+$ T-cell dependent eosinophil response to *Pneumocystis* infection, we sought to define the cell populations in the bronchoalveolar lavage (BAL) fluid of wild type and CD4-depleted animals at day 14. Cell populations in naïve mice were also analyzed. A population of cells with high side scatter was present in animals with intact $CD4^+$ T-cell responses, but absent in naïve and CD4-depleted animals infected with *Pneumocystis* (**Figure 2-2A,** *left panel*). After gating on all cells, a population of $SiglecF^+CD11b^+$ cells was noted in the wild type animals, but this population was substantially reduced back to naïve levels in animals treated with GK1.5 (**Figure 2-2A,** *right panel*). The $SiglecF^+CD11b^+$ population represented over 60% of cells in BAL fluid in wild type mice, while less than 2% of cells were $SiglecF^+CD11b^+$ in mice treated with GK1.5 (**Figure 2-2B**). Additionally, the RNA from BAL cell pellets was enriched for transcripts associated with eosinophils; *Epx* and *Prg2* expression was nearly 1000-fold higher in BAL cell pellets from wild type mice when compared to naïve and CD4-depleted mice (**Figure 2-2C**).

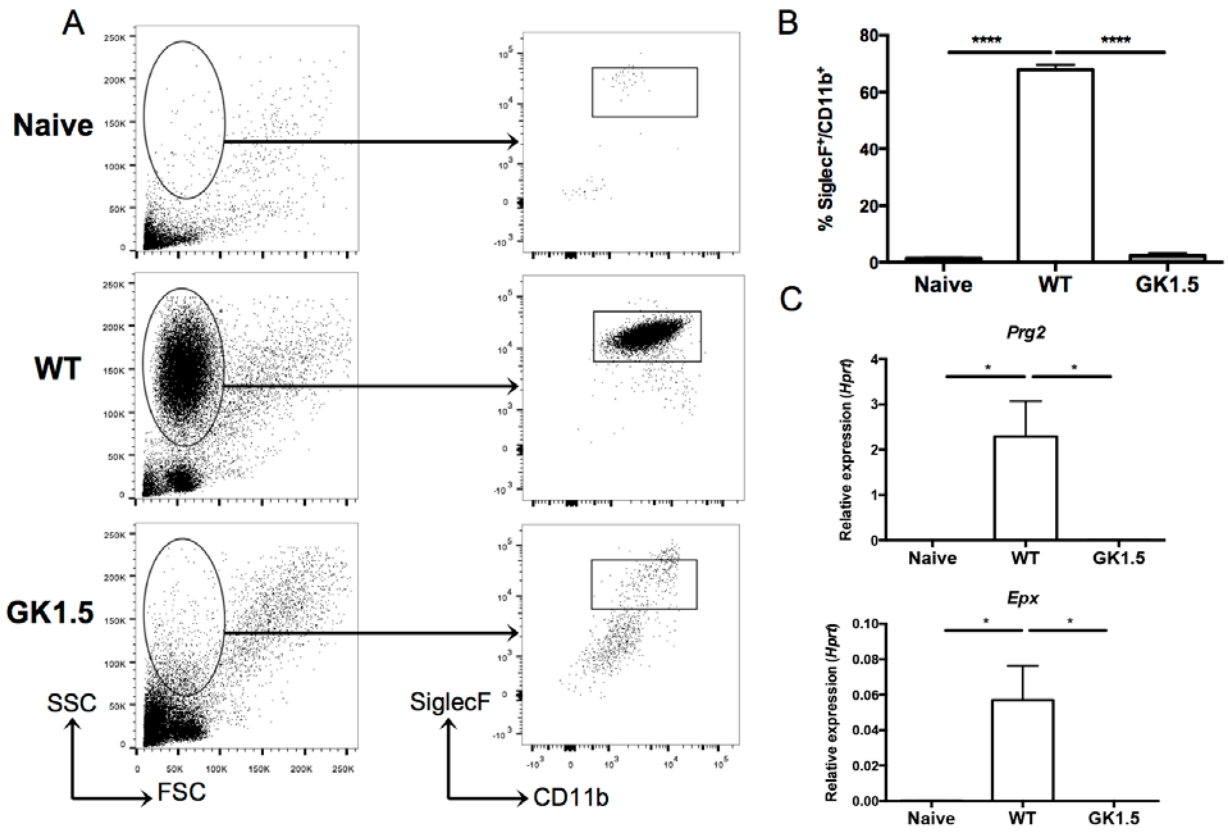

Figure 2-2. CD4-dependent recruitment of eosinophils to the lung at day 14 of *Pneumocystis* infection.

A. Bronchoalveolar lavage (BAL) of naïve (uninfected), wild type, and GK1.5 treated CD4-depleted mice 14 days post-inoculation with *Pneumocystis* shows a large population of cells with high side-scatter in wild type mice (*left panel*). The cells were gated as shown (*left panel*), and a SiglecF^{+}CD11b^{+} population was seen in the wild type, but not the naïve or GK1.5 treated animals (*right panel*). B. Significant increase in percentage of SiglecF^{+}CD11b^{+} cells in wild type animals compared to naïve and GK1.5 treated animals (n=4-5, **** $p<0.0001$ by one-way ANOVA with Tukey's multiple comparisons). C. qRT-PCR for *Epx* (*top)* and *Prg2* (*bottom*) on RNA extracted from BAL cell pellets shows significant increase in expression in wild type animals compared to naïve and GK1.5 treated animals (* $p<0.05$ by one-way ANOVA with Tukey's multiple comparisons).

2.4.3 Eosinophils contribute to control of *Pneumocystis* infection both *in vitro* and *in vivo*

To determine the role of eosinophils in *Pneumocystis* infection, we used a loss-of-function approach and infected eosinophilopoiesis-deficient *Gata1^{tm6Sho}/J* mice and BALB/c controls. *Gata1^{tm6Sho}/J* mice had an increased *Pneumocystis* burden at day 14 post infection compared to control BALB/c mice (**Figure 2-3A**). BALB/c mice had a substantial increase in *Epx* expression and a modest increase in *Prg2* expression compared to *Gata1^{tm6Sho}/J* mice (**Figure 2-3B**). Eosinophils cultured from BALB/c bone marrow also demonstrated anti-*Pneumocystis* activity *in vitro* (**Figure 2-3C**). Furthermore, bone marrow derived eosinophils displayed increased *Pneumocystis* killing activity when co-cultured with IL-4 and IL-13 (**Figure 2-3D**).

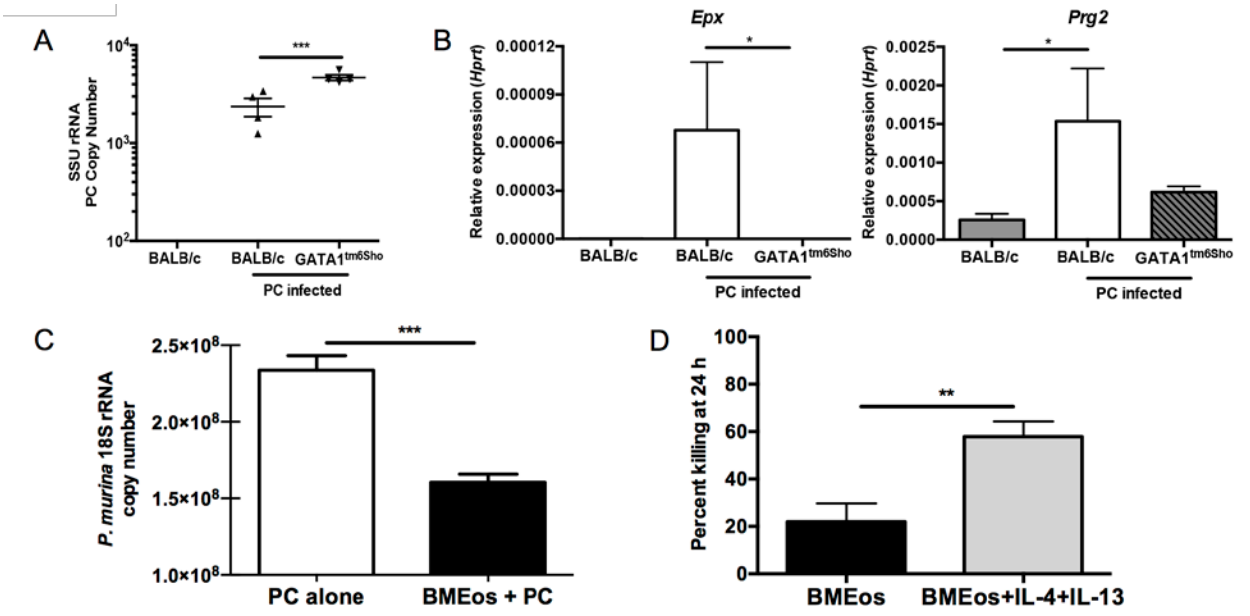

Figure 2-3. Eosinophils contribute to control of *Pneumocystis* infection both *in vitro* and *in vivo*.

A. BALB/c and *Gata1*^{tm6Sho}*/J* knockout mice were infected with *Pneumocystis* and sacrificed at day 14 post-infection and SSU burden was quantified by qRT-PCR (** $p<0.01$ by Student's T test). Uninfected BALB/c mice have no detectable *Pneumocystis* burden. B. qRT-PCR for *Epx* (*left)* and *Prg2* (*right*) on RNA from whole lung shows significant increase in BALB/c mice infected with *Pneumocystis* compared to uninfected BALB/c and infected *Gata1*^{tm6Sho}*/J* knockout mice (* $p<0.05$ by Kruskal-Wallis test with Dunn's multiple comparisons test). C. Bone marrow derived eosinophils from BALB/c mice demonstrate anti-*Pneumocystis* activity when co-cultured *in vitro* for 24 hours at an eosinophil to *P. murina* cyst ratio of 100:1 (*** $p<0.0001$, Student's t-test). D. Bone marrow derived eosinophils show enhanced killing activity when co-cultured with *Pneumocystis* in the presence of 10 ng/ml of IL-4 and IL-13 compared to *Pneumocystis* alone (** $p<0.01$ by Student's T test).

2.4.4 Hydrodynamic injection of IL-5 promotes *Pneumocystis* clearance in CD4-depleted C57BL/6 and *Rag1*-/- mice

To induce eosinophilia prior to *Pneumocystis* infection, we employed hydrodynamic injection with either a plasmid expressing IL-5 (pIL5) or an empty plasmid control (pCMV) in C57BL/6

mice treated with GK1.5 or *Rag1-/-* mice three days prior to infection (**Figure 2-4A**). At day two following infection, mice treated with pIL5 had over a log-fold increase in serum IL-5 (**Figure 2-4B**). At day 14 of infection, treatment with pIL5 resulted in an increased abundance of a high side scatter population and a SiglecF$^+$CD11b$^+$ population in both CD4-depleted C57BL/6 and *Rag1-/-* mice (**Figure 2-4C**). While these populations were present by flow cytometry in the groups treated with pCMV alone (**Figure 2-4C**, *left panel*), C57BL/6 and *Rag1-/-* mice treated with pIL5 had significantly more SiglecF$^+$CD11b$^+$ cells as measured by both percentage and total cell number recovered from the lung (**Figure 2-4D**).

Strikingly, both the CD4-depleted C57BL/6 and *Rag1-/-* mice receiving pIL5 had a statistically significant reduction in *Pneumocystis* burden by day 14 of infection when compared to mice treated with pCMV (**Figure 2-4E**). While the average difference in burden was approximately a half-log in both cohorts, some individual mice had greater than a log-reduction in *Pneumocystis* burden with pIL5 treatment (**Figure 2-4E**). Recruitment of eosinophils to the lung could also be observed by H&E staining in mice receiving pIL5 (**Figure 2-4F**). The pIL5 treated mice also had a ten-fold increase in expression of *Epx* and *Prg2* in whole lung RNA when compared to pCMV treated mice (**Figure 2-4G**).

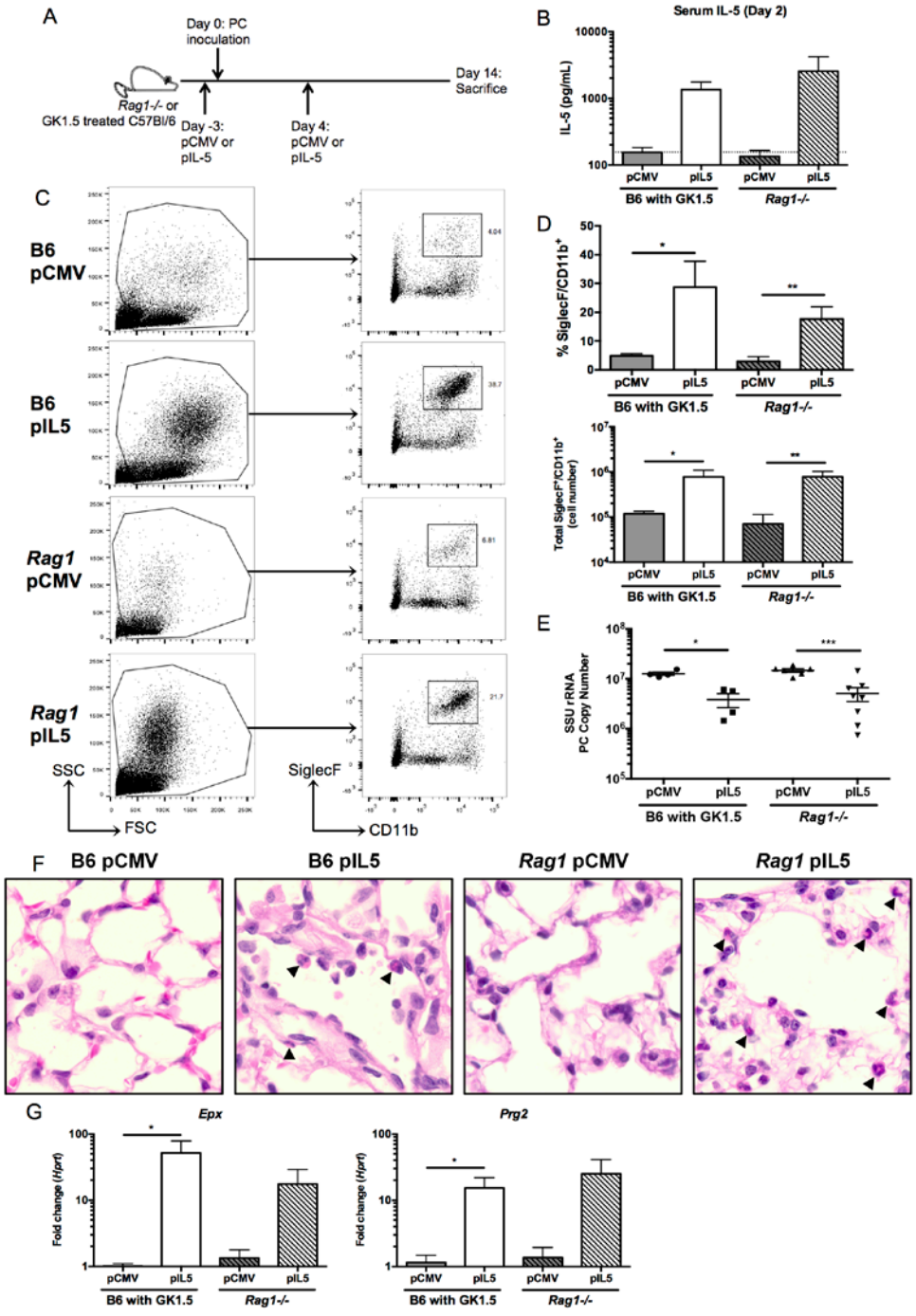

Figure 2-4. Treatment of CD4-depleted C57BL/6 and *Rag1-/-* mice with pIL5 results in eosinophilia in whole lung and decreased *Pneumocystis* burden.

A. Schematic showing timing of hydrodynamic injection of either pCMV or pIL5 (day -3 and 4) and *Pneumocystis* inoculation (day 0) into GK1.5 treated C57BL/6 (B6) or *Rag1-/-* mice. B. Serum IL-5 ELISA at day 2 post infection shows log-fold increase in IL-5 in pIL5 treated animals (n=4-7, dotted line represents limit of detection). C.

Digested whole lung shows a high side scatter population in the pIL5 groups compared to the pCMV treated groups (*left panel*). The cells were gated as shown (*left panel*), and a SiglecF^{+}CD11b^{+} population was seen in both the B6 and *Rag1-/-* mice treated with pIL5 at day 14 post infection (*right panel*). D. pIL5 treatment resulted in a statistically significant increase in percentage (*top*) and total number (*bottom*) of SiglecF^{+}CD11b^{+} cells (* $p<0.05$, ** $p<0.01$ by Student's t-test). E. pIL5 treatment results in statistically significant reduction in *Pneumocystis* burden as measured by qRT-PCR of small subunit ribosomal RNA at day 14 post infection (* $p<0.05$, *** $p<0.001$ by Student's t-test). F. H&E staining on paraffin-embedded lung sections demonstrating eosinophils (black arrowheads) in both the B6 and *Rag1-/-* mice treated with pIL5 at 60X magnification. G. qRT-PCR for *Epx* (*left)* and *Prg2* (*right*) on RNA extracted from whole lung shows significant log-fold increase in expression in pIL5 treated animals compared to pCMV treated mice (* $p<0.05$ by Student's T test).

Furthermore, although pIL5 treatment increased eosinophilic lung inflammation, this was not associated with Type 2 immune inflammation as measured by goblet cell hyperplasia or mucin expression (as measured by qRT-PCR of *Clca3*, *Muc5ac* and PAS staining) or *Il13* expression in the pIL5 treated C57BL/6 mice (**Figure 2-5**).

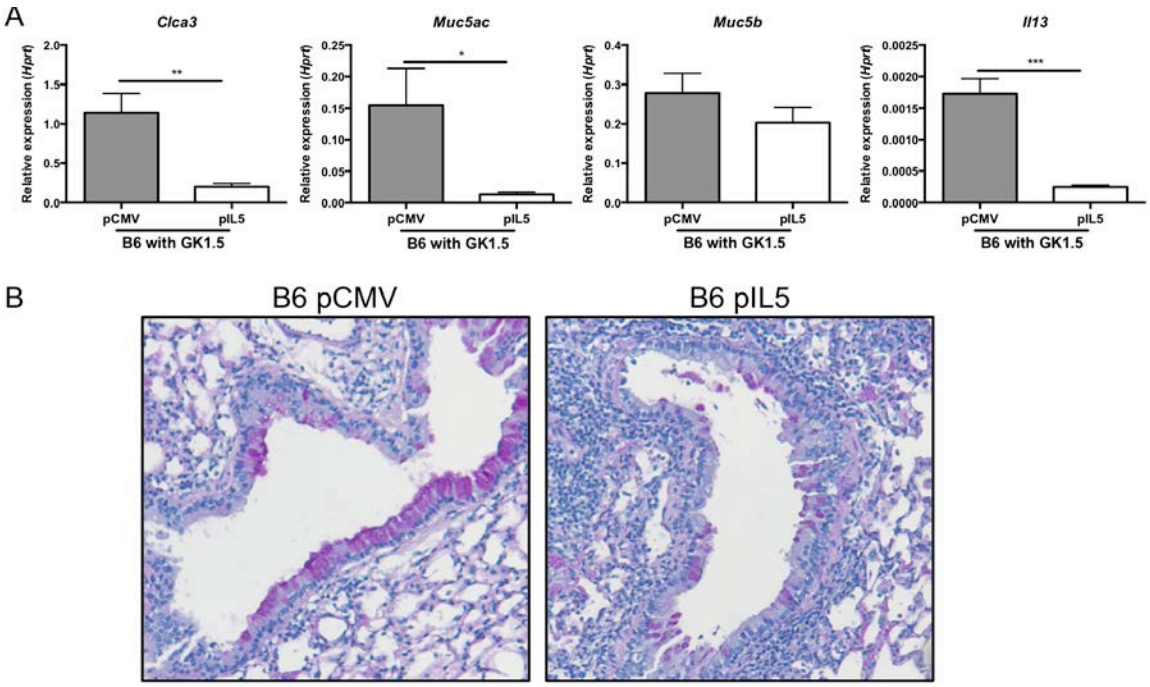

Figure 2-5. Airway markers of pathology are reduced following pIL5 treatment.

A. pIL5 treatment in B6 mice resulted in reduced *Clca3*, *Muc5ac*, and *Il13* expression in whole lung homogenate when compared to pCMV treated mice (*, **, and *** represent $p<0.05$, $p<0.01$, $p<0.005$ by Student's T test). *Muc5b* expression was not significantly different in pIL5 treated animals. B. PAS staining of airways shows reduced mucus production in pIL5 treated B6 mice when compared to mice receiving pCMV at 10X magnification.

2.4.5 IL-5 mediated decrease in *Pneumocystis* burden is abrogated in eosinophil-deficient *Gata1^{tm6Sho}/J* mice

To verify the effect of pIL5 required eosinophilopoiesis, we used a genetic approach. CD4-depleted BALB/c mice were treated with pIL5 as described above and similar levels of IL-5 were induced in the serum (**Figure 2-6A**). Similarly, increased eosinophils were noted in the lung digest of pIL5 treated BALB/c mice (**Figure 2-6B**). pIL5 treated BALB/c mice had a statistically significant increase in total number and a trend towards higher percentage of

SiglecF^{+}/CD11b^{+} cells compared to pCMV treated BALB/c mice (**Figure 2-6C**). Furthermore, upon sacrifice, BALB/c mice treated with pIL5 had nearly a 50% reduction in *Pneumocystis* burden when compared to pCMV treated animals (**Figure 2-6D**, p=0.04). Burden in this case was normalized to the pCMV group as the inoculums over three independent experiments varied; however, a similar reduction in burden was noted with C57BL/6 and *Rag1*-/- mice (**Figure 2-6E**). Also noteworthy, four pIL5 treated mice had no induction of serum IL-5 and lacked eosinophils in the lung at day 14 by flow cytometry, likely due to technical variation. If only mice that responded to pIL5 treatment were included in the analysis, the mean percentage of *Pneumocystis* remaining in pIL5 treated mice would be 26% compared to 100% of pCMV treated mice ($p<0.0002$). pIL5 treatment was also associated with significant increases in eosinophil associated genes such as *Epx* and *Prg2* (**Figure 2-6E**).

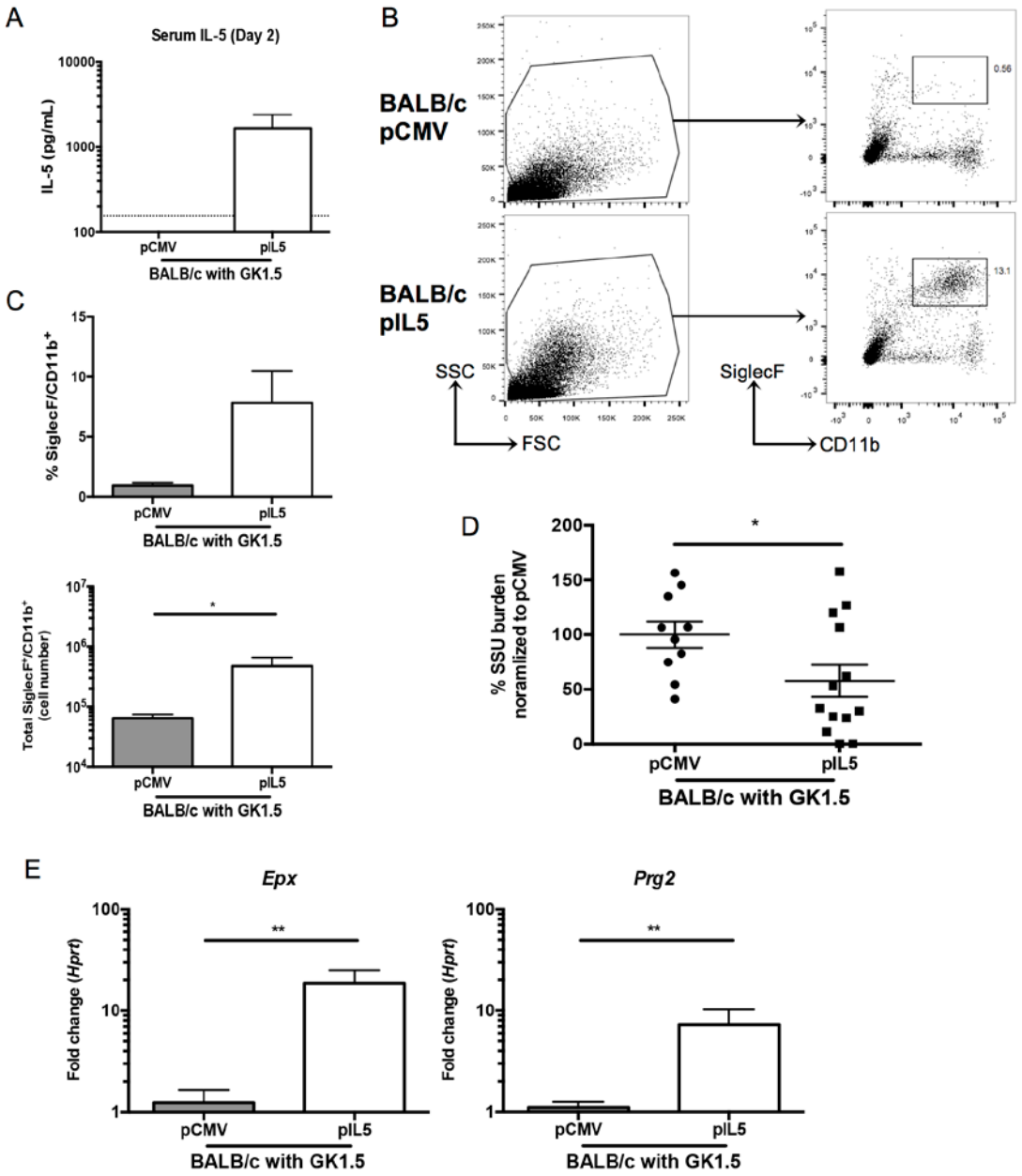

Figure 2-6. pIL5 treatment can reduce *Pneumocystis* burden in CD4-depleted BALB/c mice.

A. Serum IL-5 ELISA at day 2 post infection shows log-fold increase in IL-5 in pIL5 treated BALB/c mice (*n*=4, dotted line represents limit of detection). B. Digested whole lung shows a high side scatter population in the pIL5 groups compared to the pCMV treated groups (*left panel*). The cells were gated as shown (*left panel*), and a $SiglecF^{+}CD11b^{+}$ population was seen in the BALB/c mice treated with pIL5 (*right panel*). C. pIL5 treatment resulted in an increase in percentage (*top*) and total number (*bottom*) of $SiglecF^{+}CD11b^{+}$ cells. D. pIL5 treatment results in reduction in *Pneumocystis* burden as measured by qRT-PCR of small subunit ribosomal RNA (p=0.08 by

Student's t-test). E. qRT-PCR for *Epx* (*left)* and *Prg2* (*right*) on RNA extracted from whole lung shows significant log-fold increase in expression in pIL5 treated animals compared to pCMV treated mice (* $p<0.05$ by Student's T test).

The increased *Pneumocystis* killing in mice that recruited eosinophils to the lungs is also evident in the strong negative correlation that exists between *Pneumocystis* burden and total $SiglecF^{+}CD11b^{+}$ recruited cells in both C57BL/6 and BALB/c mice (**Figure 2-7,** $p<0.05$).

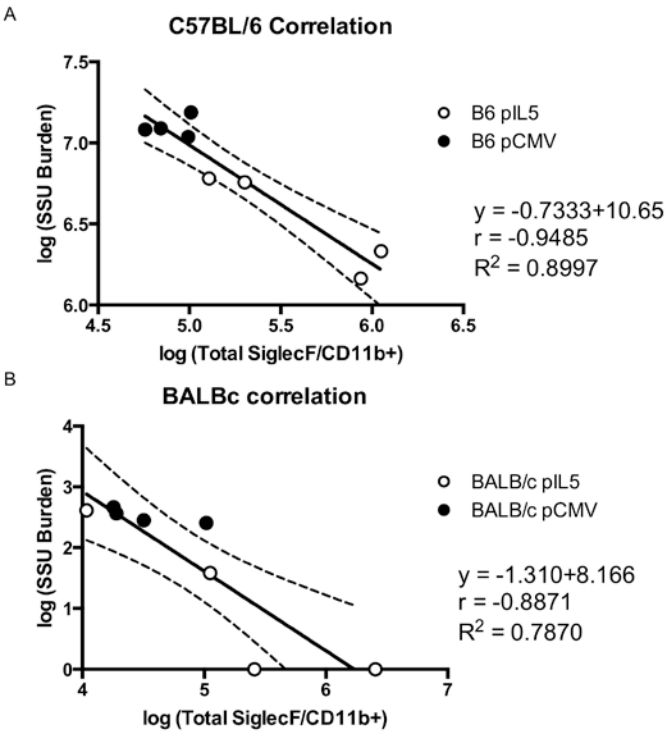

Figure 2-7. Eosinophil number correlates with *Pneumocystis* killing *in vivo*.

A. Correlation between the log of total $SiglecF^{+}CD11b^{+}$ cells with the log of *Pneumocystis* SSU burden demonstrates a strong negative correlation in B6 mice. Solid line represents linear regression of data points and dashed lines represent 95% confidence interval (r=-0.9485, p=0.0003 by Pearson's correlation). B. Similar correlation was noted in BALB/c mice, despite one pIL5 mouse recruiting few eosinophils (r=-0.8871, p=0.0033 by Pearson's correlation).

In contrast, *Gata1*^{tm6Sho}*/J* mice, which are deficient in eosinophilopoiesis, were CD4-depleted and treated with pIL5 or pCMV as described. Treated *Gata1*^{tm6Sho}*/J* mice failed to show an effect of pIL5 on fungal burden, despite similar levels of IL-5 compared to previous mouse strains (**Figure 2-8A and 2-8B**). Consistent with no reduction in fungal burden, there was no observable eosinophil recruitment was detected in the lungs of *Gata1*^{tm6Sho}*/J* mice, as neither a high side-scatter population nor a SiglecF^{+}CD11b^{+} was noted by flow cytometry (**Figure 2-8C and 2-8D**). Furthermore, there was no induction of *Epx* or *Prg2* in the *Gata1*^{tm6Sho}*/J* mice treated with pIL5 (**Figure 2-8E**).

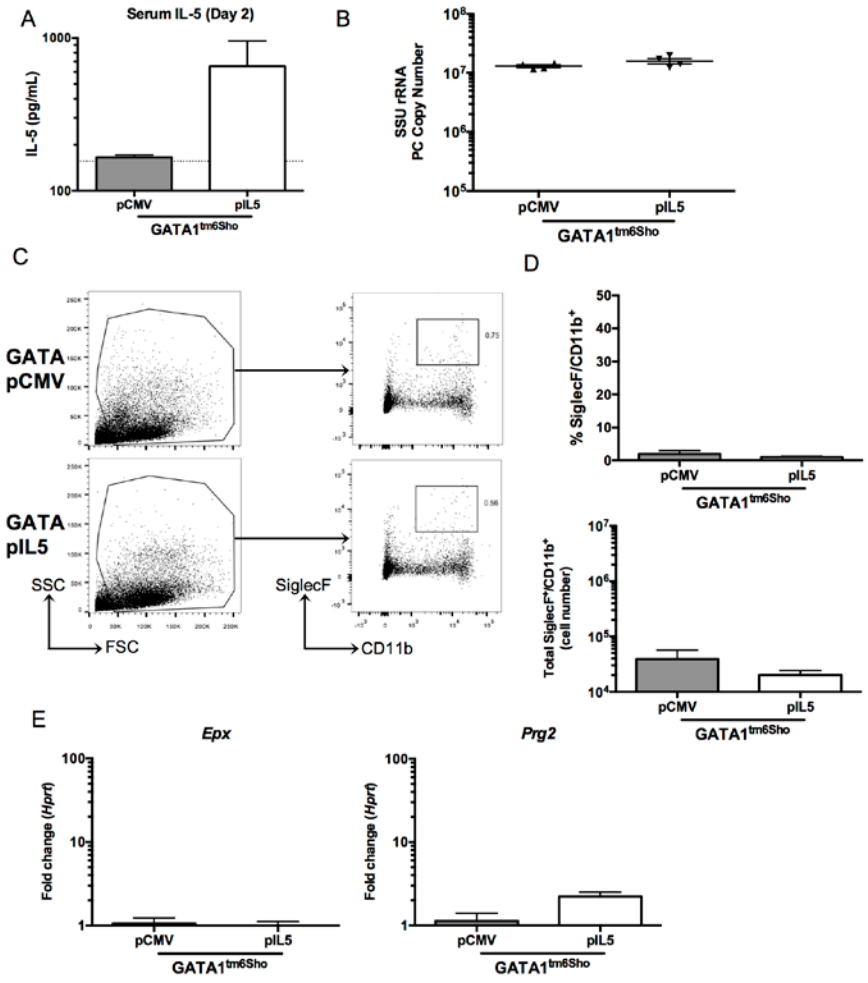

Figure 2-8. pIL5 treatment cannot rescue eosinophil-deficient *Gata1^{tm6Sho}/J* knockout mice.

A. Serum IL-5 ELISA at day 2 post infection shows nearly a log increase in *Gata1^{tm6Sho}/J* pIL5 treated animals (*n*=4, dotted line represents limit of detection). B. pIL5 treatment does not reduce *Pneumocystis* burden at day 14 post infection in *Gata1^{tm6Sho}/J* mice as measured by qRT-PCR of small subunit ribosomal RNA. C. Digested whole lung shows no difference in high side scatter populations (*left panel*) or SiglecF^{+}CD11b^{+} cells (*right panel*) independent of pIL5 treatment status. D. pIL5 treated *Gata1^{tm6Sho}/J* mice showed no difference in percentage (*top*) or total number (*bottom*) of SiglecF^{+}CD11b^{+} cells. E. qRT-PCR for *Epx* (*left)* and *Prg2* (*right*) on RNA extracted from whole lung shows no increase in eosinophil associated genes in *Gata1^{tm6Sho}/J* mice.

2.5 DISCUSSION

The current study utilized an unbiased RNA sequencing based approach towards evaluating the role of $CD4^+$ T-cells in *Pneumocystis* infection and suggested that $CD4^+$ T-cells can recruit eosinophils to the lung by day 14 of infection by RNA sequencing. Eosinophils were also shown to have a role in immunity against *Pneumocystis* in a primary challenge model of eosinophil-deficient mice and in an eosinophil-based *Pneumocystis in vitro* killing assay. Furthermore, induction of eosinophilia via hydrodynamic injection of pIL5 was capable of reducing *Pneumocystis* burden *in vivo* in both CD4-depleted C57BL/6 and *Rag1-/-* mice. Finally, the same technique was able to reduce *Pneumocystis* burden in CD4-depleted BALB/c mice but failed to provide any therapeutic benefit in CD4-depleted *Gata1^{tm6Sho}/J* mice, further implicating eosinophils as a novel cell population responsible for *in vivo* antifungal activity.

$CD4^+$ T-cells have been established as crucial mediators of *Pneumocystis* due to the high incidence of *Pneumocystis* in HIV/AIDS patients with low $CD4^+$ T-cell counts (1, 128). One clear role of $CD4^+$ T-cells in response to *Pneumocystis* is to stimulate antibody responses by providing co-stimulatory signals to B cells (79, 129). Antibodies against *Pneumocystis* are protective; however, at day 14 of infection, prior to antibody production, *Pneumocystis* burden has already plateaued in wild type animals, suggesting an antibody-independent function for CD4 cells (129). As such, $CD4^+$ T-cells appear to recruit eosinophils early in infection while B cells are undergoing maturation into antibody-producing plasma cells and provide preliminary control of *Pneumocystis* burden. Importantly, IL-5 transcription and eosinophil recruitment appear to be dependent on $CD4^+$ T-cells in this model, as such markers do not appear until after activation of the adaptive immune response at day 7 post-infection.

Eosinophils, classically recognized as mediators of immunity against helminths, have recently been implicated in host defense against a variety of pathogens, including bacterial and viral infections (98). Recently, the Steele lab demonstrated that eosinophils contribute to host defense against the fungal pathogen *Aspergillus fumigatus* through a secretory factor, as eosinophils could mediate fungal killing when separated using transwells (121). The current study extends these findings by demonstrating that eosinophil-deficient mice are more susceptible to *Pneumocystis* infection and that eosinophils display antifungal activity *in vitro*. Additionally, treatment of bone marrow derived eosinophils with IL-4 and IL-13 greatly enhanced killing of *Pneumocystis*, suggesting that Th2 cytokines in the lung may augment eosinophil-dependent antifungal activity.

There are also several lines of evidence that connect *Pneumocystis* related pathology and eosinophils in both human disease and mouse models. First, eosinophilia in the bronchoalveolar lavage fluid of HIV-positive patients with *Pneumocystis* pneumonia has been well documented; however, whether a correlation exists between high eosinophil counts and lower *Pneumocystis* burden in these patients is unknown (130, 131). Secondly, patients with a history of *Pneumocystis* or bacterial pneumonia had a significantly higher rate of physician-diagnosed asthma, a disease that has a well-established eosinophilic component in regards to pathogenesis (66). Murine models of *Pneumocystis* have also shown STAT6, a transcription factor required for Th2 responses, is necessary for the development of airway hyperresponsiveness early in the course of infection (129). While eosinophilia was also documented early in this murine model, the study further links a Th2 response, and potentially eosinophilia, with pathology in the context of *Pneumocystis* infection (129). Additionally studies have shown that $CD8^+$ T-cells may

moderate the interactions between $CD4^+$ T-cells and eosinophils, although all three cell types may contribute to *Pneumocystis* driven pulmonary pathology (132).

However, the current study suggests that eosinophils are more than just the byproduct of a misguided immune response that drives airway hyperresponsiveness and pathology. The current study demonstrates that eosinophils have antifungal effects against *Pneumocystis* infection *in vitro* and *in vivo* and appear to be recruited to the lung by $CD4^+$ T-cells early in infection. Additionally, the role of eosinophils as a potential therapeutic in the setting of HIV/AIDS may warrant further exploration, as IL-5 mediated eosinophilia can provide reduced *Pneumocystis* burden even in the setting of complete loss of T cells and B cells. Furthermore, such robust eosinophilia actually appeared to mitigate airway pathology (e.g. mucus production) suggesting that *Pneumocystis* burden may play an equally important role in driving airway hyperresonsivness. These findings provide evidence that the specific pathways responsible for protective and pathologic effects in *Pneumocystis* pneumonia may be independent and may allow for the targeted use of eosinophil-based treatments for *Pneumocystis* while avoiding concurrent pathology.

3.0 A NOVEL CD4$^+$ T-CELL DEPENDENT MURINE MODEL OF *PNEUMOCYSTIS* DRIVEN ASTHMA-LIKE PATHOLOGY

Adapted from: A novel CD4$^+$ T-cell dependent murine model of *Pneumocystis* driven asthma-like pathology

Taylor Eddens[1,2], Brian T. Campfield[1,3], Katelin Serody[1], Michelle L. Manni[5], William Horne[1], Waleed Elsegeiny[1,2], Kevin J. McHugh[5], Derek Pociask[4], Kong Chen[1], Mingquan Zheng[1], John F. Alcorn[5], Sally Wenzel[6], and Jay K. Kolls[1]

1-Richard King Mellon Foundation Institute for Pediatric Research, Children's Hospital of Pittsburgh of UPMC, Pittsburgh, Pennsylvania, USA. 2-University of Pittsburgh School of Medicine, Department of Immunology, Pittsburgh, Pennsylvania, USA. 3-Division of Pediatric Infectious Diseases, Department of Pediatrics, University of Pittsburgh School of Medicine, Pittsburgh, Pennsylvania, USA. 4-Department of Pulmonary Diseases, Critical Care, and Environmental Medicine, Tulane University School of Medicine, New Orleans, Louisiana, USA. 5-Department of Pediatrics, Children's Hospital of Pittsburgh of UPMC, Pittsburgh, Pennsylvania, USA. 6-Department of Pulmonary, Allergy, and Critical Care Medicine, Pittsburgh, Pennsylvania, USA.

PMID: 27007260 (ePub ahead of print at this time).

The American Journal of Respiratory and Critical Care Medicine is an official journal of the American Thoracic Society.

3.1 INTRODUCTION: IMMUNOBIOLOGY OF ASTHMA

Asthma affects over 300 million people worldwide and is characterized by bronchial hyperreactivity, mucus production, and airway remodeling (133). Asthma is highly prevalent, particularly in Western cultures, affecting over 1 in 10 children and 1 in 12 adults (134). In total, the medical costs and indirect costs of asthma in the United States exceed $18 billion dollars per year (133, 134). Symptoms of asthma include shortness of breath, chest tightness, wheezing, cough with sputum production, and nighttime awakenings with any of the above symptoms. Often, these patients can require hospitalization for a wheezing episode. However, outside of admissions, patients are often maintained on a bronchodilator, as well as an anti-inflammatory steroid inhaler.

Clinically, asthma is diagnosed primarily by spirometry and is defined as a forced expiratory volume in one second (FEV1) below 70% predicted (which accounts for various factors, such as height, weight, sex, etc.). A decreased FEV1 is diagnostic of obstructive lung disease, and in the case of asthma, represents the underlying airway remodeling and mucus plugging as a result of hyper-secretion. Other spirometry analyses can include decreased forced expiratory flow 25-75% (FEF25-75), which would be further indicative of obstruction in the smaller to medium sized airways. Additionally, patients with severe asthma can have such obstruction in their bronchi that air is retained or trapped in the lung; air trapping can increase the total lung capacity (TLC) and the amount of air remaining in the lungs following maximal expiration (residual volume, RV). These measurements are acquired by a technique known as plethysmography and are less routinely performed than spirometry.

Severe asthma is defined as poor symptom control with frequent severe exacerbations requiring systemic steroids or hospitalization. Additionally, patients with severe asthma have a

FEV1<80% predicted immediately following treatment with a bronchodilator (135). Asthma, however, is more and more being recognized as a heterogeneous disorder. For one, genome wide association studies have associated certain genes, such as *IL33*, *SMAD3*, and *HLA-DQ*, with the presence of asthma in all age groups (136). Furthermore, meeting the clinical definition of severe asthma does not paint the entire picture. One study used data from 856 asthmatic patients (such as demographics, spirometry, atopy, treatment, etc.) and found that asthma can divided into five clusters (137). This heterogeneity extends further than clinical data, as various –omics approaches are being applied to patients with asthma. One study used transcriptomics on nasal epithelium followed by hierarchical clustering and was able to identify a subset of patients with a high Th2-skew (138). A population of asthma patients with high Th2 gene activation could also be detected by transcriptomics techniques on sputum samples and bronchial epithelial brushes (139, 140).

While these unbiased approaches unveiled novel players in the field of asthma, it has long been known that Th2 responses play a critical role in asthma. In fact, one early study of patients with mild asthma demonstrated the presence of IL-4^+ and IL-5^+ $CD4^+$ T-cells in the bronchoalveolar lavage fluid (141). One possible detrimental effect of these Th2 cells in the lung is the promotion of IgE class-switched antibodies. IgE can bind Fc receptors on mast cells, and in the presence of cognate antigen result in the release of pathologic mediators of allergic airway inflammation such as histamine (134). The presence of antigen-specific IgEs is routinely diagnosed clinically via skin prick testing or by serum analysis. Antigen-specific IgEs are indicators of allergic sensitization to particular airborne substances (tree pollen, house dust mite, cockroach antigen, etc.).

The Th2 response in the lung has other consequences outside of IgE antibody formation. IL-13, another hallmark type II cytokine, can directly lead to bronchial hyperreactivity and airway hyperresponsiveness (142). Furthermore, IL-13 can initiate the process of goblet cell hyperplasia, essentially leading to increased epithelial differentiation to the goblet cells that produce mucus (143). Th2 cells can also produce IL-5, a cytokine that acts in the bone marrow to cause eosinophilopoiesis (see chapter 2). Eosinophils can then be recruited into the lung via local production of eotaxins – CCL11, CCL24, and CCL26 – and release of pro-inflammatory mediators can lead to increased bronchial reactivity in some cases (144). Murine models of allergic inflammation, however, have led to conflicting evidence of the pathologic role of eosinophils. The TgPHIL mouse developed by Lee *et al*., had decreased airway resistance following OVA challenge compared to wild type mice (145). Contrastingly, the dblGATA1 knockout mice deficient in eosinophilopoiesis had similar airway hyperresponsiveness compared to wild type mice following OVA challenge (146). One study attributed this discrepancy to the underlying genetic strain used to generate each model organism (147). In a second model of allergic inflammation, intranasal administration of house dust mite extract exacerbated airway resistance in both TgPHIL and dblGATA1 knockout mice, but to a lesser extent than wild type mice (148). Importantly, the Th2 response and the associated mucus production appeared to be independent of eosinophils (148).

Another cell type in the lung is capable of mediating type II pathology, the innate lymphoid cell type II (ILC2). ILC2s are not part of the adaptive immune system, as these cells do not possess antigen-specific recognition receptors (149). However, ILC2 cells mirror the response generated by Th2 cells, as ILC2s can produce IL-5 and IL-13 early in the context of infection (150). Interestingly, ILC2s respond to the epithelial derived cytokines IL-33, IL-25, and

thymic stromal lymphoprotein (TSLP) and can drive airway eosinophilia and mucus production (151, 152). The redundancy in cytokines produced between Th2 and ILC2 cells has led to the examination of the role of ILC2s in allergic airway disease. Accordingly, ILC2s have been implicated in pathogenesis of allergic airway inflammation in response to papain, a protease-dependent airway irritant, and in an acute model of *Alternaria*, a fungal allergen (153, 154). In an acute model of OVA and house dust mite exposure, ILC2 cells appear to produce IL-5 and IL-13 in a similar, if not greater, quantity compared to Th2 cells (155). ILC2s also appear to have the ability to facilitate Th2-response development, by secreting IL-13 and presumably by altering the local cytokine milieu to a more Th2-biased polarizing environment (156). In addition to secretion of Th2-skewing cytokines, ILC2 cells are capable of directly priming Th2 cells through major histocompatibility class II:T-cell receptor interactions, further suggestive of a role for ILC2s in the optimal Th2 response (157).

While all of these type II cells (Th2, eosinophils, ILC2s) collaborate to contribute to asthma pathology, they may represent a specific subtype of allergic airway disease. Revisiting the transcriptomic data described above, a high Th2 signature could only be found in less than 50% of asthma patients, suggesting other immunologic lineages are involved in asthma pathogenesis (140). One such cell implicated in the development of severe asthma is the Th17 cell. Th17 cells are thought to participate in host defense against extracellular pathogens, primarily through neutrophil recruitment, modulation of antimicrobial peptide expression, and alterations in epithelial barrier integrity (158). This inflammatory response characterized by neutrophil recruitment is present in a subset of patients with late-onset, severe forms of asthma (159–161). IL-17A, the prototypical cytokine produced by Th17 cells, has been shown to directly cause contraction of bronchial smooth muscle cells (162). Further indicative of the severe nature

of asthma caused by Th17 cells, one study in a murine model demonstrated that transfer of Th17 cells led to increased bronchial hyperreactivity that was steroid-insensitive (160).

While a litany of aspects of the immune system can contribute to the immunopathology of asthma, the triggers of this maladaptive response are the real culprits behind the pathophysiology. Viral pathogens appear to be a major exacerbating factor leading to wheezing in young children. Human respiratory syncytial virus (RSV), for example, has been well established as a pathogen capable of causing acute wheezing, cough, and mucus production resembling asthma-like pathology in children (163). Furthermore, children diagnosed with RSV bronchiolitis had a higher prevalence of asthma (39%) compared to control children (9%) 18 years after infection with RSV (164). Children with early RSV infection were also more likely to have evidence of IgE antibodies to environmental exposures compared to healthy controls (164). RSV induces a potent Th2 response in the lung and can potentially skew the immune responses to future environmental allergens (165–167). Other viral pathogens, such as human metapneumovirus and rhinovirus, are also major causes of acute wheezing episodes in children and may lead to Th2-driven pathology in the lung (168–170).

A variety of non-viral airborne exposures can exacerbate asthma, including non-infectious particles (house dust mite, cigarette smoke) and infectious airborne fungal spores (151). Fungal sensitization in asthma patients is common, as some studies found between 35-70% of severe asthmatics had evidence of anti-fungal IgE antibodies (171–173). There are a number of fungal species associated with asthma, such as *Aspergillus, Alternaria, Penicillium, Fusarium,* and patients are routinely screened for allergic sensitization by skin test or blood IgE levels (171). Interestingly, asthma patients with fungal IgE sensitization have more severe

disease as measured by diminished lung function and increased hospital admissions (170, 171, 174).

Exposure to these fungal species likely occurs early and in the home. One study found that dust obtained from homes with an asthmatic child contained a fungal protease, aspergillopepsin, found in the *Aspergillus niger* (175). Porter *et al*. then elegantly demonstrated that protease-deficient strains of *Aspergillus* were unable to cause changes in airway resistance, while wild type strains induced allergic airway inflammation (175, 176). Wild type *Aspergillus niger* was not alone in inducing allergic inflammation; one study demonstrated that exposure to over 12 strains of fungi led to varying degrees of Th2 responses and increases in airway resistance (177). Importantly, mice lacking $CD4^+$ T-cells were unable to control fungal burden and dissemination, suggesting that the Th2 response, at least in regards to a few fungal species, was protective (177).

3.2 RATIONALE AND HYPOTHESIS

Given the strong eosinophilic response to *Pneumocystis* in the lung and the abundance of exposure to *Pneumocystis* amongst the population, we hypothesized that *Pneumocystis* may generate a type II response capable of modulating a similarly type II driven disease of the lung, asthma.

3.3 METHODS

Mice

C57BL/6, BALB/c, *Gata1^{tm6Sho}/J*, *Rag1$^{-/-}$* and *Rag2$^{-/-}$Il2rg$^{-/-}$* mice were all ordered from The Jackson Laboratory. Mice were all 6-8 week old and sex-matched. Colonies were maintained in the Rangos Research Building Animal Facility and use was approved and performed in accordance with the University of Pittsburgh Institutional Care and Use Committee.

Pneumocystis inoculation

Pneumocystis murina was harvested from the lungs of an infected *Rag2$^{-/-}$Il2rg$^{-/-}$* mouse and mice were challenged with 2.0 x 10^6 cysts/mL as previously described(83, 123). CD4-depletion with GK1.5 antibody was performed as described previously(83, 124).

RNA isolation and qRT-PCR

The right middle lobe was homogenized in Trizol® (Life Technologies) followed by subsequent RNA isolation, per manufacturer's instructions. One μg of RNA was then converted to cDNA using iScript™ (Bio-Rad). Gene expression analysis was performed using SsoAdvanced™ qRT-PCR universal probes supermix (Bio-Rad). Murine primers included: *Il4*, *Il5*, *Il13*, *Clca3*, *Muc5ac*, *Prg2* (Applied Biosystems). *Pneumocystis* SSU primer/probe sequences were described above in section 2.3.

RNA sequencing

Sample preparation and RNA sequencing was performed as described previously (25994969) and are publicly available through the Sequence Read Archive BioProject (number: PRJNA276259). Data were filtered on a quality score of 10 and mined for genes associated with type II immune responses: *Il33, Il25, Muc5ac, Clca3, Il9, Il4, Il13, Chi3l3, Chi3l4, Arg1, Il9r, Il17rb, Gpr44, Tslp, Il7r, Crlf2, Il1rl1, Acta2*. *Il9* and *Il25* did not pass the quality filter.

RNA sequencing pathway analysis

The FASTQ files from our previous study were uploaded to Illumina BaseSpace cloud-based software, aligned using TopHat version 1.0.0 and assembled with Cufflinks Assembly and DE, Version 1.1.0. Pathway analysis was then performed using iPathwayGuide, Version 1.4.0. KEGG and Disease pathways were analyzed for significance using a false discovery rate.

Purification of $CD4^+$ T-cells and adoptive transfer

Spleens from C57BL/6 mice were harvested, physically digested, and passed through a 70-μm filter. $CD4^+$ T-cells were isolated using a Stemcell™ EasySep™ Mouse kit (19852) and were subsequently enumerated. Each *Rag1*-/- mouse received 5 x 10^5 cells in 200 μL via intravenous injection. Mice were infected on the day of transfer as described above and sacrificed 6 weeks post infection.

Lung protein and Luminex

The right upper lobe of lung was collected, homogenized in PBS plus protease inhibitor (14277300, Roche). The lung homogenate was then centrifuged at 5,000xg for 5 minutes to

collect debris and the supernatant was collected. Cytokine analysis was then performed on this supernatant with a 23-plex Bio-Plex Pro™ (Bio-Rad), per manufacturer's instructions.

Ex vivo whole lung cell stimulation

The right lower and post-caval lobes of lung were collected, physically digested, and incubated for an hour and a half at 37°C in collagenase/DNase. Lungs were collected from naïve, HDM-treated, PC-infected, or HDM-treated and PC-infected mice. Likewise, cells were isolated from mice treated with PCAg. Single cell suspensions were then strained using a 70-μm sterile filter, treated with red blood cell lysis buffer (NH_4Cl), and enumerated. 5 x 10^5 cells/well were stimulated with PBS (no stimulation control), 2.5 μg PCAg or HDM, or 2.5 μL of CD3/CD28 Dynabeads® (2015-07, Life Technologies). Three days post-stimulation, the cells were pelleted, supernatants were harvested and cell pellets were resuspended in Trizol® LS (Life Technologies).

Histology

The right lung was clamped and the left lung was inflated with 10% formalin through the trachea. Following fixation, the lungs were processed, sectioned, and stained with hematoxylin and eosin or periodic acid-Schiff staining.

Pneumocystis antigen preparation and treatment

A lung from a *Rag2*$^{-/-}$*Il2rg*$^{-/-}$ infected with *Pneumocystis murina* for 8 weeks was strained through a 70-μm sterile filter (83, 178). Following centrifugation, the pellet was resuspended in 1 mL of PBS, layered on top of 30 mL of Centricoll™ (C-0580, Sigma) and centrifuged at 2,000 rpm for 15 minutes. The material at the interface of the Centricoll™ and PBS was collected,

washed twice in PBS, resuspended in 1 mL PBS and sonicated for 30 seconds three times. Protein was quantified using a BCA assay. Mice were then anesthetized with isoflurane and 10 μg of PCAg or HDM was administered intranasally in 50 μL PBS. Mice were sensitized on day 0, challenged on day 7-11, and sacrificed on day 14. For ILC2 studies, mice were treated every three days intraperitoneally with 0.5 mg of anti-ST2 antibody, provided by Dr. Dirk Smith.

ELISAs

96-well plates were coated overnight in a 9.2 pH carbonate buffer with 150 ng/well of *Pneumocystis* antigen, *Aspergillus fumigatus* antigen (GM3A01, Greer®), house dust mite extract (XPB70D3A2.5, Greer®), or a heat-killed *Streptococcus pneumonia* preparation. Plates were washed 5x with PBST and blocked in PBST with 5% milk for 2 hours at room temperature. Serum was diluted 1:64 (IgG assays) or 1:10 (IgE assays) in PBST with 5% milk and 100 μL was added to each well and the plate was incubated overnight at room temperature. Plates were then washed 5x with PBST and treated with 1:1000 goat anti-mouse IgG-HRP or 1:1000 goat anti-moues IgE-HRP (1030-05, Southern Biotech) diluted in blocking buffer. Following a one-hour incubation at room temperature, plates were washed 5x with PBST, developed with 1x TMB solution (BD OptEIA™, 555214), stopped with H_2SO_4 and read at 450nm. For human serum assays, bovine serum albumin was used in place of milk and rabbit anti-human IgG (A8792, Sigma®) and goat anti-human IgE (A18793, Life Technologies) were used as secondary antibodies.

Anti-PCAg Western blotting

PCAg (5 μg) or murine lung homogenate (10 μg) was denatured at 65° in LDS buffer with β-mercaptoethanol for 10 minutes and then added to a 4-20% tris-bis gel (Bio-rad) and run at 200V for 35 minutes. Following transfer to a nitrocellulose membrane (Bio-rad), the membrane was washed for 5 minutes in TBST and blocked at room temperature in TBST with 5% BSA for 2 hours. Serum samples were diluted 1:100 in TBST with 5% BSA, applied to the membrane, and incubated at 4° overnight. Membranes were washed three times with TBST for 5 minutes each, followed by addition of secondary antibody (described in ELISA) for one hour at room temperature. Membranes were then washed, developed using SuperSignal® West Pico Chemiluminescent Substrate (#34080, Thermo Scientific) and luminescence was measured for 1 second.

Flow cytometry

Whole lung cells were isolated as described in the *ex vivo* whole lung cell stimulation methods. Briefly, cells were plated, centrifuged, and resuspended in surface antibodies diluted in PBS. Following a 1 hour incubation at 4°C, cells were washed and resuspended in the streptavidinBV421 (diluted 1:200). Following a 30 minute incubation at 4°C, cells were washed and fixed and permeabilized using the eBioscience FoxP3 staining kit per manufacturer's instructions. Intracellular antibodies, anti-CD45.2, and anti-CD90.2 antibodies were added and incubated at 4°C for 1 hour. Cells were then washed, resuspended, and analyzed on a BD LSR II Flow Cytometer with compensation via OneComp eBeads (eBioscience). Data analysis was conducted using FlowJo software (Treestar).

Antibodies used in these panels were diluted 1:200 in PBS unless otherwise specified and include: GATA3-FITC, diluted 1:5 (BD Pharmingen, Clone: L50-823), TCRβ-PerCP-Cy5.5

(eBioscience, Clone: H57-597), TCRγδ-PE (eBioscience, Clone: GL3), CD90.2-PE-Cy7, diluted 1:1500 (eBioscience, Clone: 53-2.1), RORγT-APC (BD Pharmingen, Clone: Q31-378), CD45.2-APC-e780 (eBioscience, Clone: 104), Streptavidin-BV421 (BioLegend, Cat: 405226), CD11b-Biotin (eBioscience, Clone: M1/70), F4/80-biotin (eBioscience, Clone: BM8), NK1.1-biotin (BD Pharmingen, Clone: PK136), CD11c-biotin (BD Pharmingen, Clone: HL3), CD19-biotin (BD Pharmingen, Clone: 1D3), TER119-biotin (BD Pharmingen, Cat: 553672). APC panel: GR-1-e450 (BD Biosciences, Clone: RB6-8C5), CD11b-APC (Biolegend, Clone: M1/70), F4/80-APC-e780 (eBioscience, Clone: BM8), SiglecF-PE (BD Biosciences, E50-2440), CD11c-FITC (eBioscience, Clone: N418).

Lung Mechanics and Airway Hyperresponsiveness Measurements

Pulmonary function was assessed during mechanical ventilation of anesthetized (90 mg/kg pentobarbital i.p.) and tracheotomized mice using a computer-controlled small-animal mechanical ventilator (FlexiVent; SCIREQ, Montreal, Quebec, Canada) as previously described(159, 179). Briefly, mice were mechanically ventilated at 200 breaths/min with a tidal volume of 0.25mL and a positive end expiratory pressure of 3 cmH_2O (mimicking spontaneous ventilation). The quasi-static mechanical properties of the lung (compliance and hysteresis) were calculated using pressure-volume curves derived from a step-wise inflation of the lung to a maximum pressure of 30cmH_2O. Newtonian resistance (Rn), tissue damping (G), and tissue elastance (H) were assessed prior to and following airway challenge with increasing doses of aerosolized methacholine (0, 0.75, 3.125, 12.5, and 50 mg/mL) using the forced oscillation technique and constant phase model as previously described (180, 181). Multiple linear regression was used to fit measured pressure and volume in each individual mouse to the model

of linear motion of the lung. Model fits that resulted in a coefficient of determination less than 0.8 were excluded.

Clinical measurements

All human samples were collected via the Severe Asthma Research Program (SARP) and were collected at the University of Pittsburgh. Samples were de-identified and the serum ELISAs were performed with the disease status blinded from the researcher. Symptom scores and clinical measurements were collected in accordance with the Institutional Review Board (IRB0610032) as previously described(137).

Statistics

All statistics were performed using Graph Prism version 6.0f. All data are presented with mean ± SEM, with the exception of symptom scores (presented as median). Studies with two groups used a simple Student's t-test. Time course and Flexivent studies were analyzed using a Two-way ANOVA with multiple comparisons at each time point. Studies with more than two samples were analyzed using an ordinary one-way ANOVA with Tukey's multiple comparisons. Cytokine protein levels were analyzed for normality using a D'Agostino and Pearson omnibus normality test and were found to be normally distributed. Antibody dilution studies with human serum were analyzed with a two-way ANOVA. A Chi-square test was used to analyze patient symptom scores. Linear regression was performed, the slope was analyzed for significant difference from zero, and a Pearson's correlation coefficient was calculated. All statistical analyses considered $p<0.05$ significant.

3.4 RESULTS

3.4.1 *Pneumocystis murina* infection induces a robust type II response dependent on $CD4^+$ T-cells

While we have previously shown that *Pneumocystis murina* infection leads to a $CD4^+$ T-cell dependent recruitment of eosinophils (182), several other genes associated with a type II response were upregulated in wild type mice compared to CD4-depleted mice treated with GK1.5 monoclonal antibody at day 14 post-infection by RNA sequencing (**Figure 3-1A and 3-1B**). In addition to a previously shown increase in IL-5 expression (182), IL-4 and IL-13 were also upregulated in a $CD4^+$ T-cell dependent manner (**Figure 3-1C**). Likewise, markers of goblet cell hyperplasia, *Muc5ac* and *Clca3*, had increased expression (**Figure 3-1C**). At the protein level, IL-4 production over the course of infection increased in a $CD4^+$-dependent manner, while IL-5 had sustained protein levels in wild type but not $CD4^+$-depleted animals (**Figure 3-1D**). Histologically, wild type mice had inflammatory foci at day 7 and eosinophilic perivascular inflammation at day 14, while $CD4^+$-depleted animals appeared to have a delayed and reduced inflammatory response (**Figure 3-1E**). Similarly, by day 7 and 14 of infection wild type mice had increased goblet cell activation and mucus production, while GK1.5 treated mice had minimal mucus detection at day 14 (**Figure 3-1F**).

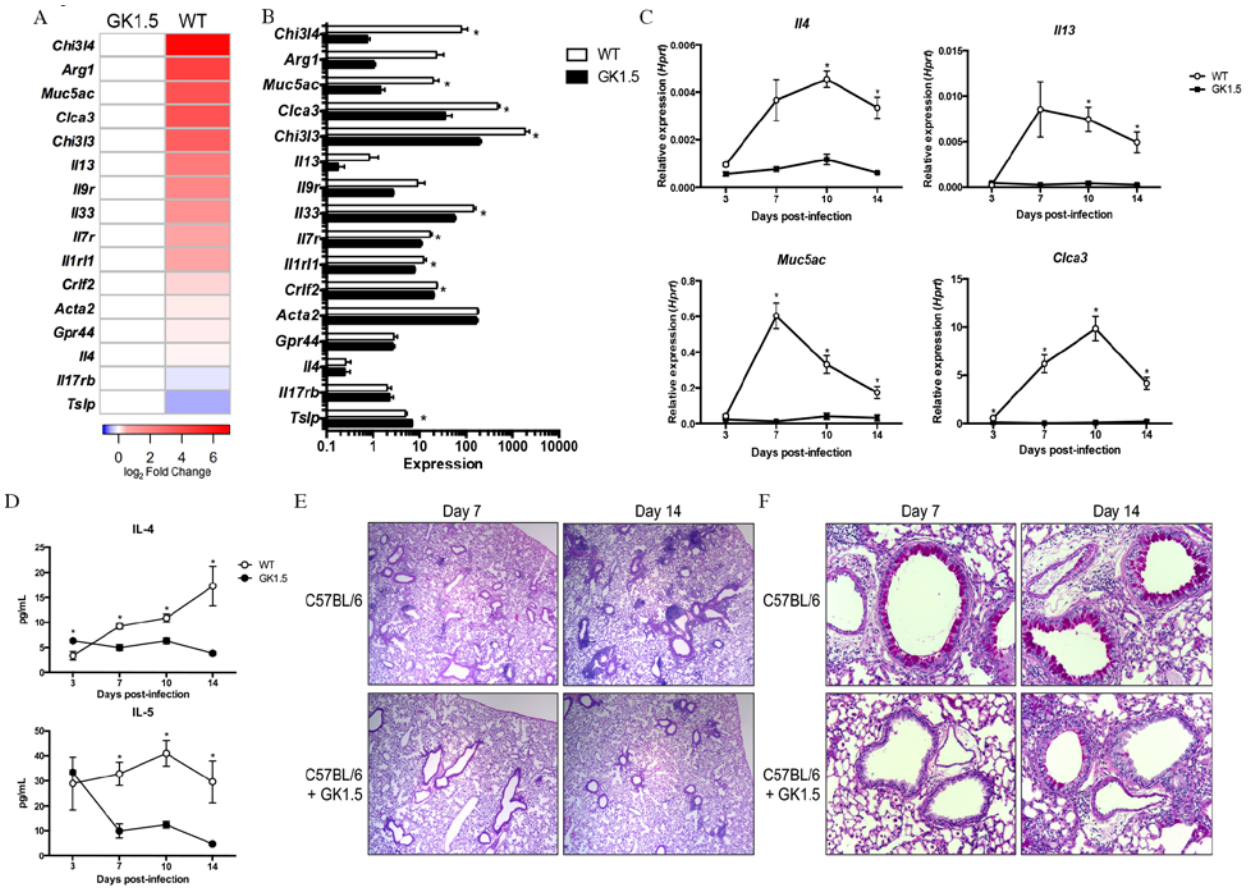

Figure 3-1. ***Pneumocystis murina*** **infection induces a CD4⁺ T-cell dependent type II response.**

Wild type (WT) or GK1.5 treated C57BL/6 mice were infected with *Pneumocystis murina* and sacrificed at day 3, 7, 10, and 14. A.) Whole lung RNA from day 14 was then isolated, sequenced using an Illumina NextSeq 500, and analyzed for differential expression of genes associated with a type II response. B.) RNA sequencing expression levels for the corresponding genes in the heat map (* $p<0.05$, Student's t-test, $n=4$ per group). C.) Expression of *Il4*, *Il13*, *Muc5ac*, and *Clca3* over the time course as measured by qRT-PCR demonstrating CD4⁺ T-cell dependent increase in gene expression (* $p<0.05$ by two-way ANOVA with multiple comparisons, $n=5$). D.) Protein levels of IL-4 and IL-5 in wild type and GK1.5 treated mice during infection. E.) Representative images of H&E staining of sectioned lung from WT and GK1.5 treated mice at days 7 and 14, demonstrating increased eosinophilic perivascular inflammation in WT mice. F.) Representative images of PAS staining of sectioned lung from WT and GK1.5 treated mice at day 7 and day 14 demonstrating increased mucus production in WT animals.

Moreover, global pathway analysis demonstrated upregulation of KEGG pathways associated with immunologic function, as well as pathways associated with allergic rhinitis, eosinophilic disorders, and asthma (**Figure 3-2**).

A

KEGG Pathway	p-value
Cytokine-cytokine receptor interaction	6.67×10^{-7}
Antigen processing and presentation	8.95×10^{-4}
Asthma	6.00×10^{-3}

B

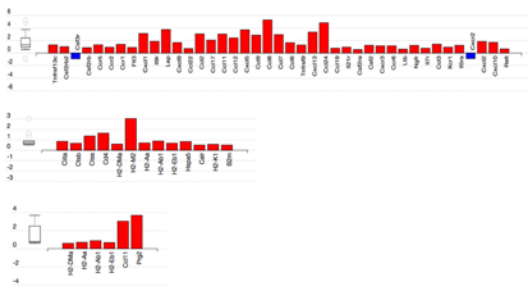

C

Disease Pathway	p-value
Allergic Rhinits	2.97×10^{-7}
Eosinophilic esophagitis	0.002
Asthma	0.029

D

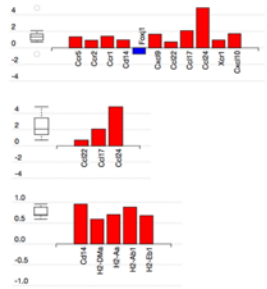

Figure 3-2. Pathway analysis on RNA sequencing shows upregulation of pathways associated with type II immunity.

A.) KEGG pathways significantly upregulated in wild type mice compared to $CD4^+$ T-cell depleted mice. B.) Individual gene expression associated with each KEGG pathway expressed as log(Fold change). C.) Disease pathways significantly upregulated in wild type mice compared to $CD4^+$ T-cell depleted mice. D.) Individual gene expression associated with each disease pathway log(Fold change).

$CD4^+$ T-cells are also sufficient to produce a type II immune response following *Pneumocystis* infection, as significant increases in *Muc5ac*, *Clca3*, *Il13*, and *Prg2* (major basic protein, an eosinophil-marker) were observed in lung homogenates of *Rag1*$^{-/-}$ mice receiving adoptive transfer of $CD4^+$ T-cells compared to no transfer controls (**Figure 3-3**).

A

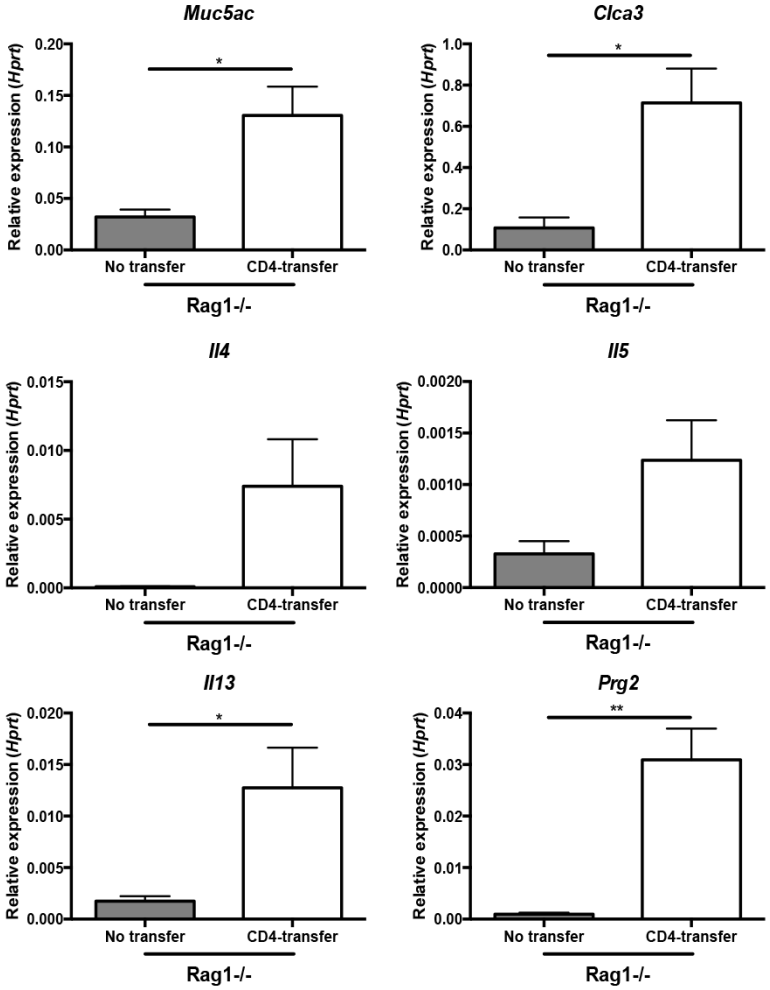

Figure 3-3. CD4$^+$ T-cells are sufficient to induce type II mediated pathology.

A.) *Rag1* -/- mice received PBS (no transfer, *n*=4) or 5 x 10^5 purified CD4$^+$ T-cells (*n=4)* via intravenous injection and were infected with *Pneumocystis murina*. Six weeks post-infection, *Rag1* -/- receiving CD4$^+$ T-cells had increased gene expression of type II related genes in lung homogenate (*p<0.05, **p<0.01, Student's t-test).

3.4.2 The immune response to *Pneumocystis* generates type II mediated lung pathology similar to that of house dust mite

We next sought to determine if concurrent *Pneumocystis* infection and exposure to a common airway allergen, house dust mite (HDM), would lead to a synergistic type II response (**Figure 3-4A**), as prior studies have suggested that *Pneumocystis* infection altered the immune response to OVA(183). Mice exposed to *Pneumocystis* infection or HDM alone generated both anti-*Pneumocystis* and anti-HDM IgG and IgE responses in the serum, respectively, while dual-treated mice generated IgG and IgE to both antigens (**Figure 3-4B**). Interestingly, even though all mice exposed to *Pneumocystis* infection had cleared the infection by day 28 (data not shown), mice infected with *Pneumocystis* alone had increases in eosinophil and goblet cell hyperplasia transcripts (**Figure 3-4C**). A synergistic response was noted in terms of a specific eosinophil marker, *Prg2* (**Figure 3-4C**). The antigen-specific responses of whole lung cells from *Pneumocystis*-infected or house dust mite exposed mice to PC antigen (PCAg) and HDM, respectively, were strikingly similar in terms of IL-4, IL-5, IL-10, IL-13, IL-17A, and IFN-γ production (**Figure 3-4D**). Dual-treatment resulted in little additive effects and appeared to prime two independent immune responses (**Figure 3-4D**). Surprisingly, mice that had been infected with and cleared *Pneumocystis* still had detectable mucus in both large and small airways (**Figure 3-4E**).

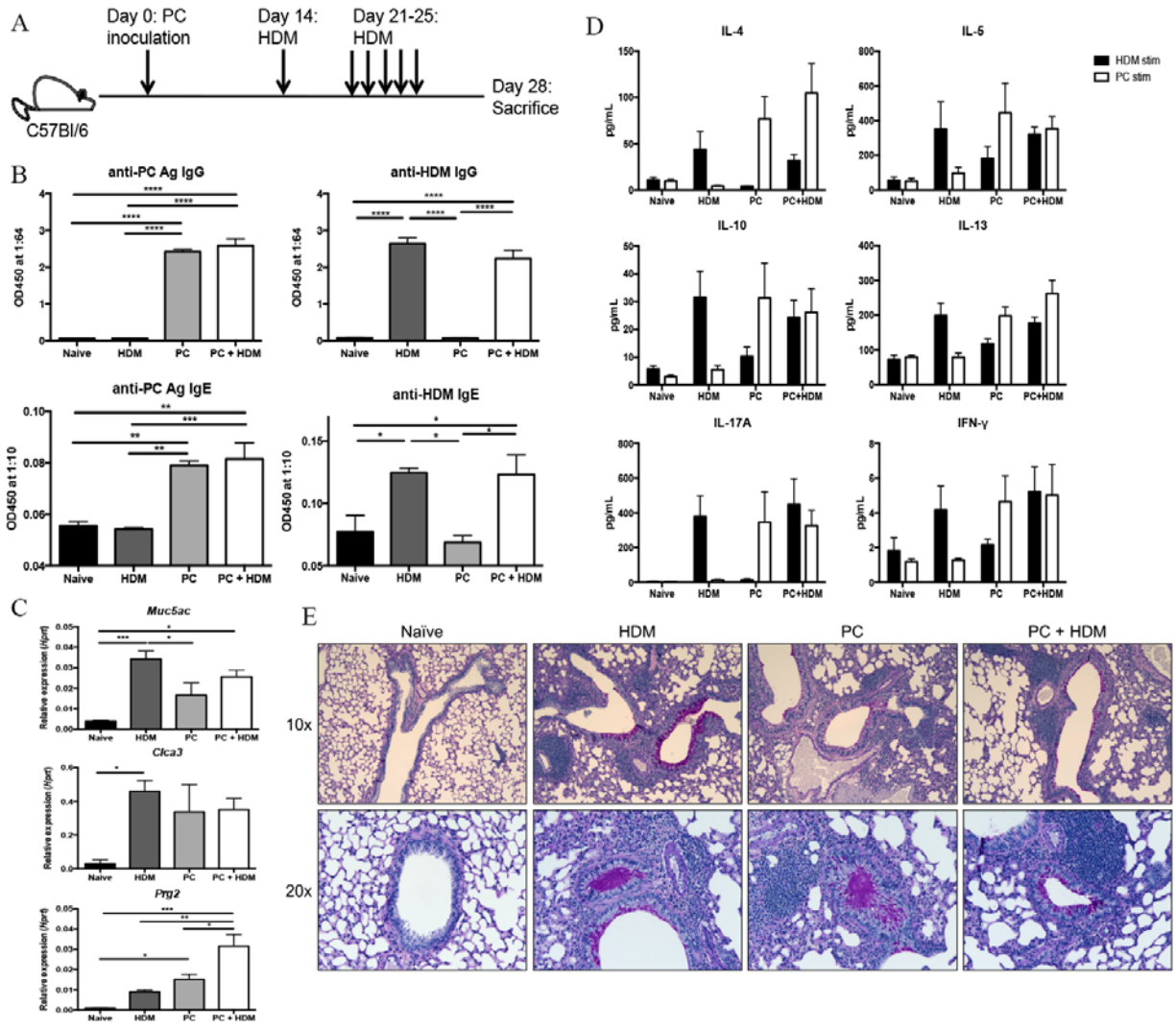

Figure 3-4. *Pneumocystis* infection and house dust mite treatment induce independent type II responses.

A.) Mice were untreated (naïve), treated with HDM alone (HDM), infected with *Pneumocystis* alone (PC), or infected with PC and subsequently treated with HDM (*n*=4 per group). B.) Infection and HDM treatment generate anti-PC and anti-HDM IgG and IgE antibodies C.) Increase in type II associated genes in PC infected, HDM treated, and PC + HDM mice in whole lung as measured by qRT-PCR. D.) *Ex vivo* cells isolated from whole lung were stimulated with either HDM or PC Ag for 72 hours and supernatants were analyzed using a Bioplex kit. E.) PAS staining of naïve, HDM, PC alone mice, and dual-treated mice demonstrating increased mucus production following each treatment. (* $p<0.05$, ** $p<0.01$, *** $p<0.001$, **** $p<0.0001$, one-way ANOVA with Tukey's multiple comparisons).

Given the similarities between the antigen-specific responses to primary *Pneumocystis* infection and HDM treatment, we next evaluated the potential of PCAg to induce a type II response and lung pathology (**Figure 3-5A**). Following sensitization and challenge, mice generated anti-HDM and anti-PC IgG and IgE (**Figure 3-5B**). PCAg treatment did increase expression of type II cytokines, mucus-associated genes and *Prg2* in a comparable manner to that of HDM treatment (**Figure 3-5C**). The antigen-specific responses to HDM were similar as described above (**Figure 3-4D**), while PCAg exposure induced an antigen-specific release of IL-4 and IL-5, but not IL-17A (**Figure 3-5D**). Additionally, both PCAg and HDM treated mice had a striking upregulation of mucus production and increased perivascular inflammation on histologic sections (**Figure 3-5E and 3-5F**).

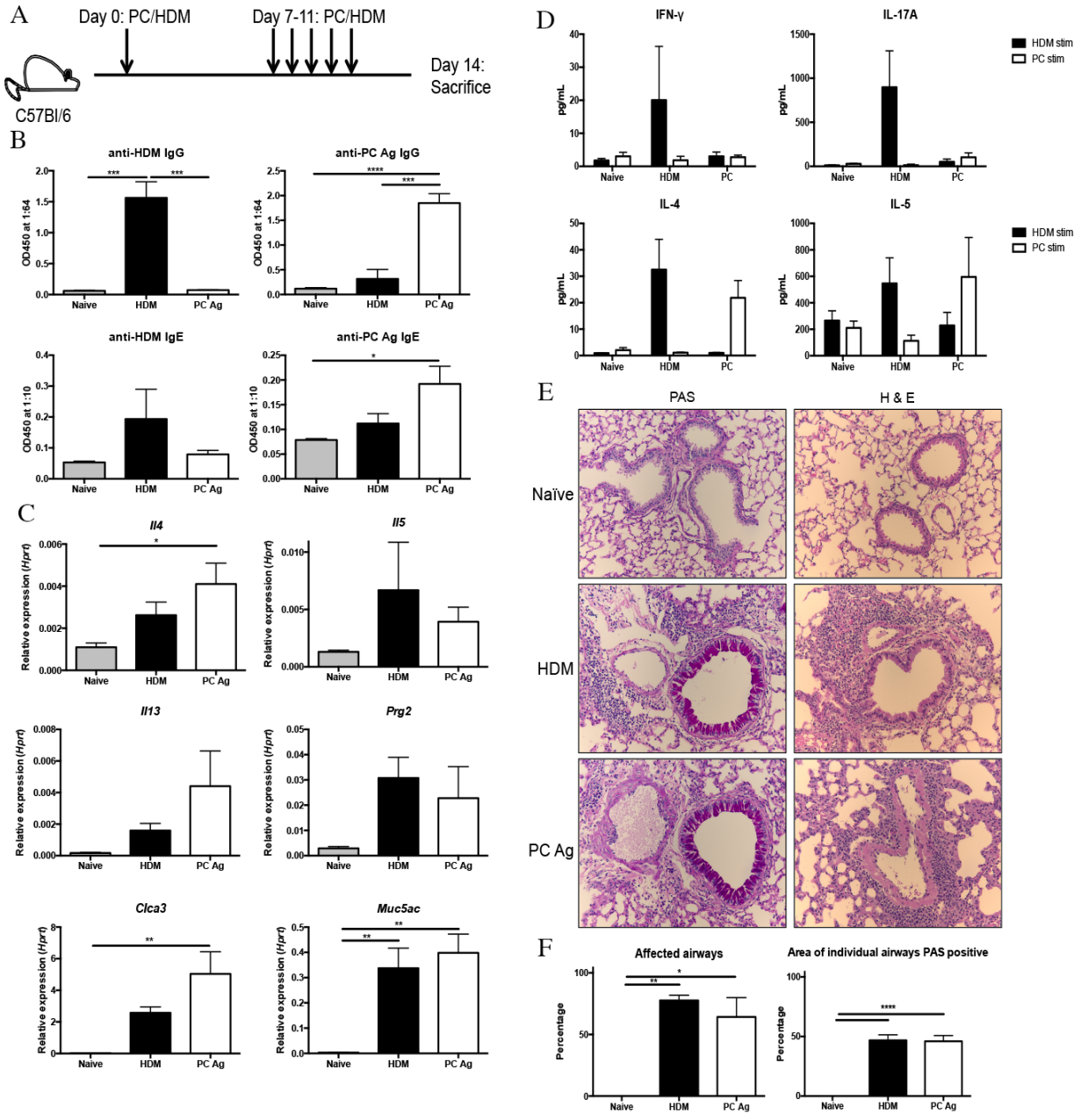

Figure 3-5. Exposure to *Pneumocystis* antigen and house dust mite generate lung pathology.

A.) Schematic of treatment of mice with 10 µg of HDM and sonicated PCAg on days 0, 7, 8, 9, 10, and 11. Naïve (*n*=9), HDM (*n*=6), and PC Ag (*n*=10) were all sacrificed at day 14 and data are from three individual experiments. B.) PCAg and HDM exposure generate anti-PC and anti-HDM IgG and IgE responses, respectively. C.) PCAg and HDM increase expression of type II related genes by qRT-PCR D.) *Ex vivo* cells isolated from whole lung were stimulated with either HDM or PCAg for 72 hours and supernatants were analyzed for IL-4, IL-5, IL-17A, and IFN-

γ. E.) Representative images from PAS and H&E staining from naïve, HDM-treated, and PCAg-treated mice demonstrating increased mucus and perivascular inflammation in the HDM and PCAg groups. All images were taken on 20x magnification. F.) HDM and PCAg treatment increased the percentage of total airways affected by mucus (left) and the area of individual airways PAS positive (right). (* $p<0.05$, **$p<0.01$, *** $p<0.001$, **** $p<0.0001$, one-way ANOVA with Tukey's multiple comparisons).

Furthermore, PCAg treated mice had an increase in antigen-specific $CD4^+$ Th2 cells, as measured by upregulation of *Gata3* expression and GATA3 protein levels (**Figures 3-6A-C**). This was not the case for Th17 cells, as *Rorc* expression and RORγT protein levels were unchanged following stimulation with PCAg (**Figures 3-6A-C**). Similarly, antigen-specific Th2 cytokine expression was increased following PCAg stimulation (**Figure 3-6D**) and eosinophils were recruited to the lung (**Figure 3-6E**). Neutrophils, a hallmark effector cell responding to IL-17-dependent chemokine expression, were not significantly recruited to the lung following PCAg stimulation (**Figures 3-6F and 3-6G**). Taken together, these results suggest that PCAg mediated pathology is mediated by the effector functions of Th2, and not Th17, cells.

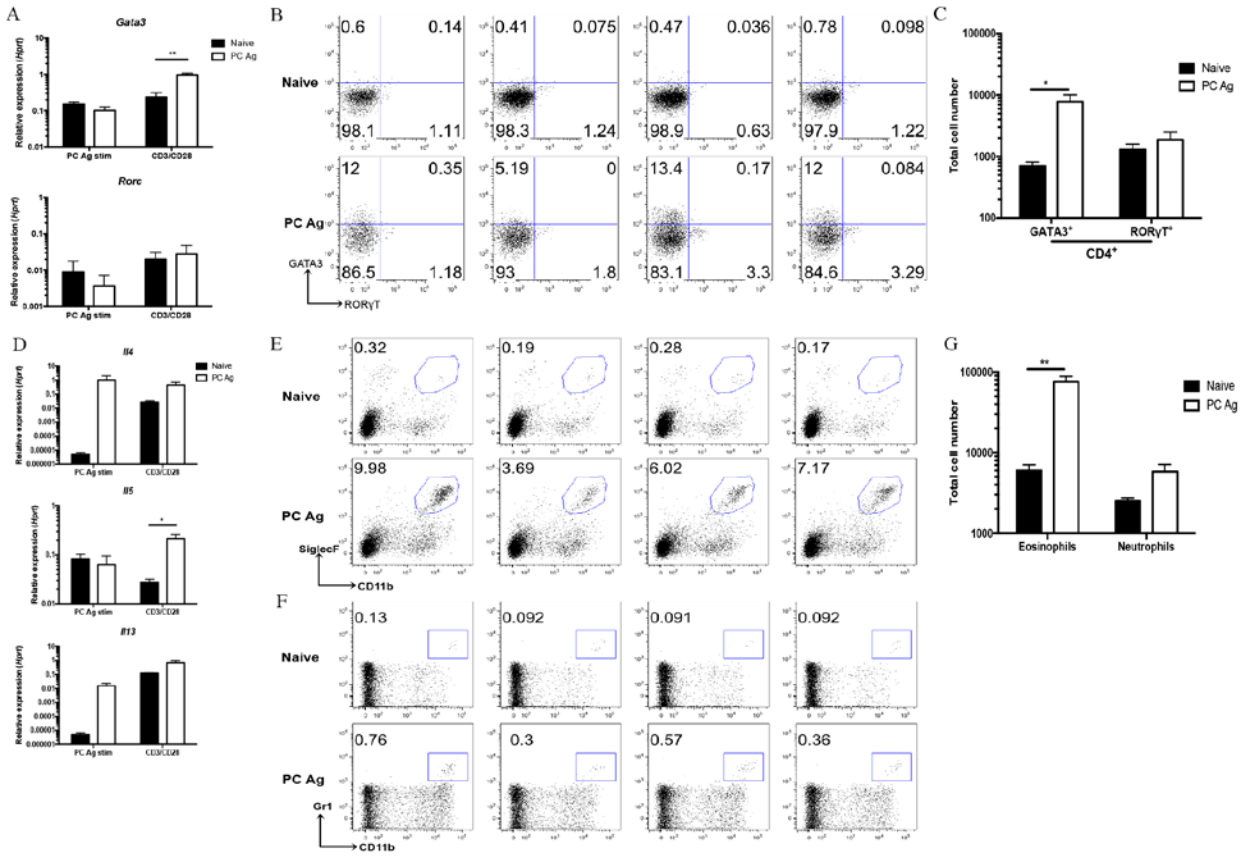

Figure 3-6. PCAg treated mice have increased Th2 cells and eosinophil recruitment in the lung.

A.) Following PCAg treatment, lung cells were isolated from lungs of PCAg treated or naïve mice and stimulated with PCAg or CD3/CD28 beads for 72 hours and analyzed for expression of *Gata3* and *Rorc* (** $p<0.01$). B.) Flow cytometry on $CD4^+$ T-cells demonstrates an increase in intracellular GATA3, but not RORγT, following PCAg treatment. C.) Quantification of Th2 $GATA3^+$ cells and Th17 $ROR\gamma T^+$ cells in naïve and PCAg treated mice ($p<0.05$, Student's t-test). D.) qRT-PCR on *ex vivo* stimulated lung cells shows increases in *Il4* and *Il13* in response to PCAg and a log increase in expression of *Il4*, *Il5*, and *Il13* following CD3/CD28 stimulation (*$p<0.05$). E.) Flow cytometry on whole lung cells shows an increase in eosinophils ($SiglecF^+CD11b^+$) following PCAg treatment. F.) Flow cytometry on whole lung cells shows minimal recruitment of neutrophils ($CD11b^+Gr1^+$) following PCAg treatment. G.) Quantification of eosinophils and neutrophils by flow cytometry shows significant increase in eosinophils following PCAg treatment ($p<0.01$, Student's t-test).

3.4.3 Both *Pneumocystis* antigen and house dust mite induce pathologic functional changes in respiratory mechanics

To assess functional changes in airway physiology, BALB/c mice were treated with PCAg or HDM. Quasi-static lung compliance was decreased with both PCAg and HDM treatment, indicative of inflammation in the lungs (**Figure 3-7A**). Similarly, both PCAg and HDM treated mice had significant increases in airway resistance compared to control animals when challenged methacholine (**Figure 3-7B**). PCAg and HDM treatment also similarly increased parameters associated with parenchymal resistance (tissue damping) and recoil (tissue elastance) compared to naïve mice (**Figure 3-7C**).

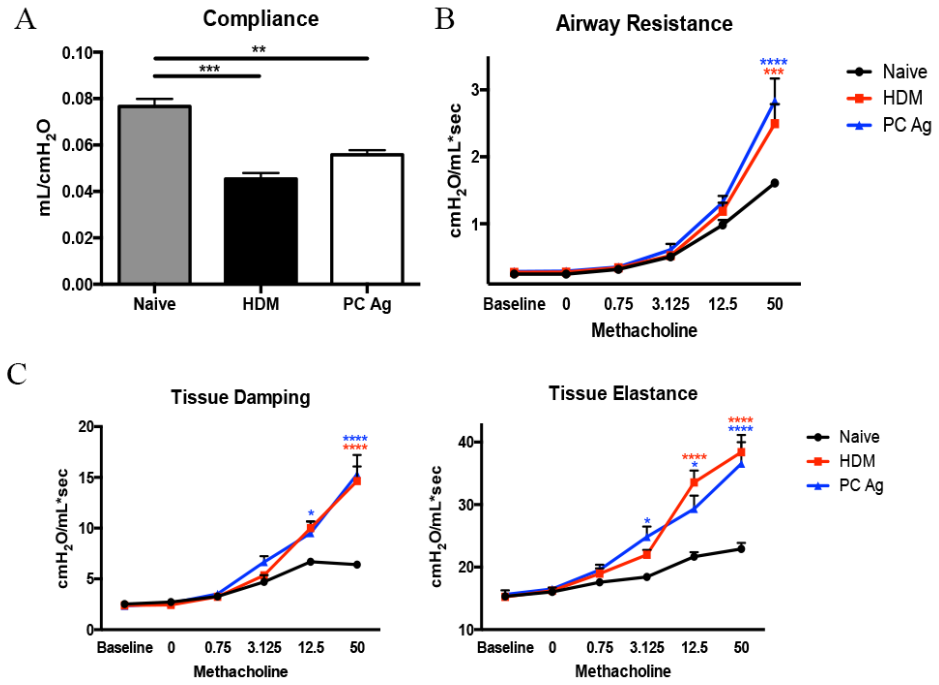

Figure 3-7. *Pneumocystis* antigen and HDM comparably reduce lung function.

BALB/c mice (n=6 per group) were treated with either HDM or PC Ag on days 0 and 7-11, and were sacrificed on day 14. Naïve BALB/c (n=3) mice were analyzed as controls. Data represent the combination of two independent experiments. A.) Following anesthetization, tracheotomized mice were ventilated and quasi-static compliance was calculated using pressure-volume curves. BALB/c mice treated with HDM and PC Ag had reduced compliance (* $p<0.05$, ** $p<0.01$ one-way ANOVA with Tukey's multiple comparisons). B.) Newtonian airway resistance was calculated following escalating doses of aerosolized methacholine (0, 0.075, 3.125, 12.5, and 50 mg/mL). PC Ag and HDM treated mice had increased resistance at higher doses of methacholine compared to naïve BALB/c mice (*** $p<0.001$, **** $p<0.0001$, two-way ANOVA with multiple comparisons). C.) Parameters associated with alveolar pathology (e.g. increased damping or elastance) were measured following treatment with methacholine and were also increased in PC Ag and HDM treated mice (* $p<0.05$, **** $p<0.0001$, two-way ANOVA with multiple comparisons).

As seen previously in C57BL/6 mice, both PCAg and HDM exposure increased expression of type II cytokines, mucus-associated genes, and *Prg2* in BALB/c mice in an equivalent manner (**Figure 3-8**).

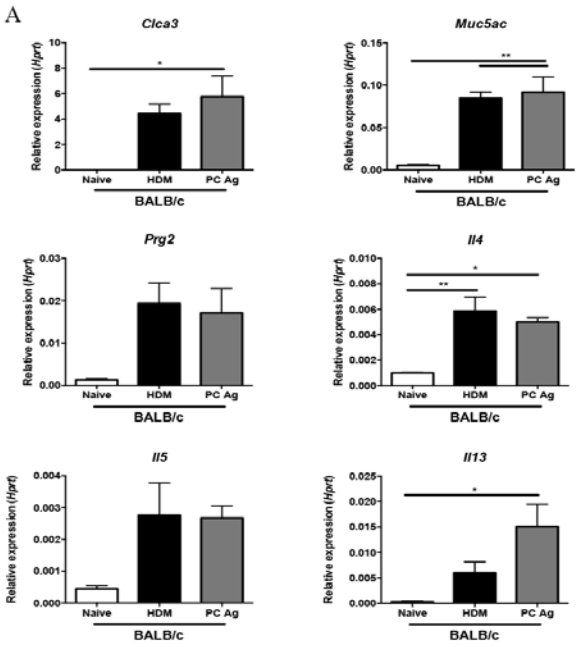

Figure 3-8. PCAg and HDM induce similar type II responses in BALB/c mice.

A.) BALB/c mice were treated with either PCAg or HDM and type II response in whole lung was analyzed by qRT-PCR (*n*=6 per group). HDM and PCAg induce comparable type II responses in BALB/c mice (* $p<0.05$, ** $p<0.01$, one-way ANOVA with Tukey's multiple comparisons).

3.4.4 The pathologic response to *Pneumocystis* antigen requires CD4$^+$ T-cells and collaboration with ILC2 cells

We next sought to determine the role of CD4$^+$ T-cells and ILC2 cells in response to PCAg. As expected, anti-*Pneumocystis* IgG and IgE production were decreased following CD4$^+$-depletion

(**Figure 3-9A**). Furthermore, $CD4^+$-depletion significantly reduced expression of type II cytokines (*Il4* and *Il13*), as well as eosinophil genes (*Prg2*) and mucus associated genes (*Muc5ac* and *Clca3*) (**Figure 3-9B**). $CD4^+$-depletion also significantly reduced PAS-positive airways indicative of mucus production (**Figures 3-9C and 3-9D**).

To assess the role of ILC2 cells as effector cells contributing to allergic inflammation, the response to PCAg treatment was also observed in *Rag1*$^{-/-}$, lacking T- and B-cells, or *Rag2*$^{-/-}$*Il2rg*$^{-/-}$, which lack adaptive immunity as well as NK cells and ILC2s. Further, *Rag1*$^{-/-}$ mice treated with PCAg were also treated with an anti-ST2 antibody, which has been shown to neutralize the IL-33/ST2 signaling pathway and ILC2 expansion (184, 185). No significant induction in type II cytokines was observed in *Rag1*$^{-/-}$ or *Rag2*$^{-/-}$*Il2rg*$^{-/-}$ mice treated with PCAg (**Figure 3-9B**). *Rag1*$^{-/-}$ did have a small increase in mucus production that was ameliorated with anti-ST2 treatment, suggesting that ILC2 cells may have a minor role in inducing mucus-associated pathology (**Figures 3-9C and 3-9D**). These results demonstrate that $CD4^+$ T-cells, and not ILC2 cells, are the primary effector cells responsible for the asthma-like pathology observed following PCAg treatment.

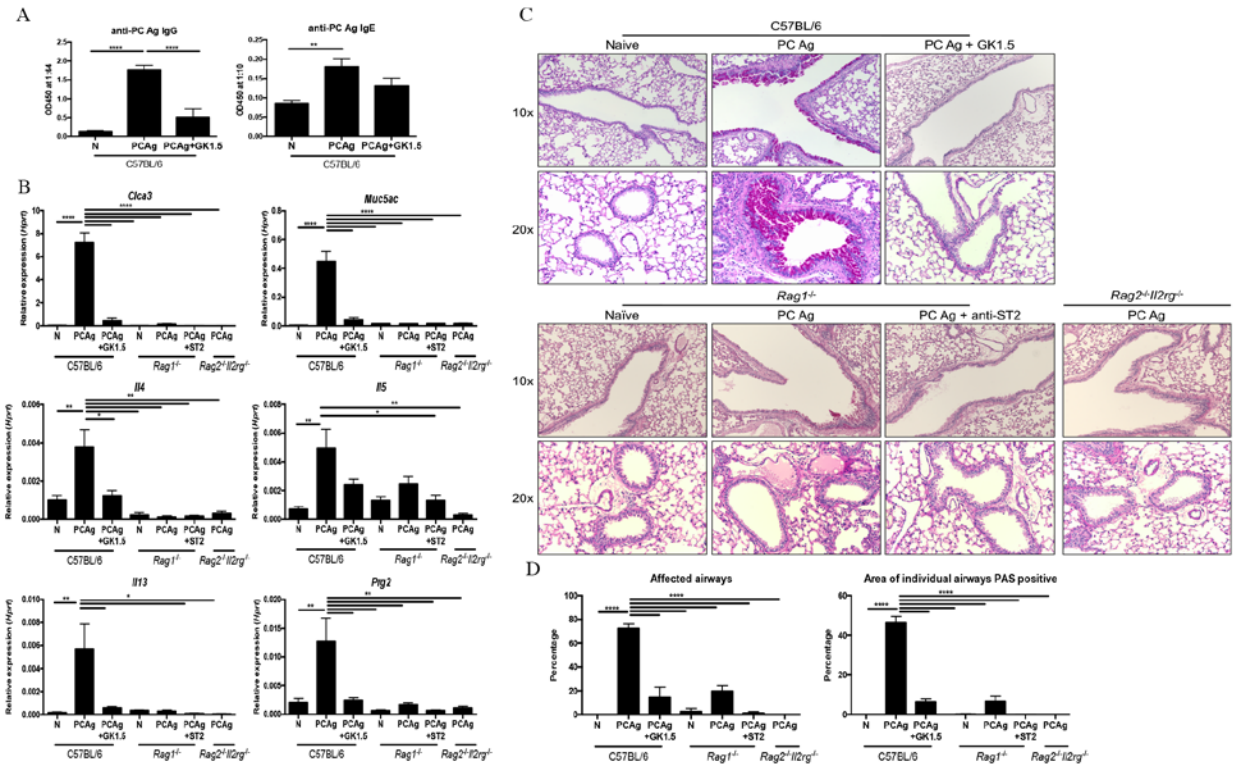

Figure 3-9. CD4$^+$ T-cells, but not ILC2s, are the primary effectors of PCAg-driven pathology.

C57BL/6 mice (*n*=6 per group) were untreated, treated with PC Ag, or treated with both PC Ag and GK1.5 monoclonal antibody and sacrificed at day 14. Data represent the combination of two independent experiments. Naïve *Rag1*$^{-/-}$ mice (*n*=3), *Rag1*$^{-/-}$ treated with PC Ag (*n*=3), *Rag1*$^{-/-}$ treated with anti-ST2 antibody and PCAg (*n*=4), and *Rag2*$^{-/-}$*Il2rg*$^{-/-}$ treated with PC Ag (*n*=3) were also analyzed. A.) Anti-PC antibody production (IgG and IgE) is dependent on CD4$^+$ T-cells. B.) Expression of type II immune response genes in whole lung homogenate at day 14 appears to be mediated by CD4$^+$ T-cells but not ILC2 cells. C.) PAS staining of whole lung shows CD4$^+$ T-cells drive the mucus response to PC Ag, while limited ILC2-dependent mucus production was noted in *Rag1*-/- mice. D.) PCAg treatment significantly increased the percentage of total airways affected by mucus (left) and the area of individual airways PAS positive (right) in a CD4-dependent manner. (* $p<0.05$, ** $p<0.01$, **** $p<0.0001$, one-way ANOVA with Tukey's multiple comparisons).

However, to assess the role of ILC2 cells upstream of the T-cell responses, C57BL/6 mice were exposed to PCAg and treated with anti-ST2 antibody. PCAg treatment did result in a

small expansion of ILC2 cells, which was neutralized by anti-ST2 treatment (**Figure 3-10A and 3-10B**). However, in addition to impairing ILC2 expansion, blockade of ST2 also reduced the percentage of $GATA3^+$ Th2 cells (**Figure 3-10B**). Anti-ST2 treatment did not impair production of anti-PC IgG or IgE, but did reduce expression of type II cytokines (*Il4, Il5*, and *Il13*) and an eosinophil-specific marker, *Prg2* (**Figure 3-10C**). However, anti-ST2 treatment was insufficient in reducing the mucus response as measured by qRT-PCR and PAS staining of the airways (**Figure 3-10D**). Taken together, these studies demonstrate that the IL-33/ST2 pathway is required for expansion of ILC2 and Th2 cells in response to PCAg. Further, these studies are suggestive that ILC2 cells may influence the Th2 response, but do not play a significant role in driving the pathology to PCAg.

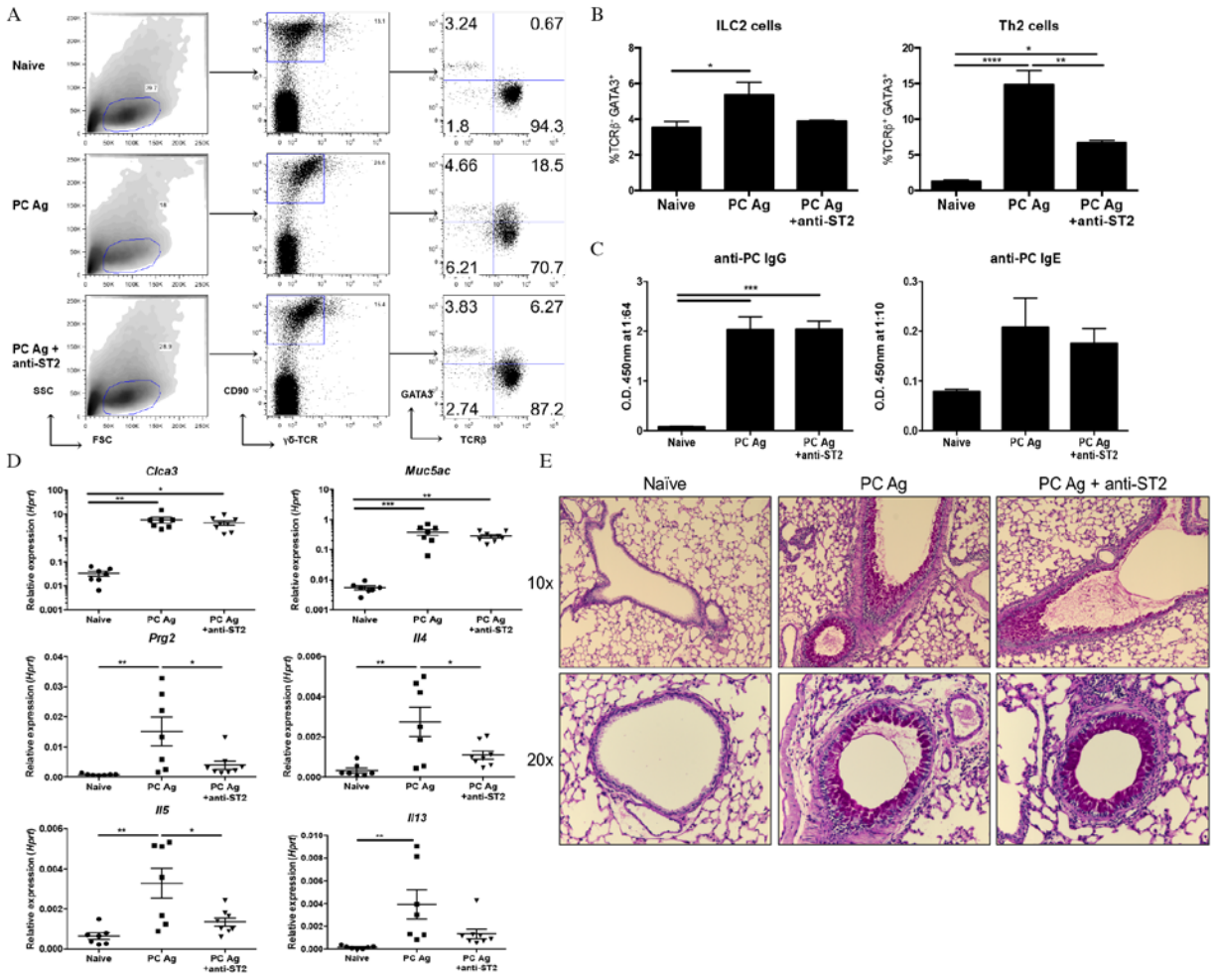

Figure 3-10. ST2-antibody treatment partially abrogates the pathologic Th2 response to PCAg.

C57BL/6 mice were untreated (naïve), treated with PCAg, or treated with PCAg and anti-ST2 blocking antibody (*n*=6-7). A.) Flow cytometry gating strategy for isolating ILC2 cells from whole lung. Cells were gated on lineage negative, γδ-TCR negative, CD90 high, TCRβ negative, GATA3 high (*n*=4). B.) Quantification of ILC2 cells ($TCR\beta^{-}GATA3^{+}$) and Th2 cells ($TCR\beta^{+}GATA3^{+}$). C.) Anti-*Pneumocystis* antigen IgG and IgE responses are unchanged with anti-ST2 treatment. D.) qRT-PCR for type II immune response genes showing decrease in type II cytokine production in anti-ST2 treated mice, but no change in mucus associated genes. E.) PAS staining demonstrating mucus production in PCAg and PCAg mice treated with anti-ST2. (* $p<0.05$, ** $p<0.01$, *** $p<0.001$, **** $p<0.0001$, one-way ANOVA with Tukey's multiple comparisons).

3.4.5 Eosinophils are dispensable for *Pneumocystis* antigen driven pathology

We next sought to characterize the role of eosinophils in the pathologic response to PCAg. *GATA1^{tm6Sho}/J* mice treated with PCAg had increased *Clca3*, *Muc5ac*, *Il4*, *Il5*, and *Il13* when compared to naïve *GATA1^{tm6Sho}/J* mice (**Figure 3-11A**). Compared to BALB/c mice treated with PCAg, *GATA1^{tm6Sho}/J* mice had significant upregulation of *Clca3*, *Muc5ac*, and *Il5*, but not *Prg2*. *GATA1^{tm6Sho}/J* mice also had a significant reduction in quasi-static compliance similar to that seen in BALB/c mice (**Figure 3-11B**). Furthermore, *GATA1^{tm6Sho}/J* mice had exacerbated airway resistance in the airways following PCAg compared to naïve *GATA1^{tm6Sho}/J* mice (**Figure 3-11C**). Although there appeared to be an increase in airway resistance in naïve *GATA1^{tm6Sho}/J* mice compared to naïve BALB/c mice, PCAg challenged *GATA1^{tm6Sho}/J* mice had significantly elevated airway resistance similar to that of challenged BALB/c mice. Significant changes in the alveolar parameters were also observed following PCAg in *GATA1^{tm6Sho}/J* mice (**Figure 3-11D**). Histologically, *GATA1^{tm6Sho}/J* mice had similar mucus production compared to BALB/c mice treated with PCAg (**Figure 3-11E**).

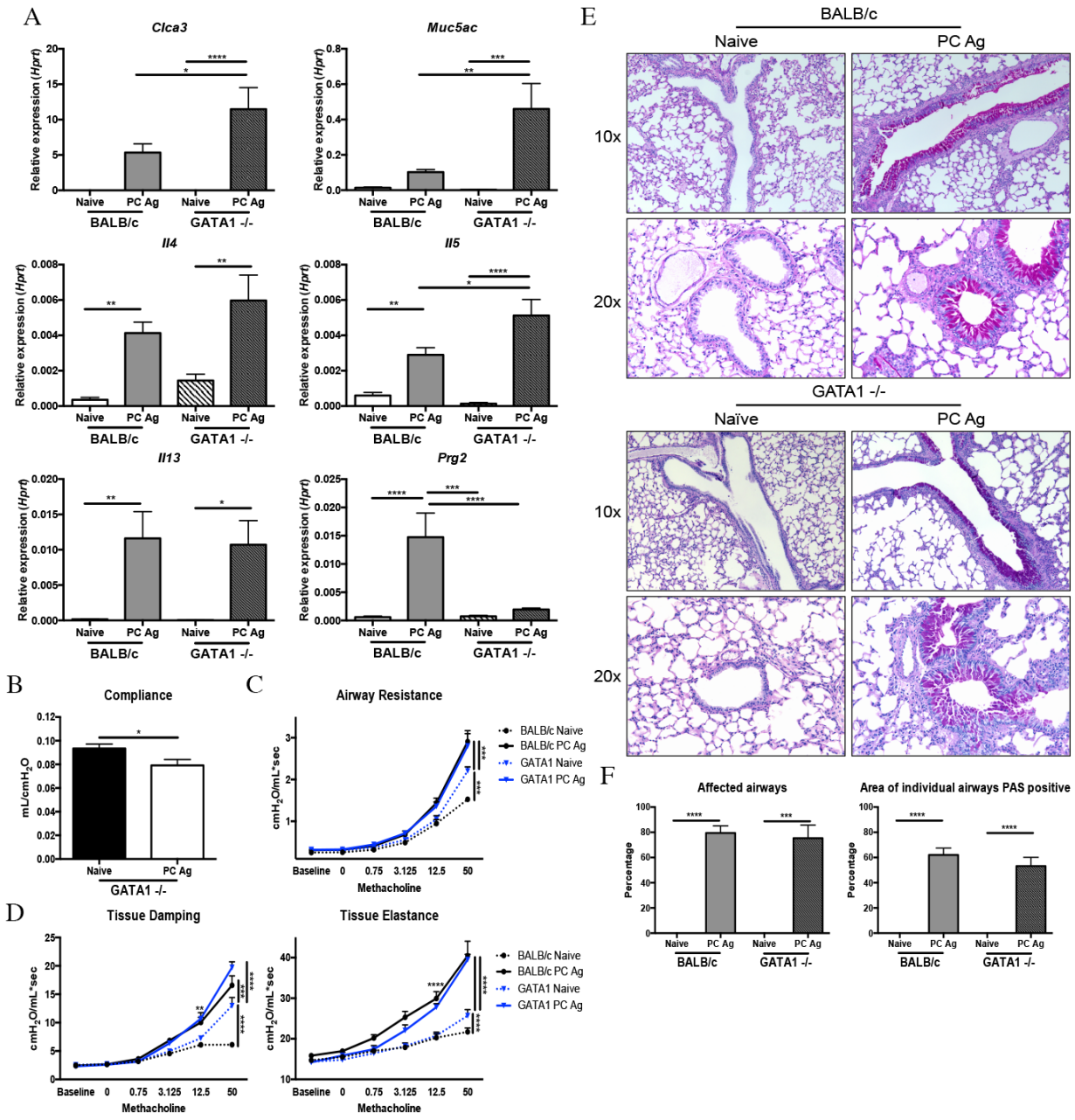

Figure 3-11. Eosinophils are dispensable for pathology following PC Ag exposure.

BALB/c and *GATA1*^{tm6Sho}*/J* mice were treated with PC Ag (*n*=5 for naïve BALB/c, *n*=8 BALB/c + PC Ag, *n*=8 for *GATA1*^{tm6Sho}*/J* groups) and sacrificed at day 14. Data represent the combination of two independent experiments. A.) RNA isolated from lung homogenate demonstrates that *GATA1*^{tm6Sho}*/J* mice are capable of mounting a type II response comparable to, if not greater than, that of BALB/c mice (* $p<0.05$, ** $p<0.01$, *** $p<0.001$, **** $p<0.0001$, one-way ANOVA with Tukey's multiple comparisons). B.) Follow anesthetization, tracheotomized mice were ventilated and quasi-static compliance was calculated using pressure-volume curves. *GATA1*^{tm6Sho}*/J* mice

treated with PC Ag had reduced compliance (* $p<0.05$, Student's t-test). C.) Newtonian airway resistance was calculated following escalating doses of aerosolized methacholine (0, 0.075, 3.125, 12.5, and 50 mg/mL). *GATA1^{tm6Sho}/J* mice, like BALB/c mice, have exacerbated airway resistance following PC Ag treatment (*** $p<0.001$, two-way ANOVA with multiple comparisons). D.) Tissue damping and tissue elastance were increased in *GATA1^{tm6Sho}/J* mice following PC Ag treatment (** $p<0.01$, *** $p<0.001$, **** $p<0.0001$, two-way ANOVA with multiple comparisons). E.) PAS staining of naïve and PC Ag BALB/c and *GATA1^{tm6Sho}/J* demonstrates similar mucus production in the PC Ag treated groups in both large and small airways. F.) Quantification of PAS demonstrates BALB/c and *GATA1^{tm6Sho}/J* have equally affected airways following PCAg treatment (*** $p<0.001$, **** $p<0.0001$, one-way ANOVA with Tukey's multiple comparisons).

3.4.6 Severe asthma patients have increased antibody titers to *Pneumocystis*

As prior studies have implicated *Pneumocystis* as a ubiquitous environmental exposure, we sought to determine if differences in anti-*Pneumocystis* antibodies correlated with asthma status. Severe asthma (SA) patients had elevated anti-*Pneumocystis* IgG levels compared to healthy control (HC) patients (**Figure 3-12A**). Both a single HC patient and a single SA patient appeared to recognize similar *Pneumocystis* antigens by Western blotting; however, the SA patient recognized these antigens with greater intensity, corroborating the ELISA findings (**Figure 3-12B**). To assess the specificity of these antibody responses, we evaluated antibody production to another respiratory pathogen, *Streptococcus pneumoniae* (SP). Interestingly, SA patients had decreased anti-SP antibodies compared to HC patients (**Figure 3-12C**). Additionally, as previously observed in the murine model of *Pneumocystis* exposure, a subset of SA patients had detectable anti-*Pneumocystis* IgE levels (**Figure 3-12D**). A strong positive correlation between anti-*Pneumocystis* IgG and IgE was observed, as patients with elevated anti-

Pneumocystis IgG were more likely to have increased anti-*Pneumocystis* IgE levels as well (**Figure 3-12E**). To rule out the possibility of non-specific binding to fungal antigens, the serum samples were also assessed for anti-*Aspergillus* antibodies and no difference was observed between HC and SA patients (**Figures 3-12F and 3-12G**). Further, no correlation existed between anti-*Pneumocystis* and anti-*Aspergillus* IgG or IgE (**Figures 3-12H and 3-12I**).

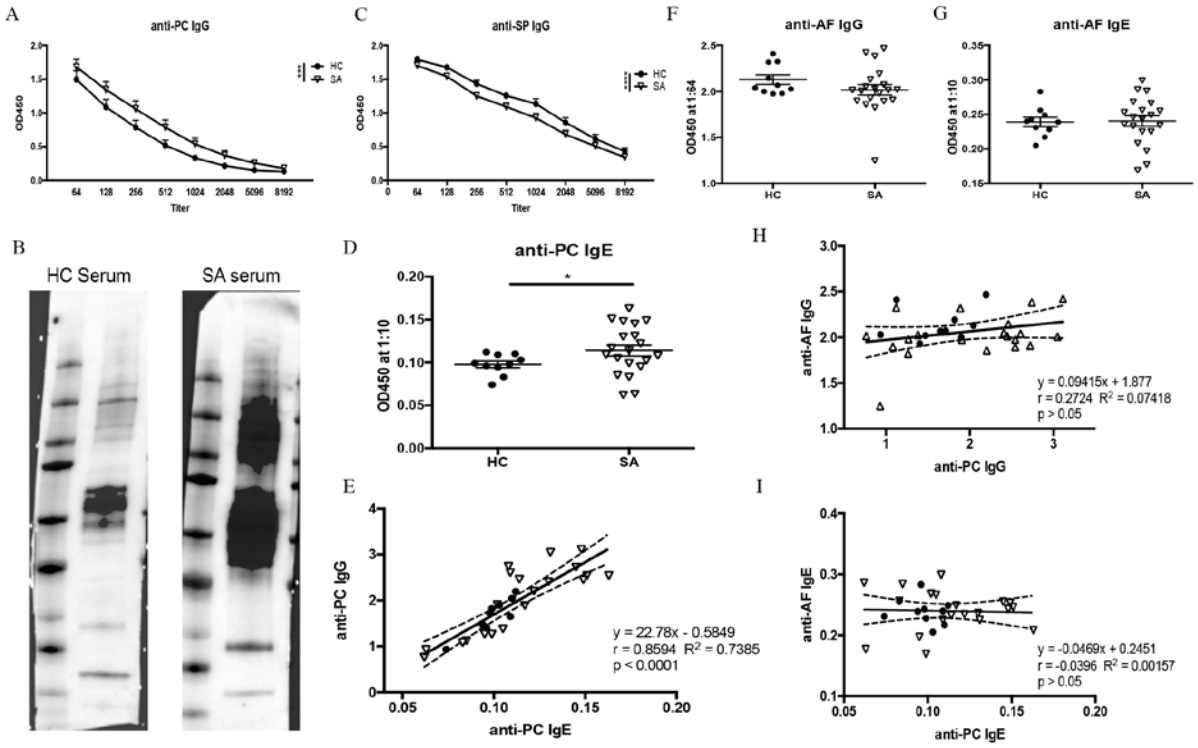

Figure 3-12. Patients with severe asthma have elevated anti-*Pneumocystis* IgG and IgE levels.

A.) Serum samples from healthy controls (HC, *n*=10) and severe asthma patients (SA, *n*=20) were analyzed for anti-PC IgG at various dilutions. SA patients had increased antibody levels against PC (*** p<0.001, two-way ANOVA). B.) Detection of anti-PC IgG from a HC patient and a patient with SA demonstrates similar banding patterns, but increased intensity in the SA patient. C.) Serum samples from HC and SA patients were also analyzed for IgG levels against *Streptococcus pneumoniae* (SP) and SA patients had reduced antibody levels (**** p<0.0001, two-way ANOVA) D.) Anti-PC IgE could be detected in the serum (diluted 1:10) of subset of patients with SA by ELISA. E.) Linear regression and Pearson's correlation analysis demonstrates a strong correlation between anti-PC IgG and anti-PC IgE levels in patients (r=0.8594, p<0.0001). F. and G.) SA patients do not have an increase in anti-*Aspergillus* IgG and IgE, respectively. H.) No correlation exists between anti-PC IgG and anti-AF IgG (r=0.2724, p>0.05). I.) No correlation exists between anti-PC IgE and anti-AF IgE (r= -0.0396, p>0.05).

Due to concerns of contaminating mouse proteins within the PCAg preparation, we probed mouse lung homogenate with the same human serum samples and found little reactivity (**Figure 3-13**).

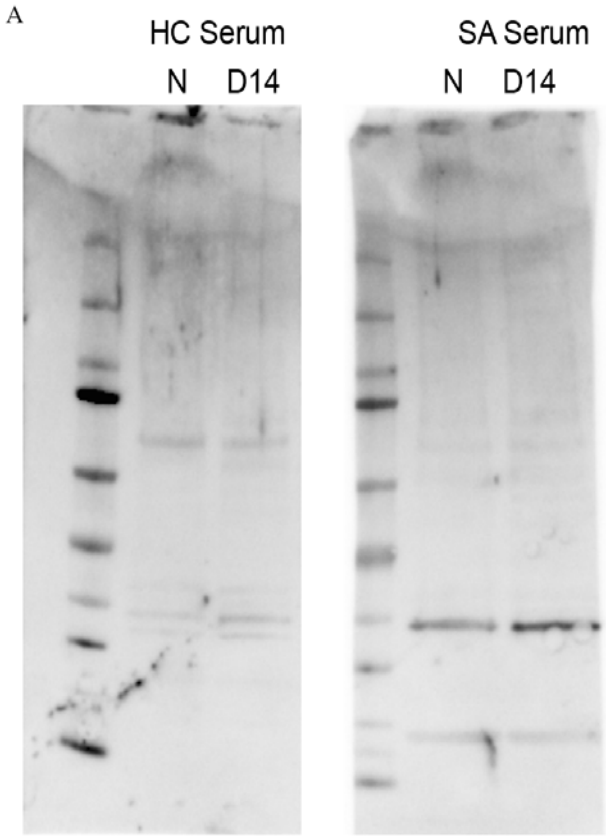

Figure 3-13. Serum from a healthy control and severe asthma patient demonstrate limited reactivity to mouse lung protein.

A.) Serum samples from a healthy control and a patient with severe asthma were probed for reactivity against lung homogenate from naïve mice (N) or mice treated previously treated with PCAg (D14). Unlike the PCAg western, the same human serum samples displayed a limited reactivity to mouse protein.

3.4.7 Severe asthma patients with increased anti-*Pneumocystis* antibody levels have worsened symptomatology and lung function

We next stratified SA patients into PC-high or PC-low subsets using a z-score approach. Any individual with an anti-PC IgG response above a z-score of one (2.02 based on the HC cohort) was considered PC-high (*n*=11); a patient with an ELISA O.D. of 2.02 or less was considered PC-low (*n*=9) (**Figure 3-14A**). The PC-high group had a significantly higher age at time of study compared to the PC-low group, while other demographics were similar (**Figure 3-14A**). The PC-low subset was 67% female and 22% ever-smokers, compared to 81% female and 36% ever-smokers in the PC-high group.

The SA PC-high subset had worsened symptom scores compared to the PC-low group with regards to cough and a trend towards increased shortness of breath (**Figure 3-14B**). Interestingly, SA PC-high patients had a trend towards reduced sputum production compared to the PC-low group (**Figure 3-14B**). On spirometry, PC-high patients had significantly decreased FEV1 and had a trend towards decreased FVC and FEF25-75 (**Figure 3-14C**). SA PC-high patients also had increased air trapping on plethysmography, as PC-high patients (*n*=7) had increased total lung capacity and residual volume compared to PC-low patients (*n*=9) (**Figure 3-14D**).

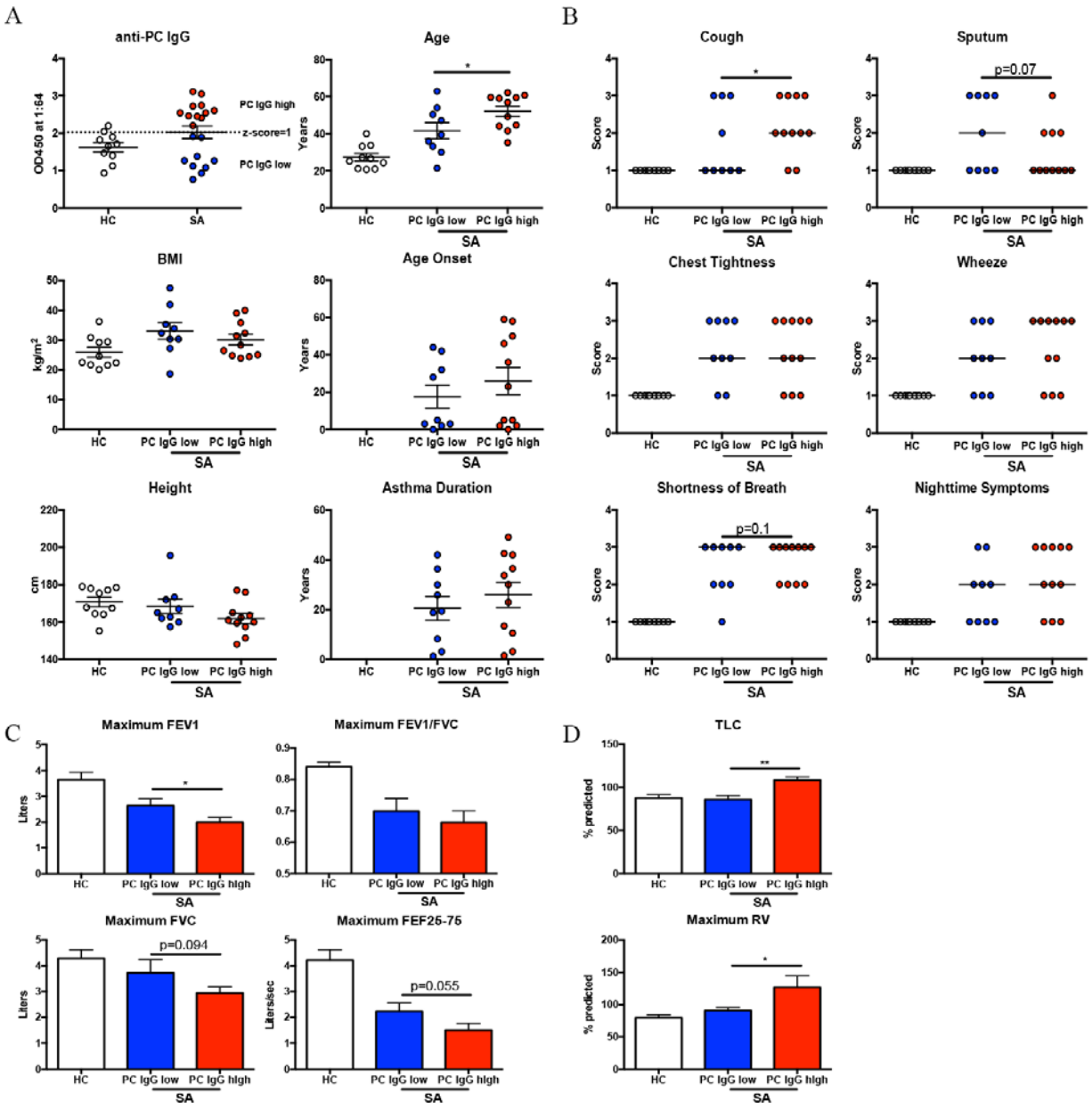

Figure 3-14. Severe asthma patients with increased anti-*Pneumocystis* IgG have worsened symptoms and decreased lung function.

A.) Patients with severe asthma were stratified into PC-high (n=11) and PC-low (n=9) groups by using a z-score of 1 within the HC population with an O.D. of 2.02 serving as the cutoff (dashed line). Demographics for these patient populations were similar with the exception of age, as PC-high patients had a significantly higher age (* $p<0.05$, Student's t-test). B.) Symptomatology as reported by the patients to a standard questionnaire shows PC-high patients having increased symptom severity in every symptom except for sputum production (* $p<0.05$, Chi-square analysis).

C.) Spirometric assessment of lung function demonstrates PC-high patients had decreased FEV1 (* $p<0.05$, Student's t-test), and trends towards decreased FVC and FEF25-75 compared to PC-low patients. D.) Plethysmography demonstrates PC-high patients have increased TLC and RV compared to PC-low patients (* $p<0.05$, ** $p<0.01$, Student's t-test).

Serum IgE levels for PC-low vs. PC-high groups were comparable, and both appeared elevated compared to HC patients (**Figure 3-15A**). Importantly, there did not appear to be a difference in allergen skin testing between groups (**Figure 3-15B**).

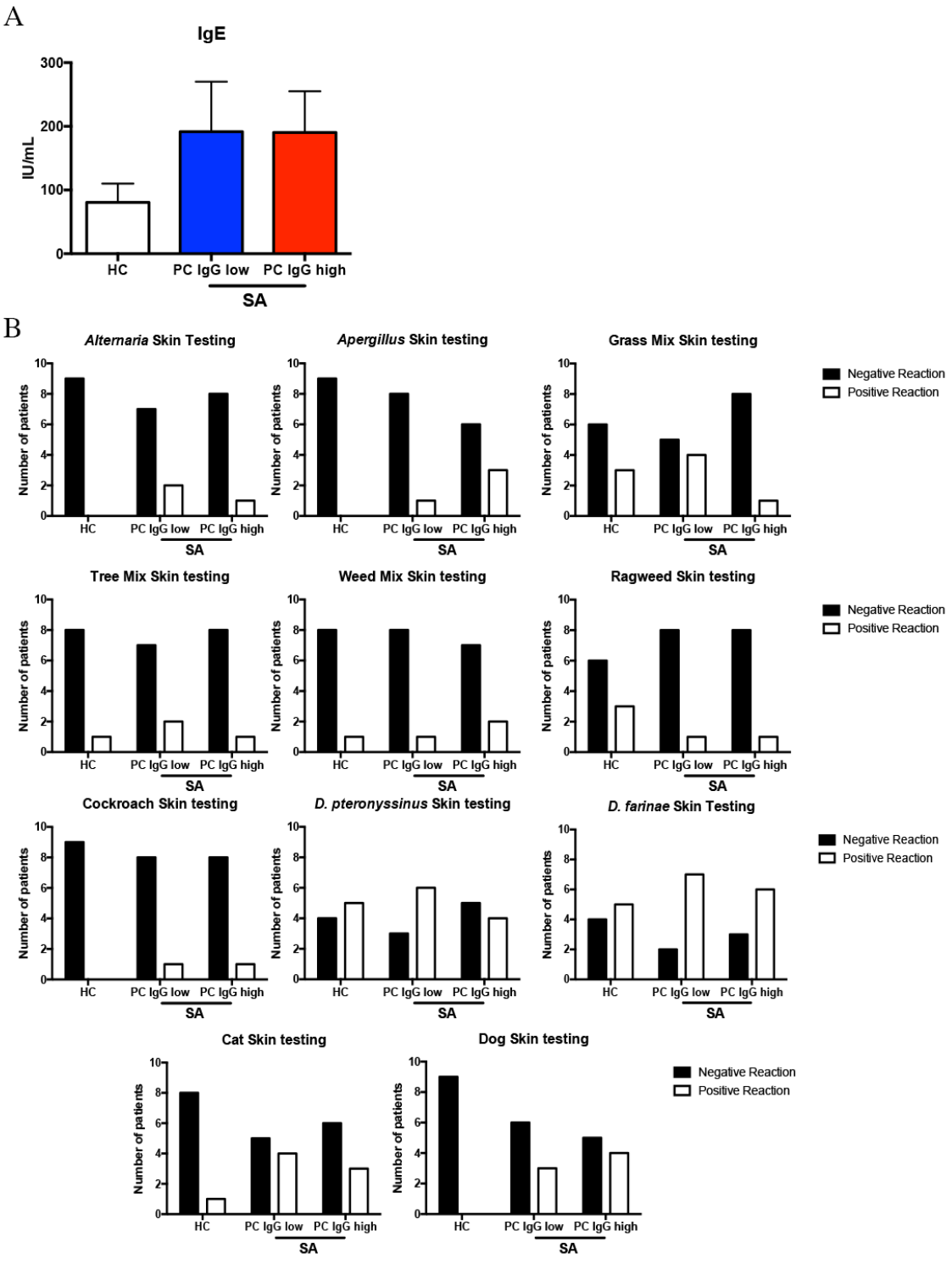

Figure 3-15. Allergic sensitization in healthy control and severe asthma patients.

A.) Serum IgE shows elevation in SA patients compared to healthy controls, but no difference based on anti-PC IgG status. B.) Allergen skin testing analysis for HC, PC IgG low, and PC IgG high patients.

Additionally, there were no differences in blood neutrophils, lymphocytes or eosinophils between PC-high and PC-low patients (**Figure 3-16A**). Similar counts of cells were also observed on bronchoalveolar lavage (**Figure 3-16B**). There were also no observed differences in inhaled or oral steroid use or steroid dose between the PC-high and PC-low group (data not shown).

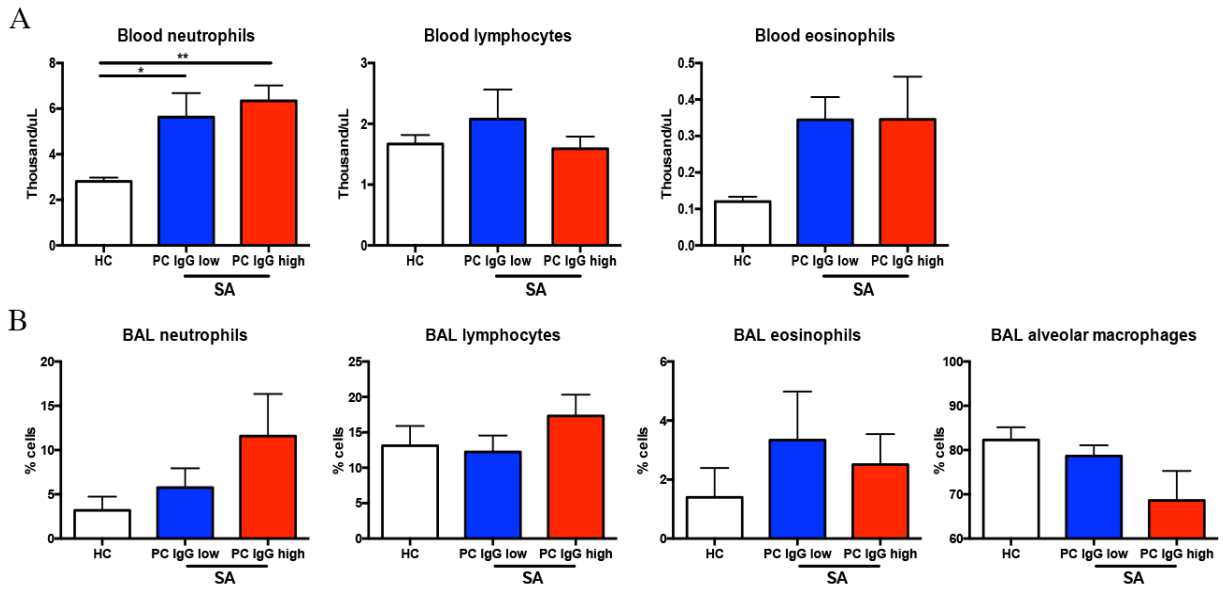

Figure 3-16. Peripheral blood and bronchoalveolar lavage cell analysis in healthy control and severe asthma patients.

A.) Number of neutrophils, lymphocytes, and eosinophils in peripheral blood in HC, PC IgG low, and PC IgG high patients (* $p<0.05$, ** $p<0.01$, one-way ANOVA with multiple comparisons). B.) Percentage of neutrophils, lymphocytes, eosinophils, and macrophages in the bronchoalveolar lavage of HC, PC IgG low, and PC IgG high patients.

3.5 DISCUSSION

These results demonstrate for the first time that *Pneumocystis* infection and antigen treatment induces an asthma-like pathologic response in the lung driven by $CD4^+$ T-cells. The ability of *Pneumocystis* to induce a strong Th2 response may have implications in the immunocompetent as it has recently been shown that the majority of healthy individuals have detectable anti-*Pneumocystis* antibodies (61). Furthermore, colonization of live *Pneumocystis* within the lung may occur as a transitional state of low *Pneumocystis* burden, with the specific host-pathogen interactions (e.g. immunosuppression) ultimately determining the difference between disease, colonization, and clearance (186). Indeed, asymptomatic infection with *Pneumocystis* may have immunologic ramifications, as infants with detectable *Pneumocystis* in the lungs had increased mucus production (187, 188), consistent with findings in our murine model.

The ubiquity in which humans are exposed to *Pneumocystis* and the specific nature of the immune response to *Pneumocystis* begs the question of how this pathogen and the subsequent host response may impact asthma. One prior study has demonstrated that *Pneumocystis* could worsen an ovalbumin murine model of asthma by altering dendritic cell subsets (183). While concurrent *Pneumocystis* infection only slightly modified a HDM model in the current study, *Pneumocystis* appeared to prime an equally potent type II response compared to HDM treated mice alone. These findings, coupled with the PCAg model, would suggest that much like HDM, *Pneumocystis* functions as an airway allergen (189, 190). As shown previously with HDM, PCAg further exacerbated airway responsiveness in *GATA1^{tm6Sho}/J* mice (148, 191). The necessity of eosinophils in mediating airway hyperresponsiveness has been difficult to show

definitively though, as variations between knockout-mouse and antigenic model have offered differing outcomes (145, 146).

There were some unique differences between the HDM and PCAg models. ILC2 cells have been shown to be prolific producers of type II cytokines in response to both pulmonary and intradermal HDM exposure (155, 192). Similarly, murine models of fungal allergen exposure, *Alternaria*, have also demonstrated a role for ILC2 cells as cytokine producers (153, 193). In the current *Pneumocystis* model, ILC2 cells appeared to have a greater function in maintaining the optimal Th2 response as opposed to directly contributing to pathology via cytokine production. This priming function has been shown previously to require MHC class II expression on ILC2 cells, although it is unclear if direct antigen presentation is required in the PCAg model (157, 194). One further difference between the HDM and PCAg model appears to be the specificity of the respective antigens and antibody responses. The antigen-specific recall responses and antibody-responses to PCAg and HDM did not cross-react, suggesting that distinct antigens, and not molecular patterns such as chitin, are recognized in these two models (195, 196).

While evidence in the mouse model shows that *Pneumocystis* infection and exposure can lead to lung pathology, this has yet to formally be studied in a population of immunocompetent patients with asthma. One study found an association between HIV-positive patients with prior pneumonia with either *Pneumocystis* or a bacterial pathogen and doctor-diagnosed asthma (66). A second study in HIV-positive individuals demonstrated that history with *Pneumocystis* was associated with an obstructed spirometry pattern on lung function testing (197). While these prior studies focused on fulminant infection in an HIV-positive host, the current study examined immune exposure by measuring anti-*Pneumocystis* antibody levels in the blood of patients with and without asthma. Strikingly, a cohort of patients with severe asthma had elevated anti-

Pneumocystis IgG and IgE antibodies in their serum compared to healthy controls. Importantly, this did not appear to be the result of non-specific immune activation to all pathogens, as severe asthma patients had decreased antibody responses to *S. pneumoniae* and similar antibody responses to *Aspergillus* compared to healthy controls. These findings are suggestive of increased exposure of *Pneumocystis* in severe asthma patients compared to healthy individuals; whether this is exposure is persistent colonization or transient contact with airborne spores is unclear. One possibility is that this increase in *Pneumocystis* exposure is due to the use of both inhaled and oral corticosteroids in severe asthmatics (135).

Thus, the current study cannot differentiate between a model where *Pneumocystis* exposure increases the likelihood of developing severe asthma and a model where severe asthmatics are more likely to be exposed to *Pneumocystis* as a result of steroid exposure. Monitoring *Pneumocystis* colonization status by molecular techniques could be useful in understanding the effects of local immunosuppression on *Pneumocystis* colonization, and such techniques could be applied longitudinally to a healthy cohort of patients to assess the development of asthma.

Importantly, the current study identifies the presence of anti-*Pneumocystis* IgE in serum samples of asthmatic patients. Type-I hypersensitivity to *Pneumocystis*, therefore, may be diagnosed much like that of other allergens routinely tested in the clinical setting. This also raises the exciting possibility of intervening with trimethoprim-sulfamethoxazole (TMP-SMX), the hallmark of treatment and prophylaxis for *Pneumocystis*, in severe asthma patients with known sensitization and/or colonization with *Pneumocystis*. While further studies elucidating the interplay between *Pneumocystis* and asthma are essential to inform future clinical investigations,

the current study demonstrates in both a murine model and in human patients that *Pneumocystis* may lead to the development of lung pathology and thus a clinical phenotype similar to asthma.

4.0 TH2 AND TH17 CELLS COOPERATIVELY REGULATE CXCL13 EXPRESSION IN *PNEUMOCYSTIS*-DEPENDENT INDUCIBLE BRONCHUS ASSOCIATED LYMPHOID TISSUE FORMATION

Taylor Eddens[1], Javier Rangel-Moreno[2], Patricia Castillo[1], Katelin Serody[1], Brian Campfield[1,3], Kong Chen[1], Jay K. Kolls[1]

[1]-Richard King Mellon Foundation Institute for Pediatric Research, Children's Hospital of Pittsburgh of UPMC, Pittsburgh, Pennsylvania, USA.

[2]-University of Rochester Medical Center, School of Medicine and Dentistry, Rochester, NY, USA.

[3]-Division of Pediatric Infectious Diseases, Department of Pediatrics, University of Pittsburgh School of Medicine, Pittsburgh, Pennsylvania, USA.

This work is currently in preparation for submission.

4.1 INTRODUCTION: IMMUNOLOGY OF INDUCIBLE BRONCHUS ASSOCIATED LYMPHOID TISSUE

The immune system interacts with almost every organ system. Immunologic cells can travel through the lymphatic or circulatory system to reach a site of effector function. However, there are also dedicated lymphoid organs where immune cells reside. The traditional primary lymphoid organs consist of the bone marrow and thymus, where B- and T-cells develop. Here, the processes of positive and negative selection occur and lead to the generation of a diverse, self-restricted repertoire of adaptive immune cells. Post-development, these cells can traffic to secondary lymphoid organs (SLOs). SLOs, consisting of lymph nodes, Peyer's patches in the small intestine, and the spleen, function to house naïve lymphocytes until priming and activation by a cognate antigen (198). Once primed, effector lymphocytes can travel to the site of infection and/or inflammation and contribute to the ongoing immune response, be it pathologic or protective.

One illustrative example of the complexities associated with the development of SLOs is the lymph node. Lymph nodes appear to begin development *in utero* and continue in some species up to three weeks after birth (199). Following lymphatic development, circulating lymphoid tissue-inducer (LTi) cells colonize the rudimentary lymph node (200). LTi cells are derived from the fetal liver progenitor and maturation of LTi cells is dependent on the transcription factor RORγT (201). LTi cells interact with stromal cells in the lymph node and through unknown mechanisms appear to promote the development of high endothelial venules (202). These high endothelial venules facilitate lymphocyte entry into the lymph node through a peripheral node addressin (PNAd) and L-selectin interaction (203).

Once lymphocytes have entered the lymph node, the tumor necrosis factor-lymphotoxin family of proteins, including lymphotoxin-alpha (*Lta*, gene name, LTα, protein name), and lymphotoxin-beta (LTβ), are crucial for lymphoid organ development (204). *Lta*$^{-/-}$ mice, for example, fail to develop lymph nodes and Peyer's patches (205). To compliment this loss-of-function approach, transgenic mice expressing LTα under a constitutive promoter can direct lymphoid neogenesis in organs such as the pancreas and kidney (206). LTα is unique in the sense that it can signal through TNFR family members, or it can form a heterotrimer with LTb ($LT\alpha_1LT\beta_2$) and signal through the lymphotoxin receptor LT-βR. Mice treated with an LT-βR antibody had decreased lymphocyte homing, PNAd expression, and lymph node number compared to isotype treated mice (207). Furthermore, blockade of LT-βR led to the decreased production of the lymphoid chemokine family, which act as critical orchestrators of the lymph node compartmentalization (204, 207).

The lymphoid chemokine family includes CCL19 and CCL21, ligands for the receptor CCR7, and CXCL13, a ligand for the receptor CXCR5 (208). CCL19 and CCL21 are constitutively expressed by stromal cells and together organize the homing of naïve T-cells and dendritic cells to the T-cell zone of the lymph node (209). Moreover, CCL21 is also expressed by the high endothelial venules and appears to have a more direct effect in dendritic cell immigration into the lymph node (209, 210). CXCL13, on the other had, has a more direct role in the recruitment of $CXCR5^+$ B-cells into the follicles (211). CXCL13, like LTα, can be overexpressed and appears to be sufficient to generate lymphoid neogenesis (212). These three chemokines control the development and homeostasis of the mature lymph node. Once formed, the lymph node is an encapsulated, bean-shaped organ containing compartmentalized

lymphocytes, antigen-presenting cells, and intricate vasculature systems connecting to both the systemic circulation and the lymphatic system.

Although T-cell priming in the SLOs happens regularly, ectopic lymphoid structures can form in the context of chronic inflammation or persistent antigen (204). These structures, called tertiary lymphoid organs (TLOs), can form in non-lymphoid locations through a process called lymphoid neogenesis. Lymphoid neogenesis has been shown to occur in almost every tissue, ranging from major organs such as brain, lung, liver, and intestine, to the smaller, more specialized tissues such as the aorta, salivary glands, and synovial tissue (198). Given such a broad range of tissues capable of harboring TLOs, it is not surprising that these ectopic lymphoid structures are found in a variety of disease states, such as: arthritis, multiple sclerosis, atherosclerosis, inflammatory bowel disease, cancer, hepatitis infection, Lyme disease, transplantation, and chronic obstructive pulmonary disease (COPD) (198). Although this is a brief overview of the abundance of TLOs in pathologic conditions, the remainder of this introduction will focus on TLOs in the lung.

The formation of TLOs in the lung has been preferentially referred to as inducible bronchus associated lymphoid tissue (iBALT) and much of our understanding of iBALT has stemmed from murine studies looking at key mediators of SLO maturation. In one influenza model of iBALT, mice lacking SLOs not only generated antigen-specific T- and B-cell responses, but also had decreased mortality (213). Moreover, the lymphoid chemokine family members CXCL13 and CCL21 were expressed in lungs containing iBALT in a LTα-independent manner (213). CXCL13 appears to be the predominant driver of iBALT formation, as mice lacking CCR7 spontaneously develop lymphoid follicles in the lung (214). Furthermore, *plt/plt*

mice lacking the genes encoding CCL19 and CCL21 develop iBALT to influenza but appear to have altered organization (215).

Given the crucial role of CXCL13 in iBALT formation, several studies have examined the cellular producers of the chemokine. First, Rangel-Moreno *et al*. demonstrated using bone marrow chimera experiments that the predominant producers of *Cxcl13* in the lung are non-hematopoietic cells (215). Using immunofluorescent staining, CXCL13 was localized to the B-cell follicles following influenza infection, while CCL21 appeared to be expressed by $PNAd^{+}$ high endothelial venules (215). In another model of influenza-iBALT, $CD11c^{+}CD11b^{+}$ dendritic cells expressed *Cxcl13* although depletion of these cells did not alter the total expression of *Cxcl13* (216). Blockade of LT-βR, however, did reduce *Cxcl13* expression in the lung (216). Interestingly, in patients with COPD, as well as in mice exposed to cigarette smoke extract, CXCL13 can be induced in the lung (217). Furthermore, in patients with COPD, CXCL13 appears to be expressed by follicular B-cells as part of a positive feedback loop; CXCL13 signals through CXCR5 to induce LTα, which then signals through LT-βR to induce more CXCL13 (218). Patients with pulmonary complications of rheumatoid arthritis are also susceptible to developing lymphoid follicles. The presence of iBALT in a subset of patients with rheumatoid arthritis correlated with expression of CXCL13, as well as other chemokines, and LTα (219).

One elegant study by Rangel-Moreno *et al*. explored a novel regulator of iBALT formation: IL-17A (220). Here, the authors administered LPS to neonatal mice followed by subsequent challenge with influenza. Neonatal mice were more susceptible to iBALT formation, a finding consistent with human biopsy and autopsy data demonstrating the presence of iBALT in infants and young children at high frequencies (220–222). The study then went on to exclude a role of LTi cells, as $Rorc^{-/-}$ mice were able to develop iBALT. However, $Il17a^{-/-}$ mice, as well as

Il17ra$^{-/-}$ mice, had defects in iBALT formation. These two findings are very counterintuitive, as *Rorc* expression is thought to be critical for Th17 cell development (223); it is also possible that some compensatory mechanism exists in the *Rorc*$^{-/-}$ mice, such as alterations in the microbiome (224). The study by Rangel-Moreno *et al*. convincingly implicated a role for IL-17A though, as neonatal pulmonary fibroblasts stimulated with IL-17A upregulated *Cxcl13* expression and appeared to be a critical mediator of initiation of iBALT (220).

Although IL-17A emerged as a novel regulator of iBALT formation, IL-17A belongs to a broader, more complex family of proteins that signal through the IL-17 receptors. IL-17A can form a homodimer or a heterodimer with IL-17F and signal through a heterodimeric complex of IL-17RA and IL-17RC (225). Likewise, IL-17F can also homodimerize and signal through the IL-17RA:IL-17RC complex. The IL-17RA:IL-17RC complex can signal through the canonical NF-κB pathway via ACT1 and induce chemokine, cytokine, and pro-inflammatory gene transcription (225). IL-17RC is specific to IL-17A and IL-17F signaling, while IL-17RA is ubiquitously expressed on tissues and is more promiscuous. IL-17RA can also heterodimerize with IL-17RB to signal in response to the ligand IL-25 (226). IL-25 sufficiently induces the production of type II cytokines such as IL-5 and IL-13 via activation of both Th2 and ILC2 cells (152, 155, 226). Given the propensity of IL-25 to amplify type II responses, IL-25 has been highly studied in relation to asthma and allergic airway disease (227–229). Interestingly given the connection to *Pneumocystis*, patients with asthma have an increased likelihood of developing iBALT (230).

4.2 RATIONALE AND HYPOTHESIS

We observed the formation of perivascular lymphocytic clusters following *Pneumocystis* infection that resembled architecture previously described as iBALT. We hypothesized that these structures were iBALT composed of $CD4^+$ T-cells and B-cells and that this *Pneumocystis* driven iBALT would be dependent on CXCL13, IL-17A signaling, and lymphotoxin-alpha.

4.3 METHODS

Mice

All mouse colonies were maintained in the Rangos Research Building Animal Facility and use was approved and performed in accordance with the University of Pittsburgh Institutional Care and Use Committee (Protocol: 14084329 and 16027674). C57BL/6, BALB/c, *Cxcr5*$^{-/-}$, *Lta*$^{-/-}$, *Stat6*$^{-/-}$, *Gata1*^{tm6Sho}*/J*, *Rag1*$^{-/-}$ and *Rag2*$^{-/-}$*Il2rg*$^{-/-}$ mice were all ordered from The Jackson Laboratory. The *Il17ra*$^{-/-}$ and *Il17rb*$^{-/-}$ mice were generated at Amgen. The *Il17rc*$^{-/-}$ mice were generated at GenenTech.

Reagents

Mice were depleted of $CD4^+$ cells by weekly intraperitoneal injection of 0.3 mg of GK1.5 monoclonal antibody as previously described (182, 231). $CD20^+$ cells were depleted using intraperitoneal injections of 0.1 mg 5D2 monoclonal antibody every three days. Recombinant IL-17A and IL-13 (R&D Systems) was used at a final concentration of 100ng/mL. Recombinant IL-6 (R&D Systems) was used at a final concentration of 40 ng/mL.

Pneumocystis inoculation

Pneumocystis murina was harvest from the lungs of an infected *Rag2*$^{-/-}$*Il2rg*$^{-/-}$ mouse. Following straining through a 70-μm sterile filter, mice were challenged with $2.0x10^6$ cysts/mL as previously described (83, 123).

Immunofluorescence staining and histologic analysis

The left lobe was fixed by injecting 10% formalin into the left main stem bronchus. Lung tissue was processed, paraffin-embedded, and sectioned. Hematoxylin and eosin staining was performed by the Children's Hospital of Pittsburgh Histology Core. For immunofluorescence, slides were hydrated in PBS and were blocked for 30 mins at room temperature in Fc block (10 ug/mL) and 5% vol/vol normal donkey serum in PBS. Slides were then incubated in primary antibody diluted in PBS for 30 minutes at room temperature: anti-PNAd, anti-Lyve-1, proliferating cell nuclear antigen (PCNA), peanut agglutinin (PNA), anti-B220, anti-CD3, anti-CXCL13, anti-CD21, anti-CD35, anti-FDC-M1. Images were collected with Zeiss Axioplan 2 microscope and the outline tool in Zeiss Axiovision software was used for morphometric analysis. I would also like to take this time to acknowledge our collaborator, Dr. Javier Rangel-Moreno. I want to avoid feeling like Jeremy Grey, who once said "the painting was a gift and I'm taking it with me." The pictures from Dr. Rangel-Moreno are an incredible gift and are only included in my dissertation, as the data he provided are instrumental in telling the story of the *Pneumocystis* driven iBALT. To Dr. Rangel-Moreno, thank you sincerely.

qRT-PCR

The right middle lobe was homogenized in Trizol® (Life Technologies) followed by RNA isolation per manufacturer's instructions. Following quantification using a Nanodrop 2000 (Thermo Scientific), 500 ng of RNA was converted to cDNA using iScript™ (Bio-Rad). Gene expression analyses were then perfomed using SsoAdvanced™ qRT-PCR universal probes supermix (Bio-Rad). Murine primers included: *Ccl19*, *Ccl21*, *Ifng*, *Prg2*, *Il6*, *Il17a*, *Ccl11* (Applied Biosciences) and *Cxcl13*, *Il5*, *Il13*, and *Cxcl1* (IDT). *Pneumocystis* SSU burden was quantified as described previously (231).

Ex vivo *antigen restimulation assay*

The right lower lobe of lung was collected, physically digested, and incubated in collagenase/DNase for one hour at 37°C as described previously(182, 231). Single cell suspensions were then strained using a 70-μm sterile filter. Red blood cells were lysed using a NH_4Cl solution and the cells were enumerated using Trypan Blue staining. Cells were then plated at $5x10^5$ cells per well, stimulated with either 5 μg *Pneumocystis* antigen or 2.5 μL of CD3/CD28 Dynabeads® (2015-07, Life Technologies). Following 72-hours, the cells were pelleted and the supernatants were collected. The remaining cells were resuspended in Trizol® LS (Life Technologies) for RNA isolation.

Flow Cytometry

Whole lung cells were isolated prepared as described in the *ex vivo* whole lung cell stimulation methods. Briefly, cells were plated, centrifuged, and stimulated with 50 ng/mL PMA and 750 ng/mL ionomycin for 4 hours. After one hour, 1 μL GolgiStop (BD Pharmingen) was added.

Following incubation, cells were then washed, and resuspended in surface antibodies diluted in PBS at 1:200 unless otherwise specified. Surface staining included: CD3-Alexa700 (eBioscience, Clone: 17A2) TCRβ-PerCP-Cy5.5 (eBioscience, Clone: H57-597), TCRγδ-FITC (eBioscience, Clone: GL3), CD90.2-PE-Cy7, diluted 1:1500 (eBioscience, Clone: 53-2.1), CD11b-Biotin (eBioscience, Clone: M1/70), F4/80-biotin (eBioscience, Clone: BM8), NK1.1-biotin (BD Pharmingen, Clone: PK136), CD11c-biotin (BD Pharmingen, Clone: HL3), CD19-biotin (BD Pharmingen, Clone: 1D3), TER119-biotin (BD Pharmingen, Cat: 553672). Following a 1 hour incubation at 4°C, cells were washed and resuspended in the streptavidin-BV421 (diluted 1:200). Following a 30 minute incubation at 4°C, cells were washed and fixed and permeabilized using the eBioscience FoxP3 staining kit per manufacturer's instructions. Intracellular antibodies, anti-IL-17A-APC (eBioscience, clone: 17B7) and anti-IL-13 (eBioscience, clone: eBio13A) antibodies were added and incubated at 4°C for 1 hour. Cells were then washed, resuspended, and analyzed on a BD LSR II Flow Cytometer with compensation via OneComp eBeads (eBioscience). Data analysis was conducted using FlowJo software (Treestar).

Pulmonary fibroblast culture and stimulation

Whole lung cells were isolated as described above and plated at a 1:10 dilution in 24-well plates. Cells were incubated for three days at 37°C to allow for adherence, washed once with PBS, and left to grow in complete IMDM until reaching 50-70% confluence. The cells were then stimulated with the various cytokine mixtures described above and incubated at 37°C for 6 or 24 hours. Supernatants were collected for use in a CXCL13 ELISA (BioLegend®). The cells were then harvested in 1 mL Trizol and RNA isolation and qRT-PCR was performed as described above.

Statistics

All statistical analyses were performed using GraphPad Prism version 6.0f. All data are presented as mean ± standard error of the mean (SEM). Studies with two groups were analyzed with a Student's t-test. Studies with three or more groups were analyzed using an ordinary one-way ANOVA with Tukey's multiple comparisons. All statistical analyses considered $p<0.05$ significant.

4.4 RESULTS

4.4.1 Inducible bronchial associated lymphoid tissue develops following *Pneumocystis* infection and exposure

Over the course of murine *Pneumocystis* infection, we observed perivascular lymphocytic follicle formation beginning at day 7, expanding at day 14, and contracting by day 28 (**Figure 4-1A**). The lymphocytic follicles appeared to have other characteristics of inducible bronchus associated lymphoid tissue at day 14. For one, $PNAd^{+}$ high endothelial venules, described in both lymph nodes and iBALT structures, were detectable outside of the follicle (**Figure 4-1B**). Furthermore, Lyve-1^{+} lymphatic vessels were also present in the surrounding areas of the follicle (**Figure 4-1B**). Importantly the formation of iBALT following *Pneumocystis* infection was not an artifact of oropharyngeal infection with a large inoculum. C57BL/6 mice co-housed with a *Pneumocystis* infected *Rag2*$^{-/-}$*Il2rg* $^{-/-}$ double knockout mouse for two weeks also had formation of perivascular follicles four-weeks post-exposure (**Figure 4-1C**). Formation of iBALT

following co-housing required adaptive immunity, as *Rag1*$^{-/-}$ mice did not have lymphoid follicles following co-housing (**Figure 4-1C**). Interestingly, both C57BL/6 and *Rag1*$^{-/-}$ mice co-housed with an infected *Rag2*$^{-/-}$*Il2rg* $^{-/-}$ mouse had detectable *Pneumocystis* burden four weeks removed from exposure (**Figure 4-1D**).

We also sought to characterize the lymphoid populations contained within the structures. In C57BL/6 mice inoculated with *Pneumocystis* oropharyngeally, these structures contained proliferating cell nuclear antigen (PCNA) positive B220^{+} B cells as well as intrafollicular CD3^{+} T-cells (**Figure 4-1E**). CD4^{+} T-cells are crucial for the development of these structures, as depletion with an anti-CD4 monoclonal antibody (GK1.5) completely abrogated the accumulation and proliferation of B-cells (**Figure 4-1F**). Likewise, depletion of B-cells with an anti-CD20 monoclonal antibody (5D2) reduced the accumulation of lymphocytes in the lung (**Figure 4-1G**). Quantification of these iBALT structures demonstrated that both CD4^{+} and CD20^{+} depletion resulted in the reduction of lymphoid follicle size, number, and area occupied per lung section (**Figure 4-1H**).

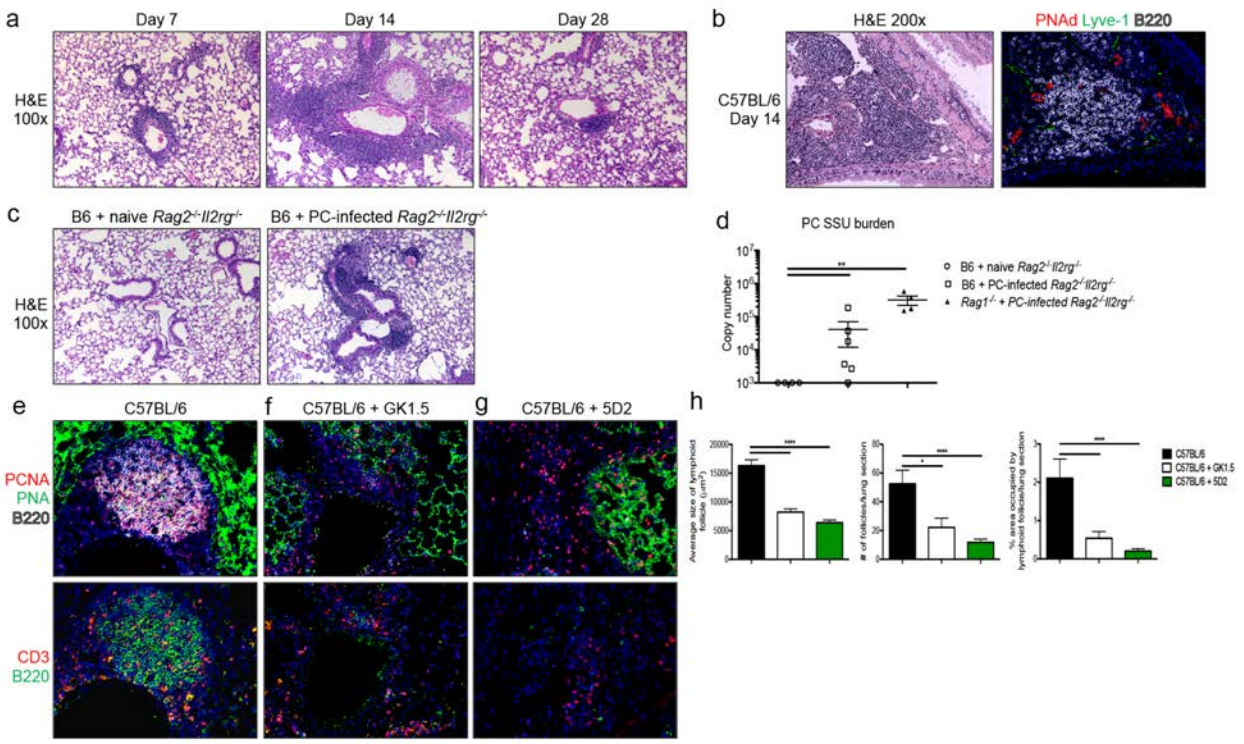

Figure 4-1. **Inducible bronchus associated lymphoid tissue (iBALT) forms following *Pneumocystis* infection and exposure.**

A.) iBALT development over the course of *Pneumocystis* infection. B.) Immunofluorescent staining of an iBALT structure 14 days post-infection with *Pneumocystis* demonstrating the presence of $PNAd^+$ high endothelial venules and Lyve-1^+ lymphatic vessels. C.) C57BL/6 mice co-housed for two weeks with a *Pneumocystis* infected *Rag2*$^{-/-}$ *Il2rg*$^{-/-}$ mouse have iBALT structures four weeks following separation. D.) C57BL/6 mice co-housed for two weeks with a *Pneumocystis* infected *Rag2*$^{-/-}$*Il2rg*$^{-/-}$ mouse have detectable *Pneumocystis* burden. ** $p<0.01$ by one-way ANOVA with Tukey's multiple comparisons. E.) Immunofluorescent staining of rapidly dividing B-cells ($PCNA^+B220^+$) cells and $CD3^+$ T-cells in the lung of a C57BL/6 mouse 14 days after *Pneumocystis* infection. F.) iBALT structures are reduced following $CD4^+$ T-cell depletion with GK1.5 monoclonal antibody. G.) iBALT structures are reduced following $CD20^+$ B-cell depletion with 5D2 monoclonal antibody. H.) Quantification of iBALT structures in C57BL/6 mice, C57BL/6 mice treated with GK1.5, and C57BL/6 mice treated with 5D2. * $p<0.05$, **** $p<0.0001$ by one-way ANOVA with Tukey's multiple comparisons.

Fungal exposure of any species was not sufficient to induce iBALT, as *Aspergillus* infected mice did not have lymphoid follicles in the lung 14 days post-infection (**Figure 4-2A**). At this time point, *Aspergillus* burden was undetectable, as were any residual inflammatory changes (**Figure 4-2B**).

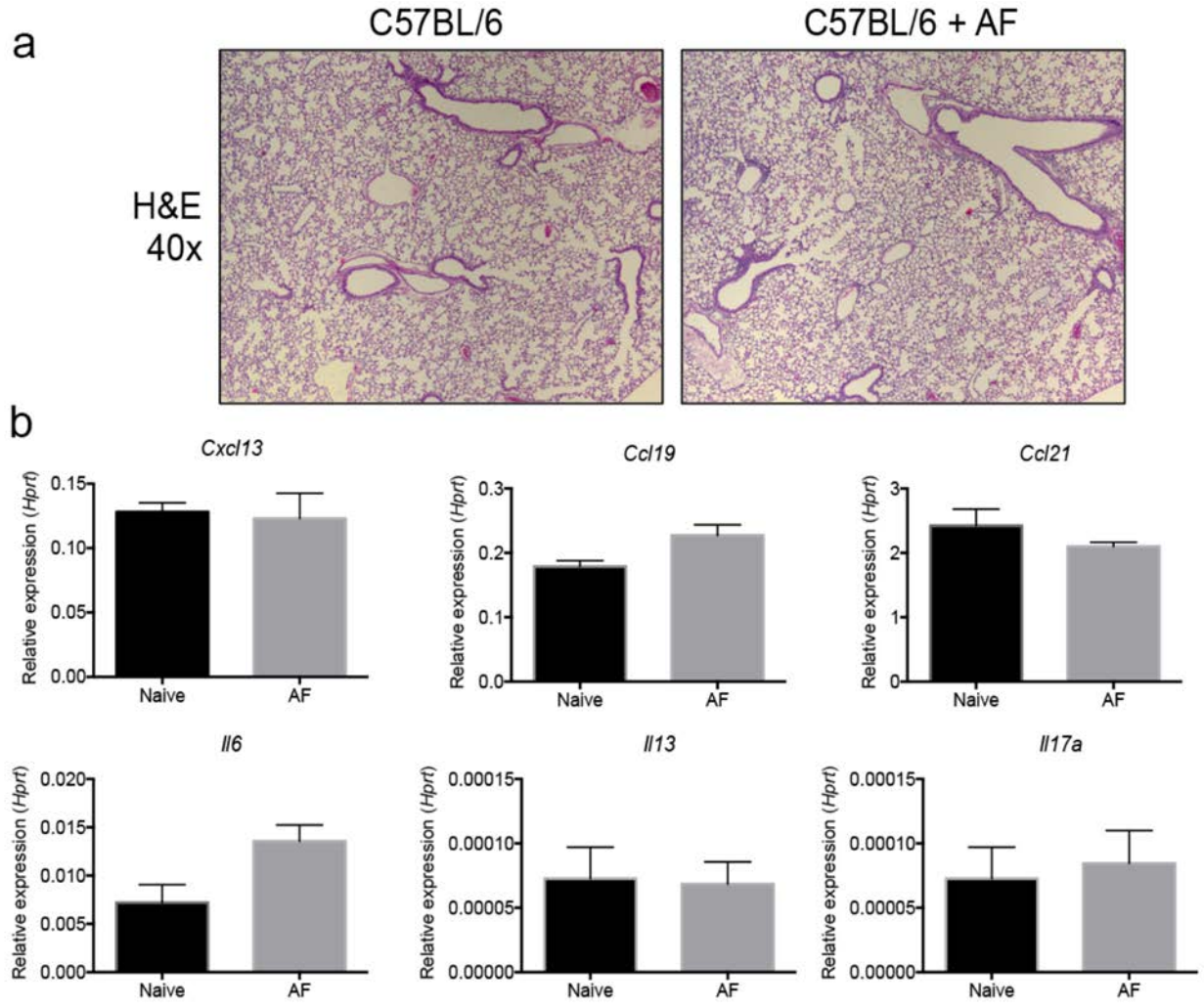

Figure 4-2. ***Aspergillus* infection does not result in formation of iBALT**.

A.) H&E staining reveals little inflammation 14 days post-infection with *Aspergillus fumigatus* (AF). B.) qRT-PCR on whole lung reveals no changes in *Cxcl13*, *Ccl19*, *Ccl21*, *Il6*, *Il13*, or *Il17a* 14 days post-infection with *Aspergillus*.

4.4.2 CXCR5, but not lymphotoxin-alpha, is required for *Pneumocystis* iBALT formation

Ligands for both CXCR5 (CXCL13) and CCR7 (CCL19 and CCL21) have previously been implicated in the formation of inducible bronchus associated lymphoid formation in both mice and humans (215–217). Over the course of *Pneumocystis* infection, CXCL13, but not CCL19 or CCL21, was induced concomitantly with iBALT formation (**Figure 4-3A**) However, CXCL13 induction was absent in GK1.5 treated mice, suggesting $CD4^+$ T-cells regulate expression of the chemokine (**Figure 4-3A**). Likewise, wild type mice that developed iBALT following exposure to a *Pneumocystis*-infected *Rag2*$^{-/-}$*Il2rg* $^{-/-}$ mouse had increased CXCL13, but not CCL19 or CCL21 expression (**Figure 4-3B**). Further implicating CXCL13 as a crucial mediator of *Pneumocystis* iBALT formation, *Cxcr5*$^{-/-}$ mice lacked organized follicles in the lung 14 days post-infection (**Figures 4-3C and 4-3D**).

Lymphotoxin-alpha has been previously implicated as an upstream mediator iBALT formation in response to influenza (220) and as a regulator of *Cxcl13* production following smoke exposure in mice (232). Strikingly, *Lta*$^{-/-}$ mice had enhanced iBALT formation with rapidly dividing B-cells and architecture similar to that of C57BL/6 mice (**Figure 4-3E**). Likewise, both *Cxcr5*$^{-/-}$ and *Lta*$^{-/-}$ mice had comparable levels of *Cxcl13* production compared to C57BL/6 mice (**Figure 4-3F**). Both *Cxcr5*$^{-/-}$ and *Lta*$^{-/-}$ mice, which are devoid of all secondary lymphoid organs, were also capable of controlling *Pneumocystis* burden similar to that of wild type mice, suggesting these iBALT structures are sufficient, but not required, to provide anti-fungal immunity (**Figure 4-3G**). Taken together, these results demonstrate that CXCR5-signaling is required for *Pneumocystis* iBALT formation in a lymphotoxin-alpha independent manner.

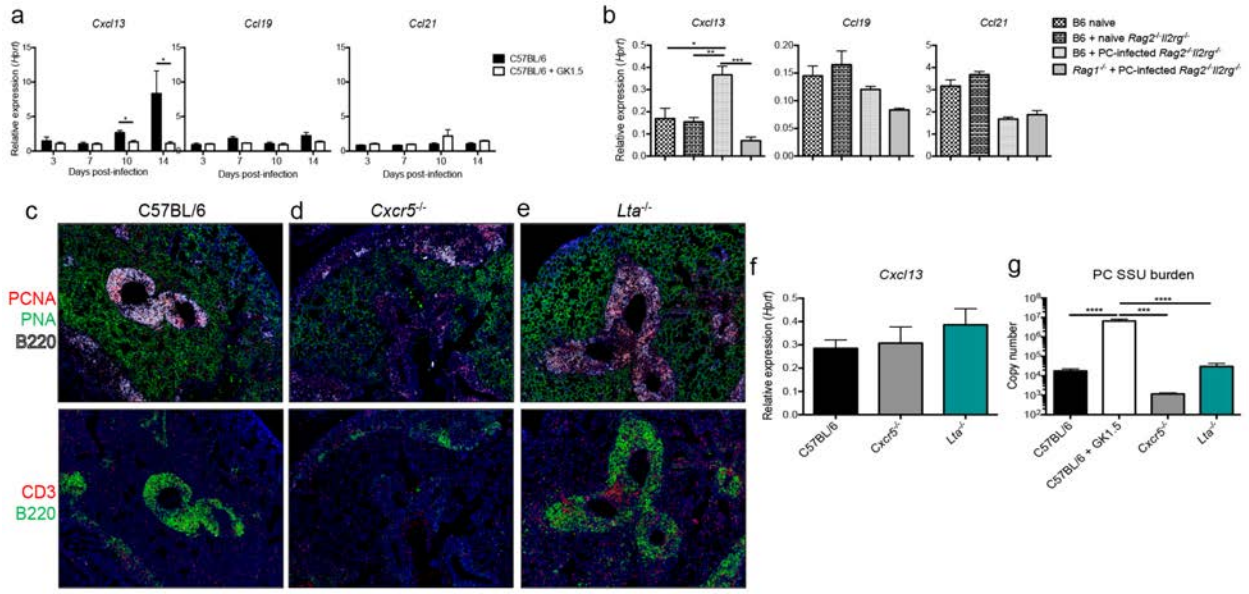

Figure 4-3. **CXCR5, but not lymphotoxin-alpha, is required for *Pneumocystis* iBALT formation**.

A.) *Cxcl13* is induced over the course of *Pneumocystis* infection in C57BL/6 mice in a $CD4^+$ T-cell dependent manner. *Ccl19* and *Ccl21* expression levels are unchanged throughout *Pneumocystis* infection. * $p<0.05$ by multiple t-tests. B.) C57BL/6 mice co-housed with a *Pneumocystis* infected *Rag2*$^{-/-}$*Il2rg*$^{-/-}$ mouse for two weeks, followed by four weeks of separation, upregulate *Cxcl13* but not *Ccl19* or *Ccl21*. * $p<0.05$, ** $p<0.01$, *** $p<0.001$ by one-way ANOVA with Tukey's multiple comparisons. C-E.) Immunofluorescent staining of C57BL/6, *Cxcr5*$^{-/-}$, and *Lta*$^{-/-}$ mice 14 days post-*Pneumocystis* infection demonstrating iBALT formation in C57BL/6 and *Lta*$^{-/-}$ mice and unorganized follicle structure in *Cxcr5*$^{-/-}$ mice. F.) *Cxcl13* expression is similar in C57BL/6, *Cxcr5*$^{-/-}$, and *Lta*$^{-/-}$ mice. G.) C57BL/6, *Cxcr5*$^{-/-}$, and *Lta*$^{-/-}$ mice control *Pneumocystis* burden at 14 days post-infection compared to CD4-depleted mice. *** $p<0.001$, **** $p<0.0001$ by one-way ANOVA with Tukey's multiple comparisons.

4.4.3 *Pneumocystis* iBALT is dependent on IL-17R family member signaling

We next evaluated members of the IL-17 family, IL-17RA, IL-17RB, and IL-17RC, in *Pneumocystis* driven iBALT formation. IL-17A signals through a heterodimer of IL-17RA and IL-17RC, while the Th2-promoting cytokine IL-25 (IL-17E) signals through an IL-17RA and IL-17RB heterodimer (225, 226). IL-17A has been previously implicated in *Cxcl13* induction and

iBALT formation in neonatal LPS-influenza and tuberculosis models of immunopathology (220, 233). Similar to those models, *Pneumocystis* iBALT was disrupted in *Il17ra*$^{-/-}$ mice compared to wild type controls, as *Il17ra*$^{-/-}$ mice had a drastic reduction in PCNA^{+}-B220^{+} cells and little organization of T-cell and B-cell zones (**Figures 4-4A and 4-4B**). Surprisingly, *Il17rb*$^{-/-}$ mice also had disrupted iBALT organization (**Figure 4-4C**). Likewise, *Il17rc*$^{-/-}$ mice had reduced iBALT size and abnormal architecture (**Figure 4-4D**). Upon quantification, *Il17ra*$^{-/-}$, *Il17rb*$^{-/-}$, and *Il17rc*$^{-/-}$ mice all had reduced follicle number and size, as well as area occupied within the lung (**Figure 4-4E**). In concordance with the histologic data, *Il17ra*$^{-/-}$, *Il17rb*$^{-/-}$, and *Il17rc*$^{-/-}$ mice had reduced expression of *Cxcl13* in the lung (**Figure 4-4F**).

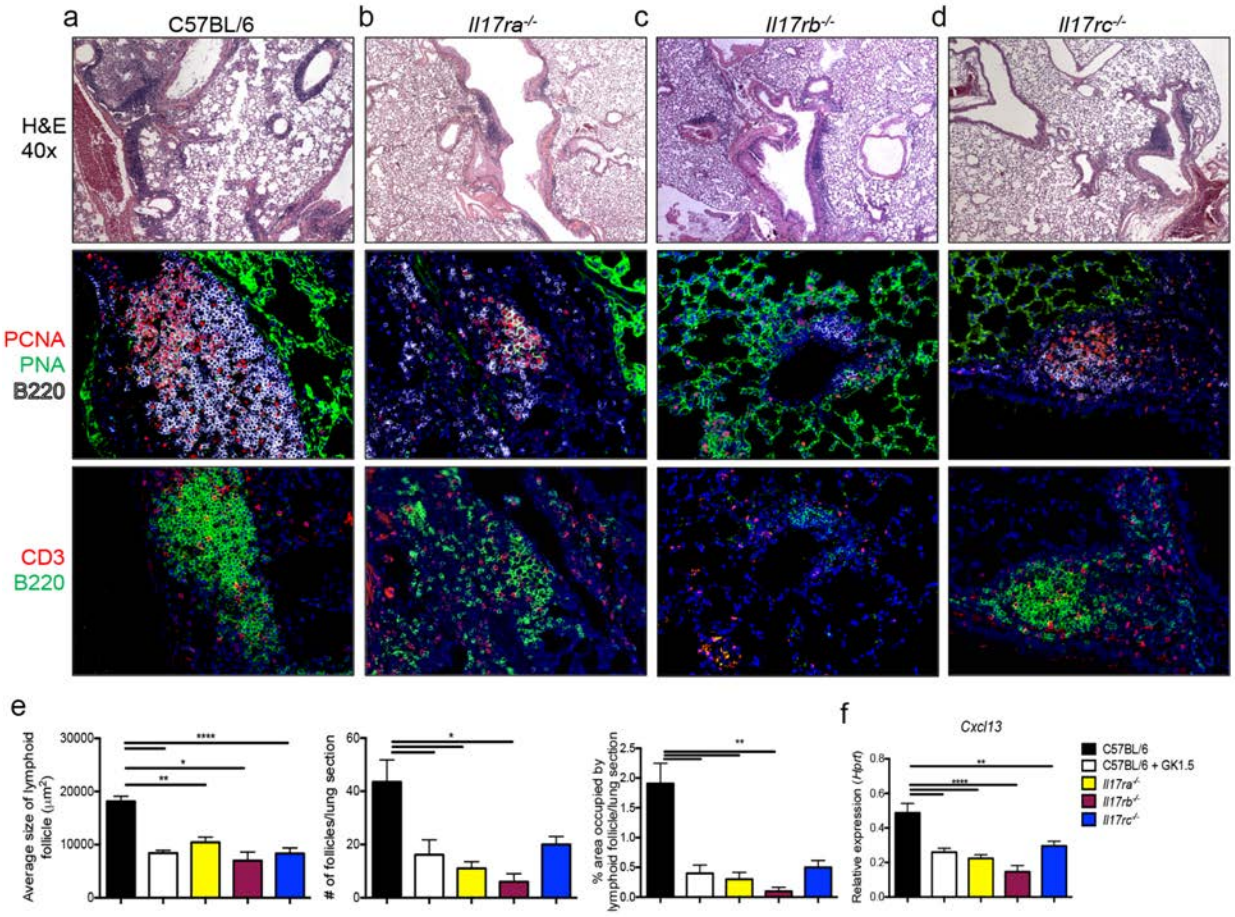

Figure 4-4. **IL-17R family members are required for the development of *Pneumocystis* iBALT**.

A-D.) Immunofluorescent staining of C57BL/6, *Il17ra*$^{-/-}$, *Il17rb*$^{-/-}$, and *Il17rc*$^{-/-}$ mice, respectively, 14 days following *Pneumocystis* infection demonstrates decreased iBALT formation (top). *Il17ra*$^{-/-}$, *Il17rb*$^{-/-}$, and *Il17rc*$^{-/-}$ mice all have reduced proliferating B-cells (middle) and disorganized T-cell and B-cell zones (bottom). E.) Quantification of size, number, and area occupied by iBALT structures. * $p<0.05$, ** $p<0.01$, **** $p<0.0001$ by one-way ANOVA with Tukey's multiple comparisons. F.) *Cxcl13* expression is reduced in *Il17ra*$^{-/-}$, *Il17rb*$^{-/-}$, and *Il17rc*$^{-/-}$ mice. ** $p<0.01$, **** $p<0.0001$ by one-way ANOVA with Tukey's multiple comparisons.

We next assessed the T-cell responses from each genotype at day 14 post-infection. *Il17ra*$^{-/-}$ and *Il17rb*$^{-/-}$ mice had diminished expression of *Il5* following *ex vivo* stimulation with *Pneumocystis* antigen (**Figure 4-5A**). *Il17rc*$^{-/-}$ mice had *Il5* expression comparable to that of

C57BL/6 mice, suggestive of intact Th2 priming and differentiation (**Figure 4-5A**). Importantly, cells from *Il17ra*$^{-/-}$ and *Il17rb*$^{-/-}$ mice did not appear to be intrinsically defective in Th2 polarization, as non-specific stimulation with CD3/CD28 was capable of inducing robust *Il5* expression (**Figure 4-5A**). Similarly, cells from *Il17ra*$^{-/-}$ and *Il17rb*$^{-/-}$, but not *Il17rc*$^{-/-}$ mice, had striking defects in *Il13* expression comparable to CD4-depleted mice (**Figure 4-5B**). Again, the capacity of these cells to make *Il13* was not defective following CD3/CD28 stimulation (**Figure 4-5B**). In contrast, Th17 polarization was reduced in cells from *Il17ra*$^{-/-}$ and *Il17rc*$^{-/-}$ mice, which are defective in IL-17A signaling (**Figure 4-5C**). However, cells from *Il17rb*$^{-/-}$ mice had intact antigen-specific production of IL-17A (**Figure 4-5C**). Production of the Th1 cytokine, interferon-γ (*Ifng)*, appeared to be slightly reduced in all genotypes (**Figure 4-5D**).

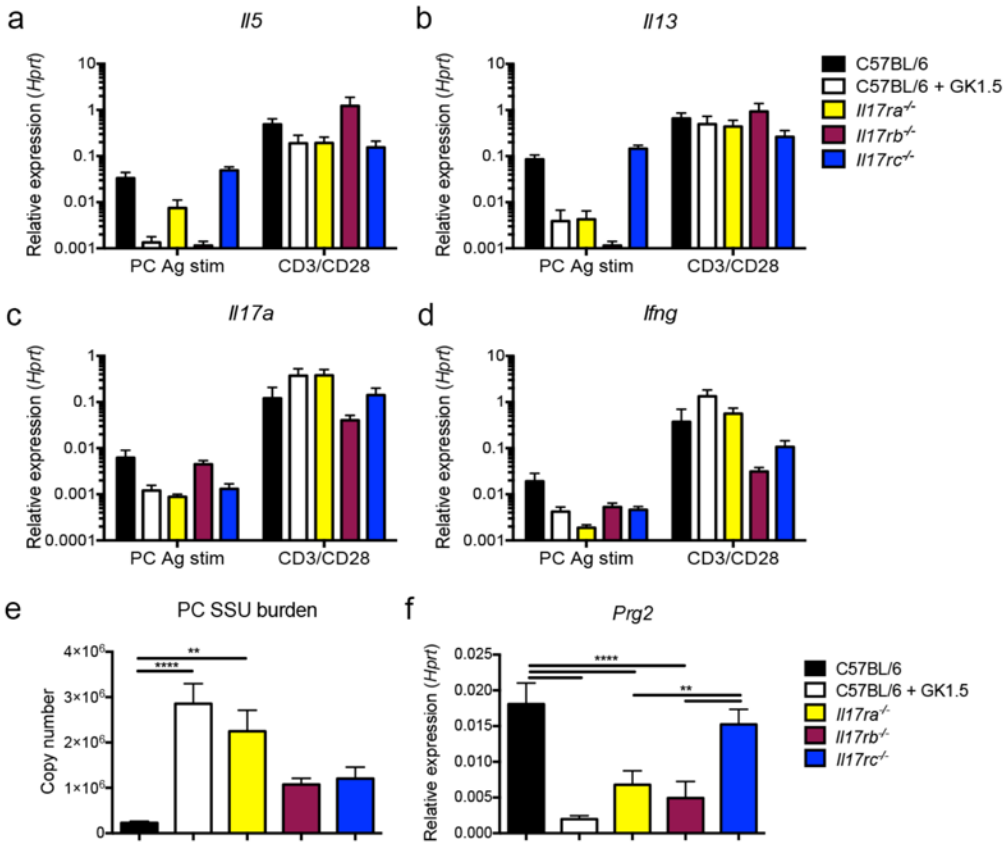

Figure 4-5. Defective *Pneumocystis* specific T-cell responses in *Il17ra*$^{-/-}$, *Il17rb*$^{-/-}$, and *Il7rc*$^{-/-}$ mice.

A-D.) Whole lung cells were isolated 14 days post-*Pneumocystis* infection from each genotype and were stimulated with either *Pneumocystis* antigen or CD3/CD28. Expression of *Il5*, *Il13*, *Il17a*, and *Ifng* was measured by qRT-PCR. E.) *Il17ra*$^{-/-}$ mice have increased *Pneumocystis* burden comparable to that of CD4-depleted animals, while *Il17rb*$^{-/-}$ and *Il17rc*$^{-/-}$ have a trend towards increased burden. F.) Eosinophil recruitment as measured by *Prg2* expression is diminished in *Il17ra*$^{-/-}$ and *Il17rb*$^{-/-}$ mice. ** $p<0.01$, **** $p<0.0001$ by one-way ANOVA with Tukey's multiple comparisons.

Strikingly, *Il17ra*$^{-/-}$ mice had *Pneumocystis* burden levels comparable to that of CD4-depleted mice, while both *Il17rb*$^{-/-}$ and *Il17rc*$^{-/-}$ had trends towards increased burden at day 14 post-infection (**Figure 4-5E**). As we have shown previously that eosinophils are protective in response to *Pneumocystis* (182), we next examined the expression of the eosinophil marker major basic protein (*Prg2*). Both *Il17ra*$^{-/-}$ and *Il17rb*$^{-/-}$ had significantly reduced expression of the eosinophil marker *Prg2* similar to that of CD4-depleted animals (**Figure 4-5F**). On the contrary, *Il17rc*$^{-/-}$ mice had similar eosinophil recruitment compared to C57BL/6 mice (**Figure 4-5F**). Eosinophils did not seem to actively participate in the formation of iBALT, as dblGATA1$^{-/-}$ mice formed lymphoid follicles and expressed *Cxcl13* in a manner similar to that of BALB/c controls (**Figure 4-6A**). Furthermore, in agreement with previously published data in a sterile *Pneumocystis* antigen model (231), the T-cell responses were unperturbed in dblGATA1$^{-/-}$ mice (**Figure 4-6B**).

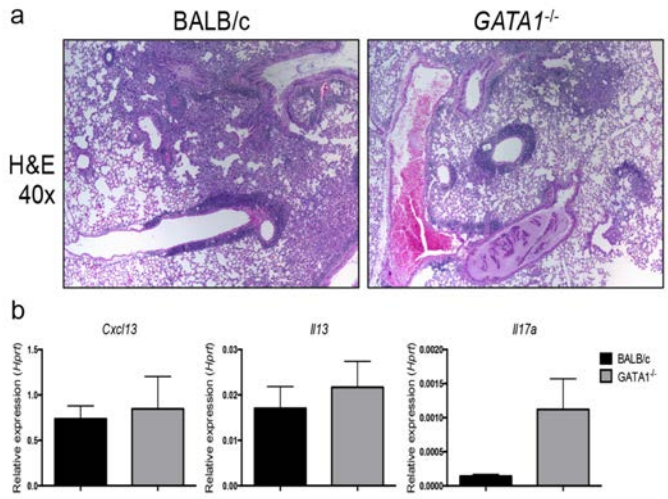

Figure 4-6. **Eosinophils are dispensable for *Pneumocystis* iBALT formation**.

A.) *Pneumocystis* dependent iBALT formation is present in both BALB/c and *GATA1*$^{-/-}$ mice fourteen days post-infection by H&E staining. B. *Cxcl13, Il13,* and *Il17a* expression is similar in BALB/c and *GATA1*$^{-/-}$ mice.

To confirm that these antigen-specific responses were CD4^{+} T-cell responses, we examined the nature of IL-17A and IL-13 producing cells early in *Pneumocystis* infection. Mice infected with *Pneumocystis* had significant increases in both IL-17A and IL-13 single-producing αβ T-cells compared to naïve controls (**Figures 4-7A-4-7C**). Furthermore, IL-17A and IL-13 double-producing cells also expanded following *Pneumocystis* infection (**Figure 4-7D**). γδ T-cells and ILCs, however, appeared to have unchanged production of IL-17A and IL-13 following *Pneumocystis* infection (**Figures 4-7A-4-7C**). Likewise, at day 14 post-infection, αβ CD4^{+} T-cells greatly outnumbered both innate lymphoid cells and γδ T-cells in the lungs (**Figure 4-7E**).

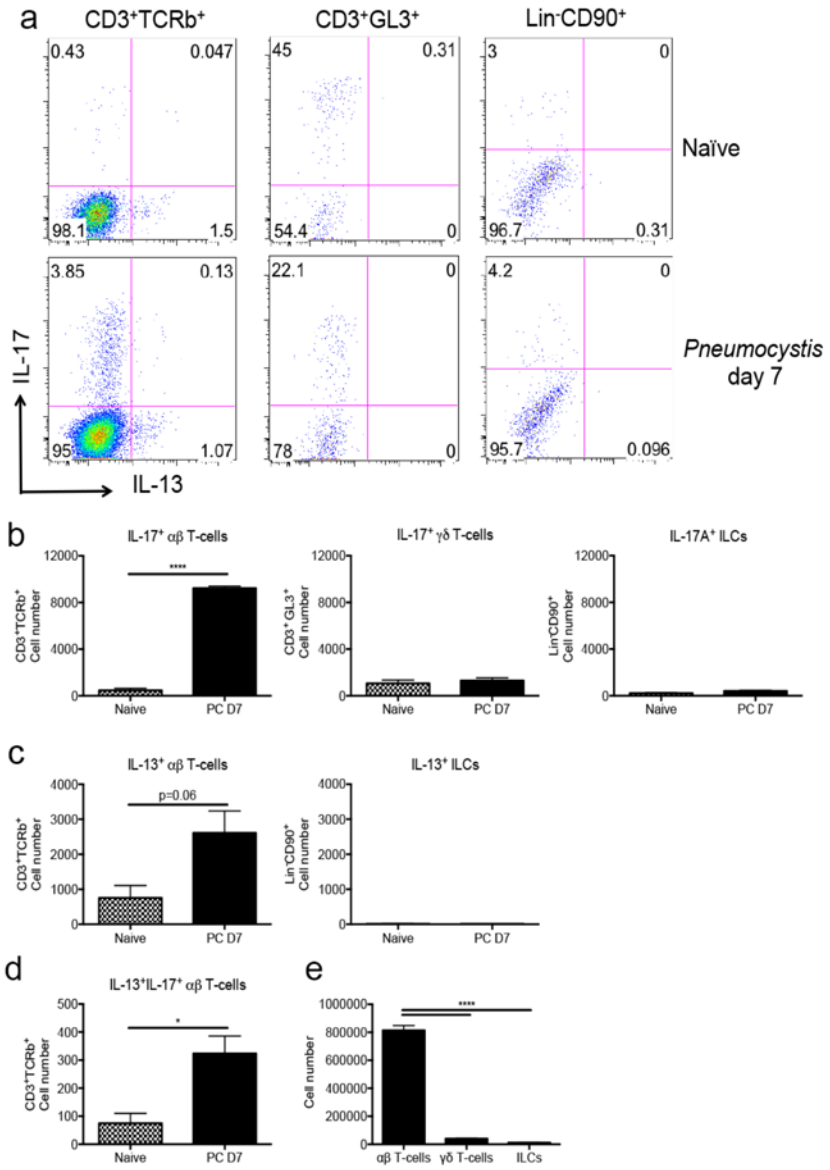

Figure 4-7. **αβ T-cells produce IL-17A and IL-13 following *Pneumocystis* infection**.

A.) Representative flow cytometry plot of IL-17A and IL-13 producing cells in naïve and *Pneumocystis* infected mice at day 7 post-infection. *Pneumocystis* infection results in expansion of $CD3^+TCRb^+$ cells expressing both IL-17A and IL-13, while no change was observed in the γδ T-cell ($GL3^+$) or ILC (Lin^-CD90^+) compartments. B.) Quantification of $IL\text{-}17A^+$ cells demonstrating expansion of αβ T-cells, but not γδ T-cells or ILCs. **** $p<0.0001$ by Student's T-test C.) Quantification of $IL\text{-}13^+$ cells demonstrating expansion of αβ T-cells but not ILCs. D.) αβ T-cells expressing both IL-13 and IL-17A were also expanded following *Pneumocystis* infection. * $p<0.05$ by Student's t-test. E.) αβ T-cells are the vast majority of cells present in the lung at day 14 post-*Pneumocystis* infection. **** $p<0.0001$ by one-way ANOVA with Tukey's multiple comparisons.

As both *Il17ra*$^{-/-}$ and *Il17rb*$^{-/-}$ mice had reduced antigen-specific Th2 responses and iBALT development, we next sought to confirm the role of IL-25 in iBALT formation. C57BL/6 mice were treated with an anti-IL25 monoclonal antibody, and at day 14 post-infection with *Pneumocystis*, anti-IL25 treatment reduced lung inflammation, as well as the structural organization of iBALT (**Figures 4-8A and 4-8B**). Both the size and total area of iBALT follicles were reduced following anti-IL25 treatment, while number of follicles was unchanged (**Figure 4-8C**).

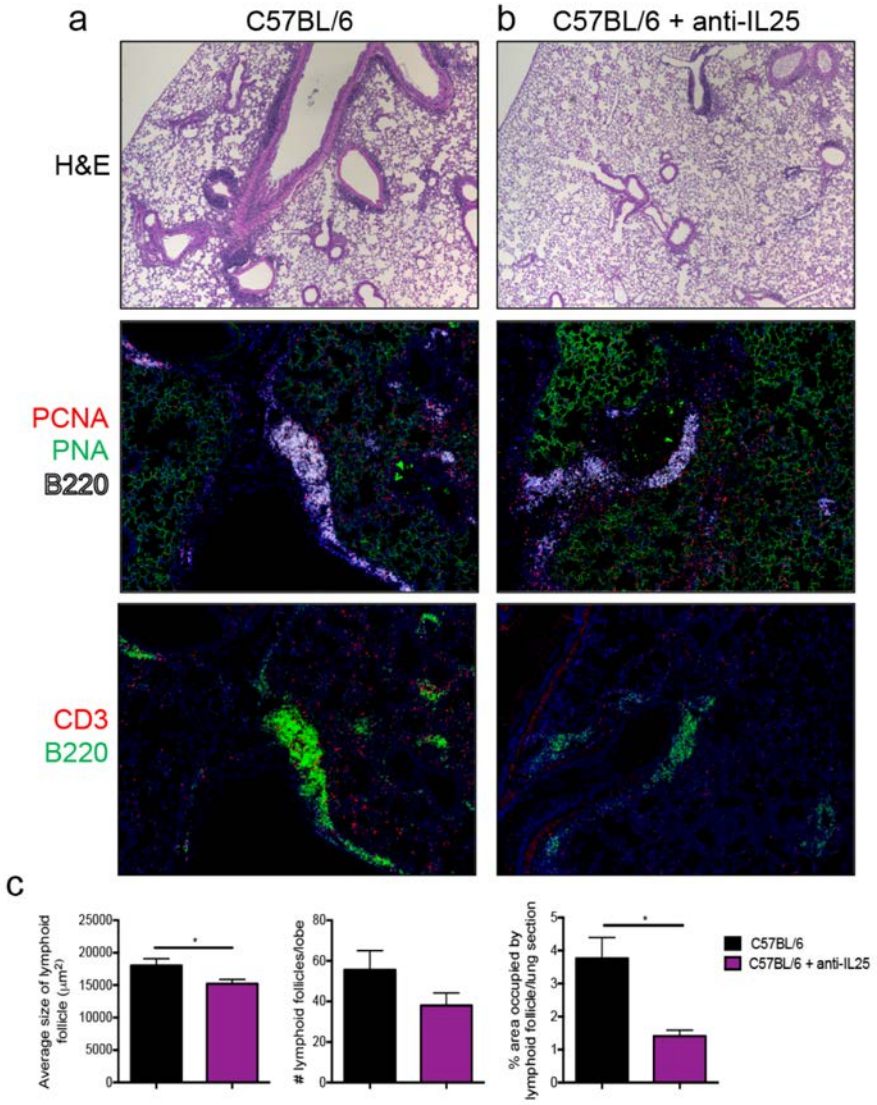

Figure 4-8. **Treatment with anti-IL25 antibody reduces *Pneumocystis* driven iBALT formation.**

A-B.) iBALT structures on H&E and immunofluorescent staining is reduced in C57BL/6 mice receiving anti-IL25 antibody compared to untreated C57BL/6 mice. C.) Quantification of iBALT structures demonstrates reduced size and area occupied in mice receiving anti-IL25 compared to untreated mice.

Altogether, these results suggest that *Il17ra*$^{-/-}$ and *Il17rb*$^{-/-}$ mice had defective Th2 priming and iBALT in part due to defective IL-25 signaling, while *Il17ra*$^{-/-}$ and *Il17rc*$^{-/-}$ mice

unsurprisingly have defective Th17 responses. Importantly, disruption of either the Th2 or Th17 responses alone was capable of reducing iBALT structures.

4.4.4 IL-13 and IL-17A synergistically induce *Cxcl13* expression

Formation of *Pneumocystis* iBALT is dependent on CXCL13 production, but surprisingly both mice lacking IL-17 signaling and Th2 cell polarization have defective *Cxcl13* expression. To assess the mechanism of *Cxcl13* induction, we first determined that the CXCL13 protein was localized to the center of the lymphoid follicles (**Figure 4-9A**). CXCL13 was undetectable in the airway epithelium and vascular endothelium (**Figure 4-9A**). Another known producer of CXCL13, $CD21^{+}CD35^{+}$FDC-$M1^{+}$ follicular dendritic cells, were also absent in the *Pneumocystis*-driven follicles (data not shown). These histologic findings suggest that a stromal cell, such a pulmonary fibroblast, was the primary cellular source of CXCL13.

Based on these data, we hypothesized that *Cxcl13* expression in pulmonary fibroblasts was being driven by IL-17 and/or the local Th2 response in the lung. Cultured primary pulmonary fibroblasts from adult mice responded to both IL-17A and IL-13 six hours following stimulation, as the respective conditions led to upregulation of *Cxcl1* and *Ccl11* (**Figure 4-9B**). However, *Cxcl13* was not induced six hours following stimulation with IL-17A, IL-13, or the combination of the two cytokines (**Figure 4-9B**). However, at 24 hours post-stimulation, *Cxcl13* was significantly upregulated in fibroblasts treated with both IL-17A and IL-13 compared to single stimulation controls (**Figure 4-9C**). *Cxcl1* induction at this time point had waned, while *Ccl11* expression remained high in IL-13 treated cells (**Figure 4-9C**).

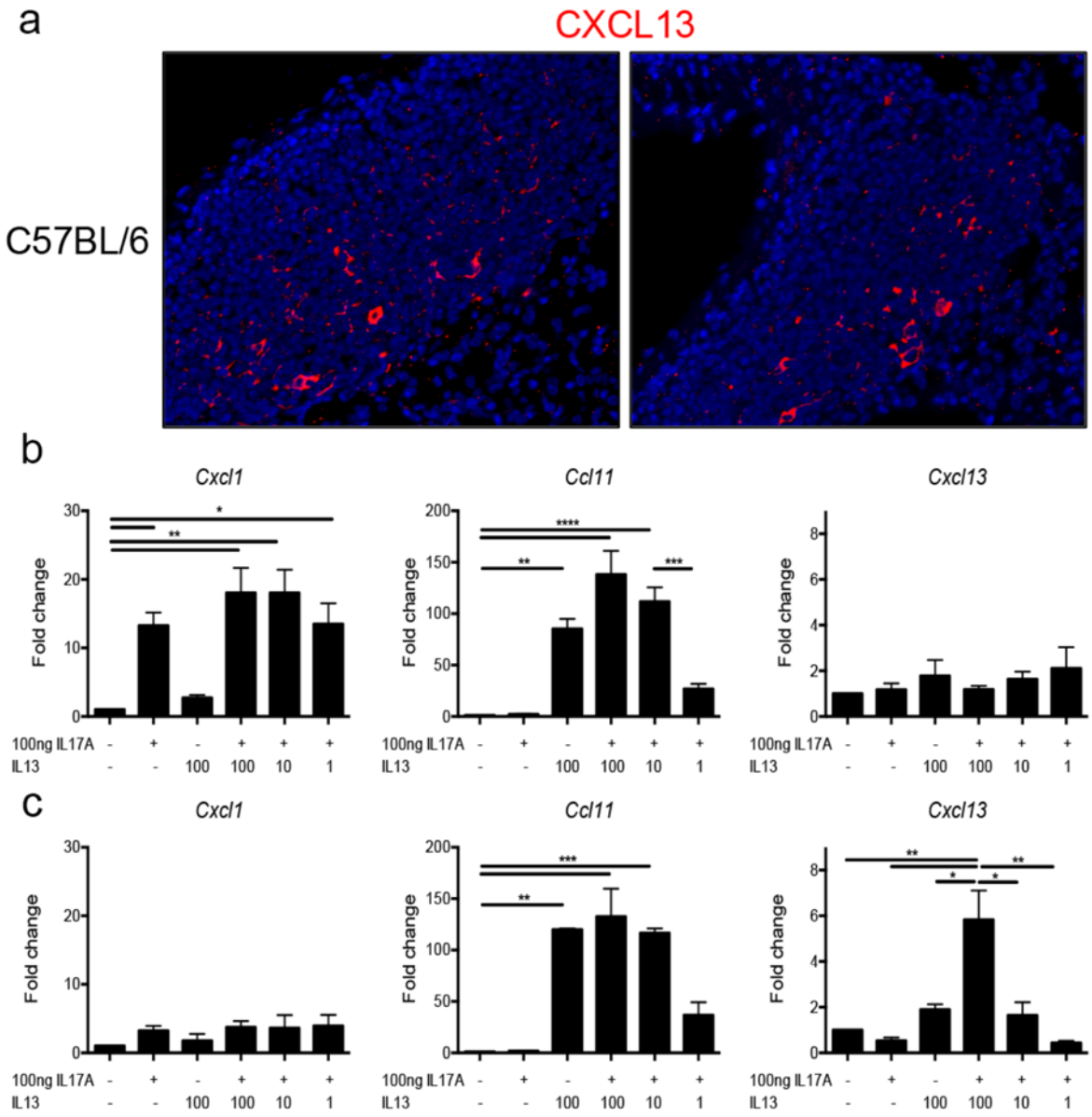

Figure 4-9. **IL-17A and IL-13 synergistically regulate *Cxcl13* expression in pulmonary fibroblasts.**

A.) Immunofluorescent staining demonstrates CXCL13 protein in a lymphoid follicle 14 days post-infection with *Pneumocystis*. B.) Pulmonary fibroblasts upregulate *Cxcl1* and *Ccl11* following a six hour stimulation with IL-17A and IL-13, respectively. *Cxcl13* expression is unchanged in all conditions at six hours post-stimulation C.) *Cxcl1* expression is reduced at 24 hours post-stimulation, while *Ccl11* expression persists. Stimulation with both IL-17A and IL-13 leads to upregulation of *Cxcl13* at 24 hours post-stimulation. * $p<0.05$, ** $p<0.01$, *** $p<0.001$, **** $p<0.0001$ by one-way ANOVA with Tukey's multiple comparisons.

The direct induction of *Cxcl1* by IL-17A coupled with the delayed induction of *Cxcl13*, led us to hypothesize an indirect effect of IL-17A was synergizing with IL-13. Stimulation of pulmonary fibroblasts with IL-17A for six hours induced a four-fold increase in IL-6 production (**Figure 4-10A**). Interestingly, IL-6 coupled with IL-13 induced similar levels of *Cxcl13* expression compared to IL-13 and IL-17A co-stimulated cells (**Figure 4-10B**). As IL-6 signaling leads to activation of STAT3 and IL-13 signaling leads to activation of GATA3 through STAT6, we next sought to determine if these transcription factors were required for *Cxcl13* induction. *Stat3*$^{fl/fl}$ and *Gata3*$^{fl/fl}$ fibroblasts were treated with adenovirus-Cre, followed by 24-hour stimulation with IL-6 and IL-13 (**Figure 4-10C**). Strikingly, *Cxcl13* expression was attenuated in both *Stat3*$^{fl/fl}$ and *Gata3*$^{fl/fl}$ fibroblasts, suggesting that both transcription factors are required.

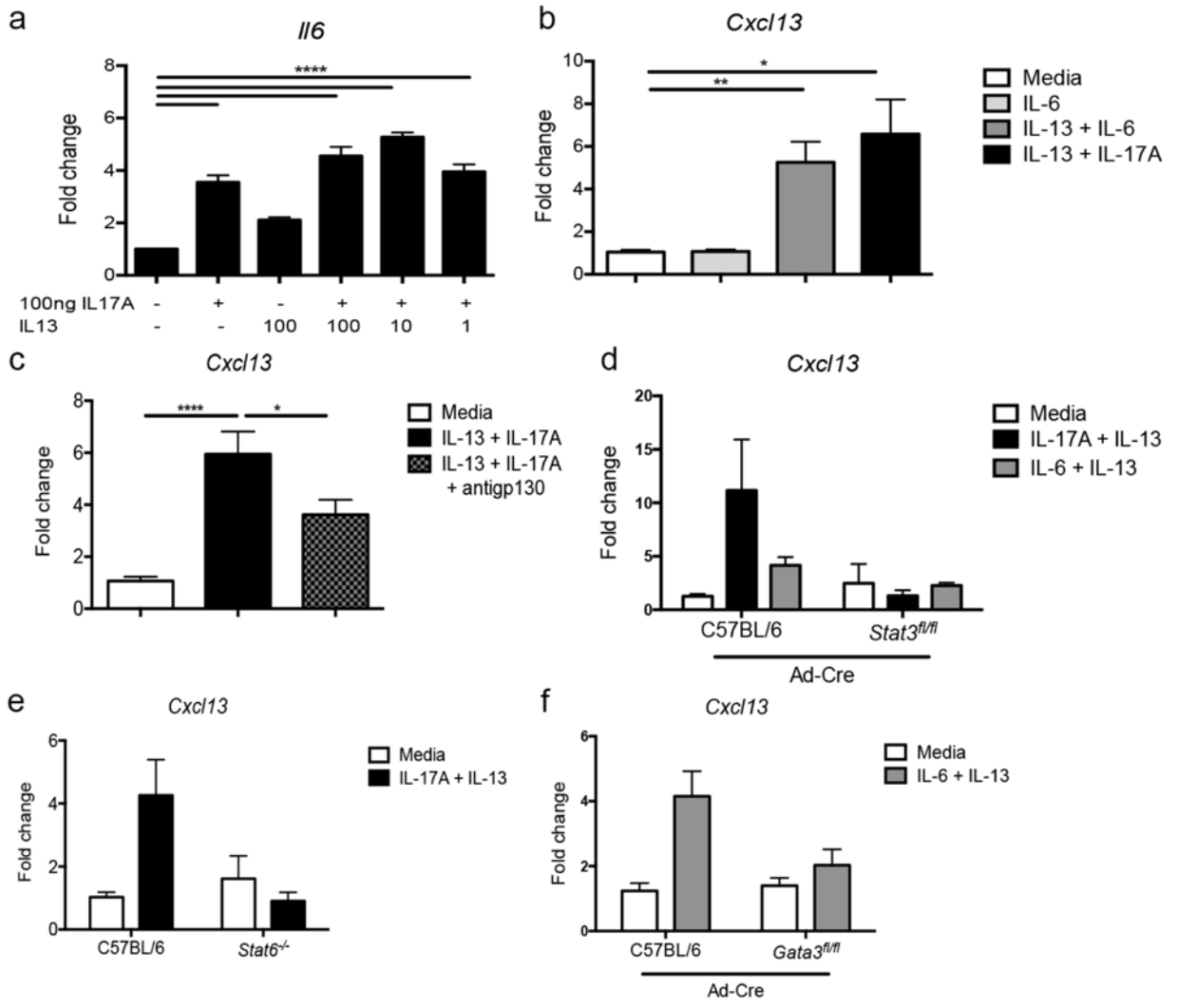

Figure 4-10. ***Cxcl13*** **expression is dependent on STAT3 and GATA3 activation**.

A.) Expression of *Il6* is upregulated in pulmonary fibroblasts following a six-hour stimulation with IL-17A (*n*=4). B.) *Cxcl13* is induced in pulmonary fibroblast by 24-hour stimulation with IL-13 in combination with either IL-6 or IL-17A (*n*=4-10). C.) *Cxcl13* upregulation is partially blocked by treatment with an anti-gp130 antibody (*n*=7-9). D.) *Cxcl13* expression is attenuated in pulmonary fibroblasts from *Stat3*$^{fl/fl}$ mice following *in vitro* treatment with adenovirus-Cre (*n*=4-12). E.) *Stat6*$^{-/-}$ fibroblasts fail to upregulate *Cxcl13* following stimulation with IL-17A and IL-13 (*n*=3-6). F.) *Cxcl13* expression is attenuated in pulmonary fibroblasts from *Gata3*$^{fl/fl}$ mice following *in vitro* treatment with adenovirus-Cre (*n*=3-4). Data are shown as mean ± standard error of the mean. * $p<0.05$, ** $p<0.01$, **** $p<0.0001$ by one-way ANOVA with Tukey's multiple comparisons.

4.5 DISCUSSION

The current study demonstrates that *Pneumocystis* infection via either oropharyngeal inoculation or natural transmission results in induction of CXCL13 and iBALT formation. Furthermore, the *Pneumocystis*-dependent iBALT structures required signaling through IL-17 family members for formation, and mice with either defective Th17 or Th2 responses failed to induce CXCL13 expression and develop iBALT. Finally, pulmonary fibroblasts from adult mice stimulated with both IL-17A and IL-13 synergistically upregulate CXCL13 expression in a STAT3- and GATA3-dependent manner.

Importantly, this study identifies a novel fungal pathogen capable of inducing iBALT. Previously studied models include bacterial (*Pseudomonas*) and viral (influenza, modified vaccinia virus Ankara (MVA)) infection and subtle differences have begun to emerge in iBALT formation depending on the pathogen of interest (213, 216, 234, 235). For example, *Pseudomonas* iBALT formation requires CXCL12-producing stromal cells, while MVA induces iBALT through a CXCL13-producing follicular dendritic cell dependent mechanism (234). Likewise, CXCL13 expression has been implicated in influenza-mediated iBALT formation (213, 215, 216). However, unlike MVA infection, CXCL13 expression in response to influenza is mediated primarily by a stromal, and not hematopoietic, source (215). Influenza mediated iBALT requires additional soluble factors, such as lymphotoxin-alpha, for development. Blockade of the receptor for lymphotoxin-alpha (LTβR) was sufficient to reduce influenza driven-iBALT and neonatal *Lta*$^{-/-}$ exposed to LPS and then influenza failed to develop iBALT (216, 220). *Pneumocystis*, on the other hand, requires CXCL13 signaling, but not lymphotoxin-alpha, for iBALT formation. These findings further highlight the need to study iBALT in a pathogen-specific manner, as differences in mechanism may arise from differences in pathogen.

Furthermore, despite the requirement for CXCL13 in both the neonatal LPS-influenza and *Pneumocystis* models, the mechanism of *Cxcl13* transcript induction appears to be different. Rangel-Moreno *et al*. elegantly demonstrated that neonatal pulmonary fibroblasts upregulate *Cxcl13* expression following stimulation with IL-17A (220). However, in adult pulmonary fibroblasts, IL-17A stimulation is not sufficient to upregulate *Cxcl13*. Surprisingly, IL-13 and IL-17A, products of the mixed Th2 and Th17 inflammatory response generated by *Pneumocystis,* potently induce *Cxcl13* expression in adult pulmonary fibroblasts. The mechanism of IL-13 and IL-17A synergy appears to be dependent on the hallmark downstream transcription factors, STAT3 and GATA3. These findings suggest that transcriptional regulation of *Cxcl13* is tightened over the course of development, perhaps through epigenetic modifications, or that neonatal fibroblasts have differing baseline activation of either STAT3 or GATA3.

The synergistic induction of *Cxcl13* highlights a unique aspect of *Pneumocystis* driven inflammation. Strikingly, mice lacking either IL-17A signaling (*Il17ra*$^{-/-}$ and *Il17rc*$^{-/-}$) or IL-25 signaling (*Il17ra*$^{-/-}$ and *Il17rb*$^{-/-}$) failed to upregulate *Cxcl13* and subsequently form iBALT. Although IL-17A signaling has previously been implicated in iBALT formation (220, 233), *Il17rb*$^{-/-}$ mice with intact IL-17A responses, but defective production of *Il5* and *Il13,* failed to form iBALT. Several studies in mice lacking Th2 cells (e.g. *Stat6*$^{-/-}$ and CD4-cre *Gata3*$^{fl/fl}$ mice) are pending and will be crucial in verifying the role of Th2 cells in the mechanism of iBALT formation. Importantly, IL-13 was produced solely by TCRβ^{+} cells and not ILC2s, further strengthening the role of Th2 cells in induction of *Cxcl13*. Together, these results demonstrate for the first time that Th2 responses can be required for iBALT formation.

While mechanistic studies in the murine model clearly indicate that natural transmission of *Pneumocystis* can induce iBALT, the incidence of iBALT formation in humans exposed to

Pneumocystis is unknown. Several key populations have been shown previously to develop iBALT: infants (222), and patients with COPD (218, 236), asthma (230), or pulmonary complications of rheumatoid arthritis (219). Importantly, colonization of *Pneumocystis* in all of these populations has been documented. Infants are nearly ubiquitously colonized with *Pneumocystis* by the age of 4 months; furthermore, *Pneumocystis* colonization in young children correlates with the increase in a mucus-associated gene, suggestive of a pathologic immune response (187, 188, 231). Likewise, patients with COPD and *Pneumocystis* have more severe disease and increases in proteases and inflammatory markers (68, 237, 238). While colonization has yet to be fully studied in asthma, a subset of patients with severe asthma have increased anti-*Pneumocystis* IgG and IgE antibodies, which correlates with worsened disease (231). Finally, patients with rheumatoid arthritis can have asymptomatic colonization of *Pneumocystis*, or depending on the therapeutic regimen, can become immunosuppressed enough to become susceptible to *Pneumocystis* pneumonia (239, 240). In all of these pathologic conditions, the correlation between *Pneumocystis* colonization or infection and iBALT formation is unknown. However, future studies examining the causality of *Pneumocystis* in iBALT formation in humans would be highly informative in supporting and/or validating the novel findings in a murine model of *Pneumocystis* exposure.

5.0 EVALUTATION OF THE *PNEUMOCYSTIS* KINOME: FROM INITIAL ANNOTATION TO DEVELOPMENT OF NOVEL ANTIFUNGAL THERAPEUTICS

Taylor Eddens[1], Teresa M. Buck[2], Zhiwei Feng[3], William T. Horne[1], Waleed Elsegeiny[1], Xiang-Qun Xie[3], Jeffrey L. Brodsky[2], Jay K. Kolls[1]*

[1]- Richard King Mellon Foundation Institute for Pediatric Research, Children's Hospital of Pittsburgh of UPMC, Pittsburgh, Pennsylvania, USA

[2]- Avinoff Chair of Biological Sciences, Department of Biological Sciences, University of Pittsburgh, Pittsburgh, Pennsylvania, USA

[3]- School of Pharmacy, University of Pittsburgh, Pittsburgh, Pennsylvania, USA

The data contained in this chapter is currently unpublished.

5.1 INTRODUCTION

As mentioned in Chapter 1, *Pneumocystis jirovecii* pneumonia remains one of the most common serious opportunistic infections in individuals with HIV/AIDS (1, 128, 241). *Pneumocystis* pneumonia mortality rates in the HIV-positive patients have remained largely unchanged over the past twenty years, despite the implementation of combined antiretroviral therapy in developed countries (2). Additionally, *Pneumocystis* infections are re-emerging in the clinical setting of immunosuppressive therapy for hematologic malignancy and post-transplantation rejection (13, 14). Alarmingly, HIV-negative patients with *Pneumocystis* pneumonia tend to have worse clinical outcomes, such as increased mechanical ventilation and mortality, when compared to HIV-positive patients (29).

The mainstay of treatment and prophylaxis for *Pneumocystis* is trimethoprim-sulfamethoxazole (TMP-SMX), which inhibits folate synthesis and *de novo* nucleic acid synthesis in microbial organisms (94, 242). Unfortunately, TMP-SMX has numerous side effects, which prove to be intolerable in up to 20% of patients, and TMP-SMX cannot be used in patients with sulfa allergies (94, 95). Second line agents, such as dapsone, are less effective and more toxic than TMP-SMX and tend to target similar microbial pathways (94, 95).

Of greater concern is the emergence of mutations in the *Pneumocystis* enzymes, dihydropteroate synthase (*Dhps*) and dihydrofolate reductase (*Dhfr*), targeted by TMP-SMX. Interestingly, the *Dhps* gene appears to be under greater selective pressure compared to the *Dhfr* gene. Out of a cohort of 37 patients, 16 had mutations in the *Dhps* gene compared to one synonymous substitution in the *Dhfr* gene (243) Interestingly, certain geographic areas, such as San Francisco, appear to have higher rates of resistant strains, suggestive of transmissibility of these *Dhps* mutant strains (244). In one recent observational clinical study, over 80% of patients

had detectable mutations in the *Dhps* gene and these patients had a greater likelihood of requiring mechanical ventilation and mortality (245). However, it is also worth noting that the majority of patients with *Dhps* mutations in this study survived despite TMP-SMX being utilized as the primary therapeutic agent, raising the question of the clinical relevance of these mutations clinically (245). Despite unclear clinical significance, *Saccharomyces cerevisiae* complemented with the mutated *Pneumocystis Dhps* gene clearly grow better in the presence of TMP/SMX (246). Although *Dhps* mutations are far more common, more recent studies are also finding evidence of mutations in the *Dhfr* gene that correlate with failure of TMP/SMX prophylaxis (247).

Given the challenge of using conventional therapies and the emerging risk of increased antimicrobial resistant *Pneumocystis* strains, discovery of novel therapeutic targets is imperative. Kinases are especially attractive candidates for rationale drug development, as these proteins are highly conserved and play important roles in proliferation, cellular signaling, and stress responses. One kinase family in particular, the phosphoinositide-3-kinase (PI3K) family, may be an attractive drug target, as these kinases mediate cell proliferation and survival, and as such, have been exploited in the development of recent anti-cancer therapeutics (248, 249).

Most antifungals utilized clinically target enzymes associated with cell wall or nucleic acid synthesis. To our knowledge, kinases have not been targeted clinically in fungal infections. However, *in vitro* studies are suggestive of a possible therapeutic effect of targeting kinases. One interesting study performed by De Souza *et al*. demonstrated that *Aspergillus nidulans* contained 128 kinases. The authors went on to characterize functional mutations for each kinase (250). Importantly, deletion of two VPS kinases (*vps34* and *vps15*) resulted in defective endosomal trafficking and *A. nidulans* growth arrest (250). In *S. cerevisiae*, deletion of VPS34 leads to

defective vacuolar sorting and decreased growth at high temperature or in high salt (251). The drastic effects of VPS34 deletion have been attributed to the dual roles of VPS34 as both a protein kinase and a PI3K (252). VPS34 appears to be a highly conserved protein throughout evolution, and orthologs of the fungal VPS34 proteins are present in mammals (253). Recently, the VPS34 protein from *Drosophila* was crystallized and the structure of the binding pockets were mapped (254, 255).

5.2 RATIONALE AND HYPOTHESIS

Given the use of anti-kinase therapeutics used clinically, we hypothesized that the *Pneumocystis* kinome may be targeted for the development of anti-fungal compounds. To test this hypothesis, we utilized a top-down approach, beginning with genome annotation and ultimately leading to selection of a viable druggable target (**Figure 5-1**).

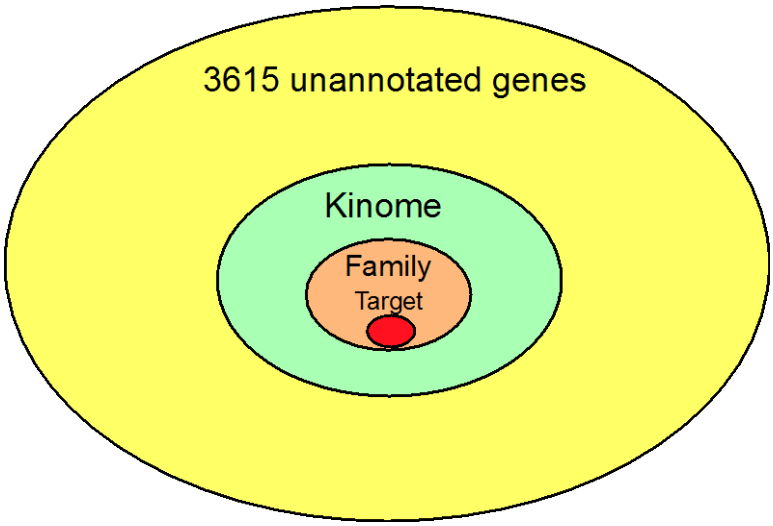

Figure 5-1. Top-down approach to identifying targets within the kinome to target pharmaceutically.

5.3 METHODS

Pneumocystis kinome annotation and characterization

A collection of all hypothetical *Pneumocystis murina* proteins was downloaded from the Broad Institute *Pneumocystis* sequencing project. Each hypothetical protein was analyzed using the NCBI Blast algorithm and the closest annotated ortholog to each protein was recorded. Every *Pneumocystis* protein with a predicted kinase function or domain was then aligned using Clustal Omega Alignment algorithms and a phylogenetic tree was created using MEGA5 software using the Maximum Likelihood method based on the JTT matrix-based model. Each kinase was then analyzed again with NCBI Blast restricted to the following taxa: *Pneumocystis* (taxid: 4753), *Saccharomyces cerevisiae* (taxid: 4932), *Schizosaccharomyces pombe* (taxid: 4896). Percent identity and e-value were then recorded. This process was repeated for all identifiable cyclins and major surface glycoproteins within the *Pneumocystis murina* genome and 50 randomly selected non-kinase *Pneumocystis murina* genes.

Pneumocystis murina time course

All animal procedures were approved by the University of Pittsburgh Institutional Care and Use Committee. Ten C57Bl/6 female mice were CD4-depleted using GK1.5 monoclonal antibody as previously described (83, 123, 182) and were subsequently challenged with 2.0 x 10^6/mL *Pneumocystis murina* cysts using oropharyngeal inoculation. Ten C57Bl/6 female mice were inoculated at the same time, but were not CD4-depleted. Five mice from each group were then sacrificed at day 10 and day 14, and lung RNA was purified using Trizol® Reagent (Life Technologies). Briefly, lungs were homogenized and following the addition of chloroform, RNA in the aqueous phase was collected and precipitated in isopropanol. Following centrifugation, the

RNA was washed with 75% ethanol, centrifuged again, and then resuspended in nuclease-free water. Following incubation at 55°, RNA was quantified using a Nanodrop and 1 μg of RNA was converted to cDNA using iScript™ cDNA synthesis kit per manufacturer's instructions (Bio-Rad). *Pneumocystis* burden was then quantified using SsoAdvanced qRT-PCR universal probes supermix (Bio-Rad) as well as primers and a probe specific for *Pneumocystis murina* large subunit (LSU) rRNA with a standard curve of known *Pneumocystis* LSU rRNA concentrations. Prior to sequencing, the RNA was further purified using a Qiagen RNA cleanup kit with DNAse treatment. An Aglient assessment of RNA purity was performed with an Agilent Tape Station 2200.

RNA sequencing

RNA sequencing was performed as described in Chapter 2. Following sequencing, the samples were aligned to the *Pneumocystis murina* genome using Genesifter. For the adult case of *Pneumocystis* pneumonia, .fastq files were downloaded and aligned to the *Pneumocystis jirovecii* genome (256).

VPS34 cloning

Pneumocystis murina VPS34 was cloned from the cDNA above using Phusion High-fidelity polymerase (Thermo-Scientific). VPS34 *Pneumocystis murina* primers: Forward- 5'-CACCATGGGAAATTCTACATATTCTTTTTGTACTTCATCTCAACTAC; Reverse- 5'-AAAGTCGACTCAGCTTCTCCAATATTGTGCGATATTATGAACTC. VPS34 from *S. cerevisiae* was cloned from genomic DNA using the following primers: Forward- 5'-CACCATGTCACTGAACAACATAACATTCTGTGTCTC; Reverse- 5'-

AAAGTCGACTCAGGTCCGCCAGTATTGTGCCAGATTATGTAAATG. Overlap extension PCR was performed to create the domain mutants. Briefly, the 5' *S. cerevisiae* forward primer and the 3' *P. murina* reverse primer were used. For the HC mutant, the domains were cloned using the overlapping primers: Reverse in the *S. cerevisiae* domain 5'- GTTAGGTTTTAGCTCTCTGTCCAAGTTTGCATTTTTAGATGC and Forward in the *P. murina* domain 5'- GCATCTAAAAATGCAAACTTGGACAGAGAGCTAAAACCTAAC. For the C mutant, the following primers were used: Reverse in the *S. cerevisiae* domain 5'- GCCAGCAATTCTGCCTGTCTTTGATCGTTCAGTATATTC and Forward in the *P. murina* domain 5'- GAATATACTGAACGATCAAAGACAGGCAGAATTGCTGGC. Once the two domains were cloned, the samples were ligated and amplified using a 30-cycle PCR reaction with Phusion polymerase. PCR products were gel purified using a QIAQuick Gel extraction kit (Qiagen) per manufacturer's protocol. Purified PCR products were inserted into pENTR™/D-TOPO® vector following manufacturer's instructions (Life Technologies). Briefly, the pENTR™/D-TOPO® vector was incubated with PCR product in a salt buffer for 30 minutes, followed by transformation with One Shot® Max Efficiency® DH5α™ competent cells and overnight growth at 37°. Colonies were selected and 5 mL starter cultures were prepared following overnight growth using a QIAprep Spin Miniprep Kit (Qiagen) per manufacturer's protocol. The indentity of the insert was then confirmed by M13 PCR screen and by sequencing (GENEWIZ®). The domain mutants were then inserted into pYES-DEST52 destination vector using an LR Recombination reaction. Following isolation of vector from starter cultures (QIAprep) the products were again verified via PCR and sequencing.

Δvps34 growth rescue

To transform yeast, wild-type and *Δvps34* strains of *S. cerevisiae* were grown overnight at 30° in yeast extract peptone dextrose (YPD) media. The cultures were then pelleted and resuspended in 5 mL of YPD. The cultures were then incubated at 30° for 4 hours prior to centrifugation for 3 mins at 3000 rpm. Cells were resuspended in 5mL of distilled water, centrifuged, and resuspended in 5 mL of 1x Te/LiAc buffer. Following centrifugation, pellets were resuspended in 1.1 mL of 1x Te/LiAc buffer and incubated for one hour at room temperature. Ten μL of sonicated salmon sperm DNA and approximately one μg of each vector (VPS34 or control) were added and cells were incubated at room temperature for 30 minutes. Following incubation, 750 μL of 9:1 PEG:10xTe/LiAc was added to each tube, followed by a 30 minute incubation at room temperature, and a ten minute incubation at 42°. Cells were spun at 5000 rpm for 2 minutes, decanted, and resuspended in appropriate selection media, plated, and grown overnight at 30°. Following initial colony selection, each strain was grown at 26°, 30°, and 37°.

Pneumocystis killing assay

Pneumocystis murina was purified from a frozen *Rag2*$^{-/-}$*Il2rg*$^{-/-}$ double knockout lung, resuspended to a final concentration of 2.0 x 10^6 cysts/mL in PBS, and 1.0 x 10^5 cysts were added to a 96-well plate. Fifty μL of 20 μM stock compounds in PBS were added to each well. Equivalent quantities of *Pneumocystis murina* input were harvested at the time of plating, while the remainder of the wells were incubated for 24 hours at 37°. RNA was isolated using Trizol® LS Reagent as described above.

In silico modeling of VPS34

The crystal structure of the *Drosophila* VPS34 protein was downloaded from NCBI Structure Summary (MMDB). Using MacPyMOL software, the catalytic subunits of the *Pneumocystis* VPS34 was modeled using the *Drosophila* VPS34 as a scaffold. After building the model, individual amino acids, as well as three-dimensional rendering, were performed on MacPyMOL software suite. Analysis of the chemical library of Dr. Xie was performed in the Xie lab as previously described.

5.4 RESULTS

5.4.1 Initial characterization of the *Pneumocystis murina* kinome

One hurdle to compiling and characterizing the *Pneumocystis murina* kinome is the fact that the recently released genome remains largely unannotated (**Figure 5-2**).

A

PNEG_01183	hypothetical protein
PNEG_01184	hypothetical protein
PNEG_01185	hypothetical protein
PNEG_01186	hypothetical protein
PNEG_01187	hypothetical protein
PNEG_01188	hypothetical protein
PNEG_01189	hypothetical protein
PNEG_01190	hypothetical protein
PNEG_01191	hypothetical protein
PNEG_01192	hypothetical protein
PNEG_01193	hypothetical protein
PNEG_01194	phenylalanyl-tRNA synthetase, beta subunit
PNEG_01195	hypothetical protein
PNEG_01196	hypothetical protein
PNEG_01197	hypothetical protein
PNEG_01198	hypothetical protein
PNEG_01199	hypothetical protein
PNEG_01200	hypothetical protein
PNEG_01201	hypothetical protein
PNEG_01202	hypothetical protein
PNEG_01203	hypothetical protein
PNEG_01204	translation elongation factor EF-1, subunit alpha
PNEG_01205	hypothetical protein
PNEG_01206	hypothetical protein
PNEG_01207	hypothetical protein
PNEG_01208	unnamed protein product *C
PNEG_01209	hypothetical protein
PNEG_01210	hypothetical protein

B

PNEG_01183	conserved hypothetical protein *C
PNEG_01184	ATP synthase subunit 4 *C
PNEG_01185	CBF/Mak21 family protein *C
PNEG_01186	40S ribosomal protein S12-B
PNEG_01187	3-oxo-5-alpha-steroid 4-dehydrogenase, C-terminal
PNEG_01188	mediator complex subunit Med15
PNEG_01189	unknown hypothetical protein
PNEG_01190	solute carrier family 35 member F1
PNEG_01191	Similar to WD repeat-containing protein
PNEG_01192	rRNA-processing protein
PNEG_01193	GLG1/glycogen synthesis initiator (glycogenin) *C
PNEG_01194	phenylalanyl-tRNA synthetase, beta subunit *C
PNEG_01195	phosphatase PP2A regulatory subunit A *C
PNEG_01196	Similar to Ankyrin repeat-containing protein *C
PNEG_01197	DNA-directed RNA polymerase subunit *C
PNEG_01198	60S ribosomal protein L16 *C
PNEG_01199	conserved hypothetical protein *C
PNEG_01200	protein efr3 *C
PNEG_01201	Similar to Protein sls1 *C
PNEG_01202	methyltransferase involved in endocytosis *C
PNEG_01203	Vid24 family protein *C
PNEG_01204	translation elongation factor EF-1, subunit alpha *C
PNEG_01205	Uridine diphosphate-N-acetylglucosamine transporter Hut1 *C
PNEG_01206	MAPK phosphatase PMP1 *C
PNEG_01207	unnamed protein product *C
PNEG_01208	unnamed protein product *C
PNEG_01209	GTP binding protein
PNEG_01210	PXA domain-containing protein

Figure 5-2. Annotation of the *Pneumocystis murina* genome.

A.) Representative image of the original annotation of the 3615 hypothetical proteins within the Broad Institute *Pneumocystis murina* genome. B.) Following NCBI Blast analysis for each individual hypothetical protein, the *Pneumocystis* genome was fully annotated.

To annotate the kinome, we analyzed each of the 3615 hypothetical proteins in the Broad Institute *Pneumocystis murina* genome using the NCBI BLAST algorithm. Each *Pneumocystis murina* protein was compared to orthologues in similar fungal species (e.g. *Schizosaccharomyces pombe, Saccharomyces cerevisiae, Aspergillus nidulans, etc*.) and a gene name for each protein was recorded.

Upon annotation of the *Pneumocystis murina* genome, a total of 120 kinases were identified and further evaluated (**table not included due to size**). Using the NCBI BLAST algorithm, each kinase was characterized for percent identity and E-value (NCBI's measure of

homology) when compared to *Pneumocystis jirovecii*, *S. pombe*, and *S. cerevisiae*. Each *Pneumocystis* kinase protein sequence was aligned using Clustal Omega alignment algorithms and the evolutionary history of these kinases was detailed using MEGA5 software **(Figure 5-3)**. Importantly, several conserved kinase families that have been well studied in model organisms were clustered together using these methods. Nineteen CMGC kinases (cyclin-dependent, mitogen-activated, glycogen synthase, and cyclin-dependent protein kinase-like kinases) were found in 3 clusters, while 10 CAMK kinases (Ca^{2+}/calmodulin-dependent protein kinases), 9 AGC kinases (protein kinase A, G, or C), and 10 STE kinases (sterile kinases) clustered with their related kinase family members. Interestingly, 12 PIKK kinases (phosphoinositide-3-kinases (PI3K) and PI3K-like kinases) resided in the genome, but these proteins seemed more scattered throughout the evolutionary tree when compared to the other protein kinase families.

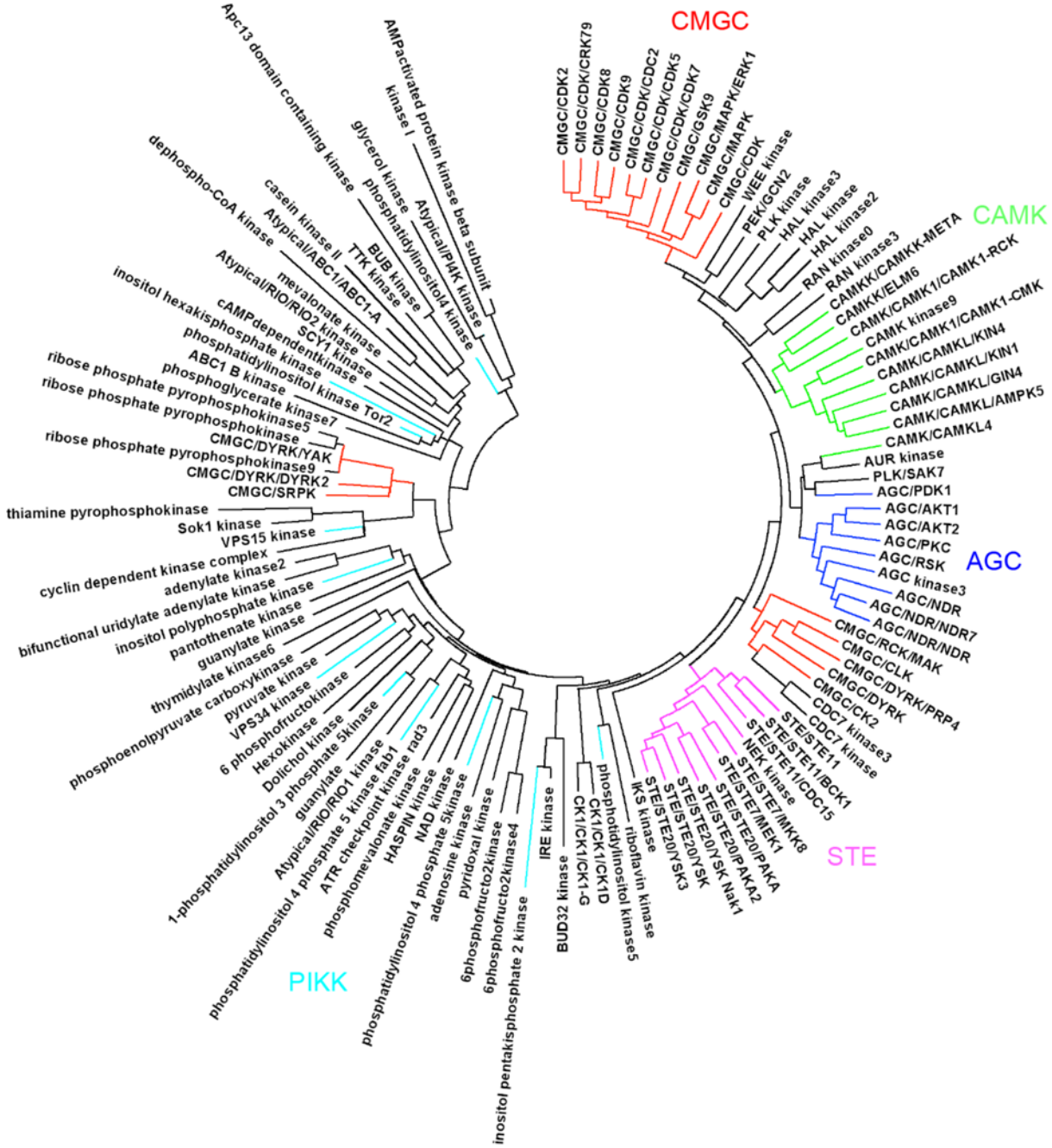

Figure 5-3. Molecular Phylogenetic analysis of the *Pneumocystis* kinome.

Clustal Omega was used to align the 119 predicted kinases in the *Pneumocystis murina* genome and the evolutionary history was inferred by using the Maximum Likelihood method based on the JTT matrix-based model (257). The tree with the highest log likelihood is shown. The tree is drawn to scale, with branch lengths measured in the number of substitutions per site. Evolutionary analyses were conducted in MEGA5 (258). Individual protein kinase families (CMGC, CAMK, AGC, STE, and PIKK) are colored.

To establish the level of conservation for the entire kinome, we compared the *Pneumocystis murina* kinome to *Pneumocystis jirovecii, S. pombe,* and *S. cerevisiae* to see how conserved each kinase was in relation to its ortholog in those species. On average, kinases between *Pneumocystis murina* and *Pneumocystis jirovecii* had 72.8% identity, while these same kinase were less conserved between *Pneumocystis murina* and *S. pombe* (49.9% identical) and *S. cerevisiae* (45.8%) **(Figure 5-4A)**. A similar trend was noted with each E-value, a more comprehensive measure of conservation, as kinases were highly conserved between *Pneumocystis murina* and *Pneumocystis jirovecii* **(Figure 5-4B)**.

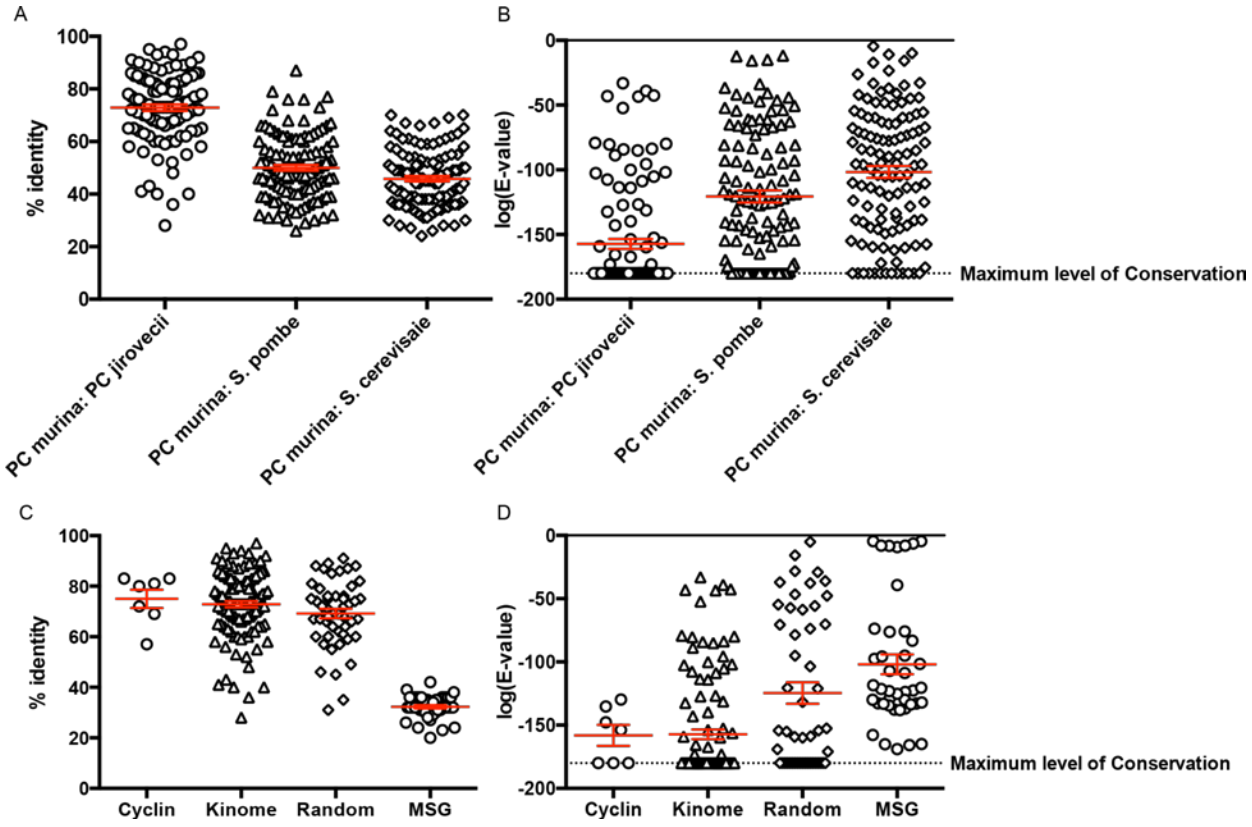

Figure 5-4. The *Pneumocystis* kinome is conserved between fungal species and in comparison to other protein families.

The percent identity (A) and E-value (B, shown in log scale) were calculated for each predicted kinase in comparison to *Pneumocystis jirovecii*, *S. cerevisiae*, and *S. pombe*, with an e-value of -180 representing the maximum level of conservation. The identity (C) and E-value (D) of each *P. murina* kinase, cyclin family member, major surface glycoprotein family member, and fifty genes selected at random were calculated in relation to *P. jirovecii.*

Along with examining the conservation between other genera and species, we sought to characterize how conserved the kinome was in relation to other protein families between *Pneumocystis murina* and *Pneumocystis jirovecii*. Cyclins, a protein family known to have a high degree of conservation (259), and the kinome had similar means of percent identity (75% vs.

72.8%) and E-values (-158 vs. -157.2) **(Figures 5-4C and 5-4D)**. The kinome also appears to be more conserved in comparison to other genes; 50 non-kinase genes selected at random had lower percent identities and E-values when compared to the kinome. Finally, there is a unique gene family within *Pneumocystis,* known as the major surface glycoprotein family, which tends to be more divergent and undergo genetic variation. Interestingly, these MSG proteins were less conserved than randomly chosen genes and the kinome.

After characterizing the kinome as a whole, we next sought to determine if a particular protein kinase family was more conserved, as a member of such a family might be a therapeutic target. Importantly, the CAMK, AGC, PIKK, CMGC, and STE kinases were all similarly conserved with the majority of the kinases in each family demonstrating high conservation by E-value **(Figures 5-5A and 5-5B)**. Similar to the kinome as a whole, these results suggest that individual protein kinase families share a high level of conservation.

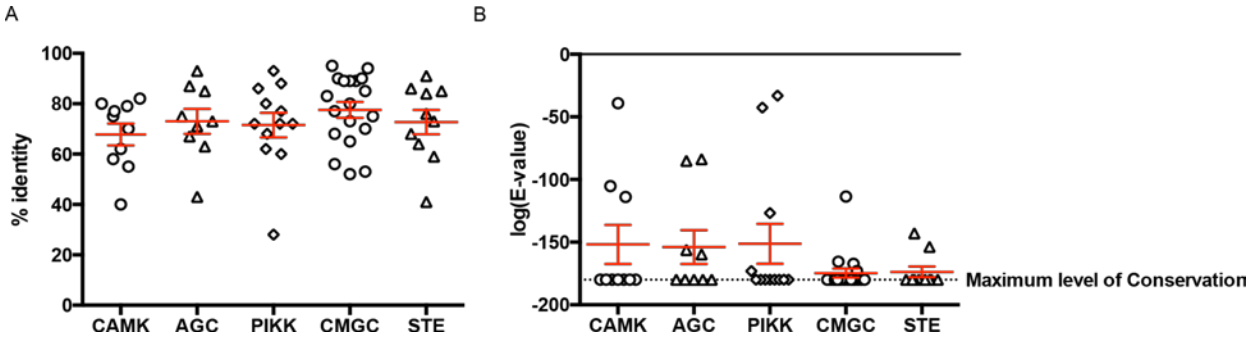

Figure 5-5. Kinase families are conserved within the *Pneumocystis* kinome.

Percent identity (A) and E-value (B, shown in log scale) of each *Pneumocystis murina* kinase within the CAMK, AGC, PIKK, CMGC, and STE kinase families when compared to the ortholog within the *Pneumocystis jirovecii* genome. An E-value of -180 represents the maximum level of conservation.

5.4.2 The *Pneumocystis* kinome is expressed during murine and clinical infection

To better select potential therapeutic targets, we next sought to assess the expression of each kinase in several different models of *Pneumocystis* infection. First, we examined the kinome expression profile in the lung 10 and 14 days following infection with *Pneumocystis murina* in both wild-type (WT) and CD4-depleted mice treated with GK1.5 monoclonal antibody (**Figure 5-6A**). *Pneumocystis* burden is similar in WT and GK1.5-treated mice at day 10 (**Figure 5-6B**). However, in CD4-depleted mice, several kinases from a variety of families are more highly expressed than in WT controls. Similarly, at day 14 when *Pneumocystis* burdens are divergent, there is a cluster of kinases that are more highly expressed in CD4-depleted mice. Strikingly, there are also kinases that are expressed at higher quantities in WT mice at day 10, suggesting that the transcriptome of *Pneumocystis* may be altered when challenged with an immune response. There are also patterns that appear independent of CD4-status, as two groups of kinases are more highly expressed at day 10 and day 14 regardless of GK1.5 treatment. Taken together, these data suggest that the kinome is dynamically expressed over the course of infection and may be sensitive to immune pressure.

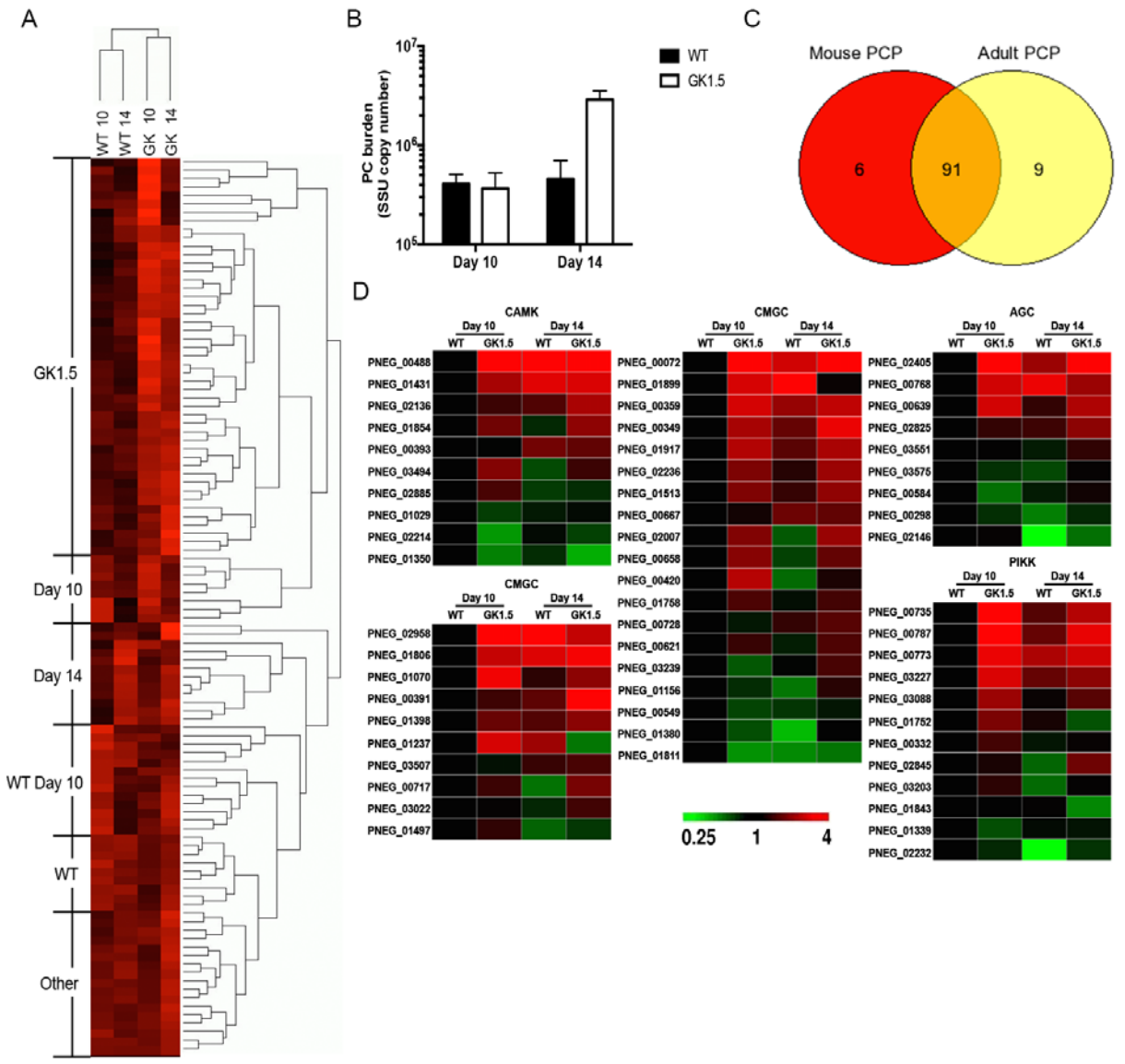

Figure 5-6. The *Pneumocystis* kinome is expressed during models of infection and during clinical infection.

A.) Expression map of the *Pneumocystis* kinome at 10 and 14 days following infection in GK1.5 treated CD4-depleted vs. wild type mice. B.) *Pneumocystis* burden of wild type and GK1.5 treated mice at days 10 and 14 as measured by qRT-PCR. C.) Venn diagram demonstrating overlap in kinase expression during a murine model of *Pneumocystis* infection and a patient with clinical *Pneumocystis* infection. D.) Expression of each kinase in the CAMK, CMGC, STE, AGC, and PIKK families during the course of infection in wild type (WT) and GK1.5 treated mice at day 10 and day 14 post-infection.

We next sought to determine if the expression of the *Pneumocystis* kinome could be detected in a patient with fulminant *Pneumocystis* pneumonia secondary to immunosuppressive drug therapies for chronic lymphocytic leukemia (256). Out of the 97 kinases expressed in murine infection, 91 were also expressed in this patient with *Pneumocystis* pneumonia (**Figure 5-6C**). Interestingly, nine kinases were uniquely expressed in this patient compared to the murine model of infection.

Given the abundance of kinases expressed during both murine and clinical infection, we again looked at individual kinase families to identify possible expression patterns (**Figure 5-6D**). Again, there was heterogeneity in terms of expression depending on the immune status and day of infection within protein kinase families. Interestingly, there appeared to be very few kinases that were expressed evenly despite immune pressure or status of infection. One PIKK family member, VPS34, a class III PIKK family member, was highly expressed in wild type and CD4-depleted animals at all four time points. Class I and class II kinases within the PIKK family have multiple different proteins, suggesting that there may be redundancy among the classes. As VPS34 represents the single class III PIKK family member, we hypothesized that this may be a viable drug target with little compensatory mechanisms in *Pneumocystis*. Furthermore, VPS34 is highly conserved among fungal species, suggestive of a critical function (**Table 5-1**). Finally, the *Drosophila* VPS34 protein structure has recently been crystallized, which can be used as a template for accurate *in silico* modeling.

Table 5-1. **Bioinformatic analysis of the conservation of VPS34 between species.**

Predicted kinase name	PNEG name	PNEJI name	% homology between *murina* and jirovecii (E-value)	*S. cerevisiae* homologue	% homology between *murina* and *cerevisiae* (E-value)	*S. pombe* homologue	% homology between *murina* and *pombe* (E-value)
VPS34 protein kinase	PNEG_03203	PNEJI1_000867	80% (0.0)	Vps34p	40% (0.0)	NP_594699.1	50% (0.0)

5.4.3 Evaluation of VPS34 as a therapeutic target

Based on the data presented above, we next sought to evaluate the function and druggability of the *Pneumocystis* VPS34 protein by complementing *Δvps34 S. cerevisiae* strains. Several attempts to express the full length *Pneumocystis* VPS34 were unsuccessful in *Δvps34 S. cerevisiae* despite the expression vector and transformation system working sufficiently for other *Pneumocystis* proteins. Interestingly, we hypothesized that lack of expression may have been due to missing regulatory elements in the *Pneumocystis* gene. Closer analysis of the VPS34 locus in *S. cerevisiae* indicated two large regions of amino acid sequences that were absent in both the *Pneumocystis murina* and *Pneumocystis jirovecii* genes (**Figure 5-7A**). However, the majority of residues were conserved in the 3' catalytic domain of VPS34 across species (**Figure 5-7A**). To circumvent the inability to express the full length *Pneumocystis* VPS34, we designed domain mutants (**Figure 5-7B**). The HC mutant contained the 5' N-terminal domain from *S. cerevisiae* and the helical and catalytic domains from *Pneumocystis*. The C mutant contained only the catalytic domain from *Pneumocystis* VPS34. These constructs are fully cloned and sequenced, and complementation studies in *Δvps34 S. cerevisiae* are underway. Prior to complementation with the various *Pneumocystis* constructs, we optimized the expression system by transforming

Δvps34 S. cerevisiae with the full length VPS34 from *S. cerevisiae* (**Figure 5-7C**). Adding back VPS34 in this system rescued the growth defect of *Δvps34* at 37°C (**Figure 5-7C**).

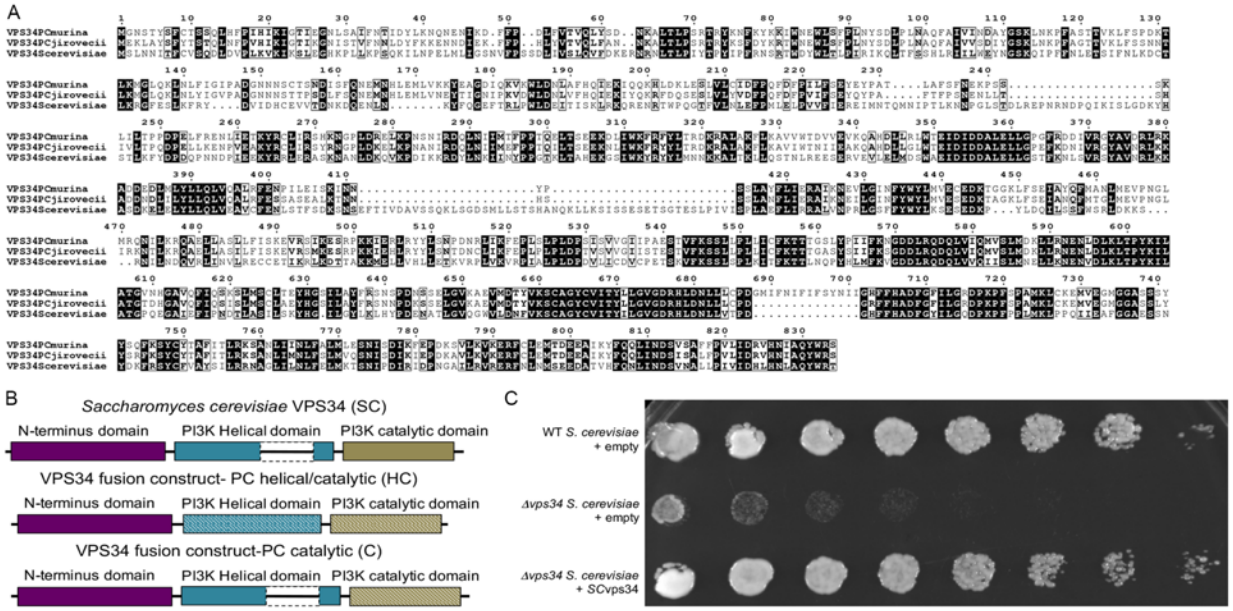

Figure 5-7. **Schematic for complementation of *Pneumocystis* VPS34 in *Δvps34 S. cerevisiae.***

A.) Alignment of VPS34 amino acid sequences from *P. murina*, *P. jirovecii*, and *S. cerevisiae* showing two large amino acid segments missing in the *Pneumocystis* sequences B.) Schematic of fusion proteins containing either both the helical and catalytic domains from *Pneumocystis* (middle) or the catalytic domain alone (lower). C.) Optimization of the VPS34 expression system in *Δvps34 S. cerevisiae* showing rescue of the growth defect with full length VPS34 from *S. cerevisiae*.

While *in vitro* studies to examine the function of *Pneumocystis* VPS34 were underway, we next sought to determine the druggability of *Pneumocystis* VPS34 via *in silico* analysis. The catalytic domain of *Pneumocystis* VPS34 was modeled using the crystal structure of *Drosophila* VPS34, which demonstrates high structural similarity (**Figure 5-8A**). The binding pockets between *Drosophila* and *Pneumocystis*, however, contained four amino acid substitutions: L744 to V613, Y746 to F615, V774 to I616, I822 to A692 (**Figure 5-8B**). Three-dimensional

rendering demonstrated that *Drosophila* VPS34 binding pocket appeared to be more compact due to a higher degree of electrostatic interactions compared to *Pneumocystis* VPS34 (**Figure 5-8C**).

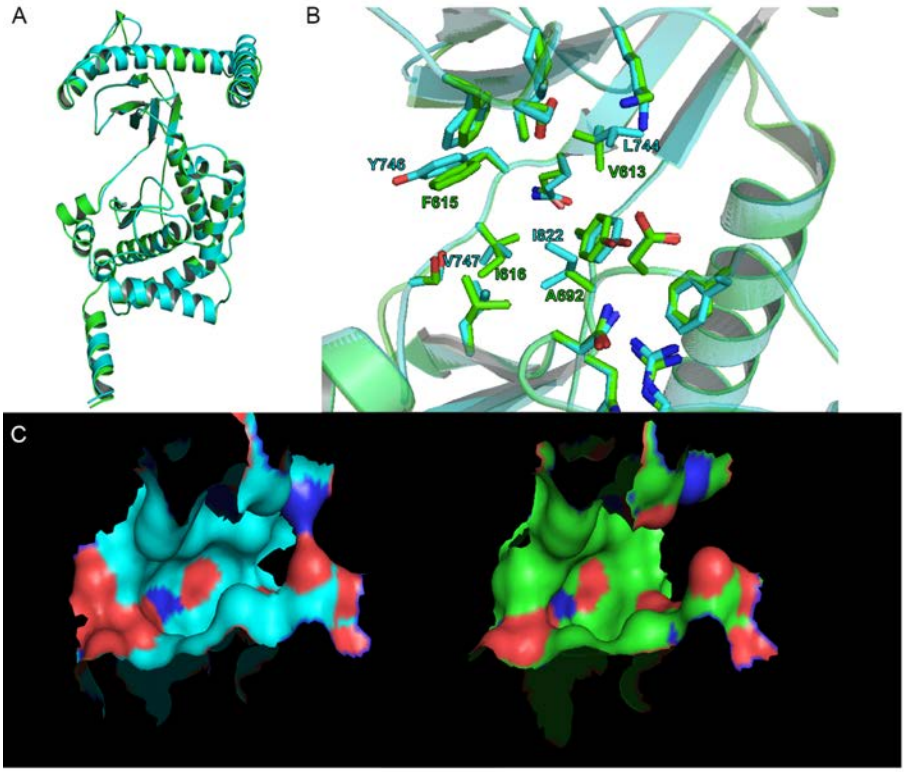

Figure 5-8. **Modeling of the *Pneumocystis* VPS34 binding pocket.**

A.) The catalytic domain of *Pneumocystis* VPS34 (green) modeled off the crystallized *Drosophila* VPS34 (cyan). B.) Map of the binding pocket showing four amino acid substitutions in the *Pneumocystis* (green) VPS34 compared to the *Drosophila* protein (cyan). C.) Three-dimensional reconstruction of *Drosophila* (left) and *Pneumocystis* (right) VPS34 showing a more open, less compact binding pocket in the *Pneumocystis* VPS34.

To screen novel compounds to target *Pneumocystis* VPS34, a library of over 22,000 chemicals created by the laboratory of Dr. Xiangqun Xie was screened *in silico* for binding to the VPS34 pocket (**Figure 5-9A**). While there were several hits, eight compounds (14, 16b, 17, 24,

41, 45, 81, and 203) were selected for further analysis as antifungals. Each compound has a unique chemical structure that is undisclosed at this point for possible proprietary reasons. Interestingly, two compounds, 16b and 24, reduced *Pneumocystis* viability by nearly 50% *in vitro* (**Figure 5-9B**).

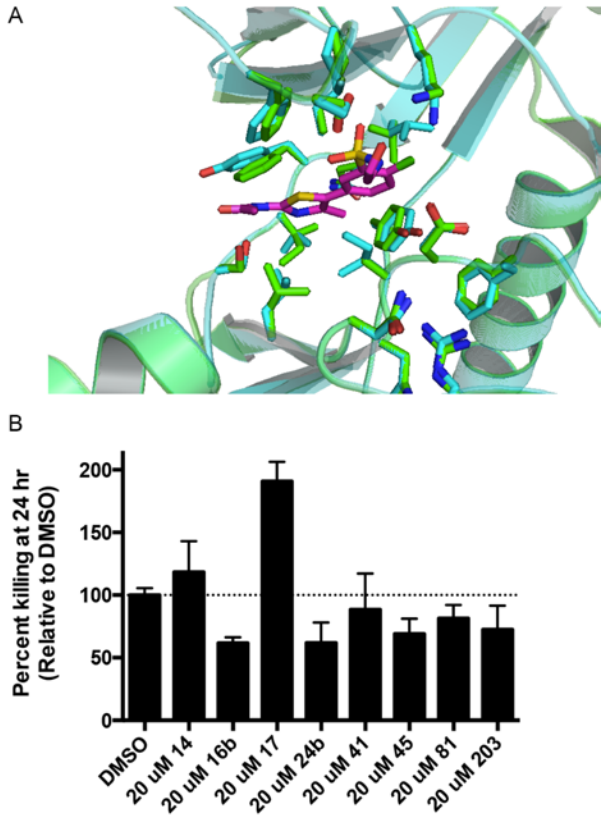

Figure 5-9. ***In silico*** **analysis of potential inhibitors of VPS34 and** ***in vitro*** **killing assay.**

A.) Compounds interfacing with the VPS34 binding pocket *in silico*. B) *Pneumocystis murina* cultured with eight compounds (14, 16b, 17, 24b, 41, 45, 81, and 203) for 24 hours at 37°C. Following incubation, RNA was isolated and *Pneumocystis* burden was calculated by qRT-PCR.

5.5 DISCUSSION

The current study demonstrates a novel top-down approach to design novel therapeutics against *Pneumocystis* pneumonia. Annotation of the 3615 genes within the *Pneumocystis* genome allows for more thorough, rational target selection. Here, we evaluated the *Pneumocystis* kinome, which contains over 100 proteins that are dynamically expressed throughout infection. As a proof-of-principle, we further demonstrated that by targeting a conserved, highly expressed kinase, VPS34, using *in silico* analysis and drug design, we could identify novel inhibitors against *Pneumocystis*.

These techniques could be of the utmost importance as antibiotic resistance continues to emerge. Prophylaxis and treatment for *Pneumocystis* relies heavily on trimethoprim-sulfamethoxazole (TMP-SMX), which targets the nucleotide synthesis pathway (94, 95, 243). However, documented resistance to TMP-SMX has begun to become more prevalent in patients, leading to increased failure of prophylaxis (242, 243, 247, 260, 261). Additionally, TMP-SMX has over a 20% treatment failure rate, as use is limited by sulfa allergy and other unwanted side effects (94, 95). Second-line therapies, such as dapsone, are less effective and tolerable than TMP-SMX (94, 95). Together, these clinical problems necessitate the discovery of novel antifungal targets.

While the current study only examines a single target, VPS34, several novel findings lay the groundwork for possible high-throughput screening. *Pneumocystis*, at present, remains unculturable *in vitro* and 99% of the inoculum will die within 24 hours as measured by qRT-PCR. This remains a large limitation in the field and greatly hinders the development of any high throughput assay. Here, we utilized a complementation approach in *Saccharomyces cerevisiae* to demonstrate functionality of the *Pneumocystis* protein VPS34. This technique, coupled with the

in silico analysis of protein structure, could lead to an assay where druggability of specific *Pneumocystis* proteins is assessed *in vitro* in *S. cerevisiae*. As *S. cerevisiae* mutants can have growth phenotypes, using a spectrophotometer could allow for assessment of broth density in a 96-well or 384-well plate, allowing for high-throughput screening. Likewise, using a luminescent or fluorescent *S. cerevisiae* could allow for quantification of growth visually (262, 263).

Given the identification of one potential target, further studies are needed to assess the viability of a strategy to drug *Pneumocystis* VPS34. VPS34, a hallmark PI3K, is expressed in most species and any compound directed towards the *Pneumocystis* VPS34 may have unwanted off-target effects. Both *in vitro* studies on mammalian cell lines and *in vivo* safety studies need to be performed prior to developing VPS34 inhibitors. Indeed, current PI3K inhibitors used clinically are directed at cancerous cells, suggesting that these compounds can target mammalian cells (248, 249). Furthermore, as existing PI3K inhibitors have yet to be screened for antifungal activity, it is possible that a currently used chemotherapy for cancer may actually have anti-*Pneumocystis* effects. This, of course, would again be limited by unwanted side effects, but it does raise the possibility of repurposing an already approved drug as a novel antifungal.

While the top-down approach successfully identifyied a single target, annotation of the *Pneumocystis* genome should facilitate antifungal development. For example, the use of unbiased screens to identify novel targets may no longer be required (264), as researchers interested in pathway ‘X’ or protein ‘Y’ can now query a fully annotated genome. Likewise, known inhibitors of proteins can be screened for anti-*Pneumocystis* activity if the protein is contained within the genome and is expressed during infection. Together, the current study furthers our knowledge of *Pneumocystis* biology and demonstrates that a top-down approach of genome annotation can identify novel drug targets.

6.0 USING TRANSCRIPTOMICS AND PROTEOMICS TO IDENTIFY NOVEL LIFE-CYCLE SPECIFIC VACCINE CANDIDATES FOR *PNEUMOCYSTIS*

This project is funded by the NIAID (1F30AI114146-01).

Parts of this work were published in: Zheng, M., Cai, Y., Eddens, T., Ricks, D.M., and Kolls, J.K. 2014. Novel *Pneumocystis* antigen discovery using fungal surface proteomics. *Infect Immun* 82: 2417-2423.

The remainder of this work is unpublished at this time.

6.1 INTRODUCTION

Pneumocystis (*PC*) is a fungal species that is best known for causing an opportunistic pneumonia in immunocompromised individuals, such as patients with HIV/AIDS (265). Even after the advent of highly active antiretroviral therapy (HAART), *Pneumocystis* pneumonia *(PCP)* remains one of the most feared complications of HIV/AIDS. One retrospective study demonstrated that *PCP* prior to HAART had a mortality rate of 10.1%; following the implementation of HAART, the mortality rate of *PCP* was modestly reduced to 9.7% (2). Furthermore, another retrospective study in the early 2000's demonstrated that overall *PCP* mortality in HIV-patients was 11.6%, while the mortality rose to 29% in patients requiring intensive care (266). Although HAART has helped reduce the incidence, *PCP* remains the most common AIDS-defining opportunistic infection in the United States (1).

PC is also emerging in the clinical setting in the HIV-negative patient population. A study conducted in Sweden demonstrated that 75% of patients presenting to the hospital with *PCP* were HIV-negative (13). Another study conducted in the U.K. between 2000-2010 found that the number of hospital episodes of *PCP* more than doubled during the study period, with transplant and hematologic malignancy patients representing the highest risk groups (14). Furthermore, patients receiving certain immunosuppressive medications such as methotrexate, steroids, or TNF-antagonists also have an increased susceptibility to *PCP*; these newer immunosuppressive agents are often the hallmark of treatment for conditions like rheumatoid arthritis, autoimmune conditions, and post-transplant rejection (30, 267–270). Perhaps more troubling, HIV-negative patients infected with *PC* tend to have worse outcomes such as higher mechanical ventilation and mortality rates when compared to HIV-positive patients (29, 30).

The current standard of care for prophylaxis and treatment of *PC* is trimethoprim-sulfamethoxazole (TMP-SMX). However, approximately 8% of patients have sulfa allergies and are unable to take TMP-SMX (96). Furthermore, one out of five patients will fail to complete the therapeutic course of TMP-SMX due to adverse effects (94, 95). Interestingly, HIV infection seems to increase the likelihood of having an adverse reaction to sulfa drugs, again limiting the use of TMP-SMX (97). Another growing concern is the emergence of TMP-SMX resistance strains of *PC* due to mutations in dihydrofolate synthase (242). Second line therapies, such as pentamidine, tend to have increased treatment failure rates and adverse events (94, 95).

Although treating *PC* remains a clinical challenge, it is clear that an intact immune system is capable of resolving *PC* infection. The HIV epidemic highlighted the importance of $CD4^+$ T cells in maintaining immunity against *PC*. Additionally, several lines of evidence suggest that an intact B cell response, facilitated by $CD4^+$ T cells, is crucial in eliminating *PC*. First, patients with common variable immunodeficiency and other inherited forms of hypogammaglobulinemia are susceptible to developing *PCP* (271). Second, patients with mutations in IL-21 receptor are susceptible to numerous opportunistic pathogens, including *PC* (78). IL-21 is a hallmark cytokine produced by T follicular helper cells, which are important for shaping a high-affinity antibody response (272). Third, patients treated with Rituximab, an anti-CD20 antibody, frequently develop *PCP*. These findings are also corroborated in several mouse models, as B cell deficient mice, IL-21 receptor knockout mice, and mice treated with an anti-CD20 antibody are unable to clear *PC* infection ((79, 178), unpublished data). Together, these findings all demonstrate that a humoral immune response is a crucial component of maintaining immunity against *PC*.

Ideally, a vaccine could be developed which induces a humoral immune response capable of protecting patients with profound immunosuppression. For example, the use of HAART can potentially reconstitute the immune system to the point where vaccination can induce a protective response even after the $CD4^+$ T cell count drops precipitously (273–275). Furthermore, a vaccine to protect non-HIV infected patients against *PC*, in theory, would be easier to implement because these patients have induced immunosuppression in the clinic. To generate such an immune response would require the presence and identification of strong antigenic proteins on the surface of *PC*. Thus, discovering and evaluating the immunogenic potential of novel antigens on *PC*, along with characterizing the immune response these antigens generate, are the crucial first steps in therapeutic and vaccine development**.**

6.2 METHODS

Separation of cysts and trophs

Total *PC* was isolated from whole lung of a *PC* infected *RAG2/γ-common chain* double knockout mouse and stained with CD45, *PC* antisera (total *PC*), an anti-*PC* antibody (6F5), and a dectin-Fc fusion protein (a complex produced in our laboratory) (127). Cysts stained $CD45^-$*PC*$^+$$Dectin^+$ while trophs stained $CD45^-$*PC*$^+$$Dectin^-$ and were sorted accordingly. RNA was extracted using Trizol and was sequenced was performed as described in prior chapters.

Meu10 and GSC-1 Elispot and peptide immunization

A total of eight fungal proteins were chosen for epitope analysis based on surface peptide identification (Table I, Supplemental Table 1). Potential MHCII-binding peptides were predicted

for each potential protein antigen using the Immune Epitope Database and Analysis Resource T cell epitope prediction tools for peptide binding to MHC class II molecules (http://tools.immuneepitope.org/mhcii). This tool employs a consensus approach to predict MHC Class II epitopes based upon Sturniolo, ARB, and SMM_align algorithms (276). For each gene product, the predicted peptide binding results for mouse MHC Class II were sorted by top percentile using the consensus score, and 10-14 of the highest ranked peptides with a unique Average Relative Binding (ARB) matrix core sequence were selected for each of the 8 fungal surface protein candidates. A total of 96 peptides were chosen for peptide synthesis and screening (Table II). C57/BL6 wild type mice were inoculated with *P. murina* for two weeks. Total lymphocytes include T cells, B cells, and antigen-presenting cells from lung draining lymph node of *P. murina* inoculated mice were collected. Total lymphocytes were resuspended in complete IMDM medium (Invitrogen, Grand Island, NY), and then distributed at 200,000 cells/well in 96 well manufactory pretreated of mouse Interferon gamma (IFN-□), Interleukin-5, and IL-17 ELISpot plates (R&D, Minneapolis, MN). Cells were then incubated at 37°C in 5% CO2 in the presence of each identified peptides pools at 1 μg/ml for four days. PC antigen and ovalbumin (OVA) proteins were used as positive and negative controls. Spot frequency of IFN-□, IL-5, and IL-17 were developed following the manufacturer's instructions and spot forming units were scanned and calculated by Cellular Technology Ltd's plate reader and its spot calculation software. For peptide immunization, mice were immunized with remaining peptides complexed in Sigma Adjuvant system and injected intraperitoneally. Serum was collected 14 days after injection.

ELISAs

Antigens (*Pneumocystis,* Meu10, GSC-1, cell lysates at a concentration of 150 ng/well) in coating buffer were then added to a 96-well plate and incubated at 4° overnight. Plates were then washed, blocked with PBST plus 5% dry-milk, and stained with 1:1000 diluted *P. murina* convalescent serum or naïve serum overnight at 4°. Plates were then washed, stained with goat anti-mouse IgG (Southern Biotech), washed, and developed with TMB substrate. Absorbance was measured at 450 nm and groups were compared using unpaired Student's t-test.

DNA vaccination

Mice were anesthetized with a combination of ketamine and xylizine. Vector (100 μg/mouse) was then injected intramuscularly into the tibialis anterior every two weeks for a total of three doses. *Pneumocystis* inoculation was performed as described in previous chapters.

Pneumocystis staining

P. murina samples were heat-fixed onto glass slides, followed by further fixation using ice-cold methanol. Slides were washed with PBS and blocked for 15 minutes in PBS with 5% dry milk. Anti-Meu10 serum (generated from mice immunized with the Meu10 peptide pool) was diluted 1:1000 in PBS and added to the slides for 15 minutes. Following PBS washes, slides were stained with 1:1000 diluted goat anti-mouse IgG conjugated to DyLight 488 (Thermo Scientific). Slides were washed with PBS, counterstained with DAPI (1:2000 for 15 minutes), washed again and coverslips were mounted with VectaMount™ AQ mounting media (Vector Laboratories). Slides were visualized using 63X magnification.

Expression of recombinant GSC-1 and protein immunization

Briefly, GSC-1 was cloned into the pYES-DEST52 expression vector and sequence confirmation was obtained from Genewiz. *S. cerevisiae* was then transformed (as described on pg. 134) and GSC-1 expression was induced by growth in S.C. –ura media containing galactose. Following 24-hours, the yeast was pelleted via centrifugation and lysed using a BeadBeater for 3 mins in ice. The lysate was then applied to a nickel-affinity column, and was cycled through at 1 mL/min. Flow through was obtained at each step. Elution was performed in an imidazole solution and buffer exchange was performed to resuspend the protein in PBS. A BCA assay was performed to calculate the concentration of protein and GSC-1-Myc tag was confirmed via Western blot. Mice were then immunized with 150 ng of GSC-1 complexed 1:1 in alum via intraperiotneal injection.

Co-housing

Mice were immunized with recombinant GSC-1 complexed in alum. Mice were then CD4-depleted as described in above chapters, and co-housed with a *Pneumocystis* infected *Rag2*$^{-/-}$ *Il2rg*$^{-/-}$ double knockout mouse for four weeks. Mice were then sacrificed and lung tissue was processed as described above.

6.3 RESULTS AND DISCUSSION

We first sought to identify extracellular antigens using a surface biotinylation process on recovered, viable *Pneumocystis*. Following biotinylation, mass spectrometry was performed on the samples and specific extracellular proteins were identified as described previously (264). Following characterization of extracellular proteins on *Pneumocystis*, we next wanted to identify the life form on which these proteins are expressed. Purified *Pneumocystis* was obtained from bronchoalveolar lavage fluid from an infected *Rag2*$^{-/-}$*Il2rg*$^{-/-}$ and cysts were labeled using a dectin-1:Fc construct (127), while trophs were dectin negative (**Figure 6-1A**). Following separation, RNA was isolated and sequenced. Interestingly, of the proteins identified via surface proteomics, Meu10 seemed to have increased expression on trophs, while GSC-1 transcript was enriched in the cyst (**Figures 6-1B and 6-1C**).

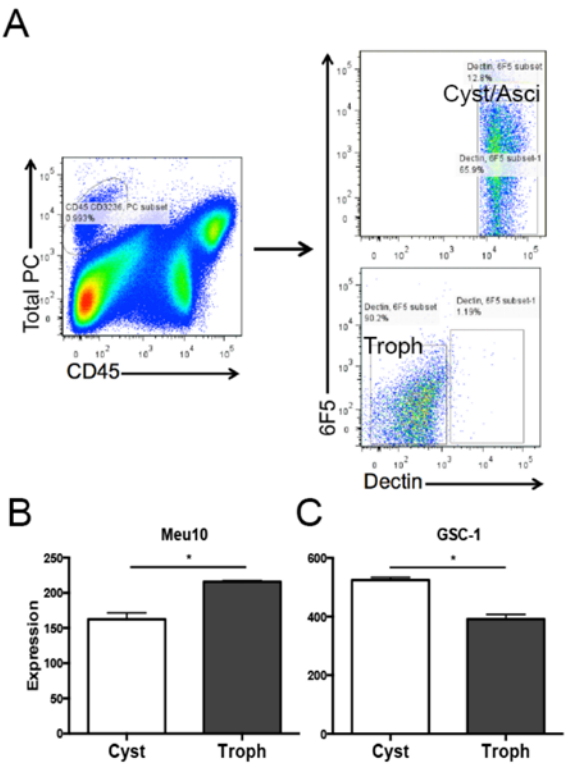

Figure 6-1. RNA sequencing of separated cysts and trophs.

A.) Gating strategy on separating cysts and trophs. Whole *Pneumocystis* was stained with *PC* anti-sera and was $CD45^{-}$. Cysts were sorted on $Dectin^{+}$, while trophs were $Dectin^{-}$. B.) Meu10 had a 1.3-fold higher expression on trophs, while GSC-1 had a 1.3 fold higher expression on cysts (* denotes $p<0.05$).

After identifying two differentially expressed targets, Meu10 and GSC-1, we next sought to characterize the immunogenicity of each protein. T-cells from a *Pneumocystis* infected mouse recognized peptides from both Meu10 and GSC-1 and released IFN-γ, IL-5, and IL-17 (**Figures 6-2 A-C**). These results suggest that both Meu10 and GSC-1 are antigens recognized by antigen-specific T-cells during the course of *Pneumocystis* infection.

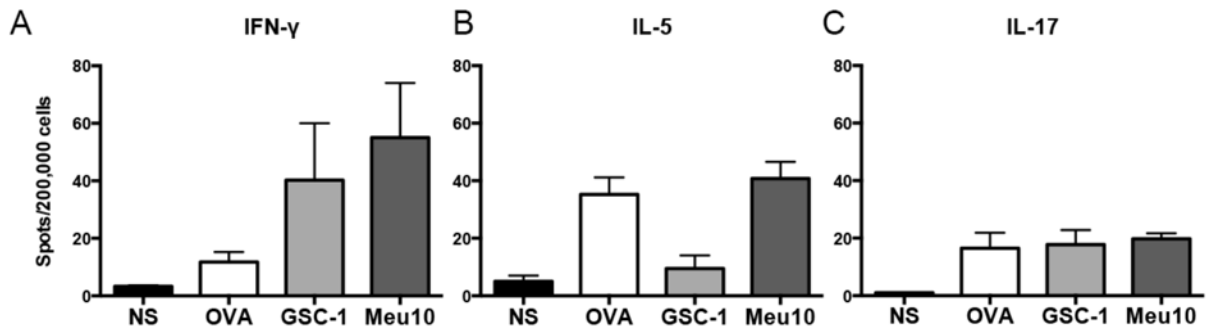

Figure 6-2. . **Meu10 and GSC-1 are antigens seen during natural infection.**

Lymphocytes collected from *Pneumocystis* infected mice were either stimulated with Meu10 peptides, GSC-1 peptides, OVA peptide, or were unstimulated (NS). Meu10 stimulation resulted in a statistically significant increase in IFN-γ positive cells ($p<0.05$), while GSC-1 stimulation resulted in a trend towards greater IFN-γ positive cells ($p=0.09$) as calculated by a Kruskal-Wallis nonparametric ANOVA with Dunn's multiple comparison test. IL-5 and IL-17 production appeared to be nonspecific.

As Meu10 and GSC-1 appeared to be T-cell epitopes, we next sought to determine if B-cells recognized either protein over the course of infection. Following immunization with Meu10 and GSC-1 peptides, a significant increase in anti-*Pneumocystis* IgG over adjuvant alone control was observed (**Figure 6-3**).

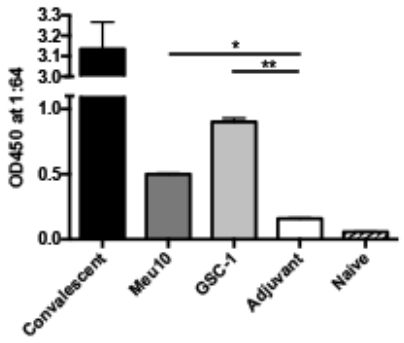

Figure 6-3. **Meu10 and GSC-1 immunization produces anti-Pneumocystis IgG.**

Meu10 and GSC-1 immunized mice had significantly higher anti-PC antibodies as measured by ELISA. * denotes $p<0.05$, ** denotes $p<0.01$ as determined by a one-way ANOVA with Holm-Sidak's multiple comparisons.

While the immunogenicity of Meu10 and GSC-1 made both targets viable vaccine candidates, the above data is limited by the peptide-based approach. To examine if Meu10 protein was immunogenic, 293T cells were transfected with an expression vector containing the nucleotide sequence for the Meu10 ectodomain. Meu10 was readily expressed in 293T cells (**Figure 6-4A**). As further evidence that Meu10 is recognized during natural *Pneumocystis* infection, serum from infected animals bound Meu10 lysate significantly more than serum from a naïve animal (**Figure 6-4B**). Furthermore, when mice were immunized intramuscularly with the Meu10-containing expression vector, sera could recognize both the cyst and the troph form of *Pneumocystis* (**Figure 6-4C**).

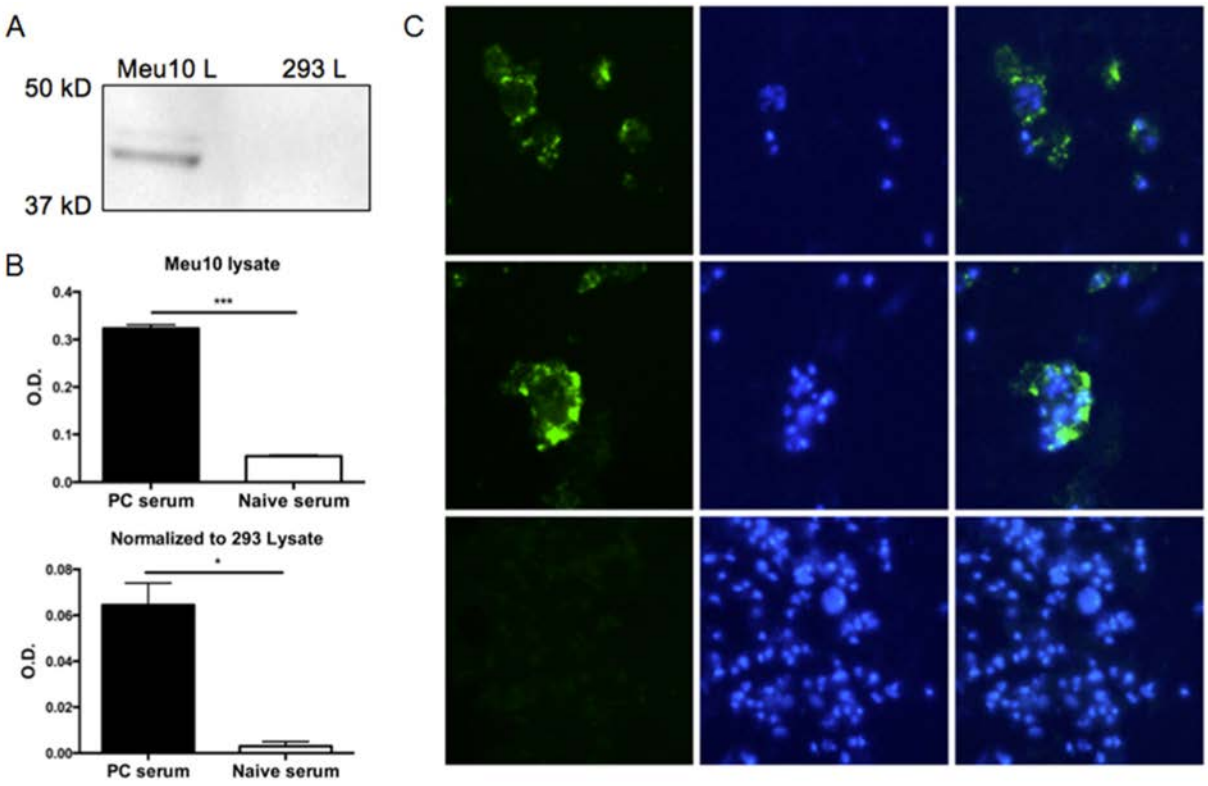

Figure 6-4. **Meu10 is an extracellular antigen capable of inducing a humoral immune response.**

A.) Recombinant myc-tagged Meu10 protein identified by SDS-PAGE and Western blotting in transfected 293 cell lysate. B). Anti-PC serum recognizes Meu10 lysate by ELISA compared to naïve serum (top panel, p=0.0009). Further normalization of the data to non-transfected 293 lysate (background) demonstrates that anti-PC serum recognizes Meu10 greater optical density (O.D.) than naïve serum (bottom panel, p=0.024). C.) Immunofluorescent staining of whole PC with anti-Meu10 serum binds to both the PC cyst (top row) and troph (middle row). Naïve serum (bottom row) demonstrated very little specific binding.

As this DNA vaccine approach was immunogenic, we next immunized mice three times with our Meu10 expression vector, followed by CD4-depletion and challenge with *Pneumocystis* (**Figure 6-5A**). Following 6 weeks of infection, Meu10 immunized mice had significantly reduced burden by qRT-PCR compared to mice receiving an empty vector control (pBUD) (**Figure 6-5B**). These findings were corroborated via a histologic approach, as GMS staining was

significantly reduced in Meu10 immunized mice (**Figure 6-5C**). As seen previously, Meu10 immunization generated anti-*Pneumocystis* IgG by ELISA (**Figure 6-5D**).

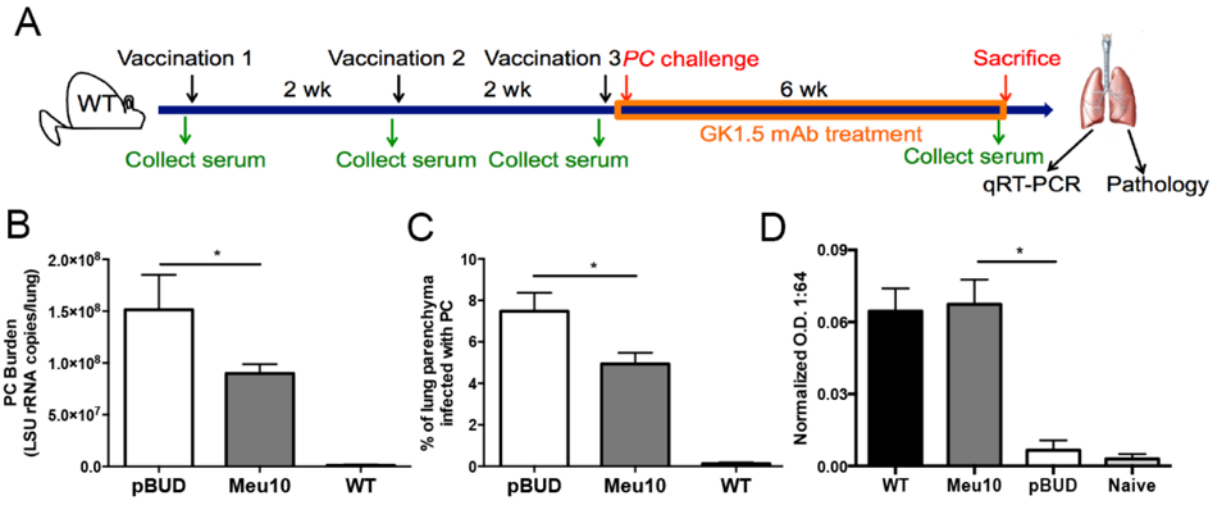

Figure 6-5. Meu10 DNA vaccination provides protection against Pneumocystis challenge and generates Meu10-specific antibodies.

A.) Vaccination scheme demonstrating three vaccination doses, followed by CD4-depletion with GK1.5 monoclonal antibody treatment, and Pneumocystis challenge. B.) Quantitative reverse transcription PCR (qRT-PCR) of large subunit (LSU) rRNA of lung homogenate following vaccination and challenge. C.) Histological analysis of Meu10 DNA vaccination demonstrates that Meu10 provided significant protection. D.) Meu10 pBudCE4.1 was transfected into 293 cells and lysates were used to coat ELISA plates. Serum collected at the time of sacrifice showed that Meu10 vaccinated animals had significantly increased O.D. when normalized to empty pBud 293 lysate. * denotes $p<0.05$ as determined by a one-way ANOVA with Holm-Sidak's multiple comparisons test.

As the DNA vaccination approach appeared to be successful in providing limited protection against *Pneumocystis* challenge, we next sought to use a protein-based approach. Expression of Meu10 recombinant protein, however, was unsuccessful in both yeast and bacteria (data not shown). To further validate our DNA vaccine findings, we then immunized mice with

the MHC-restricted Meu10 peptides designed for the ELISpot assay (**Figure 6-2**). Following immunization, mice receiving Meu10 peptides had significantly reduced *Pneumocystis* burden (**Figure 6-6A**). Upon histologic quantification, Meu10 immunization reduced GMS staining *Pneumocystis* significantly (**Figures 6-6B and 6-6C**). Again, Meu10 immunization led to significantly increased anti-*Pneumocystis* IgG levels comparable to that of C57BL/6 mice (**Figure 6-6D**).

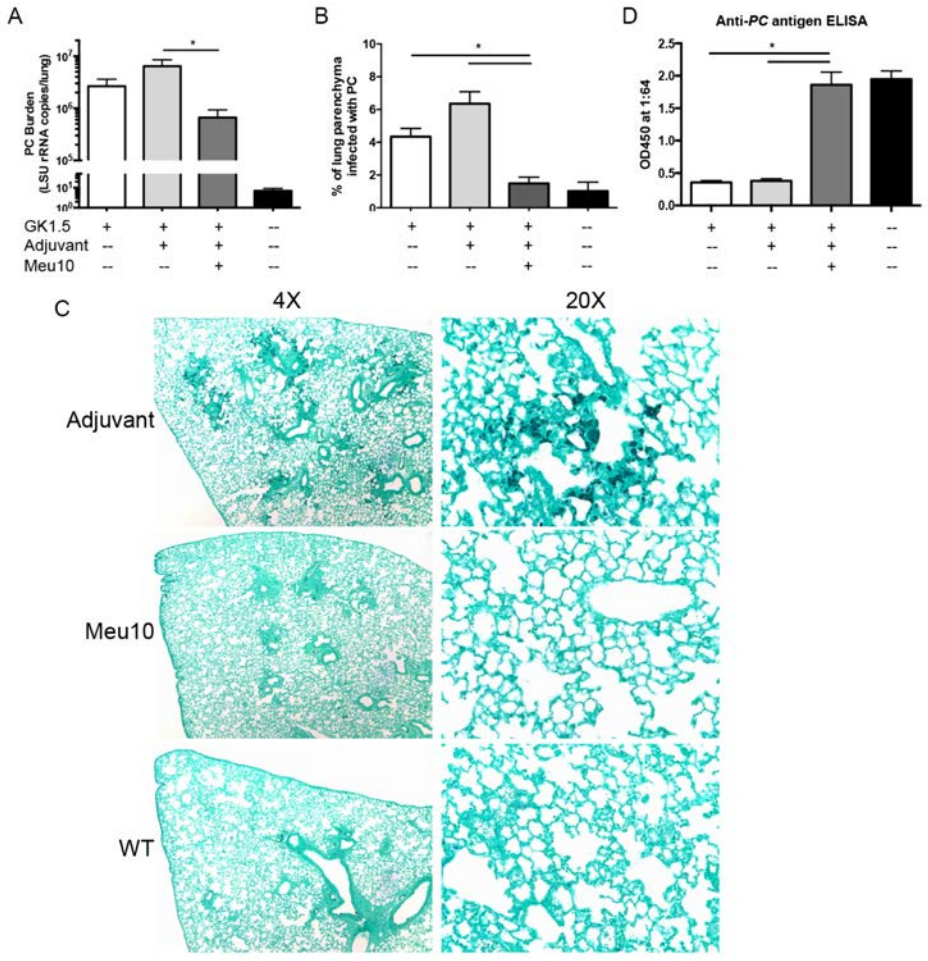

Figure 6-6. **Vaccination with Meu10 peptides decreases *Pneumocystis* burden and results in *Pneumocystis*-specific antibody generation.**

Mice received two doses of Meu10 peptides + Sigma Adjuvant System® i.p. followed by CD4-depletion with GK1.5 and challenge with *Pneumocystis*. A.) qRT-PCR on lung homogenate following 4 weeks of infection demonstrates that Meu10 vaccinated mice had significant decrease in *Pneumocystis* burden when compared to mice receiving adjuvant alone. B.) Histologic analysis of lungs stained with GMS demonstrating Meu10 vaccination provides significant protection. C.) *Pneumocystis* antigen ELISA demonstrating that Meu10 vaccinated mice had significantly higher anti-*Pneumocystis* IgG. * denotes $p<0.05$ as determined by a one-way ANOVA with Holm-Sidak's multiple comparisons test.

After demonstrating Meu10 immunization provided limited protection using two vaccination strategies, we next sought to determine the protective capabilities of GSC-1. Using a comparable DNA vaccine approach, GSC-1 was unable to provide protection following challenge with *Pneumocystis* (data not shown). We next turned to a recombinant protein approach. The ectodomain of GSC-1 was successfully cloned and expressed in *S. cerevisiae* at 24-hour post-galactose induction (**Figure 6-7A**). Furthermore, GSC-1 ectodomain protein was recognized by convalescent sera, indicating this portion of GSC-1 is recognized during natural *Pneumocystis* infection (**Figure 6-7B**).

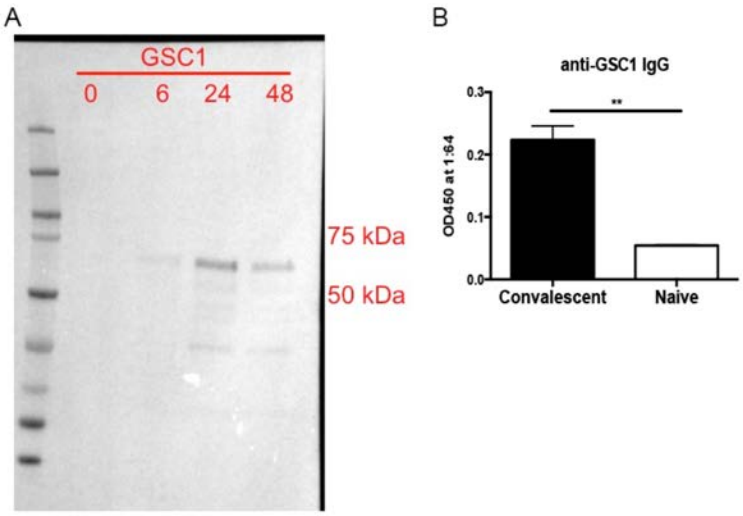

Figure 6-7. **GSC-1 protein is seen during natural *Pneumocystis* infection**.

A.) Expression of the ectodomain of GSC-1 (approximately 67 kDa) in *S. cerevisiae*. Protein was purified using a nickel affinity-column and was detected using an anti-myc Western blot. B.) Purified GSC-1 is recognized by convalescent *Pneumocystis* sera. ** $p<0.01$ by Student's t-test.

Immunization with GSC-1 induced a strong antibody response that was enhanced following a second immunization (**Figure 6-8A**). Furthermore, anti-GSC-1 sera collected

following the second immunization was capable of recognizing the *Pneumocystis* cyst, while anti-OVA sera did not (**Figure 6-8B**). Following CD4-depletion and *Pneumocystis* challenge, however, GSC-1 immunization failed to provide protection as measured by *Pneumocystis* burden (**Figure 6-8C**).

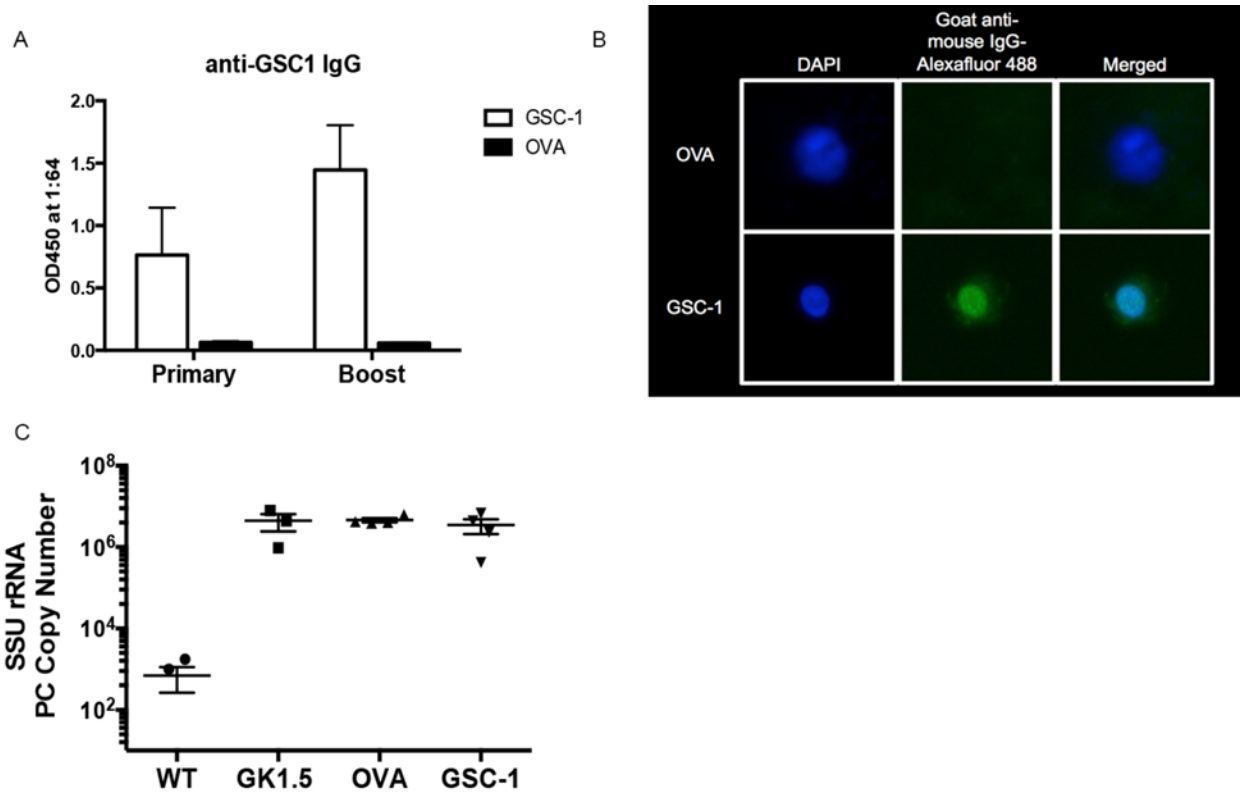

Figure 6-8. **GSC-1 protein immunization induces a strong antibody response, but fails to provide protection**. A.) Anti-GSC-1 antibodies are elicited following GSC-1 immunization and boost. B.) Serum from GSC-1 immunized mice recognizes the surface of the *Pneumocystis* cyst, while serum from OVA immunized animals does not. C.) *Pneumocystis* burden is unaffected by GSC-1 ectodomain immunization.

GSC-1 protein immunization failed to provide protection against challenge with both *Pneumocystis* cysts and trophs. However, RNA sequencing data suggests that GSC-1 is expressed on transmissible form of *Pneumocystis*, the cyst. Prior work by Andrew Limper's lab

also demonstrated that GSC-1 is expressed exclusively by the cyst (277). We therefore hypothesized that GSC-1 immunization would block transmission in a co-housing model. Mice were immunized with two doses of GSC-1 or OVA in alum and GSC-1 immunization again elicited a strong anti-GSC-1 IgG response (**Figure 6-9A**). Following CD4-depletion, immunized mice were co-housed with a *Pneumocystis* infected *Rag2*$^{-/-}$*Il2rg*$^{-/-}$ mouse for four weeks. In the first preliminary experiment, GSC-1 immunized mice had noticeably reduced *Pneumocystis* burden compared to OVA immunized mice (**Figure 6-9B**).

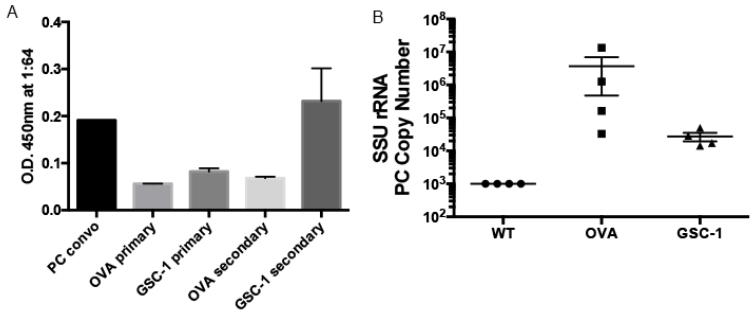

Figure 6-9. **GSC-1 immunization blocks transmission of *Pneumocystis* infection**.

A.) GSC-1 immunization induces anti-GSC-1 IgG production. B.) *Pneumocystis* burden is reduced following GSC-1 immunization and subsequent CD4-depletion and co-housing with an infected *Rag2*$^{-/-}$*Il2rg*$^{-/-}$ mouse.

Taken together, these results demonstrate the identification of two novel vaccine targets for *Pneumocystis* pneumonia. Meu10 and GSC-1, which appear to be life-form specific based on RNA sequencing data, are both recognized by T- and B-cells during natural infection. Furthermore, immunization with both proteins appears to be immunogenic as measured by production of anti-*Pneumocystis*, anti-Meu10, and anti-GSC-1 IgG production. Meu10 immunization was capable of providing limited protection against *Pneumocystis* challenge, while

GSC-1 immunization could block transmission of *Pneumocystis* but failed to reduce burden in a challenge model.

These findings, while still preliminary, are encouraging for a number of reasons. First, the validation of both Meu10 and GSC-1 demonstrates the ability of unbiased, -omic based approaches towards discovering novel antigens. Meu10 and GSC-1 were identified as candidates based on life-form specific transcriptomics and surface proteomics, two techniques that were previously never applied to *Pneumocystis*. This was especially important in the setting of an unannotated genome (which was the case when this project was initiated). Second, each antigen was capable of inducing anti-*Pneumocystis* IgG using various vaccine strategies and in isolation, both Meu10 and GSC-1 provided benefit to the host. Meu10 antibodies were capable of reducing *Pneumocystis* burden in a challenge model; however, this raises the possibility that passive transfer of anti-*Pneumocystis* antibodies into an infected host may be therapeutic. Discovery of high-affinity monoclonal antibodies targeting infectious diseases is an area of active research, as administration of a biologic agent could vastly enhance treatment regimens currently comprised of antibiotics. GSC-1, on the other hand, was more effective at blocking transmission than reducing burden. Future studies will examine the length of GSC-1 provided protection and possibly translate these findings to a non-human primate model.

However, these antigens may be best utilized in a collaborative setting, where dual vaccination could target both the cyst and the troph life-form. The life cycle of *Pneumocystis* is complicated (see Chapter 1) and it is possible that a multivalent vaccine targeting multiple life forms would provide the best protection. Unfortunately, these vaccine studies are time-intensive and a multivalent approach, although tenable, was not performed during the course of my thesis. Our future studies will therefore explore the synergistic or additive effects of adding multiple

antigens in each vaccination. Furthermore, as our knowledge of the microbiology of *Pneumocystis* expands, identification of further antigens could aid in rationale, multivalent vaccine development.

7.0 OVERALL CONCLUSIONS AND FUTURE DIRECTIONS

The findings contained in this dissertation describe the early immune response to *Pneumocystis* infection and exposure. What fascinated me about these projects was how an incredible opportunist like *Pneumocystis* generates such a strong, protective immune response that can eliminate the pathogen, but can also result in damage to the host. While we describe several novel facets of the immune system in response to *Pneumocystis*, there are additional studies that could compliment the projects contained in this thesis or lead to entirely new avenues of research.

My thesis work truly began with the *Pneumocystis* time course experiment, which led to the discovery of a strong eosinophilic signature in the lungs of infected, but not CD4-depleted, mice (**Figure 2-1**). While that project culminated with the use of hydrodynamic injection to drive eosinophilia and reduce *Pneumocystis* burden, the true antifungal mechanism of eosinophils remains unknown. Murine eosinophils have been previously shown to have fungicidal properties against *Aspergillus fumigatus* in a manner that did not require contact (121). These studies are highly suggestive of a cytotoxic mediator released via degranulation, but as described in Chapter 2, these eosinophilic granules are highly complex. More detailed *in vitro* studies could be performed with recombinant major basic protein, eosinophil peroxidase, eosinophilic cationic protein, and eosinophil-derived neurotoxin to see if any or all of these proteins contain antifungal properties. Other proteins within eosinophils, such as eosinophil associated ribonucleases, have

been shown to have anti-viral properties against respiratory syncytial virus (RSV) (personal communication S. Cormier). As transcripts for eosinophil associated ribonucleases were highly upregulated in *Pneumocystis* infected lungs, this protein family could also be a potential target for *in vitro* screening of antifungal activity. These *in vitro* studies will be limited by the fact that 99% of *Pneumocystis* dies within 24-hours outside of a suitable host. While *Pneumocystis* killing assays *in vitro* are possible with sufficiently high inoculums, a second technique would be to give recombinant proteins oropharyngeally to a *Pneumocystis* infected mouse and monitor burden *in vivo*. This type of *in vivo* killing assay has been performed by our group previously with an antimicrobial peptide; however, it is also possible that these eosinophilic granule derived proteins would cause host damage as well (109). Studies examining the antifungal properties of these eosinophil-derived proteins could also be performed *in vitro* with a culturable fungus, such as *Aspergillus*. Furthermore, the mechanistic studies could also be performed with recombinant human eosinophilic proteins or human eosinophils. These further studies would be especially interesting, as identification of a fungicidal protein could potentially lead to a novel therapeutic avenue for *Pneumocystis* pneumonia.

While the exact mechanism of the anti-*Pneumocystis* effects of eosinophils was not elucidated in the current study, driving eosinophilia was sufficient to reduce *Pneumocystis* burden (**Figure 2-4**). In natural infection, $CD4^+$ T-cell release of IL-5, coupled with the induction of eotaxin-1 (CCL11), appears to be the major driver of eosinophilia (**Figure 2-1**). However, eosinophils have been shown to respond to a number of cytokines, such as GM-CSF, IL-4, IL-13, and IL-33 (98). Furthermore, eosinophils have a number of chemoattractant receptors, as well as pattern recognition receptors that may be directly triggered by pathogen-associated molecular patterns (PAMPs) on *Pneumocystis* itself (98). One component of the

Pneumocystis cell wall, chitin, triggers airway eosinophilia and allergic airway inflammation in mice (278–280). Much like the *in vivo* studies described above with granule proteins, giving recombinant proteins in the airway and monitoring eosinophil influx could elucidate which chemokines, cytokines, or PAMPs drive eosinophil recruitment. These studies could also be performed in an *in vitro* transwell system with possible chemoattractants in the basolateral chamber, with the primary outcome measure of eosinophil transmigration (281). Eosinophil activating cytokines could also be studied in an *in vitro* assay, as various doses of cytokine (e.g. GM-CSF) could be added and changes in *Pneumocystis* burden could be monitored.

Understanding the molecules responsible for driving pulmonary eosinophilia could also be informative in the clinical setting. A subset of patients with HIV/AIDS, particularly those with lower $CD4^+$ T-cell counts, can have an increased absolute eosinophil count in the periphery (282). AIDS patients with peripheral eosinophilia rarely have active urinary or gastrointestinal parasitic infection, although eosinophilia was correlated with increased anti-parasitic antibody titers, lower $CD4^+$ T-cell counts, and prior diagnosis of an AIDS-defining infection (283). Of course, this exact cohort of AIDS patients with low $CD4^+$ T-cell counts is the one most susceptible to *Pneumocystis* pneumonia. All of the above studies beg the question: do patients with HIV/AIDS and peripheral eosinophilia have decreased incidence of *Pneumocystis* pneumonia?

While it is unfortunate that this particular study has yet to be performed, a few different outcomes are possible. First, it is possible that peripheral eosinophilia in AIDS patients does not alter the incidence of *Pneumocystis* infection. One such reason for this finding could be that peripheral eosinophilia does not correlate to pulmonary eosinophilia. While driving eosinophilia in our murine model certainly resulted in more eosinophils in the bronchoalveolar lavage fluid,

this may not be the same in humans with AIDS. It could therefore be the case that patients with peripheral eosinophilia and *Pneumocystis* pneumonia could benefit from inhaled delivery of a chemoattractive substance capable of recruiting the eosinophils to the lung. Another alternative explanation is that an eosinophil activating factor may be lacking in patients with such profound immunodeficiency. Similar human eosinophil antifungal assays as described above could be performed with samples from these AIDS patients with peripheral eosinophilia to determine if these cells are defective in fungal killing. This could again lead to discovery of activation factors capable of stimulating these cells *in vivo* to further combat the fungal burden in the lungs.

However, a second outcome in the hypothetical study examining peripheral eosinophilia and *Pneumocystis* pneumonia incidence is that patients with peripheral eosinophilia may have transient colonization, but not fulminant infection, with *Pneumocystis*. Perhaps the eosinophils are sufficient to keep *Pneumocystis* burden contained, but not clear infection. This outcome has some preliminary evidential support, as one small study found increased bronchoalveolar lavage eosinophils in patients harboring *Pneumocystis* infection (130). However, the study by Fleury-Feith *et al*. did not examine if a negative correlation between eosinophil number and *Pneumocystis* burden existed. It may therefore be possible that eosinophils, which act as a protective and temporary bridge until the adaptive immune system responds in the murine model, exist in equilibrium in the context of *Pneumocystis* colonization or infection in an immunocompromised patient. The peripheral eosinophilia in this case is not protective *per se*, but could be used to raise clinical suspicion of *Pneumocystis* pneumonia in addition to parasitic infections.

A third speculative outcome for this proposed study is that peripheral eosinophilia does decrease the incidence of *Pneumocystis* pneumonia. This outcome would certainly be consistent

with the murine studies contained in this dissertation and would further justify exploring the use of eosinophils as a therapeutic agent against *Pneumocystis*. Biologic therapies such as treatment with recombinant IL-5 could therefore be used in severe or TMP-SMX resistant *Pneumocystis* pneumonia cases and could represent a new pathway of targeted pharmaceuticals. Furthermore, peripheral eosinophilia could then be used as a biomarker to identify patients at lower risk of developing *Pneumocystis* infection.

The concept of potentially exploiting eosinophils as immunologic mediators against fungal infection was and continues to be limited by the pathologic role of eosinophils in allergic airway inflammation. A subset of patients with asthma has increased eosinophilia and a strong type II immune signature (137, 140, 284). In eosinophilic asthma patients, blockade of IL-5 signaling significantly reduced steroid dependence and exacerbations compared to a placebo control (285). These findings, coupled with murine studies that implicate eosinophils as pro-inflammatory airway irritants, suggest that increased eosinophilia is detrimental in the lungs (148). Therefore, any proposed therapeutic interventions for *Pneumocystis* pneumonia that induced or stimulated eosinophils would have to be thoroughly vetted for unwanted changes in ventilation and airway resistance. Inducing an asthma exacerbation in a patient with a fulminant pneumonia would be less than ideal.

Therefore, a balance would need to be struck between the protective role of Th2 cells and subsequent eosinophilia in response to *Pneumocystis* and the pathologic role of Th2 cells and subsequent eosinophilia in asthma exacerbations. Essentially, the immune response to *Pneumocystis* closely mirrors that seen in a subset of asthmatics, which led us to explore the question: Could *Pneumocystis* exposure be contributing to asthma pathogenesis?

In our murine model, repetitive exposure of *Pneumocystis* antigen led to Th2-polarization, increased airway hyperresponsiveness, and goblet cell hyperplasia similar to that of known airway allergen, house dust mite (**Figures 3-5 and 3-7**). While this model induced robust pathology in a $CD4^+$ T-cell dependent manner (**Figure 3-9**), this may not represent the most physiologic form of inoculation. While both primary *Pneumocystis* infection (**Figure 3-1**) and natural transmission via a co-housing model (data not shown) induce a strong Th2-response, it is unclear at this time if either model is capable of inducing the hallmark functional changes of airway hyperresponsiveness. In particular, studying the mechanisms of allergic airway inflammation in the co-housing model would be fascinating, as this model, despite its technical challenges, would represent the mechanism of infection thought to occur in the human population.

The current model of *Pneumocystis* antigen exposure studied in this dissertation was highly informative in a number of ways. First, *Pneumocystis* antigen model allowed for direct comparison to the previously studied and validated model of house dust mite exposure by controlling the timing and protein dose of inoculation (286, 287). The immunologic similarities between the two models strongly suggest that like house dust mite, *Pneumocystis* is capable of behaving as a common airway allergen. Second, exposure to sterile *Pneumocystis* antigen allowed for the use of knockout mice that would have been otherwise susceptible to *Pneumocystis* infection, such as $Rag1^{-/-}$, $Rag2^{-/-}Il2rg^{-/-}$, and $Gata1^{-/-}$ knockout mice. Use of genetic tools, coupled with antibody-mediated depletion of $CD4^+$ T-cells, allowed for the examination of the cellular populations responsible for the pathology. In the sterile antigen model, $CD4^+$ Th2 cells appeared to be the predominant mediator of the detrimental inflammation (**Figure 3-9**). ILC2s, as well as eosinophils, appeared to be largely dispensable as effector cells

causing inflammation (**Figures 3-9 and 3-11**). However, preliminary studies contained in this dissertation implicate ILC2s as upstream mediators responsible for maintaining the optimal Th2 response (**Figure 3-10**). Therefore, the pathology mediated in this model was largely dependent on $CD4^+$ T-cells —the same cell that is critical for the protective response in both mice and humans.

The immunologic sensors that lie upstream of the $CD4^+$ T-cell response remain largely unknown. For example, the bronchial epithelial cells and intraepithelial dendritic cells are likely the first cells exposed to *Pneumocystis* in the airway. Understanding the pattern recognition receptors (PRRs), such as toll-like receptors (TLRs) and C-type lectin receptors (CLRs), that respond to *Pneumocystis* and initiate the immunologic cascade that follows would be highly informative (151, 288, 289). C-type lectin receptors, such as Dectin-1, Dectin-2, Mincle, and others, are responsible for sensing sugar and protein moieties contained within fungal cell walls (288). Future studies examining the role of these CLRs in initiation of the pathologic response would be informative for three reasons. First, by identifying the receptors required for recognizing *Pneumocystis*, mediators downstream of these receptors could then be evaluated for a role in the host response against *Pneumocystis*. Second, if the receptors lead to a pathologic response, blocking the accompanying signaling could lead to novel strategies to pharmacologically limit such pathology. Third, identifying a receptor would provide further information about the ligand from *Pneumocystis* that triggers such a pathologic response. Establishing the pathway of *Pneumocystis* recognition and identifying targets downstream of the initial ligand:receptor interaction would facilitate further understanding of the immune response against *Pneumocystis,* both pathologic and protective.

In addition to possible pathogen associated molecular patterns interacting with PRRs, other virulence factors from *Pneumocystis* could contribute to asthma-like pathology. For example, in *Aspergillus* mediated allergic airway disease, fungal proteases appear to initiate the inflammatory process in the lung (176, 177). The target of the proteolytic cleavage appears to be fibrinogen, which once cleaved, can signal through a TLR4-dependent pathway to upregulate mucus production and fibrin clot formation in the airway (290). In an *Alternaria* model of murine allergic airway inflammation, a fungal serine protease triggers the release of IL-33 from bronchial epithelial cells and initiates a Th2-skewed response (193). Interestingly, proteolytic activity does not appear to be necessary for *Pneumocystis* driven airway inflammation. The genome of *Pneumocystis* encodes multiple proteases with homology to proteases in *Aspergillus* and *Alternaria*. However, protease activity in the *Pneumocystis* antigen preparations was assessed by casein zymography and by *in vitro* cleavage of fluorescently labeled peptides; both techniques revealed little proteolytic activity (data not shown). While this lack of proteolytic activity could be an artifact of the *Pneumocystis* antigen purification process, the very same antigen preparation was sufficient to induce allergic airway disease. Therefore, unlike *Aspergillus*, which requires protease activity to induce asthma-like pathology, *Pneumocystis* may have a protease-independent mechanism.

While the novel murine model of *Pneumocystis* driven allergic airway inflammation is highly informative for elucidating mechanisms of disease, it is unable to answer if this phenomenon is observed clinically. *Pneumocystis* exposure is common over time in humans, as 80% of individuals will have anti-*Pneumocystis* antibodies by the age of 13 (61). Interestingly, in a cohort of adult healthy controls and severe asthmatics, anti-*Pneumocystis* IgG antibodies could

be detected ubiquitously (**Figure 3-14**). However, the intensity of binding was higher in a subset of severe asthmatics, which correlated with worsened lung function (**Figure 3-14**).

While this initial study of antibody levels yielded exciting, positive results, measuring anti-*Pneumocystis* IgGs does not accurately reflect infection status. For example, a patient may have a robust IgG response against *Pneumocystis* from multiple prior exposures, but may not be actively colonized with *Pneumocystis*. Therefore, understanding the *Pneumocystis* colonization rates amongst patients with severe asthma would be a next logical step. This could be done in several different ways. First, a noninvasive nasal swab could be used to screen for *Pneumocystis* RNA by qRT-PCR. This has been done previously in the laboratory and would be very easy to perform in an outpatient or emergency room setting. The second, more invasive option would be to collect bronchoalveolar lavage fluid from patients with severe asthma. In addition to quantifying *Pneumocystis* RNA, bronchoalveolar lavage fluid could be assessed for cellular infiltrates (e.g. eosinophils) and pro-inflammatory cytokines (e.g. IL-13). Furthermore, correlations between *Pneumocystis* colonization and pulmonary function could be performed at the time of screening, similar to that performed in this thesis (**Figure 3-14**). Either approach would provide excellent information regarding the snapshot colonization rates of *Pneumocystis* in patients with severe asthma at a specific time.

The other variable that these studies would aim to address is the role of steroid use in enhancing *Pneumocystis* exposure. *Pneumocystis* is a remarkable opportunist that thrives under settings of immunosuppression; severe asthmatics, by definition, all have local pulmonary immunosuppression at the very least (135). Oral steroid courses are frequently used to treat asthma exacerbations and some patients, regardless of asthma severity, see little change in disease progression following steroid administration (133, 137). It is therefore possible that

Pneumocystis colonization rates in patients with severe asthma would then positively correlate with dose of inhaled corticosteroid, length of corticosteroid use, and/or courses of systemic steroids. Depending on the cohort, it may also be possible to follow *Pneumocystis* colonization pre- and post-initiation of inhaled corticosteroids in children not otherwise exposed to steroids. Of course, defining the relationship between steroid initiation and *Pneumocystis* may be difficult in a clinical setting. Should this be the case, *Pneumocystis* colonization rates could be assessed in our mouse model of natural transmission, with a cohort of mice receiving local or systemic steroid exposure.

While characterizing the one-time colonization rate studies described above would be informative to get a greater sense of the prevalence of *Pneumocystis* colonization, both studies would fail to assess causality of *Pneumocystis* infection. To address that question, a cohort of patients would need to be followed from birth or infancy. The study design would include nasal screens for *Pneumocystis* at all routine visits to the pediatrician during the first year of life, coupled with assessment of wheezing, cough, rhinitis, etc. The children would then be enrolled in the study for years (approximately until adolescence) and diagnosis and severity of asthma would be followed. This study, while challenging to execute, would be informative for a number of reasons. First, one study in Chile found near universal prevalence of *Pneumocystis* by qRT-PCR or immunostaining in infants that passed away at four months of age (187). The proposed study above would aim to validate the ubiquity of *Pneumocystis* colonization in young children using non-invasive measures. Second, this study could address the temporal relationship of *Pneumocystis* colonization and development of asthma (or vice versa). This would need to be a fairly large study, although the prevalence rate of asthma (~30%) is high enough to make enrollment feasible.

All of the above clinical studies examining the role of *Pneumocystis* in development or worsening of asthma are critically important in the sense that if a relationship does exist, this would allow for potential therapeutic intervention. Trimethoprim-sulfamethoxazole (TMP-SMX) is used clinically for prophylaxis in high-risk patients and for therapy in patients with diagnosed *Pneumocystis* pneumonia (95). While failure of TMP-SMX does occur, the fact that a pharmaceutical exists and is deemed safe for long-term use in certain patients, including children, offers an exciting possibility that intervention in patients with asthma and *Pneumocystis* colonization could improve disease. Although we are likely several critical studies away from initiation of a phase I clinical trial, the ability to prevent or reduce colonization of *Pneumocystis* and reduce disease severity of asthma with TMP-SMX would represent a tremendous opportunity to impact clinical care for a large patient population.

Another fascinating implication of *Pneumocystis* exposure occurring early in life is the possible relationship to a histologic finding common in infants: inducible bronchus associated lymphoid tissue (iBALT). iBALT structures were observed in nearly half of autopsy specimens from infants passing away from trauma or congenital defects (222). One study by Emery *et al*. further demonstrated that iBALT formation occurs in the majority infants by the age of 10 weeks and is nearly ubiquitously detected in children by three years (221). However, estimations of iBALT structure prevalence in adults varies widely, from completely absent in some cohorts to detectable in 70% in others (230, 291). Interestingly, the percentage of iBALT in adults does appear to rise in patients with pulmonary pathology, such as smoking or asthma (230). iBALT is also present in patients with chronic inflammatory processes such as pulmonary complications of rheumatoid arthritis and chronic obstructive pulmonary disease (COPD) (219, 230, 236). Strikingly, the conditions associated with iBALT formation (e.g. infancy, asthma, autoimmune

disease, and COPD) are very similar to the conditions associated with *Pneumocystis* colonization and infection. These connections, coupled with our remarkable histologic findings in our murine model of *Pneumocystis* infection, led us to further explore the formation of *Pneumocystis* dependent iBALT.

Much like the earlier studies looking at type II pathology, we were able to demonstrate that both inoculation and natural transmission of *Pneumocystis* lead to the development of iBALT (**Figure 4-1**). *Pneumocystis* iBALT was dependent on CXCL13, which was regulated by both Th17 cytokines (IL-17A) and Th2 cytokines (IL-13) (**Figures 4-3 and 4-9**). Interestingly, as mentioned in Chapter 4, these findings represent the first model of fungal iBALT in mice. However, as this iBALT project is more in its infancy than the eosinophil or asthma projects, there are a number of future studies to conduct to complete this story.

For one, the exact mechanism of *Cxcl13* transcript induction requires further exploration. While the current studies elucidated two novel transcription factors capable of regulating *Cxcl13*, STAT3 and GATA3, how this mechanism occurs is unknown. For example, the *Cxcl13* promoter and gene contain both STAT3 and GATA3 binding sites. However, chromatin immunoprecipitation assays with anti-STAT3 or anti-GATA3 antibodies would be required to assess transcription factor binding to the *Cxcl13* promoter. Another hypothesis for the requirement of two transcriptions could be that one transcription factor is required for modification of the epigenetic landscape of the *Cxcl13* promoter, while the other is required for initiation of transcription (292). Such modification could include demethylation or deacetylation, both of which would make the chromatin more accessible to transcription factor binding. Experimentally, the role of demethylation in regulating *Cxcl13* expression could be determined by performing single cytokine stimulation (e.g. IL-13 or IL-17A alone) coupled with inhibitors

of DNA methylation, such as 5-azacytidine (293). Likewise, an inhibitor of DNA acetylation, such as trichostatin (294), could be added to cultures of pulmonary fibroblasts with IL-13 or IL-17A stimulation to assess induction of *Cxcl13*.

Two pieces of evidence support the epigenetic modification hypothesis. First, Rangel-Moreno *et al*. has shown previously that IL-17A stimulation alone was able to induce *Cxcl13* in neonatal pulmonary fibroblasts (220). However, in the current study, *Cxcl13* transcript levels were unchanged following stimulation of adult pulmonary fibroblasts with IL-17A (**Figure 4-9**). These findings could suggest that the *Cxcl13* epigenetic landscape changes, and while open during development, becomes more closed in adulthood. Epigenetic changes certainly occur during development, as methylation states change greatly in peripheral blood cell populations from neonatal cord blood to adulthood (295). Second, using a luciferase reporter system, increases in *Cxcl13* transcription were observed following stimulation with sodium butyrate, a short chain fatty acid that has histone deacetylase inhibitor activity (296). Furthermore, *Cxcl13* transcription was enhanced with pre-treatment with 5-azacytidine and/or trichostatin (296). Taken together, these results would suggest that epigenetic modifications may be occurring in the *Cxcl13* locus.

While further *in vitro* experiments need to be performed to elucidate the precise mechanism of *Cxcl13* regulation, several questions remain about the development of iBALT *in vivo*. First, although suggested by studies with *Il17rb*$^{-/-}$ mice, the role of Th2 cells in initiating or propagating *Pneumocystis* iBALT could be further explored. Using CD4-cre *Gata3*$^{fl/fl}$ mice to abolish Th2 differentiation could be a useful system to determine if Th2 cytokines from an αβ T-cells are required (297). Upstream mediators of the Th2-polarization (e.g. CLRs) as described above could then also be evaluated as important initiators of *Pneumocystis* driven iBALT.

Furthermore, the role of iBALT itself in host defense or *Pneumocystis* driven pathology is unclear. Much like prior publications examining iBALT in influenza (213), mice lacking peripheral lymphoid organs (*Lta*$^{-/-}$) can clear *Pneumocystis* pneumonia comparable to that of wild type mice (**Figure 4-3**). However, *Cxcr5*$^{-/-}$ mice lacking CXCL13 signaling and iBALT also clear *Pneumocystis* adequately (**Figure 4-3**), suggesting that iBALT is sufficient, but not necessary, for immunity against *Pneumocystis*. In terms of pathology, however, it is unclear if these iBALT structures would contribute to the allergic airway inflammation seen following repetitive exposure to *Pneumocystis* antigen. It would be worthwhile to explore changes in airway hyperresponsiveness in the *Cxcr5*$^{-/-}$ and *Lta*$^{-/-}$ mice to evaluate if the presence of iBALT structures contributes to the functional changes associated with *Pneumocystis* exposure. This could also be evaluated on re-exposure to live *Pneumocystis* infection, as iBALT structures are thought to contain memory T-cell responses that would presumably expand upon stimulation with the cognate antigen. These studies would undoubtedly begin to address the role of iBALT in *Pneumocystis*-driven allergic airway inflammation, and possibly strengthen the link between iBALT and asthma (230, 298).

Assessing the role of *Pneumocystis*-driven iBALT in humans would also be highly informative, although it would be challenging from the perspective of obtaining a piece of lung tissue for histologic analysis. Therefore, it may be worthwhile to retrospectively look at sample cohorts previously obtained. For example, the cohort described in the work of Vargas *et al*. detecting colonization of *Pneumocystis* in deceased infants would a fascinating population to examine (187, 188). This cohort has archived histology and RNA samples, both of which could be assessed for iBALT and expression of *Cxcl13* transcript, respectively. Immunologic markers, such as *Il13* and *Il17a*, could also be evaluated. Interestingly, this cohort contains subjects with a

range of *Pneumocystis* burden, so correlations between all of the above markers and fungal colonization status could be explored. Mining these previously collected samples would represent a crucial first step in examining the role of *Pneumocystis* colonization in infants contributing to iBALT formation.

All of the above experiments explored the expansive host response to *Pneumocystis* and elucidated novel protective mechanisms of immunity against the fungus, such as eosinophil-mediated killing and iBALT formation. The findings contained within this dissertation, therefore, could be utilized for the development of novel anti-*Pneumocystis* therapeutics. However, the above studies fail to account for the populations most susceptible to *Pneumocystis* infection: the immunocompromised. The individuals that have the most morbidity and mortality inflicted by *Pneumocystis* uniformly have a suppressed or defective immune response, and thus are unable to combat the infection. Therefore, designing a therapeutic that exploits the host response may have little benefit in an immunodeficient or immunosuppressed patient.

In addition to understanding the host's immune response, we also utilized a top-down approach to discover potential antifungal drug targets within the *Pneumocystis* genome. Following annotation of the *Pneumocystis* genome, we characterized the *Pneumocystis* kinome (**Figure 5-3**). The kinome was highly conserved and dynamic throughout *Pneumocystis* infection (**Figures 5-4 and 5-5**). Finally, we used an *in silico* approach to target a class III PI3K, VPS34, and discovered several compounds capable of killing *Pneumocystis in vitro* (**Figure 5-8**).

There are several additional experiments that could further the potential use of anti-VPS34 compounds. For one, although three of the compounds had anti-*Pneumocystis* effects *in vitro*, there is no guarantee that this is due to targeting VPS34. Pharmaceuticals often have off-target effects and it is certainly possible that these compounds are perturbing a different system

within the fungus. To analyze this possibility, we plan to explore the fungicidal properties of these compounds in the *S. cerevisiae* system (**Figure 5-7**). Complementation of a *Δvps34* strain of *S. cerevisiae* with a vector encoding wild-type *S. cerevisiae* VPS34 rescued the observable growth defect of the yeast. However, similar complementation experiments could be performed with the VPS34 from *Pneumocystis*. Presuming this VPS34 was capable of rescuing the growth defect of the *Δvps34* strain, we could then use this system to examine the specificity of our compounds. Ideally, culture with our anti-VPS34 compounds would inhibit the growth or kill the *S. cerevisiae* expressing *Pneumocystis* VPS34, but not the *S. cerevisiae* VPS34 protein. This complementation system would also be highly useful in developing a high-throughput screening system where efficacy of a compound could be measured by alterations in growth (O.D.), as opposed to RNA yield of *Pneumocystis*.

The above complementation system could also be utilized to examine any off-target effects these compounds may have on the host VPS34. Addition of a mammalian (mouse or human) VPS34 back into the *Δvps34* strain would allow for screening of toxicity of the anti-VPS34 compounds against a non-fungal VPS34. However, it is also possible that these compounds have off-target effects extending beyond binding to VPS34. To explore off-target toxicity, I would examine the growth rates and apoptosis rates of murine or human cell lines grown in the presence of the anti-VPS34 compounds. These experiments would allow for examination of toxicity in a broader fashion.

While a novel therapeutic against *Pneumocystis* would be highly utilized and important clinically, one of the tenets of providing care to patients at high-risk for *Pneumocystis* is to block transmission. While this can be done via prophylactic administration of trimethoprim-sulfamethoxazole, adverse side effects as well as difficulty implementing a daily treatment limit

the efficacy of such therapy. Towards that end, we sought to identify novel vaccine targets capable of inducing protective humoral immunity capable of preventing *Pneumocystis* infection. This approach would utilize a patient's immune system while intact and would hopefully provide protection even after disruption of the immune system by HIV progression or initiation of immunosuppressive medications.

To identify novel antigens, we used unbiased –omics based techniques. Previously, we utilized surface biotinylation and proteomic analysis to identify extracellular proteins (264). Here, we explored the ascus and troph specific expression of these extracellular proteins and found that two, GSC-1 and Meu10, had enhanced expression in the ascus and the troph, respectively, using RNA-sequencing (**Figure 6-1**). While immunization with Meu10 was capable of reducing *Pneumocystis* burden, vaccination with the extracellular region of GSC-1 was capable of preventing *Pneumocystis* transmission in a co-housing model of infection (**Figure 6-9**).

The above findings highlight a number of novel aspects of *Pneumocystis*. First, the ascus form of *Pneumocystis* is transmissible form of the fungus. Pharmacologic depletion of the ascus with an echinocandin antibiotic prevented transmission of infection in a murine model (55). The findings above further support the notion of the ascus as the infectious form, as prevention of ascus transmission was sufficient to limit *Pneumocystis* infection in an immunocompromised mouse. Future experiments will examine the length of protection of GSC-1 immunization in the murine co-housing model. In addition to primary vaccination and CD4-depletion, wild-type mice could be immunized with GSC-1 and sera could be passively transferred to *Rag1*$^{-/-}$ mice. The recipients of GSC-1 sera could then be co-housed with an infected mouse to demonstrate that the protective component of the vaccine is a soluble factor (e.g. antibody). If these experiments

further demonstrate that anti-GSC-1 antibodies are protective over a long period of time, the next step would be to move to a non-human primate model of immunization and *Pneumocystis* infection.

Secondly, in the murine model of *Pneumocystis* infection, immunocompromised mice with anti-Meu10 antibodies had reduced *Pneumocystis* burden by qRT-PCR and histologic analysis. These findings suggest that antibodies targeting the trophic form of infection may have therapeutic benefit in the setting of a fulminant *Pneumocystis* pneumonia. Towards that end, the effect of passively transferred anti-Meu10 antibodies in the context of high *Pneumocystis* burden in an immunocompromised mouse could be explored. Furthermore, the use of Meu10 in the co-housing model described above could add to our understanding of *Pneumocystis* transmission/infection, as the protection against the trophic form should not prevent transmission.

BIBLIOGRAPHY

1. Morris, A., J. D. Lundgren, H. Masur, P. D. Walzer, D. L. Hanson, T. Frederick, L. Huang, C. B. Beard, and J. E. Kaplan. 2004. Current epidemiology of Pneumocystis pneumonia. *Emerging Infect Dis* 10: 1713–1720.

2. Walzer, P. D., H. E. Evans, A. J. Copas, S. G. Edwards, A. D. Grant, and R. F. Miller. 2008. Early predictors of mortality from Pneumocystis jirovecii pneumonia in HIV-infected patients: 1985-2006. *Clin Infect Dis* 46: 625–633.

3. Antiretroviral Therapy Cohort Collaboration (ART-CC), A. Mocroft, J. A. Sterne, M. Egger, M. May, S. Grabar, H. Furrer, C. Sabin, G. Fatkenheuer, A. Justice, P. Reiss, A. d' Arminio Monforte, J. Gill, R. Hogg, F. Bonnet, M. Kitahata, S. Staszewski, J. Casabona, R. Harris, and M. Saag. 2009. Variable impact on mortality of AIDS-defining events diagnosed during combination antiretroviral therapy: not all AIDS-defining conditions are created equal. *Clin Infect Dis* 48: 1138–1151.

4. Huang, L., A. Cattamanchi, J. L. Davis, S. den Boon, J. Kovacs, S. Meshnick, R. F. Miller, P. D. Walzer, W. Worodria, H. Masur, International HIV-associated Opportunistic Pneumonias (IHOP) Study, and Lung HIV Study. 2011. HIV-associated Pneumocystis pneumonia. *Proc Am Thorac Soc* 8: 294–300.

5. Malin, A. S., L. K. Gwanzura, S. Klein, V. J. Robertson, P. Musvaire, and P. R. Mason. 1995. Pneumocystis carinii pneumonia in Zimbabwe. *The Lancet* 346: 1258–1261.

6. Ruffini, D. D., and S. A. Madhi. 2002. The high burden of Pneumocystis carinii pneumonia in African HIV-1-infected children hospitalized for severe pneumonia. *AIDS* 16: 105–112.

7. Chakaya, J. M., C. Bii, L. Ng'ang'a, E. Amukoye, T. Ouko, L. Muita, S. Gathua, J. Gitau, I. Odongo, J. M. Kabanga, K. Nagai, S. Suzumura, and Y. Sugiura. 2003. Pneumocystis carinii pneumonia in HIV/AIDS patients at an urban district hospital in Kenya. *East Afr Med J* 80: 30–35.

8. Tansuphasawadikul, S., P. Pitisuttithum, A. D. Knauer, W. Supanaranond, J. Kaewkungwal, B. M. Karmacharya, and A. Chovavanich. 2005. Clinical features, etiology and short term outcomes of interstitial pneumonitis in HIV/AIDS patients. *Southeast Asian J Trop Med Public Health* 36: 1469–1478.

9. Nissapatorn, V., C. K. Lee, M. Rohela, and A. K. Anuar. 2004. Spectrum of opportunistic infections among HIV-infected patients in Malaysia. *Southeast Asian J Trop Med Public Health* 35 Suppl 2: 26–32.

10. Udwadia, Z. F., A. V. Doshi, and A. S. Bhaduri. 2005. Pneumocystis carinii pneumonia in HIV infected patients from Mumbai. *J Assoc Physicians India* 53: 437–440.

11. Panizo, M. M., V. Reviákina, T. Navas, K. Casanova, A. Sáez, R. N. Guevara, A. M. Cáceres, R. Vera, C. Sucre, and E. Arbona. 2008. [Pneumocystosis in Venezuelan patients: epidemiology and diagnosis (2001-2006)]. *Rev Iberoam Micol* 25: 226–231.

12. Chernilo, S., S. Trujillo, M. Kahn, M. Paredes, G. Echevarría, and C. Sepúlveda. 2005. [Lung diseases among HIV infected patients admitted to the "Instituto Nacional del Torax" in Santiago, Chile]. *Rev Med Chil* 133: 517–524.

13. Mikaelsson, L., G. Jacobsson, and R. Andersson. 2006. Pneumocystis pneumonia--a retrospective study 1991-2001 in Gothenburg, Sweden. *J Infect* 53: 260–265.

14. Maini, R., K. L. Henderson, E. A. Sheridan, T. Lamagni, G. Nichols, V. Delpech, and N. Phin. 2013. Increasing Pneumocystis pneumonia, England, UK, 2000-2010. *Emerging Infect Dis* 19: 386–392.

15. Catherinot, E., F. Lanternier, M. E. Bougnoux, M. Lecuit, L. J. Couderc, and O. Lortholary. 2010. Pneumocystis jirovecii Pneumonia. *Infect Dis Clin North Am* 24: 107–138.

16. Carmona, E. M., and A. H. Limper. 2011. Update on the diagnosis and treatment of Pneumocystis pneumonia. *Ther Adv Respir Dis* 5: 41–59.

17. Goto, N., and S. Oka. 2011. Pneumocystis jirovecii pneumonia in kidney transplantation. *Transpl Infect Dis* 13: 551–558.

18. Mussini, C., C. Manzardo, M. Johnson, A. D. Monforte, C. Uberti-Foppa, A. Antinori, M. J. Gill, L. Sighinolfi, V. Borghi, A. Lazzarin, J. M. Miró, C. Sabin, and Late Presenter Investigators. 2008. Patients presenting with AIDS in the HAART era: a collaborative cohort analysis. *AIDS* 22: 2461–2469.

19. Neff, R. T., R. M. Jindal, D. Y. Yoo, F. P. Hurst, L. Y. Agodoa, and K. C. Abbott. 2009. Analysis of USRDS: incidence and risk factors for Pneumocystis jiroveci pneumonia. *Transplantation* 88: 135–141.

20. Sepkowitz, K. A. 2002. Opportunistic infections in patients with and patients without Acquired Immunodeficiency Syndrome. *Clin Infect Dis* 34: 1098–1107.

21. Wolfe, R. A., E. C. Roys, and R. M. Merion. 2010. Trends in organ donation and transplantation in the United States, 1999-2008. *Am J Transplant* 10: 961–972.

22. Rodriguez, M., and J. A. Fishman. 2004. Prevention of infection due to Pneumocystis spp. in human immunodeficiency virus-negative immunocompromised patients. *Clin Microbiol Rev* 17: 770–82, table of contents.

23. Louie, G. H., Z. Wang, and M. M. Ward. 2010. Trends in hospitalizations for Pneumocystis jiroveci pneumonia among patients with rheumatoid arthritis in the US: 1996-2007. *Arthritis Rheum* 62: 3826–3827.

24. Stamp, L. K., and M. Hurst. 2010. Is there a role for consensus guidelines for P. jiroveci pneumonia prophylaxis in immunosuppressed patients with rheumatic diseases? *J Rheumatol* 37: 686–688.

25. Falagas, M. E., K. G. Manta, G. I. Betsi, and G. Pappas. 2007. Infection-related morbidity and mortality in patients with connective tissue diseases: a systematic review. *Clin Rheumatol* 26: 663–670.

26. Poppers, D. M., and E. J. Scherl. 2008. Prophylaxis against Pneumocystis pneumonia in patients with inflammatory bowel disease: toward a standard of care. *Inflamm Bowel Dis* 14: 106–113.

27. De Castro, N., S. Neuville, C. Sarfati, P. Ribaud, F. Derouin, E. Gluckman, G. Socié, and J. M. Molina. 2005. Occurrence of Pneumocystis jiroveci pneumonia after allogeneic stem cell transplantation: a 6-year retrospective study. *Bone Marrow Transplant* 36: 879–883.

28. Martin-Garrido, I., E. M. Carmona, U. Specks, and A. H. Limper. 2013. Pneumocystis pneumonia in patients treated with rituximab. *Chest* 144: 258–265.

29. Monnet, X., E. Vidal-Petiot, D. Osman, O. Hamzaoui, A. Durrbach, C. Goujard, C. Miceli, P. Bourée, and C. Richard. 2008. Critical care management and outcome of severe Pneumocystis pneumonia in patients with and without HIV infection. *Crit Care* 12: R28.

30. Mori, S., and M. Sugimoto. 2012. Pneumocystis jirovecii infection: an emerging threat to patients with rheumatoid arthritis. *Rheumatology (Oxford)* 51: 2120–2130.

31. Saltzman, R. W., S. Albin, P. Russo, and K. E. Sullivan. 2012. Clinical conditions associated with PCP in children. *Pediatr Pulmonol* 47: 510–516.

32. Fallo, A. A., W. DobrzanskiNisiewicz, N. Sordelli, M. A. Cattaneo, G. Scott, and E. L. López. 2002. Clinical and epidemiologic aspects of human immunodeficiency virus-1-infected children in Buenos Aires, Argentina. *Int J Infect Dis* 6: 9–16.

33. De Armas Rodríguez, Y., G. Wissmann, A. L. Müller, M. A. Pederiva, M. C. Brum, R. L. Brackmann, V. Capó de Paz, and E. J. Calderón. 2011. Pneumocystis jirovecii pneumonia in developing countries. *Parasite* 18: 219–228.

34. Thomas, C. F., and A. H. Limper. 2004. Pneumocystis pneumonia. *N Engl J Med* 350: 2487–2498.

35. Kanne, J. P., D. R. Yandow, and C. A. Meyer. 2012. Pneumocystis jiroveci pneumonia: high-resolution CT findings in patients with and without HIV infection. *AJR Am J Roentgenol* 198: W555–W561.

36. Wakefield, A. E., F. J. Pixley, S. Banerji, K. Sinclair, R. F. Miller, E. R. Moxon, and J. M. Hopkin. 1990. Detection of Pneumocystis carinii with DNA amplification. *The Lancet* 336: 451–453.

37. Reid, A. B., S. C. Chen, and L. J. Worth. 2011. Pneumocystis jirovecii pneumonia in non-HIV-infected patients: new risks and diagnostic tools. *Curr Opin Infect Dis* 24: 534–544.

38. Flori, P., B. Bellete, F. Durand, H. Raberin, C. Cazorla, J. Hafid, F. Lucht, and R. T. Sung. 2004. Comparison between real-time PCR, conventional PCR and different staining techniques for diagnosing Pneumocystis jiroveci pneumonia from bronchoalveolar lavage specimens. *J Med Microbiol* 53: 603–607.

39. Desmet, S., E. Van Wijngaerden, J. Maertens, J. Verhaegen, E. Verbeken, P. De Munter, W. Meersseman, B. Van Meensel, J. Van Eldere, and K. Lagrou. 2009. Serum (1-3)-beta-D-glucan as a tool for diagnosis of Pneumocystis jirovecii pneumonia in patients with human immunodeficiency virus infection or hematological malignancy. *J Clin Microbiol* 47: 3871–3874.

40. Nakamura, H., M. Tateyama, D. Tasato, S. Haranaga, S. Yara, F. Higa, Y. Ohtsuki, and J. Fujita. 2009. Clinical utility of serum beta-D-glucan and KL-6 levels in Pneumocystis jirovecii pneumonia. *Intern Med* 48: 195–202.

41. Edman, J. C., J. A. Kovacs, H. Masur, D. V. Santi, H. J. Elwood, and M. L. Sogin. 1988. Ribosomal RNA sequence shows Pneumocystis carinii to be a member of the fungi. *Nature* 334: 519–522.

42. Stringer, S. L., K. Hudson, M. A. Blase, P. D. Walzer, M. T. Cushion, and J. R. Stringer. 1989. Sequence from ribosomal RNA of Pneumocystis carinii compared to those of four fungi suggests an ascomycetous affinity. *J Protozool* 36: 14S–16S.

43. Wakefield, A. E., S. E. Peters, S. Banerji, P. D. Bridge, G. S. Hall, D. L. Hawksworth, L. A. Guiver, A. G. Allen, and J. M. Hopkin. 1992. Pneumocystis carinii shows DNA homology with the ustomycetous red yeast fungi. *Mol Microbiol* 6: 1903–1911.

44. Pixley, F. J., A. E. Wakefield, S. Banerji, and J. M. Hopkin. 1991. Mitochondrial gene sequences show fungal homology for Pneumocystis carinii. *Mol Microbiol* 5: 1347–1351.

45. Ypma-Wong, M. F., W. A. Fonzi, and P. S. Sypherd. 1992. Fungus-specific translation elongation factor 3 gene present in Pneumocystis carinii. *Infect Immun* 60: 4140–4145.

46. Cushion, M. T., A. G. Smulian, B. E. Slaven, T. Sesterhenn, J. Arnold, C. Staben, A. Porollo, R. Adamczak, and J. Meller. 2007. Transcriptome of Pneumocystis carinii during fulminate infection: carbohydrate metabolism and the concept of a compatible parasite. *PLoS ONE* 2: e423.

47. Frenkel, J. K. 1976. Pneumocystis jiroveci n. sp. from man: morphology, physiology, and immunology in relation to pathology. *Natl Cancer Inst Monogr* 43: 13–30.

48. Aliouat-Denis, C. M., M. Chabé, C. Demanche, E. L. M. Aliouat, E. Viscogliosi, J. Guillot, L. Delhaes, and E. Dei-Cas. 2008. Pneumocystis species, co-evolution and pathogenic power. *Infect Genet Evol* 8: 708–726.

49. Keely, S. P., J. M. Fischer, and J. R. Stringer. 2003. Evolution and speciation of Pneumocystis. *J Eukaryot Microbiol* 50 Suppl: 624–626.

50. Wright, T. W., F. Gigliotti, C. G. Haidaris, and P. J. Simpson-Haidaris. 1995. Cloning and characterization of a conserved region of human and rhesus macaque Pneumocystis carinii gpA. *Gene* 167: 185–189.

51. Wright, T. W., T. Y. Bissoondial, C. G. Haidaris, F. Gigliotti, and P. J. Haidaris. 1995. Isoform diversity and tandem duplication of the glycoprotein A gene in ferret Pneumocystis carinii. *DNA Res* 2: 77–88.

52. Peters, S. E., A. E. Wakefield, K. E. Whitwell, and J. M. Hopkin. 1994. Pneumocystis carinii pneumonia in thoroughbred foals: identification of a genetically distinct organism by DNA amplification. *J Clin Microbiol* 32: 213–216.

53. Aliouat-Denis, C. M., A. Martinez, E. L. M. Aliouat, M. Pottier, N. Gantois, and E. Dei-Cas. 2009. The Pneumocystis life cycle. *Mem Inst Oswaldo Cruz* 104: 419–426.

54. Chabé, M., C. M. Aliouat-Denis, L. Delhaes, E. L. M. Aliouat, E. Viscogliosi, and E. Dei-Cas. 2011. Pneumocystis: from a doubtful unique entity to a group of highly diversified fungal species. *FEMS Yeast Res* 11: 2–17.

55. Cushion, M. T., M. J. Linke, A. Ashbaugh, T. Sesterhenn, M. S. Collins, K. Lynch, R. Brubaker, and P. D. Walzer. 2010. Echinocandin treatment of pneumocystis pneumonia in rodent models depletes cysts leaving trophic burdens that cannot transmit the infection. *PLoS ONE* 5: e8524.

56. Itatani, C. A. 1994. Ultrastructural demonstration of a pore in the cyst wall of Pneumocystis carinii. *J Parasitol* 80: 644–648.

57. Cushion, M. T. 2004. Pneumocystis: unraveling the cloak of obscurity. *Trends Microbiol* 12: 243–249.

58. Martinez, A., E. L. M. Aliouat, A. Standaert-Vitse, E. Werkmeister, M. Pottier, C. Pinçon, E. Dei-Cas, and C. M. Aliouat-Denis. 2011. Ploidy of cell-sorted trophic and cystic forms of Pneumocystis carinii. *PLoS ONE* 6: e20935.

59. Martinez, A., M. C. Halliez, E. L. M. Aliouat, M. Chabé, A. Standaert-Vitse, E. Fréalle, N. Gantois, M. Pottier, A. Pinon, E. Dei-Cas, and C. M. Aliouat-Denis. 2013. Growth and airborne transmission of cell-sorted life cycle stages of Pneumocystis carinii. *PLoS ONE* 8: e79958.

60. Schildgen, V., S. Mai, S. Khalfaoui, J. Lüsebrink, M. Pieper, R. L. Tillmann, M. Brockmann, and O. Schildgen. 2014. Pneumocystis jirovecii can be productively cultured in differentiated CuFi-8 airway cells. *MBio* 5: e01186–e01114.

61. Respaldiza, N., F. J. Medrano, A. C. Medrano, J. M. Varela, C. de la Horra, M. Montes-Cano, S. Ferrer, I. Wichmann, D. Gargallo-Viola, and E. J. Calderon. 2004. High seroprevalence of Pneumocystis infection in Spanish children. *Clin Microbiol Infect* 10: 1029–1031.

62. Vargas, S. L., C. A. Ponce, F. Gigliotti, A. V. Ulloa, S. Prieto, M. P. Muñoz, and W. T. Hughes. 2000. Transmission of Pneumocystis carinii DNA from a patient with P. carinii pneumonia to immunocompetent contact health care workers. *J Clin Microbiol* 38: 1536–1538.

63. Miller, R. F., H. E. Ambrose, and A. E. Wakefield. 2001. Pneumocystis carinii f. sp. hominis DNA in immunocompetent health care workers in contact with patients with P. carinii pneumonia. *J Clin Microbiol* 39: 3877–3882.

64. Morris, A., and K. A. Norris. 2012. Colonization by Pneumocystis jirovecii and its role in disease. *Clin Microbiol Rev* 25: 297–317.

65. Fily, F., S. Lachkar, L. Thiberville, L. Favennec, and F. Caron. 2011. Pneumocystis jirovecii colonization and infection among non HIV-infected patients. *Med Mal Infect* 41: 526–531.

66. Gingo, M. R., S. E. Wenzel, C. Steele, C. J. Kessinger, L. Lucht, T. Lawther, M. Busch, M. E. Hillenbrand, R. Weinman, W. A. Slivka, D. K. McMahon, Y. Zhang, F. C. Sciurba, and A. Morris. 2012. Asthma diagnosis and airway bronchodilator response in HIV-infected patients. *J Allergy Clin Immunol* 129: 708–714.e8.

67. Shipley, T. W., H. M. Kling, A. Morris, S. Patil, J. Kristoff, S. E. Guyach, J. E. Murphy, X. Shao, F. C. Sciurba, R. M. Rogers, T. Richards, P. Thompson, R. C. Montelaro, H. O. Coxson, J. C. Hogg, and K. A. Norris. 2010. Persistent pneumocystis colonization leads to the development of chronic obstructive pulmonary disease in a nonhuman primate model of AIDS. *J Infect Dis* 202: 302–312.

68. Norris, K. A., and A. Morris. 2011. Pneumocystis infection and the pathogenesis of chronic obstructive pulmonary disease. *Immunol Res* 50: 175–180.

69. Kluge, R. M., D. M. Spaulding, and A. J. Spain. 1978. Combination of pentamidine and trimethoprim-sulfamethoxazole in therapy of Pneumocystis carinii pneumonia in rats. *Antimicrob Agents Chemother* 13: 975–978.

70. Chandler, F. W., J. K. Frenkel, and W. G. Campbell. 1979. Pneumocystis pneumonia. Animal model: pneumocystis cartinii pneumonia in the immunosuppressed rat. *Am J Pathol* 95: 571–574.

71. Hughes, W. T., R. A. Price, H. K. Kim, T. P. Coburn, D. Grigsby, and S. Feldman. 1973. Pneumocystis carinii pneumonitis in children with malignancies. *J Pediatr* 82: 404–415.

72. Phair, J., A. Muñoz, R. Detels, R. Kaslow, C. Rinaldo, and A. Saah. 1990. The risk of Pneumocystis carinii pneumonia among men infected with human immunodeficiency virus type 1. Multicenter AIDS Cohort Study Group. *N Engl J Med* 322: 161–165.

73. Shellito, J., V. V. Suzara, W. Blumenfeld, J. M. Beck, H. J. Steger, and T. H. Ermak. 1990. A new model of Pneumocystis carinii infection in mice selectively depleted of helper T lymphocytes. *J Clin Invest* 85: 1686–1693.

74. Rudner, X. L., K. I. Happel, E. A. Young, and J. E. Shellito. 2007. Interleukin-23 (IL-23)-IL-17 cytokine axis in murine Pneumocystis carinii infection. *Infect Immun* 75: 3055–3061.

75. Milner, J. D., J. M. Brenchley, A. Laurence, A. F. Freeman, B. J. Hill, K. M. Elias, Y. Kanno, C. Spalding, H. Z. Elloumi, M. L. Paulson, J. Davis, A. Hsu, A. I. Asher, J. O'Shea, S. M. Holland, W. E. Paul, and D. C. Douek. 2008. Impaired T(H)17 cell differentiation in subjects with autosomal dominant hyper-IgE syndrome. *Nature* 452: 773–776.

76. Mogensen, T. H. 2013. STAT3 and the Hyper-IgE syndrome: Clinical presentation, genetic origin, pathogenesis, novel findings and remaining uncertainties. *JAKSTAT* 2: e23435.

77. Crotty, S. 2011. Follicular helper CD4 T cells (TFH). *Annu Rev Immunol* 29: 621–663.

78. Kotlarz, D., N. Ziętara, G. Uzel, T. Weidemann, C. J. Braun, J. Diestelhorst, P. M. Krawitz, P. N. Robinson, J. Hecht, J. Puchałka, E. M. Gertz, A. A. Schäffer, M. G. Lawrence, L. Kardava, D. Pfeifer, U. Baumann, E. D. Pfister, E. P. Hanson, A. Schambach, R. Jacobs, H. Kreipe, S. Moir, J. D. Milner, P. Schwille, S. Mundlos, and C. Klein. 2013. Loss-of-function mutations in the IL-21 receptor gene cause a primary immunodeficiency syndrome. *J Exp Med* 210: 433–443.

79. Lund, F. E., M. Hollifield, K. Schuer, J. L. Lines, T. D. Randall, and B. A. Garvy. 2006. B cells are required for generation of protective effector and memory CD4 cells in response to Pneumocystis lung infection. *J Immunol* 176: 6147–6154.

80. Al-Saud, B. K., Z. Al-Sum, H. Alassiri, A. Al-Ghonaium, S. Al-Muhsen, H. Al-Dhekri, R. Arnaout, O. Alsmadi, E. Borrero, A. Abu-Staiteh, F. Rawas, H. Al-Mousa, and A. Hawwari. 2013. Clinical, immunological, and molecular characterization of hyper-IgM syndrome due to CD40 deficiency in eleven patients. *J Clin Immunol* 33: 1325–1335.

81. Tsai, H. Y., H. H. Yu, Y. H. Chien, K. H. Chu, Y. L. Lau, J. H. Lee, L. C. Wang, B. L. Chiang, and Y. H. Yang. 2015. X-linked hyper-IgM syndrome with CD40LG mutation: two case reports and literature review in Taiwanese patients. *J Microbiol Immunol Infect* 48: 113–118.

82. Costa-Carvalho, B. T., G. F. Wandalsen, G. Pulici, C. S. Aranda, and D. Solé. 2011. Pulmonary complications in patients with antibody deficiency. *Allergol Immunopathol (Madr)* 39: 128–132.

83. Zheng, M., J. E. Shellito, L. Marrero, Q. Zhong, S. Julian, P. Ye, V. Wallace, P. Schwarzenberger, and J. K. Kolls. 2001. CD4+ T cell-independent vaccination against Pneumocystis carinii in mice. *J Clin Invest* 108: 1469–1474.

84. Gigliotti, F., C. G. Haidaris, T. W. Wright, and A. G. Harmsen. 2002. Passive intranasal monoclonal antibody prophylaxis against murine Pneumocystis carinii pneumonia. *Infect Immun* 70: 1069–1074.

85. Limper, A. H., J. S. Hoyte, and J. E. Standing. 1997. The role of alveolar macrophages in Pneumocystis carinii degradation and clearance from the lung. *J Clin Invest* 99: 2110–2117.

86. Lasbury, M. E., S. Merali, P. J. Durant, D. Tschang, C. A. Ray, and C. H. Lee. 2007. Polyamine-mediated apoptosis of alveolar macrophages during Pneumocystis pneumonia. *J Biol Chem* 282: 11009–11020.

87. Steele, C., L. Marrero, S. Swain, A. G. Harmsen, M. Zheng, G. D. Brown, S. Gordon, J. E. Shellito, and J. K. Kolls. 2003. Alveolar macrophage-mediated killing of Pneumocystis carinii f. sp. muris involves molecular recognition by the Dectin-1 beta-glucan receptor. *J Exp Med* 198: 1677–1688.

88. Wells, J., C. G. Haidaris, T. W. Wright, and F. Gigliotti. 2006. Complement and Fc function are required for optimal antibody prophylaxis against Pneumocystis carinii pneumonia. *Infect Immun* 74: 390–393.

89. McAllister, F., F. Mc Allister, C. Steele, M. Zheng, E. Young, J. E. Shellito, L. Marrero, and J. K. Kolls. 2004. T cytotoxic-1 CD8+ T cells are effector cells against pneumocystis in mice. *J Immunol* 172: 1132–1138.

90. Mandujano, J. F., N. B. D'Souza, S. Nelson, W. R. Summer, R. C. Beckerman, and J. E. Shellito. 1995. Granulocyte-macrophage colony stimulating factor and Pneumocystis carinii pneumonia in mice. *Am J Respir Crit Care Med* 151: 1233–1238.

91. Paine, R., A. M. Preston, S. Wilcoxen, H. Jin, B. B. Siu, S. B. Morris, J. A. Reed, G. Ross, J. A. Whitsett, and J. M. Beck. 2000. Granulocyte-macrophage colony-stimulating factor in the innate immune response to Pneumocystis carinii pneumonia in mice. *J Immunol* 164: 2602–2609.

92. Borie, R., C. Danel, M. P. Debray, C. Taille, M. C. Dombret, M. Aubier, R. Epaud, and B. Crestani. 2011. Pulmonary alveolar proteinosis. *Eur Respir Rev* 20: 98–107.

93. Nelson, M. P., B. S. Christmann, J. L. Werner, A. E. Metz, J. L. Trevor, C. A. Lowell, and C. Steele. 2011. IL-33 and M2a alveolar macrophages promote lung defense against the atypical fungal pathogen Pneumocystis murina. *J Immunol* 186: 2372–2381.

94. Bellamy, R. J. 2008. HIV: treating Pneumocystis pneumonia (PCP). *Clin Evid* 2008.

95. Helweg-Larsen, J., T. Benfield, C. Atzori, and R. F. Miller. 2009. Clinical efficacy of first- and second-line treatments for HIV-associated Pneumocystis jirovecii pneumonia: a tri-centre cohort study. *J Antimicrob Chemother* 64: 1282–1290.

96. Jick, H. 1982. Adverse reactions to trimethoprim-sulfamethoxazole in hospitalized patients. *Rev Infect Dis* 4: 426–428.

97. Phillips, E., and S. Mallal. 2007. Drug hypersensitivity in HIV. *Curr Opin Allergy Clin Immunol* 7: 324–330.

98. Rosenberg, H. F., K. D. Dyer, and P. S. Foster. 2013. Eosinophils: changing perspectives in health and disease. *Nat Rev Immunol* 13: 9–22.

99. Jung, Y., and M. E. Rothenberg. 2014. Roles and regulation of gastrointestinal eosinophils in immunity and disease. *J Immunol* 193: 999–1005.

100. Rothenberg, M. E., and S. P. Hogan. 2006. The eosinophil. *Annu Rev Immunol* 24: 147–174.

101. Bochner, B. S., and N. Zimmermann. 2015. Role of siglecs and related glycan-binding proteins in immune responses and immunoregulation. *J Allergy Clin Immunol* 135: 598–608.

102. Kiwamoto, T., T. Katoh, C. M. Evans, W. J. Janssen, M. E. Brummet, S. A. Hudson, Z. Zhu, M. Tiemeyer, and B. S. Bochner. 2015. Endogenous airway mucins carry glycans that bind Siglec-F and induce eosinophil apoptosis. *J Allergy Clin Immunol* 135: 1329–40.e1.

103. Iwasaki, H., S. Mizuno, R. Mayfield, H. Shigematsu, Y. Arinobu, B. Seed, M. F. Gurish, K. Takatsu, and K. Akashi. 2005. Identification of eosinophil lineage-committed progenitors in the murine bone marrow. *J Exp Med* 201: 1891–1897.

104. Simon, H. U., S. Yousefi, C. Schranz, A. Schapowal, C. Bachert, and K. Blaser. 1997. Direct demonstration of delayed eosinophil apoptosis as a mechanism causing tissue eosinophilia. *J Immunol* 158: 3902–3908.

105. Kouro, T., and K. Takatsu. 2009. IL-5- and eosinophil-mediated inflammation: from discovery to therapy. *Int Immunol* 21: 1303–1309.

106. Woodcock, J. M., B. Zacharakis, G. Plaetinck, C. J. Bagley, S. Qiyu, T. R. Hercus, J. Tavernier, and A. F. Lopez. 1994. Three residues in the common beta chain of the human GM-CSF, IL-3 and IL-5 receptors are essential for GM-CSF and IL-5 but not IL-3 high affinity binding and interact with Glu21 of GM-CSF. *EMBO J* 13: 5176–5185.

107. Yu, C., A. B. Cantor, H. Yang, C. Browne, R. A. Wells, Y. Fujiwara, and S. H. Orkin. 2002. Targeted deletion of a high-affinity GATA-binding site in the GATA-1 promoter leads to selective loss of the eosinophil lineage in vivo. *J Exp Med* 195: 1387–1395.

108. Nei, Y., K. Obata-Ninomiya, H. Tsutsui, K. Ishiwata, M. Miyasaka, K. Matsumoto, S. Nakae, H. Kanuka, N. Inase, and H. Karasuyama. 2013. GATA-1 regulates the generation and function of basophils. *Proc Natl Acad Sci U S A* 110: 18620–18625.

109. Acharya, K. R., and S. J. Ackerman. 2014. Eosinophil granule proteins: form and function. *J Biol Chem* 289: 17406–17415.

110. Dvorak, A. M., P. Estrella, and T. Ishizaka. 1994. Vesicular transport of peroxidase in human eosinophilic myelocytes. *Clin Exp Allergy* 24: 10–18.

111. Spencer, L. A., R. C. Melo, S. A. Perez, S. P. Bafford, A. M. Dvorak, and P. F. Weller. 2006. Cytokine receptor-mediated trafficking of preformed IL-4 in eosinophils identifies an innate immune mechanism of cytokine secretion. *Proc Natl Acad Sci U S A* 103: 3333–3338.

112. Wang, H. B., I. Ghiran, K. Matthaei, and P. F. Weller. 2007. Airway eosinophils: allergic inflammation recruited professional antigen-presenting cells. *J Immunol* 179: 7585–7592.

113. Butterworth, A. E., M. A. Vadas, D. L. Wassom, A. Dessein, M. Hogan, B. Sherry, G. J. Gleich, and J. R. David. 1979. Interactions between human eosinophils and schistosomula of Schistosoma mansoni. II. The mechanism of irreversible eosinophil adherence. *J Exp Med* 150: 1456–1471.

114. McLaren, D. J., C. G. Peterson, and P. Venge. 1984. Schistosoma mansoni: further studies of the interaction between schistosomula and granulocyte-derived cationic proteins in vitro. *Parasitology* 88 (Pt 3): 491–503.

115. Gebreselassie, N. G., A. R. Moorhead, V. Fabre, L. F. Gagliardo, N. A. Lee, J. J. Lee, and J. A. Appleton. 2012. Eosinophils preserve parasitic nematode larvae by regulating local immunity. *J Immunol* 188: 417–425.

116. Fabre, V., D. P. Beiting, S. K. Bliss, N. G. Gebreselassie, L. F. Gagliardo, N. A. Lee, J. J. Lee, and J. A. Appleton. 2009. Eosinophil deficiency compromises parasite survival in chronic nematode infection. *J Immunol* 182: 1577–1583.

117. Lehrer, R. I., D. Szklarek, A. Barton, T. Ganz, K. J. Hamann, and G. J. Gleich. 1989. Antibacterial properties of eosinophil major basic protein and eosinophil cationic protein. *J Immunol* 142: 4428–4434.

118. Domachowske, J. B., K. D. Dyer, C. A. Bonville, and H. F. Rosenberg. 1998. Recombinant human eosinophil-derived neurotoxin/RNase 2 functions as an effective antiviral agent against respiratory syncytial virus. *J Infect Dis* 177: 1458–1464.

119. Linch, S. N., A. M. Kelly, E. T. Danielson, R. Pero, J. J. Lee, and J. A. Gold. 2009. Mouse eosinophils possess potent antibacterial properties in vivo. *Infect Immun* 77: 4976–4982.

120. Phipps, S., C. E. Lam, S. Mahalingam, M. Newhouse, R. Ramirez, H. F. Rosenberg, P. S. Foster, and K. I. Matthaei. 2007. Eosinophils contribute to innate antiviral immunity and promote clearance of respiratory syncytial virus. *Blood* 110: 1578–1586.

121. Lilly, L. M., M. Scopel, M. P. Nelson, A. R. Burg, C. W. Dunaway, and C. Steele. 2014. Eosinophil deficiency compromises lung defense against Aspergillus fumigatus. *Infect Immun* 82: 1315–1325.

122. Yoon, J., J. U. Ponikau, C. B. Lawrence, and H. Kita. 2008. Innate antifungal immunity of human eosinophils mediated by a beta 2 integrin, CD11b. *J Immunol* 181: 2907–2915.

123. Zheng, M., A. J. Ramsay, M. B. Robichaux, C. Kliment, C. Crowe, R. R. Rapaka, C. Steele, F. McAllister, J. E. Shellito, L. Marrero, P. Schwarzenberger, Q. Zhong, and J. K. Kolls. 2005. CD4+ T cell-independent DNA vaccination against opportunistic infections. *J Clin Invest* 115: 3536–3544.

124. Beck, J. M., M. L. Warnock, J. L. Curtis, M. J. Sniezek, S. M. Arraj-Peffer, H. B. Kaltreider, and J. E. Shellito. 1991. Inflammatory responses to Pneumocystis carinii in mice selectively depleted of helper T lymphocytes. *Am J Respir Cell Mol Biol* 5: 186–197.

125. Dyer, K. D., J. M. Moser, M. Czapiga, S. J. Siegel, C. M. Percopo, and H. F. Rosenberg. 2008. Functionally competent eosinophils differentiated ex vivo in high purity from normal mouse bone marrow. *J Immunol* 181: 4004–4009.

126. Nakagome, K., M. Dohi, K. Okunishi, R. Tanaka, T. Kouro, M. R. Kano, K. Miyazono, J. Miyazaki, K. Takatsu, and K. Yamamoto. 2007. IL-5-induced hypereosinophilia suppresses the antigen-induced immune response via a TGF-beta-dependent mechanism. *J Immunol* 179: 284–294.

127. Ricks, D. M., K. Chen, M. Zheng, C. Steele, and J. K. Kolls. 2013. Dectin immunoadhesins and pneumocystis pneumonia. *Infect Immun* 81: 3451–3462.

128. Eddens, T., and J. K. Kolls. 2015. Pathological and protective immunity to Pneumocystis infection. *Semin Immunopathol* 37: 153–162.

129. Swain, S. D., N. N. Meissner, D. W. Siemsen, K. McInnerney, and A. G. Harmsen. 2012. Pneumocystis elicits a STAT6-dependent, strain-specific innate immune response and airway hyperresponsiveness. *Am J Respir Cell Mol Biol* 46: 290–298.

130. Fleury-Feith, J., J. T. Van Nhieu, C. Picard, E. Escudier, and J. F. Bernaudin. 1989. Bronchoalveolar lavage eosinophilia associated with Pneumocystis carinii pneumonitis in AIDS patients. Comparative study with non-AIDS patients. *Chest* 95: 1198–1201.

131. Sadaghdar, H., Z. B. Huang, and E. Eden. 1992. Correlation of bronchoalveolar lavage findings to severity of Pneumocystis carinii pneumonia in AIDS. Evidence for the development of high-permeability pulmonary edema. *Chest* 102: 63–69.

132. Swain, S. D., N. N. Meissner, and A. G. Harmsen. 2006. CD8 T cells modulate CD4 T-cell and eosinophil-mediated pulmonary pathology in pneumocystis pneumonia in B-cell-deficient mice. *Am J Pathol* 168: 466–475.

133. Jackson, D. J., A. Sykes, P. Mallia, and S. L. Johnston. 2011. Asthma exacerbations: origin, effect, and prevention. *J Allergy Clin Immunol* 128: 1165–1174.

134. Lambrecht, B. N., and H. Hammad. 2015. The immunology of asthma. *Nat Immunol* 16: 45–56.

135. Chung, K. F., S. E. Wenzel, J. L. Brozek, A. Bush, M. Castro, P. J. Sterk, I. M. Adcock, E. D. Bateman, E. H. Bel, E. R. Bleecker, L. P. Boulet, C. Brightling, P. Chanez, S. E. Dahlen, R. Djukanovic, U. Frey, M. Gaga, P. Gibson, Q. Hamid, N. N. Jajour, T. Mauad, R. L. Sorkness, and W. G. Teague. 2014. International ERS/ATS guidelines on definition, evaluation and treatment of severe asthma. *Eur Respir J* 43: 343–373.

136. Moffatt, M. F., I. G. Gut, F. Demenais, D. P. Strachan, E. Bouzigon, S. Heath, E. von Mutius, M. Farrall, M. Lathrop, W. O. Cookson, and GABRIEL Consortium. 2010. A large-scale, consortium-based genomewide association study of asthma. *N Engl J Med* 363: 1211–1221.

137. Moore, W. C., D. A. Meyers, S. E. Wenzel, W. G. Teague, H. Li, X. Li, R. D'Agostino, M. Castro, D. Curran-Everett, A. M. Fitzpatrick, B. Gaston, N. N. Jarjour, R. Sorkness, W. J. Calhoun, K. F. Chung, S. A. Comhair, R. A. Dweik, E. Israel, S. P. Peters, W. W. Busse, S. C. Erzurum, E. R. Bleecker, and National Heart, Lung, and Blood Institute's Severe Asthma Research Program. 2010. Identification of asthma phenotypes using cluster analysis in the Severe Asthma Research Program. *Am J Respir Crit Care Med* 181: 315–323.

138. Poole, A., C. Urbanek, C. Eng, J. Schageman, S. Jacobson, B. P. O'Connor, J. M. Galanter, C. R. Gignoux, L. A. Roth, R. Kumar, S. Lutz, A. H. Liu, T. E. Fingerlin, R. A. Setterquist, E. G. Burchard, J. Rodriguez-Santana, and M. A. Seibold. 2014. Dissecting childhood asthma with nasal transcriptomics distinguishes subphenotypes of disease. *J Allergy Clin Immunol* 133: 670–8.e12.

139. Peters, M. C., Z. K. Mekonnen, S. Yuan, N. R. Bhakta, P. G. Woodruff, and J. V. Fahy. 2014. Measures of gene expression in sputum cells can identify TH2-high and TH2-low subtypes of asthma. *J Allergy Clin Immunol* 133: 388–394.

140. Woodruff, P. G., B. Modrek, D. F. Choy, G. Jia, A. R. Abbas, A. Ellwanger, L. L. Koth, J. R. Arron, and J. V. Fahy. 2009. T-helper type 2-driven inflammation defines major subphenotypes of asthma. *Am J Respir Crit Care Med* 180: 388–395.

141. Robinson, D. S., Q. Hamid, S. Ying, A. Tsicopoulos, J. Barkans, A. M. Bentley, C. Corrigan, S. R. Durham, and A. B. Kay. 1992. Predominant TH2-like bronchoalveolar T-lymphocyte population in atopic asthma. *N Engl J Med* 326: 298–304.

142. Wills-Karp, M., J. Luyimbazi, X. Xu, B. Schofield, T. Y. Neben, C. L. Karp, and D. D. Donaldson. 1998. Interleukin-13: central mediator of allergic asthma. *Science* 282: 2258–2261.

143. Grünig, G., M. Warnock, A. E. Wakil, R. Venkayya, F. Brombacher, D. M. Rennick, D. Sheppard, M. Mohrs, D. D. Donaldson, R. M. Locksley, and D. B. Corry. 1998. Requirement for IL-13 independently of IL-4 in experimental asthma. *Science* 282: 2261–2263.

144. Coyle, A. J., S. J. Ackerman, R. Burch, D. Proud, and C. G. Irvin. 1995. Human eosinophil-granule major basic protein and synthetic polycations induce airway hyperresponsiveness in vivo dependent on bradykinin generation. *J Clin Invest* 95: 1735–1740.

145. Lee, J. J., D. Dimina, M. P. Macias, S. I. Ochkur, M. P. McGarry, K. R. O'Neill, C. Protheroe, R. Pero, T. Nguyen, S. A. Cormier, E. Lenkiewicz, D. Colbert, L. Rinaldi, S. J. Ackerman, C. G. Irvin, and N. A. Lee. 2004. Defining a link with asthma in mice congenitally deficient in eosinophils. *Science* 305: 1773–1776.

146. Humbles, A. A., C. M. Lloyd, S. J. McMillan, D. S. Friend, G. Xanthou, E. E. McKenna, S. Ghiran, N. P. Gerard, C. Yu, S. H. Orkin, and C. Gerard. 2004. A critical role for eosinophils in allergic airways remodeling. *Science* 305: 1776–1779.

147. Walsh, E. R., N. Sahu, J. Kearley, E. Benjamin, B. H. Kang, A. Humbles, and A. August. 2008. Strain-specific requirement for eosinophils in the recruitment of T cells to the lung during the development of allergic asthma. *J Exp Med* 205: 1285–1292.

148. Fattouh, R., A. Al-Garawi, M. Fattouh, K. Arias, T. D. Walker, S. Goncharova, A. J. Coyle, A. A. Humbles, and M. Jordana. 2011. Eosinophils are dispensable for allergic remodeling and immunity in a model of house dust mite-induced airway disease. *Am J Respir Crit Care Med* 183: 179–188.

149. Kumar, V. 2014. Innate lymphoid cells: new paradigm in immunology of inflammation. *Immunol Lett* 157: 23–37.

150. Yasuda, K., T. Muto, T. Kawagoe, M. Matsumoto, Y. Sasaki, K. Matsushita, Y. Taki, S. Futatsugi-Yumikura, H. Tsutsui, K. J. Ishii, T. Yoshimoto, S. Akira, and K. Nakanishi. 2012. Contribution of IL-33-activated type II innate lymphoid cells to pulmonary eosinophilia in intestinal nematode-infected mice. *Proc Natl Acad Sci U S A* 109: 3451–3456.

151. Hammad, H., and B. N. Lambrecht. 2015. Barrier Epithelial Cells and the Control of Type 2 Immunity. *Immunity* 43: 29–40.

152. Fort, M. M., J. Cheung, D. Yen, J. Li, S. M. Zurawski, S. Lo, S. Menon, T. Clifford, B. Hunte, R. Lesley, T. Muchamuel, S. D. Hurst, G. Zurawski, M. W. Leach, D. M. Gorman, and D. M. Rennick. 2001. IL-25 induces IL-4, IL-5, and IL-13 and Th2-associated pathologies in vivo. *Immunity* 15: 985–995.

153. Oczypok, E. A., P. S. Milutinovic, J. F. Alcorn, A. Khare, L. T. Crum, M. L. Manni, M. W. Epperly, A. M. Pawluk, A. Ray, and T. D. Oury. 2015. Pulmonary receptor for advanced glycation end-products promotes asthma pathogenesis through IL-33 and accumulation of group 2 innate lymphoid cells. *J Allergy Clin Immunol* 136: 747–756.e4.

154. Halim, T. Y., R. H. Krauss, A. C. Sun, and F. Takei. 2012. Lung natural helper cells are a critical source of Th2 cell-type cytokines in protease allergen-induced airway inflammation. *Immunity* 36: 451–463.

155. Klein Wolterink, R. G., A. Kleinjan, M. van Nimwegen, I. Bergen, M. de Bruijn, Y. Levani, and R. W. Hendriks. 2012. Pulmonary innate lymphoid cells are major producers of IL-5 and IL-13 in murine models of allergic asthma. *Eur J Immunol* 42: 1106–1116.

156. Halim, T. Y., C. A. Steer, L. Mathä, M. J. Gold, I. Martinez-Gonzalez, K. M. McNagny, A. N. McKenzie, and F. Takei. 2014. Group 2 innate lymphoid cells are critical for the initiation of adaptive T helper 2 cell-mediated allergic lung inflammation. *Immunity* 40: 425–435.

157. Oliphant, C. J., Y. Y. Hwang, J. A. Walker, M. Salimi, S. H. Wong, J. M. Brewer, A. Englezakis, J. L. Barlow, E. Hams, S. T. Scanlon, G. S. Ogg, P. G. Fallon, and A. N. McKenzie. 2014. MHCII-mediated dialog between group 2 innate lymphoid cells and CD4(+) T cells potentiates type 2 immunity and promotes parasitic helminth expulsion. *Immunity* 41: 283–295.

158. Kolls, J. K., and S. A. Khader. 2010. The role of Th17 cytokines in primary mucosal immunity. *Cytokine Growth Factor Rev* 21: 443–448.

159. Manni, M. L., J. B. Trudeau, E. V. Scheller, S. Mandalapu, M. M. Elloso, J. K. Kolls, S. E. Wenzel, and J. F. Alcorn. 2014. The complex relationship between inflammation and lung function in severe asthma. *Mucosal Immunol* 7: 1186–1198.

160. McKinley, L., J. F. Alcorn, A. Peterson, R. B. Dupont, S. Kapadia, A. Logar, A. Henry, C. G. Irvin, J. D. Piganelli, A. Ray, and J. K. Kolls. 2008. TH17 cells mediate steroid-resistant airway inflammation and airway hyperresponsiveness in mice. *J Immunol* 181: 4089–4097.

161. Shaw, D. E., M. A. Berry, B. Hargadon, S. McKenna, M. J. Shelley, R. H. Green, C. E. Brightling, A. J. Wardlaw, and I. D. Pavord. 2007. Association between neutrophilic airway inflammation and airflow limitation in adults with asthma. *Chest* 132: 1871–1875.

162. Kudo, M., A. C. Melton, C. Chen, M. B. Engler, K. E. Huang, X. Ren, Y. Wang, X. Bernstein, J. T. Li, K. Atabai, X. Huang, and D. Sheppard. 2012. IL-17A produced by αβ T cells drives airway hyper-responsiveness in mice and enhances mouse and human airway smooth muscle contraction. *Nat Med* 18: 547–554.

163. Wu, P., and T. V. Hartert. 2011. Evidence for a causal relationship between respiratory syncytial virus infection and asthma. *Expert Rev Anti Infect Ther* 9: 731–745.

164. Sigurs, N., F. Aljassim, B. Kjellman, P. D. Robinson, F. Sigurbergsson, R. Bjarnason, and P. M. Gustafsson. 2010. Asthma and allergy patterns over 18 years after severe RSV bronchiolitis in the first year of life. *Thorax* 65: 1045–1052.

165. Martinez, F. D., D. A. Stern, A. L. Wright, L. M. Taussig, and M. Halonen. 1998. Differential immune responses to acute lower respiratory illness in early life and subsequent development of persistent wheezing and asthma. *J Allergy Clin Immunol* 102: 915–920.

166. Macaubas, C., N. H. de Klerk, B. J. Holt, C. Wee, G. Kendall, M. Firth, P. D. Sly, and P. G. Holt. 2003. Association between antenatal cytokine production and the development of atopy and asthma at age 6 years. *The Lancet* 362: 1192–1197.

167. Stephens, R., D. A. Randolph, G. Huang, M. J. Holtzman, and D. D. Chaplin. 2002. Antigen-nonspecific recruitment of Th2 cells to the lung as a mechanism for viral infection-induced allergic asthma. *J Immunol* 169: 5458–5467.

168. Williams, J. V., P. A. Harris, S. J. Tollefson, L. L. Halburnt-Rush, J. M. Pingsterhaus, K. M. Edwards, P. F. Wright, and J. E. Crowe. 2004. Human metapneumovirus and lower respiratory tract disease in otherwise healthy infants and children. *N Engl J Med* 350: 443–450.

169. Beale, J., A. Jayaraman, D. J. Jackson, J. D. Macintyre, M. R. Edwards, R. P. Walton, J. Zhu, Y. M. Ching, B. Shamji, M. Edwards, J. Westwick, D. J. Cousins, Y. Y. Hwang, A. McKenzie, S. L. Johnston, and N. W. Bartlett. 2014. Rhinovirus-induced IL-25 in asthma exacerbation drives type 2 immunity and allergic pulmonary inflammation. *Sci Transl Med* 6: 256ra134.

170. Edwards, M. R., N. W. Bartlett, T. Hussell, P. Openshaw, and S. L. Johnston. 2012. The microbiology of asthma. *Nat Rev Microbiol* 10: 459–471.

171. Denning, D. W., B. R. O'Driscoll, C. M. Hogaboam, P. Bowyer, and R. M. Niven. 2006. The link between fungi and severe asthma: a summary of the evidence. *Eur Respir J* 27: 615–626.

172. Mari, A., P. Schneider, V. Wally, M. Breitenbach, and B. Simon-Nobbe. 2003. Sensitization to fungi: epidemiology, comparative skin tests, and IgE reactivity of fungal extracts. *Clin Exp Allergy* 33: 1429–1438.

173. Zureik, M., C. Neukirch, B. Leynaert, R. Liard, J. Bousquet, F. Neukirch, and European Community Respiratory Health Survey. 2002. Sensitisation to airborne moulds and severity of asthma: cross sectional study from European Community respiratory health survey. *BMJ* 325: 411–414.

174. Vicencio, A. G., M. T. Santiago, K. Tsirilakis, A. Stone, S. Worgall, E. A. Foley, D. Bush, and D. L. Goldman. 2014. Fungal sensitization in childhood persistent asthma is associated with disease severity. *Pediatr Pulmonol* 49: 8–14.

175. Porter, P., S. C. Susarla, S. Polikepahad, Y. Qian, J. Hampton, A. Kiss, S. Vaidya, S. Sur, V. Ongeri, T. Yang, G. L. Delclos, S. Abramson, F. Kheradmand, and D. B. Corry. 2009. Link between allergic asthma and airway mucosal infection suggested by proteinase-secreting household fungi. *Mucosal Immunol* 2: 504–517.

176. Kheradmand, F., A. Kiss, J. Xu, S. H. Lee, P. E. Kolattukudy, and D. B. Corry. 2002. A protease-activated pathway underlying Th cell type 2 activation and allergic lung disease. *J Immunol* 169: 5904–5911.

177. Porter, P. C., L. Roberts, A. Fields, M. Knight, Y. Qian, G. L. Delclos, S. Han, F. Kheradmand, and D. B. Corry. 2011. Necessary and sufficient role for T helper cells to prevent fungal dissemination in allergic lung disease. *Infect Immun* 79: 4459–4471.

178. Elsegeiny, W., T. Eddens, K. Chen, and J. K. Kolls. 2015. Anti-CD20 antibody therapy and susceptibility to Pneumocystis pneumonia. *Infect Immun* 83: 2043–2052.

179. Alcorn, J. F., L. M. Rinaldi, E. F. Jaffe, M. van Loon, J. H. Bates, Y. M. Janssen-Heininger, and C. G. Irvin. 2007. Transforming growth factor-beta1 suppresses airway hyperresponsiveness in allergic airway disease. *Am J Respir Crit Care Med* 176: 974–982.

180. Hantos, Z., B. Daróczy, B. Suki, S. Nagy, and J. J. Fredberg. 1992. Input impedance and peripheral inhomogeneity of dog lungs. *J Appl Physiol* 72: 168–178.

181. Tomioka, S., J. H. Bates, and C. G. Irvin. 2002. Airway and tissue mechanics in a murine model of asthma: alveolar capsule vs. forced oscillations. *J Appl Physiol* 93: 263–270.

182. Eddens, T., W. Elsegeiny, M. P. Nelson, W. Horne, B. T. Campfield, C. Steele, and J. K. Kolls. 2015. Eosinophils Contribute to Early Clearance of Pneumocystis murina Infection. *J Immunol* 195: 185–193.

183. Swain, S. D., N. Meissner, S. Han, and A. Harmsen. 2011. Pneumocystis infection in an immunocompetent host can promote collateral sensitization to respiratory antigens. *Infect Immun* 79: 1905–1914.

184. Sedhom, M. A., M. Pichery, J. R. Murdoch, B. Foligné, N. Ortega, S. Normand, K. Mertz, D. Sanmugalingam, L. Brault, T. Grandjean, E. Lefrancais, P. G. Fallon, V. Quesniaux, L. Peyrin-Biroulet, G. Cathomas, T. Junt, M. Chamaillard, J. P. Girard, and B. Ryffel. 2013. Neutralisation of the interleukin-33/ST2 pathway ameliorates experimental colitis through enhancement of mucosal healing in mice. *Gut* 62: 1714–1723.

185. Monticelli, L. A., G. F. Sonnenberg, M. C. Abt, T. Alenghat, C. G. Ziegler, T. A. Doering, J. M. Angelosanto, B. J. Laidlaw, C. Y. Yang, T. Sathaliyawala, M. Kubota, D. Turner, J. M. Diamond, A. W. Goldrath, D. L. Farber, R. G. Collman, E. J. Wherry, and D. Artis. 2011. Innate lymphoid cells promote lung-tissue homeostasis after infection with influenza virus. *Nat Immunol* 12: 1045–1054.

186. Morris, A., K. Wei, K. Afshar, and L. Huang. 2008. Epidemiology and clinical significance of pneumocystis colonization. *J Infect Dis* 197: 10–17.

187. Vargas, S. L., C. A. Ponce, M. Gallo, F. Pérez, J. F. Astorga, R. Bustamante, M. Chabé, I. Durand-Joly, P. Iturra, R. F. Miller, E. L. M. Aliouat, and E. Dei-Cas. 2013. Near-universal prevalence of Pneumocystis and associated increase in mucus in the lungs of infants with sudden unexpected death. *Clin Infect Dis* 56: 171–179.

188. Pérez, F. J., C. A. Ponce, D. A. Rojas, P. A. Iturra, R. I. Bustamante, M. Gallo, K. Hananias, and S. L. Vargas. 2014. Fungal colonization with Pneumocystis correlates to increasing chloride channel accessory 1 (hCLCA1) suggesting a pathway for up-regulation of airway mucus responses, in infant lungs. *Results Immunol* 4: 58–61.

189. Gregory, L. G., B. Causton, J. R. Murdoch, S. A. Mathie, V. O'Donnell, C. P. Thomas, F. M. Priest, D. J. Quint, and C. M. Lloyd. 2009. Inhaled house dust mite induces pulmonary T helper 2 cytokine production. *Clin Exp Allergy* 39: 1597–1610.

190. Johnson, J. R., R. E. Wiley, R. Fattouh, F. K. Swirski, B. U. Gajewska, A. J. Coyle, J. C. Gutierrez-Ramos, R. Ellis, M. D. Inman, and M. Jordana. 2004. Continuous exposure to house dust mite elicits chronic airway inflammation and structural remodeling. *Am J Respir Crit Care Med* 169: 378–385.

191. Tournoy, K. G., J. C. Kips, C. Schou, and R. A. Pauwels. 2000. Airway eosinophilia is not a requirement for allergen-induced airway hyperresponsiveness. *Clin Exp Allergy* 30: 79–85.

192. Salimi, M., J. L. Barlow, S. P. Saunders, L. Xue, D. Gutowska-Owsiak, X. Wang, L. C. Huang, D. Johnson, S. T. Scanlon, A. N. McKenzie, P. G. Fallon, and G. S. Ogg. 2013. A role for IL-25 and IL-33-driven type-2 innate lymphoid cells in atopic dermatitis. *J Exp Med* 210: 2939–2950.

193. Snelgrove, R. J., L. G. Gregory, T. Peiró, S. Akthar, G. A. Campbell, S. A. Walker, and C. M. Lloyd. 2014. Alternaria-derived serine protease activity drives IL-33-mediated asthma exacerbations. *J Allergy Clin Immunol* 134: 583–592.e6.

194. Maizels, R. M., and D. R. Withers. 2014. MHC-II: a mutual support system for ILCs and T cells? *Immunity* 41: 174–176.

195. Walker, A. N., R. E. Garner, and M. N. Horst. 1990. Immunocytochemical detection of chitin in Pneumocystis carinii. *Infect Immun* 58: 412–415.

196. Lee, C. G., C. A. Da Silva, J. Y. Lee, D. Hartl, and J. A. Elias. 2008. Chitin regulation of immune responses: an old molecule with new roles. *Curr Opin Immunol* 20: 684–689.

197. Drummond, M. B., L. Huang, P. T. Diaz, G. D. Kirk, E. C. Kleerup, A. Morris, W. Rom, M. D. Weiden, E. Zhao, B. Thompson, and K. Crothers. 2015. Factors associated with abnormal spirometry among HIV-infected individuals. *AIDS* 29: 1691–1700.

198. Pitzalis, C., G. W. Jones, M. Bombardieri, and S. A. Jones. 2014. Ectopic lymphoid-like structures in infection, cancer and autoimmunity. *Nat Rev Immunol* 14: 447–462.

199. Eikelenboom, P., J. J. Nassy, J. Post, J. C. Versteeg, and H. L. Langevoort. 1978. The histogenesis of lymph nodes in rat and rabbit. *Anat Rec* 190: 201–215.

200. Yoshida, H., K. Honda, R. Shinkura, S. Adachi, S. Nishikawa, K. Maki, K. Ikuta, and S. I. Nishikawa. 1999. IL-7 receptor alpha+ CD3(-) cells in the embryonic intestine induces the organizing center of Peyer's patches. *Int Immunol* 11: 643–655.

201. Eberl, G., S. Marmon, M. J. Sunshine, P. D. Rennert, Y. Choi, and D. R. Littman. 2004. An essential function for the nuclear receptor RORgamma(t) in the generation of fetal lymphoid tissue inducer cells. *Nat Immunol* 5: 64–73.

202. Miyasaka, M., and T. Tanaka. 2004. Lymphocyte trafficking across high endothelial venules: dogmas and enigmas. *Nat Rev Immunol* 4: 360–370.

203. Gallatin, W. M., I. L. Weissman, and E. C. Butcher. 1983. A cell-surface molecule involved in organ-specific homing of lymphocytes. *Nature* 304: 30–34.

204. Drayton, D. L., S. Liao, R. H. Mounzer, and N. H. Ruddle. 2006. Lymphoid organ development: from ontogeny to neogenesis. *Nat Immunol* 7: 344–353.

205. De Togni, P., J. Goellner, N. H. Ruddle, P. R. Streeter, A. Fick, S. Mariathasan, S. C. Smith, R. Carlson, L. P. Shornick, and J. Strauss-Schoenberger. 1994. Abnormal development of peripheral lymphoid organs in mice deficient in lymphotoxin. *Science* 264: 703–707.

206. Drayton, D. L., X. Ying, J. Lee, W. Lesslauer, and N. H. Ruddle. 2003. Ectopic LT alpha beta directs lymphoid organ neogenesis with concomitant expression of peripheral node addressin and a HEV-restricted sulfotransferase. *J Exp Med* 197: 1153–1163.

207. Browning, J. L., N. Allaire, A. Ngam-Ek, E. Notidis, J. Hunt, S. Perrin, and R. A. Fava. 2005. Lymphotoxin-beta receptor signaling is required for the homeostatic control of HEV differentiation and function. *Immunity* 23: 539–550.

208. Cyster, J. G. 2003. Lymphoid organ development and cell migration. *Immunol Rev* 195: 5–14.

209. Luther, S. A., H. L. Tang, P. L. Hyman, A. G. Farr, and J. G. Cyster. 2000. Coexpression of the chemokines ELC and SLC by T zone stromal cells and deletion of the ELC gene in the plt/plt mouse. *Proc Natl Acad Sci U S A* 97: 12694–12699.

210. Saeki, H., A. M. Moore, M. J. Brown, and S. T. Hwang. 1999. Cutting edge: secondary lymphoid-tissue chemokine (SLC) and CC chemokine receptor 7 (CCR7) participate in the emigration pathway of mature dendritic cells from the skin to regional lymph nodes. *J Immunol* 162: 2472–2475.

211. Legler, D. F., M. Loetscher, R. S. Roos, I. Clark-Lewis, M. Baggiolini, and B. Moser. 1998. B cell-attracting chemokine 1, a human CXC chemokine expressed in lymphoid tissues, selectively attracts B lymphocytes via BLR1/CXCR5. *J Exp Med* 187: 655–660.

212. Luther, S. A., T. Lopez, W. Bai, D. Hanahan, and J. G. Cyster. 2000. BLC expression in pancreatic islets causes B cell recruitment and lymphotoxin-dependent lymphoid neogenesis. *Immunity* 12: 471–481.

213. Moyron-Quiroz, J. E., J. Rangel-Moreno, K. Kusser, L. Hartson, F. Sprague, S. Goodrich, D. L. Woodland, F. E. Lund, and T. D. Randall. 2004. Role of inducible bronchus associated lymphoid tissue (iBALT) in respiratory immunity. *Nat Med* 10: 927–934.

214. Kocks, J. R., A. C. Davalos-Misslitz, G. Hintzen, L. Ohl, and R. Förster. 2007. Regulatory T cells interfere with the development of bronchus-associated lymphoid tissue. *J Exp Med* 204: 723–734.

215. Rangel-Moreno, J., J. E. Moyron-Quiroz, L. Hartson, K. Kusser, and T. D. Randall. 2007. Pulmonary expression of CXC chemokine ligand 13, CC chemokine ligand 19, and CC chemokine ligand 21 is essential for local immunity to influenza. *Proc Natl Acad Sci U S A* 104: 10577–10582.

216. GeurtsvanKessel, C. H., M. A. Willart, I. M. Bergen, L. S. van Rijt, F. Muskens, D. Elewaut, A. D. Osterhaus, R. Hendriks, G. F. Rimmelzwaan, and B. N. Lambrecht. 2009. Dendritic cells are crucial for maintenance of tertiary lymphoid structures in the lung of influenza virus-infected mice. *J Exp Med* 206: 2339–2349.

217. Bracke, K. R., F. M. Verhamme, L. J. Seys, C. Bantsimba-Malanda, D. M. Cunoosamy, R. Herbst, H. Hammad, B. N. Lambrecht, G. F. Joos, and G. G. Brusselle. 2013. Role of CXCL13 in cigarette smoke-induced lymphoid follicle formation and chronic obstructive pulmonary disease. *Am J Respir Crit Care Med* 188: 343–355.

218. Litsiou, E., M. Semitekolou, I. E. Galani, I. Morianos, A. Tsoutsa, P. Kara, D. Rontogianni, I. Bellenis, M. Konstantinou, K. Potaris, E. Andreakos, P. Sideras, S. Zakynthinos, and M. Tsoumakidou. 2013. CXCL13 production in B cells via Toll-like receptor/lymphotoxin receptor signaling is involved in lymphoid neogenesis in chronic obstructive pulmonary disease. *Am J Respir Crit Care Med* 187: 1194–1202.

219. Rangel-Moreno, J., L. Hartson, C. Navarro, M. Gaxiola, M. Selman, and T. D. Randall. 2006. Inducible bronchus-associated lymphoid tissue (iBALT) in patients with pulmonary complications of rheumatoid arthritis. *J Clin Invest* 116: 3183–3194.

220. Rangel-Moreno, J., D. M. Carragher, M. de la Luz Garcia-Hernandez, J. Y. Hwang, K. Kusser, L. Hartson, J. K. Kolls, S. A. Khader, and T. D. Randall. 2011. The development of inducible bronchus-associated lymphoid tissue depends on IL-17. *Nat Immunol* 12: 639–646.

221. Emery, J. L., and F. Dinsdale. 1973. The postnatal development of lymphoreticular aggregates and lymph nodes in infants' lungs. *J Clin Pathol* 26: 539–545.

222. Tschernig, T., W. J. Kleemann, and R. Pabst. 1995. Bronchus-associated lymphoid tissue (BALT) in the lungs of children who had died from sudden infant death syndrome and other causes. *Thorax* 50: 658–660.

223. Ivanov, I. I., B. S. McKenzie, L. Zhou, C. E. Tadokoro, A. Lepelley, J. J. Lafaille, D. J. Cua, and D. R. Littman. 2006. The orphan nuclear receptor RORgammat directs the differentiation program of proinflammatory IL-17+ T helper cells. *Cell* 126: 1121–1133.

224. Kumar, P., L. Monin, P. Castillo, W. Elsegeiny, W. Horne, T. Eddens, A. Vikram, M. Good, A. A. Schoenborn, K. Bibby, R. C. Montelaro, D. W. Metzger, A. S. Gulati, and J. K. Kolls. 2016. Intestinal Interleukin-17 Receptor Signaling Mediates Reciprocal Control of the Gut Microbiota and Autoimmune Inflammation. *Immunity* 44: 659–671.

225. Gaffen, S. L. 2009. Structure and signalling in the IL-17 receptor family. *Nat Rev Immunol* 9: 556–567.

226. Rickel, E. A., L. A. Siegel, B. R. Yoon, J. B. Rottman, D. G. Kugler, D. A. Swart, P. M. Anders, J. E. Tocker, M. R. Comeau, and A. L. Budelsky. 2008. Identification of functional roles for both IL-17RB and IL-17RA in mediating IL-25-induced activities. *J Immunol* 181: 4299–4310.

227. Gregory, L. G., C. P. Jones, S. A. Walker, D. Sawant, K. H. Gowers, G. A. Campbell, A. N. McKenzie, and C. M. Lloyd. 2013. IL-25 drives remodelling in allergic airways disease induced by house dust mite. *Thorax* 68: 82–90.

228. Petersen, B. C., A. L. Budelsky, A. P. Baptist, M. A. Schaller, and N. W. Lukacs. 2012. Interleukin-25 induces type 2 cytokine production in a steroid-resistant interleukin-17RB+ myeloid population that exacerbates asthmatic pathology. *Nat Med* 18: 751–758.

229. Tworek, D., S. G. Smith, B. M. Salter, A. J. Baatjes, T. Scime, R. Watson, C. Obminski, G. M. Gauvreau, and P. M. O'Byrne. 2015. Interleukin 25 Receptor Expression on Airway Dendritic Cells After Allergen Challenge in Asthmatic Subjects. *Am J Respir Crit Care Med* .

230. Elliot, J. G., C. M. Jensen, S. Mutavdzic, J. P. Lamb, N. G. Carroll, and A. L. James. 2004. Aggregations of lymphoid cells in the airways of nonsmokers, smokers, and subjects with asthma. *Am J Respir Crit Care Med* 169: 712–718.

231. Eddens, T., B. T. Campfield, K. Serody, M. L. Manni, W. Horne, W. Elsegeiny, K. J. McHugh, D. Pociask, K. Chen, M. Zheng, J. F. Alcorn, S. Wenzel, and J. K. Kolls. 2016. A Novel CD4(+) T-cell Dependent Murine Model of Pneumocystis Driven Asthma-like Pathology. *Am J Respir Crit Care Med* .

232. Demoor, T., K. R. Bracke, T. Maes, B. Vandooren, D. Elewaut, C. Pilette, G. F. Joos, and G. G. Brusselle. 2009. Role of lymphotoxin-alpha in cigarette smoke-induced inflammation and lymphoid neogenesis. *Eur Respir J* 34: 405–416.

233. Gopal, R., J. Rangel-Moreno, S. Slight, Y. Lin, H. F. Nawar, B. A. Fallert Junecko, T. A. Reinhart, J. Kolls, T. D. Randall, T. D. Connell, and S. A. Khader. 2013. Interleukin-17-dependent CXCL13 mediates mucosal vaccine-induced immunity against tuberculosis. *Mucosal Immunol* 6: 972–984.

234. Fleige, H., S. Ravens, G. L. Moschovakis, J. Bölter, S. Willenzon, G. Sutter, S. Häussler, U. Kalinke, I. Prinz, and R. Förster. 2014. IL-17-induced CXCL12 recruits B cells and induces follicle formation in BALT in the absence of differentiated FDCs. *J Exp Med* 211: 643–651.

235. Halle, S., H. C. Dujardin, N. Bakocevic, H. Fleige, H. Danzer, S. Willenzon, Y. Suezer, G. Hämmerling, N. Garbi, G. Sutter, T. Worbs, and R. Förster. 2009. Induced bronchus-associated lymphoid tissue serves as a general priming site for T cells and is maintained by dendritic cells. *J Exp Med* 206: 2593–2601.

236. John-Schuster, G., K. Hager, T. M. Conlon, M. Irmler, J. Beckers, O. Eickelberg, and A. Ö. Yildirim. 2014. Cigarette smoke-induced iBALT mediates macrophage activation in a B cell-dependent manner in COPD. *Am J Physiol Lung Cell Mol Physiol* 307: L692–L706.

237. Fitzpatrick, M. E., J. R. Tedrow, M. E. Hillenbrand, L. Lucht, T. Richards, K. A. Norris, Y. Zhang, F. C. Sciurba, N. Kaminski, and A. Morris. 2014. Pneumocystis jirovecii colonization is associated with enhanced Th1 inflammatory gene expression in lungs of humans with chronic obstructive pulmonary disease. *Microbiol Immunol* 58: 202–211.

238. Morris, A., F. C. Sciurba, I. P. Lebedeva, A. Githaiga, W. M. Elliott, J. C. Hogg, L. Huang, and K. A. Norris. 2004. Association of chronic obstructive pulmonary disease severity and Pneumocystis colonization. *Am J Respir Crit Care Med* 170: 408–413.

239. Mori, S., I. Cho, H. Ichiyasu, and M. Sugimoto. 2008. Asymptomatic carriage of Pneumocystis jiroveci in elderly patients with rheumatoid arthritis in Japan: a possible association between colonization and development of Pneumocystis jiroveci pneumonia during low-dose MTX therapy. *Mod Rheumatol* 18: 240–246.

240. Mori, S., and M. Sugimoto. 2015. Pneumocystis jirovecii Pneumonia in Rheumatoid Arthritis Patients: Risks and Prophylaxis Recommendations. *Clinical medicine insights. Circulatory, respiratory and pulmonary medicine* 9: 29–40.

241. Djawe, K., K. Buchacz, L. Hsu, M. J. Chen, R. M. Selik, C. Rose, T. Williams, J. T. Brooks, and S. Schwarcz. 2015. Mortality Risk After AIDS-Defining Opportunistic Illness Among HIV-Infected Persons--San Francisco, 1981-2012. *J Infect Dis* 212: 1366–1375.

242. Queener, S. F., V. Cody, J. Pace, P. Torkelson, and A. Gangjee. 2013. Trimethoprim resistance of dihydrofolate reductase variants from clinical isolates of Pneumocystis jirovecii. *Antimicrob Agents Chemother* 57: 4990–4998.

243. Ma, L., L. Borio, H. Masur, and J. A. Kovacs. 1999. Pneumocystis carinii dihydropteroate synthase but not dihydrofolate reductase gene mutations correlate with prior trimethoprim-sulfamethoxazole or dapsone use. *J Infect Dis* 180: 1969–1978.

244. Huang, L., C. B. Beard, J. Creasman, D. Levy, J. S. Duchin, S. Lee, N. Pieniazek, J. L. Carter, C. del Rio, D. Rimland, and T. R. Navin. 2000. Sulfa or sulfone prophylaxis and geographic region predict mutations in the Pneumocystis carinii dihydropteroate synthase gene. *J Infect Dis* 182: 1192–1198.

245. Crothers, K., C. B. Beard, J. Turner, G. Groner, M. Fox, A. Morris, S. Eiser, and L. Huang. 2005. Severity and outcome of HIV-associated Pneumocystis pneumonia containing Pneumocystis jirovecii dihydropteroate synthase gene mutations. *AIDS* 19: 801–805.

246. Moukhlis, R., J. Boyer, P. Lacube, J. Bolognini, P. Roux, and C. Hennequin. 2010. Linking Pneumocystis jiroveci sulfamethoxazole resistance to the alleles of the DHPS gene using functional complementation in Saccharomyces cerevisiae. *Clin Microbiol Infect* 16: 501–507.

247. Nahimana, A., M. Rabodonirina, J. Bille, P. Francioli, and P. M. Hauser. 2004. Mutations of Pneumocystis jirovecii dihydrofolate reductase associated with failure of prophylaxis. *Antimicrob Agents Chemother* 48: 4301–4305.

248. Rodon, J., R. Dienstmann, V. Serra, and J. Tabernero. 2013. Development of PI3K inhibitors: lessons learned from early clinical trials. *Nat Rev Clin Oncol* 10: 143–153.

249. Wong, K. K., J. A. Engelman, and L. C. Cantley. 2010. Targeting the PI3K signaling pathway in cancer. *Curr Opin Genet Dev* 20: 87–90.

250. De Souza, C. P., S. B. Hashmi, A. H. Osmani, P. Andrews, C. S. Ringelberg, J. C. Dunlap, and S. A. Osmani. 2013. Functional analysis of the Aspergillus nidulans kinome. *PLoS ONE* 8: e58008.

251. Herman, P. K., and S. D. Emr. 1990. Characterization of VPS34, a gene required for vacuolar protein sorting and vacuole segregation in Saccharomyces cerevisiae. *Mol Cell Biol* 10: 6742–6754.

252. Stack, J. H., and S. D. Emr. 1994. Vps34p required for yeast vacuolar protein sorting is a multiple specificity kinase that exhibits both protein kinase and phosphatidylinositol-specific PI 3-kinase activities. *J Biol Chem* 269: 31552–31562.

253. Engelman, J. A., J. Luo, and L. C. Cantley. 2006. The evolution of phosphatidylinositol 3-kinases as regulators of growth and metabolism. *Nat Rev Genet* 7: 606–619.

254. Miller, S., B. Tavshanjian, A. Oleksy, O. Perisic, B. T. Houseman, K. M. Shokat, and R. L. Williams. 2010. Shaping development of autophagy inhibitors with the structure of the lipid kinase Vps34. *Science* 327: 1638–1642.

255. Workman, P., and R. L. van Montfort. 2010. Unveiling the secrets of the ancestral PI3 kinase Vps34. *Cancer Cell* 17: 421–423.

256. Cissé, O. H., M. Pagni, and P. M. Hauser. 2012. De novo assembly of the Pneumocystis jirovecii genome from a single bronchoalveolar lavage fluid specimen from a patient. *MBio* 4: e00428–e00412.

257. Jones, D. T., W. R. Taylor, and J. M. Thornton. 1992. The rapid generation of mutation data matrices from protein sequences. *Comput Appl Biosci* 8: 275–282.

258. Tamura, K., D. Peterson, N. Peterson, G. Stecher, M. Nei, and S. Kumar. 2011. MEGA5: molecular evolutionary genetics analysis using maximum likelihood, evolutionary distance, and maximum parsimony methods. *Mol Biol Evol* 28: 2731–2739.

259. Nugent, J. H., C. E. Alfa, T. Young, and J. S. Hyams. 1991. Conserved structural motifs in cyclins identified by sequence analysis. *J Cell Sci* 99 (Pt 3): 669–674.

260. Kazanjian, P., A. B. Locke, P. A. Hossler, B. R. Lane, M. S. Bartlett, J. W. Smith, M. Cannon, and S. R. Meshnick. 1998. Pneumocystis carinii mutations associated with sulfa and sulfone prophylaxis failures in AIDS patients. *AIDS* 12: 873–878.

261. Rabodonirina, M., L. Vaillant, P. Taffé, A. Nahimana, R. P. Gillibert, P. Vanhems, and P. M. Hauser. 2013. Pneumocystis jirovecii genotype associated with increased death rate of HIV-infected patients with pneumonia. *Emerging Infect Dis* 19: 21–8; quiz 186.

262. Edwards, S. R., and T. J. Wandless. 2010. Dicistronic regulation of fluorescent proteins in the budding yeast Saccharomyces cerevisiae. *Yeast* 27: 229–236.

263. Jakubowski, W., D. Ertel, T. Biliński, J. Kedziora, and G. Bartosz. 1998. Luminol luminescence induced by oxidants in antioxidant-deficient yeasts Saccharomyces cerevisiae. *Biochem Mol Biol Int* 45: 191–203.

264. Zheng, M., Y. Cai, T. Eddens, D. M. Ricks, and J. K. Kolls. 2014. Novel pneumocystis antigen discovery using fungal surface proteomics. *Infect Immun* 82: 2417–2423.

265. Thomas, C. F., and A. H. Limper. 2007. Current insights into the biology and pathogenesis of Pneumocystis pneumonia. *Nat Rev Microbiol* 5: 298–308.

266. Radhi, S., T. Alexander, M. Ukwu, S. Saleh, and A. Morris. 2008. Outcome of HIV-associated Pneumocystis pneumonia in hospitalized patients from 2000 through 2003. *BMC Infect Dis* 8: 118.

267. Tasaka, S., and H. Tokuda. 2012. Pneumocystis jirovecii pneumonia in non-HIV-infected patients in the era of novel immunosuppressive therapies. *J Infect Chemother* 18: 793–806.

268. Kaur, N., and T. C. Mahl. 2007. Pneumocystis jiroveci (carinii) pneumonia after infliximab therapy: a review of 84 cases. *Dig Dis Sci* 52: 1481–1484.

269. Kaneko, Y., A. Suwa, Y. Ikeda, and M. Hirakata. 2006. Pneumocystis jiroveci pneumonia associated with low-dose methotrexate treatment for rheumatoid arthritis: report of two cases and review of the literature. *Mod Rheumatol* 16: 36–38.

270. Kamel, S., S. O'Connor, N. Lee, R. Filshie, H. Nandurkar, and C. S. Tam. 2010. High incidence of Pneumocystis jirovecii pneumonia in patients receiving biweekly rituximab and cyclophosphamide, adriamycin, vincristine, and prednisone. *Leuk Lymphoma* 51: 797–801.

271. Cetin, E., and E. Y. Lee. 2007. Pneumocystis carinii pneumonia in an infant with hypogammaglobulinemia. *Pediatr Radiol* 37: 329.

272. Eto, D., C. Lao, D. DiToro, B. Barnett, T. C. Escobar, R. Kageyama, I. Yusuf, and S. Crotty. 2011. IL-21 and IL-6 are critical for different aspects of B cell immunity and redundantly induce optimal follicular helper CD4 T cell (Tfh) differentiation. *PLoS ONE* 6: e17739.

273. Potsch, D. V., L. A. Camacho, S. Tuboi, L. M. Villar, J. C. Miguel, C. Ginuíno, E. F. Silva, R. M. Mendonça, R. B. Moreira, and P. F. Barroso. 2012. Vaccination against hepatitis B with 4-double doses increases response rates and antibodies titers in HIV-infected adults. *Vaccine* 30: 5973–5977.

274. Siegrist, C. A., C. van Delden, M. Bel, C. Combescure, C. Delhumeau, M. Cavassini, O. Clerc, S. Meier, K. Hadaya, P. M. Soccal, S. Yerly, L. Kaiser, B. Hirschel, A. Calmy, H1N1 Study Group, and Swiss HIV Cohort Study (SHCS). 2012. Higher memory responses in HIV-infected and kidney transplanted patients than in healthy subjects following priming with the pandemic vaccine. *PLoS ONE* 7: e40428.

275. Abzug, M. J., M. Qin, M. J. Levin, T. Fenton, J. A. Beeler, W. J. Bellini, S. Audet, S. B. Sowers, W. Borkowsky, S. A. Nachman, S. I. Pelton, H. M. Rosenblatt, and International Maternal Pediatric Adolescent AIDS Clinical Trials Group P1024 and P1061s Protocol Teams. 2012. Immunogenicity, immunologic memory, and safety following measles revaccination in HIV-infected children receiving highly active antiretroviral therapy. *J Infect Dis* 206: 512–522.

276. Zhang, Q., P. Wang, Y. Kim, P. Haste-Andersen, J. Beaver, P. E. Bourne, H. H. Bui, S. Buus, S. Frankild, J. Greenbaum, O. Lund, C. Lundegaard, M. Nielsen, J. Ponomarenko, A. Sette, Z. Zhu, and B. Peters. 2008. Immune epitope database analysis resource (IEDB-AR). *Nucleic Acids Res* 36: W513–W518.

277. Kottom, T. J., and A. H. Limper. 2000. Cell wall assembly by Pneumocystis carinii. Evidence for a unique gsc-1 subunit mediating beta -1,3-glucan deposition. *J Biol Chem* 275: 40628–40634.

278. O'Dea, E. M., N. Amarsaikhan, H. Li, J. Downey, E. Steele, S. J. Van Dyken, R. M. Locksley, and S. P. Templeton. 2014. Eosinophils are recruited in response to chitin exposure and enhance Th2-mediated immune pathology in Aspergillus fumigatus infection. *Infect Immun* 82: 3199–3205.

279. Roy, R. M., M. Wüthrich, and B. S. Klein. 2012. Chitin elicits CCL2 from airway epithelial cells and induces CCR2-dependent innate allergic inflammation in the lung. *J Immunol* 189: 2545–2552.

280. Villegas, L. R., T. J. Kottom, and A. H. Limper. 2012. Chitinases in Pneumocystis carinii pneumonia. *Med Microbiol Immunol* 201: 337–348.

281. Nagase, H., M. Yamaguchi, S. Jibiki, H. Yamada, K. Ohta, H. Kawasaki, O. Yoshie, K. Yamamoto, Y. Morita, and K. Hirai. 1999. Eosinophil chemotaxis by chemokines: a study by a simple photometric assay. *Allergy* 54: 944–950.

282. Skiest, D. J., and P. Keiser. 1997. Clinical significance of eosinophilia in HIV-infected individuals. *Am J Med* 102: 449–453.

283. Sivaram, M., A. White, and K. W. Radcliffe. 2012. Eosinophilia: clinical significance in HIV-infected individuals. *Int J STD AIDS* 23: 635–638.

284. Ray, A., T. B. Oriss, and S. E. Wenzel. 2015. Emerging molecular phenotypes of asthma. *Am J Physiol Lung Cell Mol Physiol* 308: L130–L140.

285. Bel, E. H., S. E. Wenzel, P. J. Thompson, C. M. Prazma, O. N. Keene, S. W. Yancey, H. G. Ortega, I. D. Pavord, and SIRIUS Investigators. 2014. Oral glucocorticoid-sparing effect of mepolizumab in eosinophilic asthma. *N Engl J Med* 371: 1189–1197.

286. Plantinga, M., M. Guilliams, M. Vanheerswynghels, K. Deswarte, F. Branco-Madeira, W. Toussaint, L. Vanhoutte, K. Neyt, N. Killeen, B. Malissen, H. Hammad, and B. N. Lambrecht. 2013. Conventional and monocyte-derived CD11b(+) dendritic cells initiate and maintain T helper 2 cell-mediated immunity to house dust mite allergen. *Immunity* 38: 322–335.

287. Coquet, J. M., M. J. Schuijs, M. J. Smyth, K. Deswarte, R. Beyaert, H. Braun, L. Boon, G. B. Karlsson Hedestam, S. L. Nutt, H. Hammad, and B. N. Lambrecht. 2015. Interleukin-21-Producing CD4(+) T Cells Promote Type 2 Immunity to House Dust Mites. *Immunity* 43: 318–330.

288. Dambuza, I. M., and G. D. Brown. 2015. C-type lectins in immunity: recent developments. *Curr Opin Immunol* 32: 21–27.

289. Wagener, J., R. K. Malireddi, M. D. Lenardon, M. Köberle, S. Vautier, D. M. MacCallum, T. Biedermann, M. Schaller, M. G. Netea, T. D. Kanneganti, G. D. Brown, A. J. Brown, and N. A. Gow. 2014. Fungal chitin dampens inflammation through IL-10 induction mediated by NOD2 and TLR9 activation. *PLoS Pathog* 10: e1004050.

290. Millien, V. O., W. Lu, J. Shaw, X. Yuan, G. Mak, L. Roberts, L. Z. Song, J. M. Knight, C. J. Creighton, A. Luong, F. Kheradmand, and D. B. Corry. 2013. Cleavage of fibrinogen by proteinases elicits allergic responses through Toll-like receptor 4. *Science* 341: 792–796.

291. Pabst, R., and I. Gehrke. 1990. Is the bronchus-associated lymphoid tissue (BALT) an integral structure of the lung in normal mammals, including humans? *Am J Respir Cell Mol Biol* 3: 131–135.

292. Tripathi, S. K., and R. Lahesmaa. 2014. Transcriptional and epigenetic regulation of T-helper lineage specification. *Immunol Rev* 261: 62–83.

293. Christman, J. K. 2002. 5-Azacytidine and 5-aza-2'-deoxycytidine as inhibitors of DNA methylation: mechanistic studies and their implications for cancer therapy. *Oncogene* 21: 5483–5495.

294. Vigushin, D. M., S. Ali, P. E. Pace, N. Mirsaidi, K. Ito, I. Adcock, and R. C. Coombes. 2001. Trichostatin A is a histone deacetylase inhibitor with potent antitumor activity against breast cancer in vivo. *Clin Cancer Res* 7: 971–976.

295. Jacoby, M., S. Gohrbandt, V. Clausse, N. H. Brons, and C. P. Muller. 2012. Interindividual variability and co-regulation of DNA methylation differ among blood cell populations. *Epigenetics* 7: 1421–1434.

296. Lucero, C. M., B. Fallert Junecko, C. R. Klamar, L. A. Sciullo, S. J. Berendam, A. R. Cillo, S. Qin, Y. Sui, S. Sanghavi, M. A. Murphey-Corb, and T. A. Reinhart. 2013. Macaque paneth cells express lymphoid chemokine CXCL13 and other antimicrobial peptides not previously described as expressed in intestinal crypts. *Clin Vaccine Immunol* 20: 1320–1328.

297. Zhu, J., B. Min, J. Hu-Li, C. J. Watson, A. Grinberg, Q. Wang, N. Killeen, J. F. Urban, L. Guo, and W. E. Paul. 2004. Conditional deletion of Gata3 shows its essential function in T(H)1-T(H)2 responses. *Nat Immunol* 5: 1157–1165.

298. Foo, S. Y., and S. Phipps. 2010. Regulation of inducible BALT formation and contribution to immunity and pathology. *Mucosal Immunol* 3: 537–544.